

VOLUME 78 SEPTEMBER 12, 1974 NUMBER 19

JPCA X

THE JOURNAL OF
PHYSICAL
CHEMISTRY

PUBLISHED BIWEEKLY BY THE AMERICAN CHEMICAL SOCIETY

THE JOURNAL OF PHYSICAL CHEMISTRY

BRYCE CRAWFORD, Jr., *Editor*

WILMER G. MILLER, *Associate Editor*

ROBERT W. CARR, Jr., **FREDERIC A. VAN-CATLEDGE,** *Assistant Editors*

EDITORIAL BOARD: A. O. ALLEN (1970-1974), C. A. ANGELL (1973-1977), F. C. ANSON (1974-1978), V. A. BLOOMFIELD (1974-1978), J. R. BOLTON (1971-1975), L. M. DORFMAN (1974-1978), M. FIXMAN (1970-1974), H. S. FRANK (1970-1974), R. R. HENTZ (1972-1976), W. J. KAUZMANN (1974-1978), R. L. KAY (1972-1976), D. W. McCLURE (1974-1978), R. M. NOYES (1973-1977), J. A. POPLE (1971-1975), B. S. RABINOVITCH (1971-1975), H. REISS (1970-1974), S. A. RICE (1969-1975), F. S. ROWLAND (1973-1977), R. L. SCOTT (1973-1977), A. SILBERBERG (1971-1975), J. B. STOTHERS (1974-1978), W. A. ZISMAN (1972-1976)

AMERICAN CHEMICAL SOCIETY, 1155 Sixteenth St., N.W., Washington, D. C. 20036

Books and Journals Division

JOHN K CRUM *Director*

RUTH REYNARD *Assistant to the Director*

CHARLES R. BERTSCH *Head, Editorial Processing Department*

D. H. MICHAEL BOWEN *Head, Journals Department*

BACIL GUILLEY *Head, Graphics and Production Department*

SELDON W. TERRANT *Head, Research and Development Department*

©Copyright, 1974, by the American Chemical Society. Published biweekly by the American Chemical Society at 20th and Northampton Sts., Easton, Pa. 18042. Second-class postage paid at Washington, D. C., and at additional mailing offices.

All manuscripts should be sent to *The Journal of Physical Chemistry*, Department of Chemistry, University of Minnesota, Minneapolis, Minn. 55455.

Additions and Corrections are published once yearly in the final issue. See Volume 77, Number 26 for the proper form.

Extensive or unusual alterations in an article after it has been set in type are made at the author's expense, and it is understood that by requesting such alterations the author agrees to defray the cost thereof.

The American Chemical Society and the Editor of *The Journal of Physical Chemistry* assume no responsibility for the statements and opinions advanced by contributors.

Correspondence regarding accepted copy, proofs, and reprints should be directed to Editorial Processing Department, American Chemical Society, 20th and Northampton Sts., Easton, Pa. 18042. Department Head: CHARLES R. BERTSCH. Assistant Department Head: MARIANNE C. BROGAN. Assistant Editor: CELIA B. MCFARLAND. Editorial Assistant: JOSEPH E. YURVATI.

Advertising Office: Centcom, Ltd., 50 W. State St., Westport, Conn. 06880.

Business and Subscription Information

Send all new and renewal subscriptions *with payment to*: Office of the Controller, 1155 16th Street, N.W., Washington, D. C. 20036. Subscriptions should be renewed promptly to avoid a break in your

series. All correspondence and telephone calls regarding changes of address, claims for missing issues, subscription service, the status of records, and accounts should be directed to Manager, Membership and Subscription Services, American Chemical Society, P.O. Box 3337, Columbus, Ohio 43210. Telephone (614) 421-7230.

On changes of address, include both old and new addresses with ZIP code numbers, accompanied by mailing label from a recent issue. Allow four weeks for change to become effective.

Claims for missing numbers will not be allowed (1) if loss was due to failure of notice of change in address to be received before the date specified, (2) if received more than sixty days from date of issue plus time normally required for postal delivery of journal and claim, or (3) if the reason for the claim is "issue missing from files."

Subscription rates (1974): members of the American Chemical Society, \$20.00 for 1 year; to nonmembers, \$60.00 for 1 year. Those interested in becoming members should write to the Admissions Department, American Chemical Society, 1155 Sixteenth St., N.W., Washington, D. C. 20036. Postage to Canada and countries in the Pan-American Union, \$5.00; all other countries, \$6.00. Air freight rates available on request. Single copies for current year: \$3.00. Rates for back issues from Volume 56 to date are available from the Special Issues Sales Department, 1155 Sixteenth St., N.W., Washington, D. C. 20036.

Subscriptions to this and the other ACS periodical publications are available on microfilm. Supplementary material not printed in this journal is now available in microfiche form on a current subscription basis. For information on microfilm or microfiche subscriptions, write Special Issues Sales Department at the address above.

THE JOURNAL OF
PHYSICAL CHEMISTRY

Volume 78, Number 19 September 12, 1974

JPCHAx 78(19) 1885-1978 (1974)

ISSN 0022-3654

- Short-Lived Intermediates Formed by the Interaction between Electronically Excited Molecules and Inorganic Ions **A. R. Watkins** 1885
- Solvent-Jump Relaxation Kinetics of the Association of Rhodamine Type Laser Dyes **M. M. Wong and Z. A. Schelly*** 1891
- Anaerobic Chemiluminescent Reaction of Aryl Grignard Reagents with Aryl Peroxides **Philip H. Bolton and David R. Kearns*** 1896
- Photolysis of Liquid Cyclohexane at 1634 Å and the Effect of the Addition of Carbon Tetrachloride and Sulfur Hexafluoride **J. Nafisi-Movaghar and Yoshihiko Hatano*** 1899
- Natural and Experimental Fluorescence Lifetimes of Benzene in Various Solvents **Menahem Luria, Mira Ofran, and Gabriel Stein*** 1904
- Photolysis of Benzene in Cyclohexane at 2537 Å **Hanspeter Lutz and Gabriel Stein*** 1909
- Ultrasonic Absorption in Aqueous Solutions of Calcium Acetate and Other Bivalent Metal Acetates **Gordon Atkinson,* Mostafa M. Emara, and R. Fernández-Prini** 1913
- Derivation of Rate Equations for Fischer Glycosidation of D-Glucose and Estimation of Rate Constants Using a Computer **Dwight F. Mowery, Jr.** 1918 ■
- Stable Intermediates in Kinetic Models of Catalase Action **M. L. Kremer* and S. Baer** 1919
- Thermodynamics of Caffeine and the 1-1 Caffeine-Salicylate Complex in Water at 25° **J. H. Stern,* J. A. Devore, S. L. Hansen, and O. Yavuz** 1922
- Heats of Mixing Aqueous Electrolytes. XI. The Charge-Asymmetric Limiting Law at Low Concentrations. Barium Chloride with Sodium Chloride and Sodium Sulfate with Sodium Chloride **R. B. Cassel and R. H. Wood*** 1924
- Charge-Asymmetric Mixtures of Electrolytes at Low Ionic Strength **Harold L. Friedman* and C. V. Krishnan** 1927
- The Lithium-Lithium Hydride System **Ewald Veleckis,* Erven H. Van Deventer, and Milton Blander** 1933 ■
- Metal Ion Association in Alcohol Solutions. IV. The Existence of an Inner-Sphere Complex between Erbium(III) and Perchlorate **Herbert B. Silber** 1940
- Predicted Properties of the Superheavy Elements. III. Element 115, Eka-Bismuth **O. L. Keller, Jr.,* C. W. Nestor, Jr., and Burkhard Fricke** 1945
- Aerodynamic Drag on Bursting Bubbles **G. Frens** 1949
- Fluorescence Quenching of the Indole Ring System by Lanthanide Ions **Robert W. Ricci* and Kurt B. Kilichowski** 1953
- Electron Paramagnetic Resonance Spectra of Tetrachloromanganate(II) in Molten Tetrabutylammonium Tetrachlorocadmate **Myron Ira Pollack and Benson R. Sundheim*** 1957
- Structure and Texture of a Crushed Na-Y Zeolite **Bernard Morawek, Pierre Gallezot, Albert Renouprez,* and Boris Imelik** 1959
- Thermodynamic Properties of Systems with Specific Interactions Calculated from the Hard-Sphere Equation of State. I. Binary Systems with One Inert Component **Aleksander Kreglewski* and Randolph C. Wilhoit** 1961 ■

- Apparent Quadrupole Moments of Carbon Monoxide and Nitrogen and Their Librational Motion in the Liquid State **Ralph L. Amey** 1968
- Optimal Determination of Relaxation Times of Fourier Transform Nuclear Magnetic Resonance. Determination of Spin-Lattice Relaxation Times in Chemically Polarized Species **Kenner A. Christensen, David M. Grant, Edward M. Schulman, and Cheves Walling*** 1971

COMMUNICATIONS TO THE EDITOR

- Direct Electron Spin Resonance Detection of Free Radicals Produced in Electron-Irradiated Liquid Alcohols **Frederick Peter Sargent* and Edward Michael Gardy** 1977

- Supplementary and/or miniprint material for this paper is available separately, in photocopy or microfiche form. Ordering information is given in the paper.

* In papers with more than one author, the asterisk indicates the name of the author to whom inquiries about the paper should be addressed.

AUTHOR INDEX

- | | | | |
|---------------------------|--------------------------|---------------------------|---------------------------|
| Amey, R. L., 1968 | Friedman, H. L., 1927 | Luria, M., 1904 | Schelly, Z. A., 1891 |
| Atkinson, G., 1913 | Gallezot, P., 1959 | Lutz, H., 1909 | Schulman, E. M., 1971 |
| Baer, S., 1919 | Gardy, E. M., 1977 | Moraweck, B., 1959 | Silber, H. B., 1940 |
| Blander, M., 1933 | Grant, D. M., 1971 | Mowery, D. F., Jr., 1918 | Stein, G., 1904, 1909 |
| Bolton, P. H., 1896 | Hansen, S. L., 1922 | Nafisi-Movaghar, J., 1899 | Stern, J. H., 1922 |
| Cassel, R. B., 1924 | Hatano, Y., 1899 | Nestor, C. W., Jr., 1945 | Sundheim, B. R., 1957 |
| Christensen, K. A., 1971 | Imelik, B., 1959 | Ofran, M., 1904 | Van Deventer, E. H., 1933 |
| Devore, J. A., 1922 | Kearns, D. R., 1896 | Pollack, M. I., 1957 | Veleckis, E., 1933 |
| Emara, M. M., 1913 | Keller, O. L., Jr., 1945 | Renouprez, A., 1959 | Walling, C., 1971 |
| Fernández-Prini, R., 1913 | Kilichowski, K. B., 1953 | Ricci, R. W., 1953 | Watkins, A. R., 1885 |
| Frens, G., 1949 | Kreglewski, A., 1961 | Sargent, F. P., 1977 | Wilhoit, R. C., 1961 |
| Fricke, B., 1945 | Kremer, M. L., 1919 | | Wong, M. M., 1891 |
| | Krishnan, C. V., 1927 | | Wood, R. H., 1924 |
| | | | Yavuz, O., 1922 |

THE JOURNAL OF PHYSICAL CHEMISTRY

Registered in U. S. Patent Office © Copyright, 1974, by the American Chemical Society

VOLUME 78, NUMBER 19 SEPTEMBER 12, 1974

Short-Lived Intermediates Formed by the Interaction between Electronically Excited Molecules and Inorganic Ions

A. R. Watkins

Max-Planck-Institut für Biophysikalische Chemie, 34 Göttingen-Nikolausberg, West Germany (Received March 22, 1974)

Publication costs assisted by the Max-Planck-Institut für Biophysikalische Chemie

A flash-photolytic investigation of the intermediates formed during the quenching of electronically excited molecules by inorganic anions shows the following. (i) In all cases studied no formation of the radical anion of the initially excited molecule can be detected. It can be shown that the radical anions are sufficiently long lived to enable their detection under the experimental conditions used. (ii) The triplet state of the initially excited molecule is formed in almost every case with a quantum yield of nearly unity. From these results it can be concluded that (i) deactivation of the excited singlet state by interaction with the quencher does not proceed by way of electron transfer and (ii) the process leading to fluorescence quenching, which depends on the energetic proximity of higher lying electron transfer states, involves a very rapid (within the lifetime of the collision complex) conversion of the primarily excited molecule mainly to the triplet state. Additional data on the quenching of the triplet state are also presented; this process appears to involve a different deactivation mechanism.

It has recently been proposed^{1,2} that quenching of the fluorescence of organic molecules by inorganic anions in solution takes place neither by way of an electron-transfer reaction nor by way of a "heavy-atom" induced transition to the triplet state of the excited molecule. Instead a mechanism was proposed by which a radiationless transition from the excited singlet state of the fluorescing molecule to the triplet state could take place rapidly in a collision complex formed between the excited molecule and the anion. This complex was assumed to be bound by no forces other than van der Waals forces, and it was suggested that mixing-in of higher lying electron-transfer states of this loosely bound complex was responsible for the observed quenching effects.

The evidence for this mechanism has been based chiefly on kinetic and thermodynamic considerations. Thus, it could be shown² that the rate constant for quenching depended on the electron donor-acceptor properties of the molecules involved, and that, for a considerable number of the systems studied, an electron transfer from the inorganic anion to the excited molecule was not to be expected on thermodynamic grounds. Some preliminary flash experiments¹ have indeed shown that (with one exception) no radical ions, such as would be expected from electron-transfer fluorescence quenching, are present as intermediates, and the main product of the quenching reaction ap-

pears to be the triplet state of the initially excited molecule.

It is clear, however, that more evidence concerning the intermediates involved in the quenching process is needed in order to establish the generality of the above conclusions. The investigation to be reported here has been made primarily with the aim of showing, by flash photolysis experiments, that the quenching interaction results in the formation of triplet states, and that no radical anions, which would be produced by an electron transfer from the inorganic anion to the excited aromatic, are formed. This demonstration covers systems which include naphthalene, anthracene, and pyrene as the primarily excited aromatics. Two further aims of the investigation were (a) to measure the quantum yield of the triplet formed by the quenching reaction in order to see whether triplets are the sole products or whether an additional deactivation pathway to the aromatic ground state exists, and (b) to study the parallel quenching process whereby triplet states are deactivated by inorganic anions.

Experimental Section

The purification of the salts used in this investigation has already been described;¹ the aromatic hydrocarbons were all purified by recrystallization and zone refining. The anthracene impurity in commercial phenanthrene was re-

moved by the method of Bachmann,³ after which it was further purified by recrystallization, column chromatography over Al_2O_3 , and zone refining. The flash spectra of the phenanthrene purified in this way showed no trace of the anthracene triplet. The acetonitrile used in the flash experiments was prepared from Merck UVASOL grade by refluxing over P_2O_5 and fractionally distilling. A description of the flash apparatus has appeared elsewhere;⁴ prior to the flash experiments all samples were degassed by repeated freeze-pump-thaw cycles. Selective excitation of the aromatic (in most cases the primarily excited molecule) could be ensured (unless otherwise stated) by inserting filter solutions or Schott glass filters between the sample cell and the flash lamp. The only difficulty encountered in this respect was with the system naphthalene- $\text{N}(\text{C}_4\text{H}_9)_4\text{NO}_3$, where the nitrate ion absorbs in the same spectral region as naphthalene. In addition to the usual filter solutions, a concentration ratio of naphthalene to nitrate was chosen such that the probability of the exciting light at 330 nm (the region of interest) being absorbed by naphthalene was over 100 times larger than for absorption by NO_3^- . Unless otherwise stated all experiments were carried out in acetonitrile as solvent.

Triplet formation quantum yields could be measured by using a flash cell with two attached reservoirs, one of which contained a solution of the aromatic hydrocarbon alone, the other a solution of the inorganic salt with the same concentration of hydrocarbon. The solution in the first reservoir could be introduced into the cell compartment and flashed, after which the two solutions could be mixed by opening a break seal and the flash experiment repeated under the same conditions. The quantum yield of triplet formation from the quenching reaction is then given by

$$\phi = \phi_0(E/E_0) \quad (1)$$

where ϕ_0 is the (known) quantum yield of triplet formation for the unquenched hydrocarbon, and E and E_0 are the optical densities for triplet-triplet absorption extrapolated back to the initiation time of the flash, in the presence and absence of quencher, respectively. This relation presupposes a purely first-order decay of the triplet states being observed,⁵ a condition which was fulfilled in all except one case studied here. The quenching constants for the triplets could be estimated from the first-order decay rate constants before and after addition of the quencher.

In selecting the systems to be investigated a number of criteria had to be satisfied. In order to be sure that the intermediates observed came mainly from the quenching process, it was necessary to ensure that fluorescence quenching was as complete as possible. This in turn depended on the quenching constant for the particular system and on the solubility of the inorganic salt being used as a quencher. In addition, the importance of being able to detect the triplet state and the radical anion of the primarily excited aromatic meant that only those aromatics could be used in which the spectra of these two intermediates are well separated. In practice the choice of systems was limited to naphthalene and anthracene with various quenchers, and to pyrene-KI. In all cases no new absorption could be detected on mixing the hydrocarbon with the inorganic salt, and the spectra of these systems did not (with one exception, see below) show any change on flashing.

Results

The experimental flash spectra have been collected in Figures 1-6 for the systems studied here. Each figure has

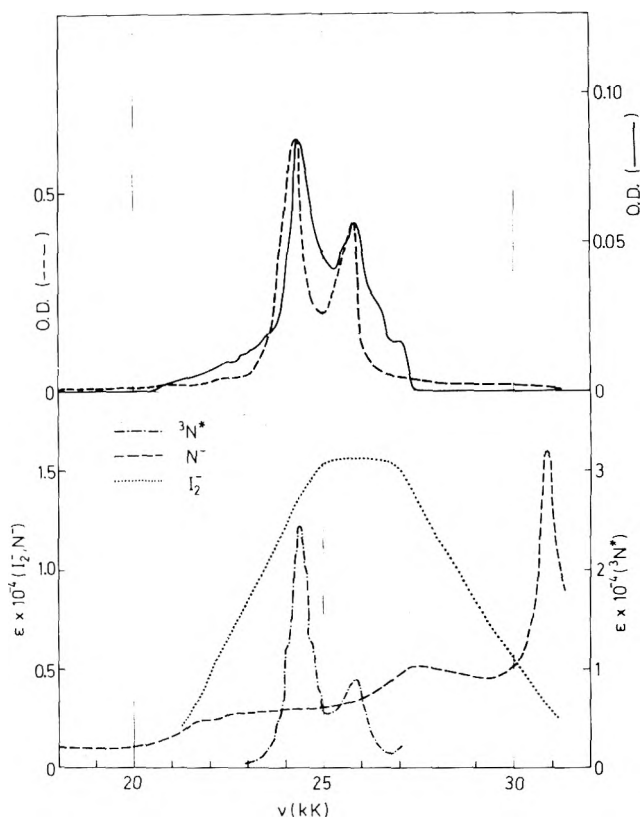


Figure 1. Transient absorption spectra of naphthalene quenched by NaI and KI in acetonitrile: (—) $[\text{naphthalene}] = 1.00 \times 10^{-2} \text{ M}$, $[\text{NaI}] = 2.00 \times 10^{-2} \text{ M}$, filter 0.1 M NaI in EtOH; (- -) $[\text{naphthalene}] = 1.00 \times 10^{-2} \text{ M}$, $[\text{KI}] = 8.7 \times 10^{-3} \text{ M}$, filter 2 M KI in H_2O . The symbols in the lower half refer to the naphthalene triplet state ($^3\text{N}^*$), radical anion (N^-), and the diiodide anion (I_2^-). A similar notation is used in the following diagrams.

been divided into an upper and lower half; the upper half in each case shows the experimentally obtained transient spectra, while the lower half contains the appropriate comparison spectra (triplet, radical anions) taken from the literature.

The spectra obtained for the naphthalene systems are shown in Figure 1 for naphthalene-NaI and naphthalene-KI, in Figure 2 for naphthalene- $\text{N}(\text{C}_2\text{H}_5)_4\text{Br}$, and in Figure 3 for naphthalene- NH_4CNS and naphthalene- $\text{N}(\text{C}_4\text{H}_9)_4\text{NO}_3$. The most prominent feature of the spectra in Figures 1-3 is the peak system centered around 25 kK; comparison with the literature spectra allows this to be assigned to the naphthalene triplet. The shift in the spectrum of naphthalene- $\text{N}(\text{C}_2\text{H}_5)_4\text{Br}$ is due to a difference in monochromator calibrations; however, the larger shift to longer wavelengths in one peak observed on flashing naphthalene- $\text{N}(\text{C}_4\text{H}_9)_4\text{NO}_3$ is not due to this, and only appears at high naphthalene concentrations. The reason for this spectral change is not known. A second important characteristic of these spectra is the absence of any significant absorption around 31 kK. The naphthalene radical anion possesses a sharp peak in this region, and the absence of this peak leads to the conclusion that no detectable radical anion formation occurs under these conditions. The only exception is naphthalene- $\text{N}(\text{C}_2\text{H}_5)_4\text{Br}$ without cutoff filters; in this case, in addition to the naphthalene triplet, a peak at 31 kK is present, which can be assigned to the naphthalene radical anion.

Figure 4 shows the experimental flash spectra for the

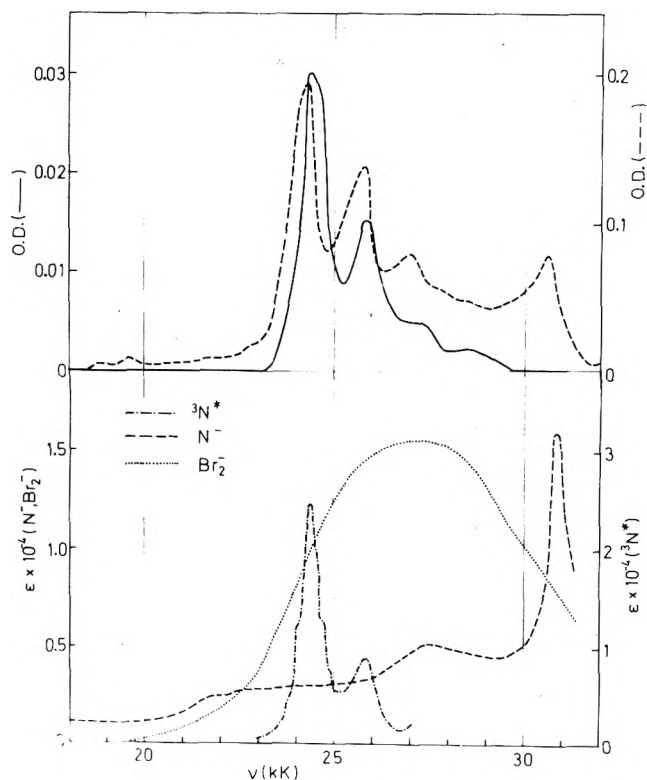


Figure 2. Transient absorption spectra of naphthalene quenched by $N(C_2H_5)_4Br$ in acetonitrile: (—) [naphthalene] = $1.31 \times 10^{-3} M$, $[N(C_2H_5)_4Br] = 0.087 M$, filter Schott WG 320; (---) same system without filter.

systems anthracene-NaI and anthracene- $N(C_2H_5)_4Br$. The anthracene radical anion has two peaks in the visible region at 30.7 and 27.1 kK, both of which occur in the region of the anthracene ground-state absorption. It was, however, possible, by keeping the anthracene concentration low ($\sim 10^{-5} M$), to carry out the experiments in such a way that any transient absorption in the region of the anion peaks could be detected with reasonable sensitivity. The picture that emerges from the flash spectra of these two systems with cutoff filters is similar to that from the naphthalene flash experiments; the anthracene radical anion does not appear to be formed, as can be seen by the absence of any transient absorption at 30.7 and 27.1 kK. The main product of the quenching process appears to be the anthracene triplet, which has peaks centered around 24 kK. The spectrum of anthracene- $N(C_2H_5)_4Br$ without any cutoff filters is more complex (see Figure 4); in addition to the triplet peaks around 24 kK, several new peaks have appeared to shorter wavelengths. Two of these can be assigned to the anthracene radical anion, while the remaining features are probably due to the broad absorption of Br_2^- , somewhat distorted by the presence of the ground-state absorption. On flashing anthracene-NaI without cutoff filters marked photochemical decomposition took place.

The flash spectrum for pyrene-KI is shown in Figure 5. As with the anthracene and naphthalene systems where appropriate cutoff filters have been used, no radical anion formation can be detected (the pyrene radical anion has a peak at 20.5 kK; this overlaps part of the pyrene triplet absorption spectrum, decreasing the sensitivity with which any radical anion formation could be detected).

The experimental results shown in Figures 1–5 were ob-

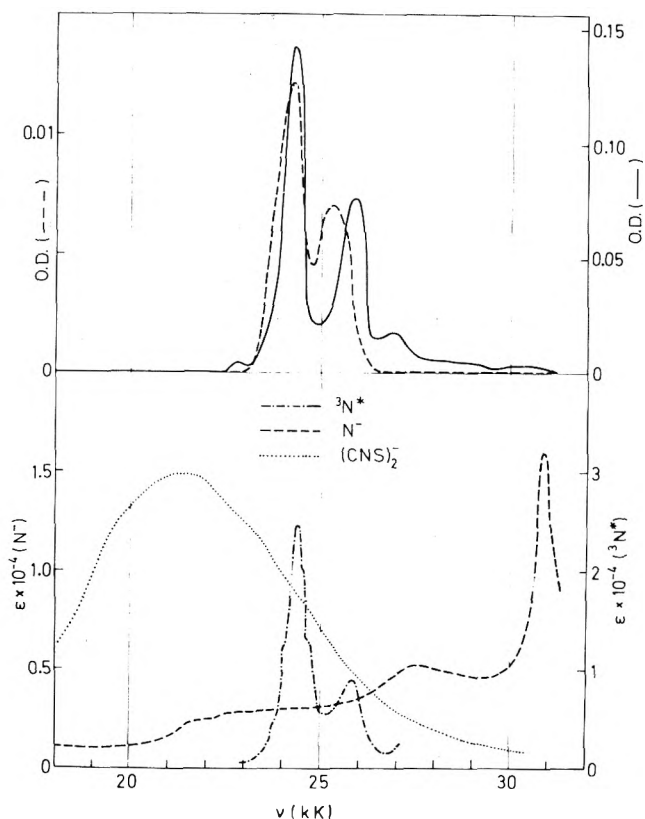


Figure 3. Transient absorption spectra of naphthalene quenched by NH_4CNS and $N(C_4H_9)_4NO_3$ in acetonitrile: (—) [naphthalene] = $1.31 \times 10^{-3} M$, $[NH_4CNS] = 0.0871 M$, filter Schott WG320; (---) [naphthalene] = 0.209 M, $[N(C_4H_9)_4NO_3] = 0.050 M$, filter 1.0 M KNO_3 in H_2O .

tained in acetonitrile in all cases; the extent of quenching exceeded 90%.

The last figure, Figure 6, shows two transient spectra obtained on flashing phenanthrene-KI and phenanthrene- NH_4CNS in ethanol. In this case no cutoff filters have been used, so that the incident flash light can be absorbed not only by the aromatic but also the inorganic ion. At the salt concentration chosen, fluorescence quenching is about 50% complete for phenanthrene-KI and very small for phenanthrene- NH_4CNS . The experimental flash spectra here are more complex than those previously considered. The most prominent peak in both cases is at 23.8 kK, and (together with peaks at 25.3 kK and, in part, at 22.0 kK) appears to belong to the phenanthrene radical anion, although there is only fair agreement with the literature spectrum shown in the lower half of this figure. The peak at 20.6 kK, together with the remainder of the peak at 22.0 kK, can be ascribed to the phenanthrene triplet.

Additional data derived from the flash experiments described above are shown in Table I. These are the percentage of fluorescence quenching, the observed triplet quantum yield ϕ_T^{obsd} , and the corrected triplet quantum yield ϕ_T for a number of the systems studied here, as well as for two biphenyl systems investigated previously.¹ ϕ_T can be derived from ϕ_T^{obsd} by the relation

$$\phi_T = (\phi_T^{obsd} - \alpha \phi_T^0) / (1 - \alpha) \quad (2)$$

where ϕ_T^0 is the triplet yield in absence of any quencher and α is the fraction of unquenched fluorescence remaining. For naphthalene- NH_4CNS the triplet decay was not

TABLE I: Quantum Yield and Kinetic Data for Various Aromatic-Inorganic Salt Systems

Primarily excited molecule	Quencher	% quenching	$\phi_T^{\text{obsd } a}$	ϕ_T^b	$k_q^T, c M^{-1} \text{ sec}^{-1}$	$\Delta G_T, d \text{ eV}$
Biphenyl	KI	89.0	0.74	0.76	6.2×10^3	1.04
	NH ₄ CNS	96.5	0.97	0.98	6.4×10^4	
Naphthalene	KI	92.7				1.35
	NH ₄ CNS	96.4	0.9 ^e			
	N(C ₂ H ₅) ₄ Br	90.9	0.87	0.88	3.8×10^3	1.85
	N(C ₄ H ₉) ₄ NO ₃	95.0			8.4×10^3	2.25
Anthracene	NaI	97.3	1.04	1.05	1.37×10^3	1.54
	N(C ₂ H ₅) ₄ Br	70.5	0.91	1.00	<10	2.04

^a Observed triplet quantum yield, based on $\phi_T^0 = 0.51$ for biphenyl, 0.75 for naphthalene, and 0.70 for anthracene.¹⁵ ^b Corrected triplet quantum yield (see text). ^c Rate constants for triplet quenching by the added salts. ^d Energy gap between triplet state and electron transfer state. ^e Estimated from triplet-triplet absorption 50 μsec after initiation of the flash.

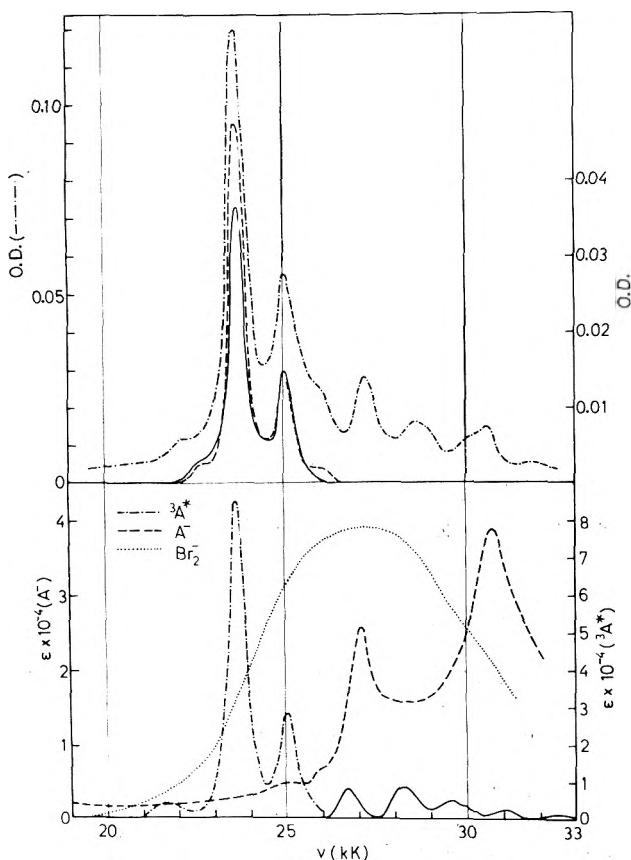


Figure 4. Transient absorption spectra of anthracene quenched by NaI and N(C₂H₅)₄Br in acetonitrile: (—) [anthracene] = 1.22×10^{-5} M, [NaI] = 0.379 M, filter Schott WG320. (---) [anthracene] = 1.22×10^{-5} M, [N(C₂H₅)₄Br] = 0.158 M, filter Schott WG320; (---) system anthracene-N(C₂H₅)₄Br without filter.

solely first order, and the value of ϕ_T^{obsd} is correspondingly less accurate. The most accurate values are those for the two anthracene systems, which were determined *via* light intensity dependence measurements. Details of this technique can be found elsewhere.⁵ Although precise values of ϕ_T^{obsd} could not be measured for the two systems naphthalene-KI and naphthalene-N(C₄H₉)₄NO₃, the triplet quantum yields were high, lying between 0.9 and 1.0.

The remaining two columns in Table I list values of k_q^T , the rate constant for quenching of the aromatic triplet state, and ΔG_T (calculated from the data of ref 2), the free energy separating the energy levels of the aromatic triplet and the electron transfer state.

Discussion

The most important conclusion to be drawn from the

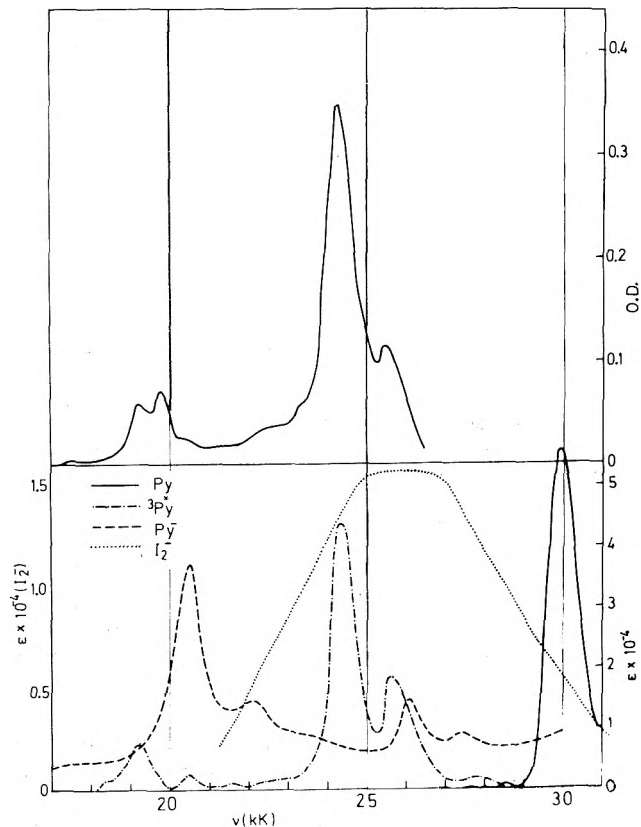
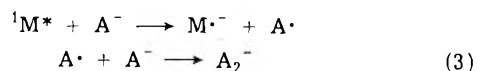


Figure 5. Transient absorption spectrum of pyrene quenched by KI in acetonitrile: (—) [pyrene] = 1.05×10^{-4} M, [KI] = 1.06×10^{-2} M, filter 0.5 MKI in H₂O.

spectra in Figures 1–5 concerns the absence of any absorption which could be ascribed to the aromatic radical anion in those cases where cutoff filters have been used. This holds true for all naphthalene systems studied (Figures 1–3), where no absorption at 31 kK due to the naphthalene radical anion can be detected. The same is true for the anthracene and pyrene systems (Figures 4 and 5) where, however, overlap of the radical anion spectrum with other spectra will make detection somewhat less reliable. It is clear that, if radical anion formation in these systems takes place, it can only be with a very small quantum yield. An electron transfer mechanism^{6,7} for the fluorescence quenching would be expected to produce not only the radical anion of the aromatic hydrocarbon, but also, in a subsequent reaction, a dihalide anion



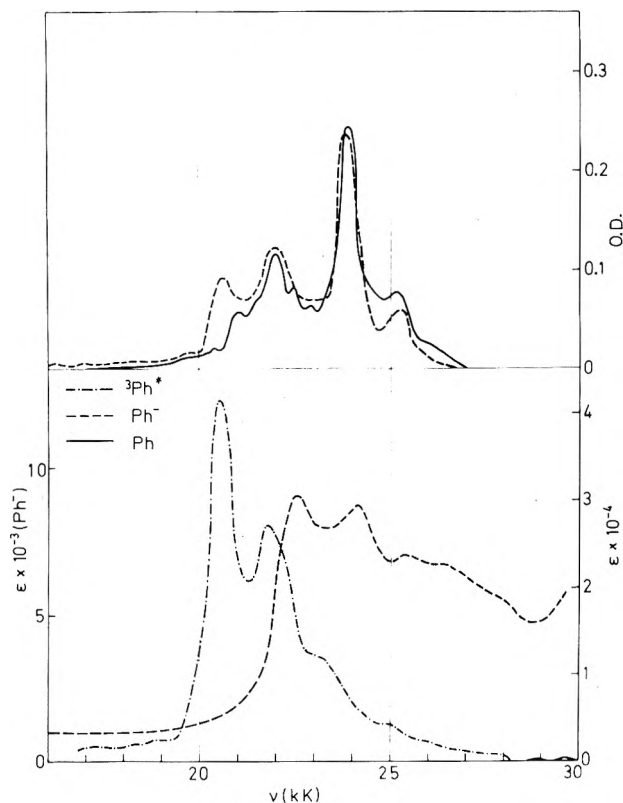


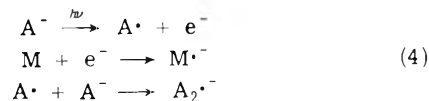
Figure 6. Transient absorption spectra of phenanthrene in the presence of KI and NH_4CNS in ethanol; no filters were inserted between sample cell and flash lamps: (—) [phenanthrene] = 2.00×10^{-3} M, [KI] = 0.139 M; (---) [phenanthrene] = 2.00×10^{-3} M, [NH_4CNS] = 0.435 M.

Figures 1–5 show that neither $\text{M}^{\cdot-}$ nor $\text{A}_2^{\cdot-}$ are formed from the quenching process on a time scale detectable in flash photolysis experiments; several explanations of this phenomenon are possible.

One of these is that, after an initial electron transfer, a very rapid reverse electron transfer occurs, leading to the molecule M in the ground state and the anion A^- . This process would have to occur while the species $\text{m}^{\cdot-}$ and A^{\cdot} were still in close proximity, that is, within a time short compared to the time required for the loose associate $\text{M}^{\cdot-} \cdots \text{A}^{\cdot}$ to diffuse apart. If it is assumed that there are no strong forces operating to keep this associate together, the half-time for the diffusion process can be calculated⁸ to be $\sim 10^{-10}$ sec. That this fast reverse electron transfer can occur is, however, doubtful when it is considered that the parallel case, where A^- is replaced by an uncharged organic electron donor or acceptor, gives rise to radical ions (from an electron transfer process) which decay on a time scale of milliseconds.⁹ There seems, therefore, no *a priori* reason to postulate disappearance of initially formed ions by reverse electron transfer in one case and not in the other.

A further possibility which must be considered is that the aromatic radical ion, after its initial formation by an electron transfer as in (3) and escape from the proximity of the A^{\cdot} radical, is in some way unstable in the presence of the inorganic salt, and disappears within some 20 μsec (the limit of the time resolution of the flash apparatus used) of its initial formation. The possible instability of the transient species produced in these experiments is an important point which we have disposed of by carrying out experiments in which the aromatic radical anions are formed

directly. This can be done by utilizing the well-known phenomenon of electron ejection from inorganic halides;¹⁰ the ejected electron is intercepted by the aromatic hydrocarbon, resulting in anion formation



This process is illustrated in Figure 6, where the two systems phenanthrene–KI and phenanthrene– NH_4CNS in ethanol have been flashed without any cutoff filters. Radical anions of phenanthrene, having lifetimes of the order of some hundreds of microseconds, are formed and can be clearly identified in the experimental spectra in Figure 6. If the aromatic without quencher is taken as the reference, the quantum yield of transient formation (triplet plus radical anion) can be calculated; these values (4.5 for phenanthrene–KI and 2.5 for phenanthrene– NH_4CNS) are considerably in excess of unity and, in the absence of any chain process, indicate that light absorption not only by the aromatic but also by the inorganic anion leads to the observed effects. In these two systems fluorescence quenching is relatively inefficient; an example of a system where fluorescence quenching is more than 90% complete can be seen in Figure 2, where the only difference between the two experimental spectra lies in the presence or absence of cutoff filters. With no cutoff filter the naphthalene radical anion (peak at 31 kK) is formed, once again with a lifetime of some hundreds of microseconds. The most plausible explanation for the appearance of the radical anion is that it is formed by reaction 4. The same considerations apply to the spectrum of anthracene– $\text{N}(\text{C}_2\text{H}_5)_4\text{Br}$ without filter (Figure 4), where an equally long-lived absorption due to the radical anion of anthracene is present. It seems reasonable to conclude that the stability, on a microsecond time scale, of the radical anion in these systems (with the possible exception of anthracene–NaI) is quite general.

If the above explanations of the flash spectra reported here can be excluded from further consideration, the only remaining alternative is to conclude that the electron-transfer mechanism (3) plays a negligibly small part in the quenching process. This is supported by the results of an investigation of the kinetics of the quenching process,² where it was shown that, by using published electrochemical data for the molecules M and calculated values of the reduction potential of A^{\cdot} , an estimate of the free-energy change on going from the excited aromatic $^1\text{M}^*$ to $\text{M}^{\cdot-} \cdots \text{A}^{\cdot}$ could be made

$$\Delta G = E(\text{A}^-/\text{A}) - E(\text{M}^{\cdot-}/\text{M}) - \Delta E \quad (5)$$

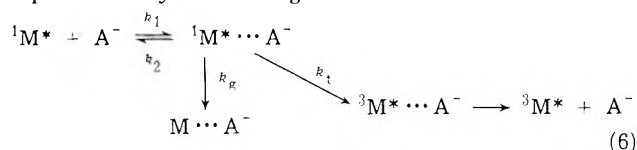
where ΔE is the zero-point energy of the aromatic hydrocarbon in its first excited singlet state. It is important to note that such an electron transfer involves a bimolecular reaction between $^1\text{M}^*$ and A^- with the formation of the radical A^{\cdot} . Energy calculations must therefore be based on the electrochemical couple $\text{A}^-|\text{A}^{\cdot}$ and not $\text{A}^-|\text{A}_2^{\cdot-}$. The values of ΔG so calculated proved to be negative for the systems biphenyl–KI and *p*-terphenyl–KI, zero or slightly positive (depending on the accuracy of the calculated $E(\text{A}^-/\text{A}^{\cdot})$) for naphthalene–KI, and positive for the remaining systems. This is in agreement with the flash experiments reported here, which, in addition to showing that ΔG for naphthalene–KI is in fact positive, confirm the calculated positive ΔG values for the other systems.

An earlier investigation¹ of biphenyl fluorescence

quenching gave rise to similar results; with the quenchers $N(C_2H_5)_4Br$ and NH_4CNS no radical anion formation could be detected in the flash experiments; similar conclusions regarding quenching by iodide and bromide ions have been reached by other authors.^{11,12} The one exception appears to be biphenyl-KI,¹ where an absorption tentatively assigned to the biphenyl radical anion is present in the flash spectrum; this observation is in agreement with the calculations of ref 2.

One possible candidate for the quenching process is a "heavy-atom" interaction¹³ between the excited molecule and the inorganic anion, leading to an enhancement of the spin-orbit coupling in the excited aromatic and a consequent increase in the rate of the transition from the singlet to the triplet manifold. This possibility has already been discussed and rejected; it will suffice to point out that, while the results in Figures 1, 2, 4, and 5 for quenching by bromides and iodides are explicable on this basis, the "heavy-atom" effect cannot explain the observed trend in the rate constants for fluorescence quenching in these systems.² Furthermore, a negligible "heavy-atom" effect would be expected for the anions NO_3^- and CNS^- , and yet the quenching properties for these anions are as marked as for iodide and bromide, and appear to conform in the same way to the general trend in quenching efficiency with changing anion.² The results presented here show that, at least for naphthalene and anthracene, fluorescence quenching by NO_3^- and CNS^- does not take place by electron transfer; the same appears to be true for the equivalent biphenyl systems.¹ The nonoccurrence of electron-transfer fluorescence quenching thus appears to be general for aromatic-inorganic anion systems; to invoke "heavy-atom" fluorescence quenching for Br^- and I^- and simultaneously some different mechanism for the remaining anions hardly seems justified, in view of the fact that quenching by Br^- and I^- can in no way be considered a special case.² The "heavy-atom" effect seems to be of minor importance, and other effects must be considered if an adequate explanation of this type of fluorescence quenching is to be found.

One such effect, mentioned in earlier publications,^{1,2} is a quantum-mechanical coupling of higher lying electron transfer states, which can induce radiationless transitions from the first excited singlet state of the aromatic to other electronic states. The model upon which this is based envisages the diffusing together of the excited aromatic $^1M^*$ and the inorganic anion A^- to form a loose associate. The binding energy is supposed to be less than kT ; no species comparable to a fluorescing exciplex or heteroexcimer¹⁴ is formed. This associate can then decay to form the aromatic triplet or the system in its ground state



The observed quenching rate constant k_q will be related to the parameters of this reaction scheme by

$$k_q = \frac{k_1}{k_t + k_g + k_2} (k_t + k_g) \quad (7)$$

The relative importance of k_t and k_g can be judged from the data on triplet quantum yields given in Table I. These quantum yields are generally high and, with one exception, lie between 0.9 and 1.0; this also appears to hold for the two

systems naphthalene-KI and naphthalene- $N(C_4H_9)_4NO_3$ for which no precise values are available. The relatively low yield for biphenyl-KI ($\phi_T = 0.76$) is doubtless due to the fact that an additional pathway for the disappearance of the associate $^1M^* \cdots A^-$ by an electron-transfer process is present,¹ leading to a lower triplet quantum yield; this possibility does not exist for any of the other systems studied here. In general, it seems that $k_t \gg k_g$ and that the deactivation of $^1M^*$ directly to the ground state is of relatively minor importance.

The rate constants k_1 and k_2 are diffusion controlled and vary little from system to system; the fate of the species $^1M^* \cdots A^-$ will be determined essentially by k_t . k_t represents the radiationless deactivation of the complex singlet state to the complex triplet state; if spin-orbit coupling effects are negligible then coupling of these two states can only occur through a third (intermediate) state, the electron transfer state $M^{\cdot-} \cdots A^-$. This state, lying higher in energy than either the initial or final states, will couple to the state $^1M^* \cdots A^-$ to an extent depending on, among other things, the inverse of the energy separation between the states $^1M^* \cdots A^-$ and $M^{\cdot-} \cdots A^-$. There are two characteristics of this mechanism which, from the point of view of the experiments, are important: (i) the dependence of the coupling on the inverse of the energy separation will explain the trend in quenching rate constants with changing aromatic or anion;² (ii) this mechanism provides an explanation of why, in the absence of heavy-atom effects or electron transfer (reaction 3), efficient fluorescence quenching can occur. A more detailed discussion can be found in a subsequent paper.

The rate constants for quenching of the corresponding triplet states, k_q^T , are much lower than the values for singlet state quenching.² In addition, there is no longer any correlation with ΔG_T , the energy separating the triplet state from the state $M^{\cdot-} \cdots A^-$. Coupling to electron-transfer states is probably no longer important for triplet quenching, due to the large energy gap ΔG_T ; it is possible that the quenching process involves a heavy-atom interaction¹³ between the triplet state and the inorganic cation. This effect is relatively unimportant for singlet quenching, which is dominated by the (faster) mechanism discussed above.

Acknowledgments. Thanks are due to Miss U. Heine and to my wife, Mrs. S. Watkins, for assistance with the experimental work, and to Dr. W. Kühnle for purifying the solvents used in this work.

References and Notes

- (1) A. R. Watkins, *J. Phys. Chem.*, **77**, 1207 (1973).
- (2) A. R. Watkins, to be submitted for publication.
- (3) W. E. Bachmann, *J. Amer. Chem. Soc.*, **57**, 555 (1935).
- (4) K. H. Grellmann, A. R. Watkins, and A. Weller, *J. Lumin.*, **1,2**, 678 (1970).
- (5) A. R. Watkins, to be submitted for publication.
- (6) Th. Förster, "Fluoreszenz Organischer Verbindungen," Vandenhoeck and Ruprecht, 1951.
- (7) R. Beer, K. M. C. Davis, and R. Hodgson, *Chem. Commun.*, 840 (1970).
- (8) M. Eigen, *Z. Phys. Chem. (Frankfurt am Main)*, **1**, 176 (1954).
- (9) H. Knibbe, D. Rehm, and A. Weller, *Ber. Bunsenges. Phys. Chem.*, **72**, 257 (1968).
- (10) L. I. Grossweiner and M. S. Matheson, *J. Phys. Chem.*, **61**, 1089 (1957).
- (11) H. Leonhardt and A. Weller, *Z. Phys. Chem. (Frankfurt am Main)*, **29**, 277 (1961).
- (12) A. R. Horrocks, T. Medinger, and F. Wilkinson, *Photochem. Photobiol.*, **6**, 21 (1967).
- (13) S. P. McGlynn, T. Azumi, and M. Kinoshita, "Molecular Spectroscopy of the Triplet State," Prentice-Hall, Englewood Cliffs, New Jersey, 1969.
- (14) H. Leonhardt and A. Weller *Ber. Bunsenges. Phys. Chem.*, **67**, 791 (1963).
- (15) J. B. Birks, "Photophysics of Aromatic Molecules," Wiley-Interscience, London, 1970.

Solvent-Jump Relaxation Kinetics of the Association of Rhodamine Type Laser Dyes¹

M. M. Wong and Z. A. Schelly*

Department of Chemistry, University of Georgia, Athens, Georgia 30602 (Received March 8, 1974)

Equilibrium spectral photometric and solvent-jump relaxation kinetic results of the monomer = dimer equilibrium of aqueous and ethanolic Rhodamine B, Rhodamine 3B, Rhodamine 6G, and Rhodamine 110 are presented. Contrary to previous suggestions we show that Rhodamine B, and also the similar Rhodamine 110, dimerizes in ethanol.

Introduction

With the rapid expansion of the applications of organic dye lasers much attention has been focused on the spectroscopic characterization,² as well as on the synthesis of new stable lasing compounds.³

Due to their excellent lasing properties, rhodamine type molecules are one of the most commonly studied. It is well known that these molecules tend to aggregate in solution,⁴ which not only leads to non-Beer's law absorption, but is also detrimental to laser action. Thus knowledge of the lifetime of aggregates is basic to the understanding and design of dye lasers. In a recent communication we presented preliminary results on the relaxation kinetics of the dimerization of Rhodamine B in aqueous solution.⁵ In the present work we extended our investigation to Rhodamine 3B, Rhodamine 6G, and Rhodamine 110 in water, and in ethanol solution. The effects of the solvent and the molecular structure of the dyes on the extent and on the rates of dimerization are discussed.

Experimental Section

Chemicals. Rhodamine 3B and Rhodamine 110 were obtained from Eastman Kodak and Rhodamine B and Rhodamine 6G from Allied Chemical. Chromatographic examination showed that each dye consisted of only one colored component. Since recrystallization did not affect the spectra and the extinction coefficients, the dyes were vacuum dried and used without further purification. Demineralized water and absolute ethyl alcohol were used for the preparation of the solutions. The alcohol was obtained from U. S. Industrial Chemicals and dried with molecular sieve Linde Type 3A. All other chemicals used (NaOH, KCl, NaCl, K₂CO₃, KClO₄) were analytical grade. The HCl gas used in the preparation of the ethanolic HCl solution was taken from a Matheson lecture bottle and dried over Mallinckrodt's Aquasorb. The dye stock solutions were stored in the dark, and the ethanolic HCl solution at 1°.

Experiments. All absorption spectra were taken on Cary 15 spectral photometer equipped with thermostated cell holders.

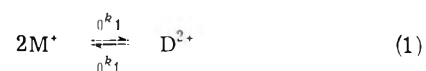
The acid-base equilibrium constant of Rhodamine 110 in ethanol was determined by Bates' method,⁶ using a Leeds and Northrup 7401 pH meter with Pt-H₂ measuring and calomel reference electrodes, at 10⁻⁴ M dye concentration and 25°.

The concentration-jump relaxation experiments⁷ were performed on a rapid flow mixing apparatus, the construction of which is based on the Durrum-Gibson-Milnes design. The experimental set-up as well as the modified mix-

ing jet used have been described elsewhere.⁸ The transient change or the steady-state value of the absorption of the relaxing reaction mixtures were observed at the absorption maximum of the respective monomers.

Analysis of Data

In our concentration-jump experiments we have utilized either of two different methods to obtain the relaxation times τ of the monomer (M⁺)-dimer (D²⁺) equilibria



of the systems involved. The transient method using a stopped flow system,⁷ or the nontransient method using a stationary flow system, where the relaxation time is determined from a single measurement of an integrated partial relaxation amplitude. In both cases after a sudden n -fold dilution the concentration C_i of species i as a function of time t is given by

$$C_i = \bar{C}_i [1 - \exp(-t/\tau)] + ({}_0C_i/n) \exp(-t/\tau) \quad (2)$$

where ${}_0C_i$ and C_i are the initial (prior to dilution) and final (at time $t \rightarrow \infty$) equilibrium concentrations respectively. In the transient method C_i is followed directly after the flow is stopped.

In the nontransient method a continuous flow is set up (Figure 1) and the steady-state absorption is measured coaxially with the flow direction. At constant flow velocity v , the age t of the relaxing mixture at any point in the pipe is given by $t = x/v$, where x is the distance variable counted from the point of mixing. Substituting x/v into (2) one obtains $C_i(x)$ and the change of absorbance dA at a given wavelength λ as $dA = \sum_i \epsilon_i(\lambda) C_i(x) dx$, where $\epsilon_i(\lambda)$ is the molar decadic absorptivity of i . The absorbance between d and l is given by an integrated partial relaxation amplitude

$$A = \int_d^l \sum_i \epsilon_i(\lambda) C_i(x) dx \quad (3)$$

After integration of (3) one can substitute the path lengths s for $(l - d)$, and the residence time t_s of the solution in the observation region for s/v , so that we finally obtain (4),

$$\frac{A - \bar{A}}{\bar{A} - A_0/n} t_s = \tau [\exp(-l/v\tau) - \exp(-d/v\tau)] \quad (4)$$

where \bar{A} and A_0 are the absorbances of the final ($t \rightarrow \infty$) and initial (prior to mixing) equilibrium solutions, respec-

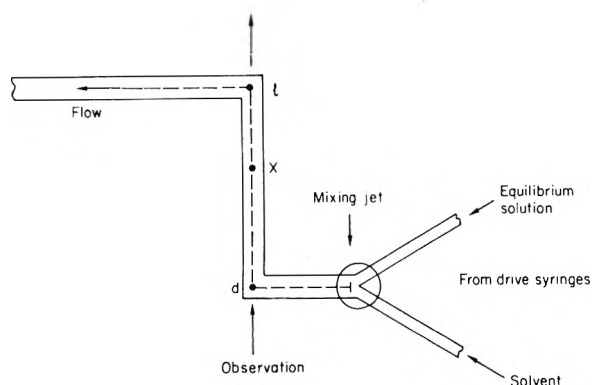


Figure 1. Schematic diagram of a flow system with uniform cross section.

tively, of path length s . All parameters in (4), except A , can be measured independently from the relaxation experiment. The unknown τ is evaluated graphically from the plot of computed values of $Y = \tau[\exp(-l/v\tau) - \exp(-d/v\tau)]$ vs. τ at constant d , l , and v . With the experimentally determined value of the left-hand side of eq 4, the correct τ can be read from the graph (see Figure 2). In exchange for the requirement of larger reactant volumes, the advantage of the nontransient method is that no fast responding detection system is needed.

With sufficiently large perturbations caused by 11-fold dilution, we could measure shorter relaxation times than the dead time of the flow system, with both transient and nontransient methods. In such a case, with the proper choice of parameters, the nonlinear part of the relaxation takes place during the dead time, and only the linear end of the relaxation is observed in the cell.

In all cases studied, single relaxation times of equilibrium 1 have been observed at 9 and 22°. The experiments were performed at natural ionic strength of the dye solutions, where the reciprocal relaxation time τ^{-1} is given by

$$\tau^{-1} = {}_0k_{-1} \frac{f_D}{f_{\ddagger}} + 4{}_0k_1 \frac{f_M^2}{f_{\ddagger}} C_M \quad (5)$$

where ${}_0k_1$ and ${}_0k_{-1}$ are the ionic strength independent forward and reverse rate constants, respectively, and f_i are the activity coefficients. The rate constants can be obtained from eq 5 in the usual manner.⁷

The concentration ratios $K = C_d/C_m^2$ were computed from the absorption spectra taken at 9 and 22°, using an iterative method previously described.⁹ The thermodynamic equilibrium constants $K_{eq} = a_d/a_m^2$ deviate very little from K in the concentration range of our measurements, nevertheless, they were calculated using the appropriate activity coefficients.

Results and Discussion

The summary of the numerical results is given in Table I, and the structure of the four rhodamine dyes in Figure 3. The carboxyphenyl substituent is held rigidly by the bulky carboxyl group in a position nearly perpendicular to the plane of the chromophore. Molecular models indicate that in Rhodamine B and Rhodamine 110 internal hydrogen bonding to the oxygen of the xanthene skeleton may give additional stability to the conformation of the molecule.

Dimerization can occur in several different ways causing distinct metachromatic behavior of the dye solution. Based on the theory of exciton interaction,¹⁰ only the high-fre-

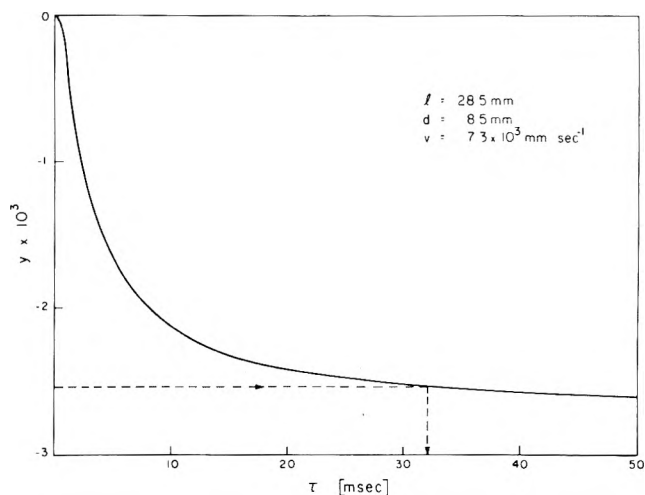


Figure 2. Determination of the relaxation time τ using eq 4 at fixed values of l , d , and v .

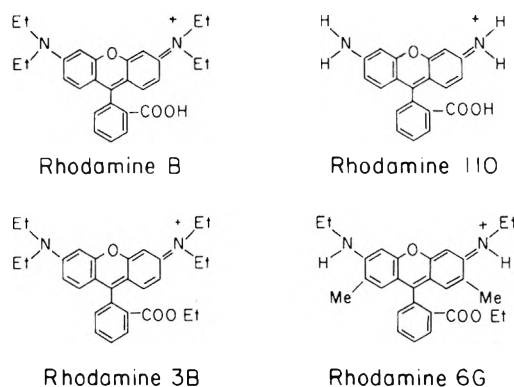


Figure 3. Structure of the rhodamines studied.

quency H band is expected to appear in a perfectly parallel dimer, whereas for a head-to-tail dimer only the red-shifted J band is allowed. For parallel dimer with twist angle, or in solutions where more than one type of dimer can be present simultaneously, an intermediate behavior is found.

Rhodamine B dimerizes in both water and ethanol. The concentration (Figure 4) and temperature dependence of the absorption spectrum in water was studied over the concentration range 5×10^{-5} to 4×10^{-6} M at 9 and 22°. At the same temperatures, and in the concentration range of 1.82×10^{-5} to 5.45×10^{-6} M, the relaxation times vary from 0.67 to 3.65 msec. Our $\Delta H = -0.9$ kcal mol⁻¹ is significantly larger than $\Delta H = -2.8$ kcal mol⁻¹ obtained by Rohatgi and Singhal.^{4b} The discrepancy is probably due to their method of analysis of the absorption spectra, which has been already pointed out by Selwyn and Steinfeld.² The addition of 0.1 M KNO₃ causes no change of the absorption spectra.

In ethanol, the spectra were studied in solutions with concentrations between 3.9×10^{-6} and 7.1×10^{-7} M. The kinetic experiments, performed at concentrations ranging from 5×10^{-5} to 1×10^{-5} M, yielded relaxation times from 1.5 to 3.2 msec. The $\Delta H = -2.3$ kcal mol⁻¹ obtained between 9 and 22° is in excellent agreement with the difference of the forward and reverse activation energies ${}_1E_a - {}_{-1}E_a = -2.4$ kcal mol⁻¹, but it is larger than the $\Delta H \approx -4$ kcal mol⁻¹ estimated² for the range between 22 and 62°. We agree with Drexhage,³ and also with Ferguson and Mau,¹¹ that in ethanol Rhodamine B is part of an acid-

TABLE I: Thermodynamic and Kinetic Data of the Dimerization of Rhodamine Dyes

Dye	$K_{\text{ASSOC}},^a M^{-1}$		$\Delta H,^b$ kcal mol $^{-1}$	$ok_1,^c M^{-1} \text{sec}^{-1}$		ok_{-1}, sec^{-1}		${}_1E_a,$ kcal mol $^{-1}$	$-{}_1E_a,$ kcal mol $^{-1}$
	9°	22°		9°	22°	9°	22°		
Rhodamine B in H ₂ O	1.55×10^3	1.44×10^3	-0.94 (-0.9)	(3.1×10^6)	(4.5×10^6)	2.0×10^2	3.2×10^2	4.9	5.8
in EtOH	2.87×10^4 (2.7×10^4)	2.4×10^4 (2.4×10^4) 2.04×10^4 ^d	-2.8 ^e -2.3 (-2.4) ~ -4.0 ^d	9.8×10^6	10.4×10^6	3.6×10^2	4.3×10^2	~ 0	2.4
Rhodamine 3B in H ₂ O	3.10×10^3 (2.8×10^3)	3.40×10^3 (3.4×10^3)	1.3 (3.0)	1.6×10^6	1.3×10^6	5.7×10^2	3.8×10^2	-2.4	-5.4
in EtOH	No association								
Rhodamine 6G in H ₂ O	1.72×10^3	1.69×10^3	~ -0.2	Too fast for flow techniques					
in EtOH	No association								
Rhodamine 110 in H ₂ O	Not soluble								
in EtOH	9.43×10^3 (1.4×10^4)	1.17×10^4 (1.3×10^4)	3.0 (3.3) ^g	3.9×10^6 (2.6×10^6)	4.8×10^6 (4.3×10^6)	2.8×10^2	3.7×10^2	2.7 (6.9) ^f	3.6

^a Photometrically determined; the values in parentheses are $(ok_1/{}_1k_0)$. ^b Obtained from optical data; the values in parentheses are $({}_1E_a - {}_{-1}E_a)$. ^c Determined from the slope of eq 5; the more accurate values in parentheses are $(K_{\text{ASSOC}} ok_{-1})$. ^d From ref 2. ^e From ref 4b. ^f Obtained using the values in parentheses for ${}_1E_a$. ^g Obtained using the value in parentheses for ${}_1E_a$.

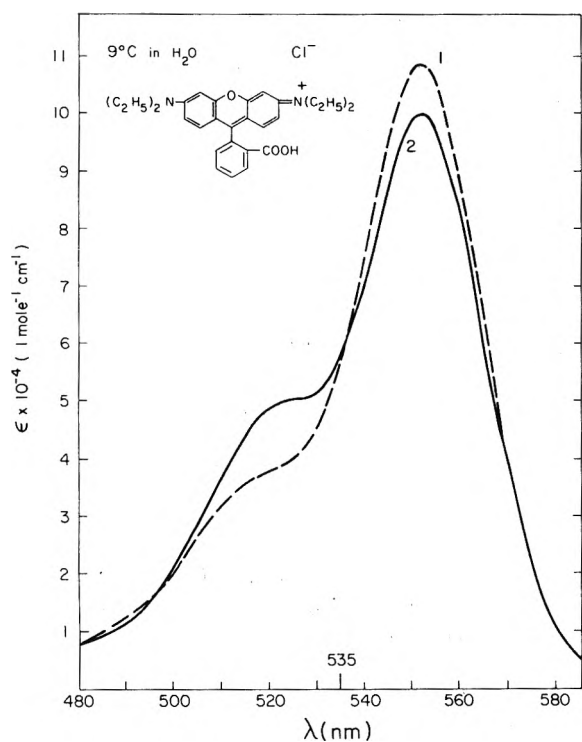


Figure 4. Absorption spectrum of Rhodamine B in water at 9°: (curve 1) $8 \times 10^{-6} M$ solution in a 1-cm cell; (curve 2) $8 \times 10^{-5} M$ solution in a 0.1-cm cell.

base equilibrium, where the main absorption band is shifted to higher frequency on deprotonation of the dye. However, we disagree with their claims that no aggregation occurs in this solvent since our kinetic results clearly indicate dimerization. A more detailed discussion of the mechanism is presented under Rhodamine 110 that behaves similarly.

Rhodamine 3B. Based on the concentration dependence of the absorption spectra, this dye does not aggregate in ethanol. Nevertheless, the solution ($2 \times 10^{-5} M$) shows hypochromic behavior and a hypsochromic shift (10 \AA) in a

$10^{-3} M$ ethanolic NaOH, with a simultaneous increase of the uv bands. In a $10^{-2} M$ ethanolic HCl solution, on the other hand, we find an increase of the unshifted visible, as well as the uv bands.

Similar pH effects, plus dimerization, but no salt effect can be observed in water. The unusual metachromatic behavior suggests a complex association mechanism, indicated also by the positive ΔH and the apparently negative activation energies of the reaction (see Table I). In the kinetic experiments, relaxation times between 1 and 3.6 msec were measured for the concentration range of 2×10^{-4} to $1 \times 10^{-5} M$.

Rhodamine 6G shows definite dimerization in water (Figure 5), but none in ethanol. The equilibrium constant at 9°, $K_{9^\circ} = 1.72 \times 10^3 M^{-1}$, is close to that previously determined² at 22°, $K_{22^\circ} = 1.69 \times 10^3 M^{-1}$. The absorption spectrum is effected by changes of the pH as well as the ionic strength, where the intensity of the dimer band is increased more by 0.1 M KNO₃ than by 0.1 M HCl, if the dye concentration is $7.6 \times 10^{-5} M$. In a ten times more dilute dye solution, however, both monomer and dimer band intensities increase under the same conditions.

No reliable kinetic data could be obtained for this system because the relaxation times are too short for flow techniques. Although we attempted to use a 16° temperature jump to perturb the equilibrium, the ΔH of the reaction is too small ($\approx -0.2 \text{ kcal mol}^{-1}$) to yield measurable effects.

Rhodamine 110. The solubility of the dye in water is about $10^{-6} M$, below which concentration only monomer is present in the solution. The reason for the low solubility is probably the formation of large aggregates with $-\text{COOH}-$ $-\text{NH}_2-$ links.

The concentration and pH dependence of the ethanolic spectra (Figure 6) closely resembles to that of Rhodamine B.² The main absorption band of the pure dye is increased by the addition of protons, and is decreased with a blue shift if OH⁻ ions are added. Although, such spectral behavior could be caused also by specific ion interactions with sensitive chromophoric sites alone,¹² in the present case we

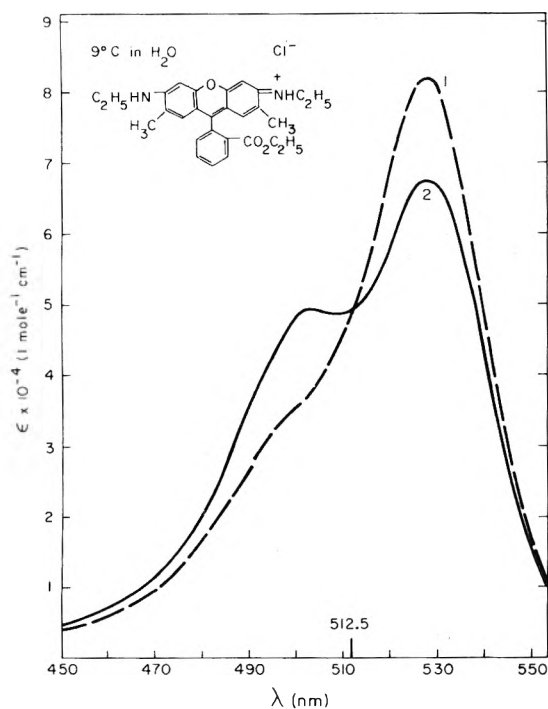


Figure 5. Absorption spectrum of Rhodamine 6G in water at 9°C: (curve 1) 7.45×10^{-6} M solution in a 1-cm cell; (curve 2) 7.45×10^{-5} M solution in a 0.1-cm cell.

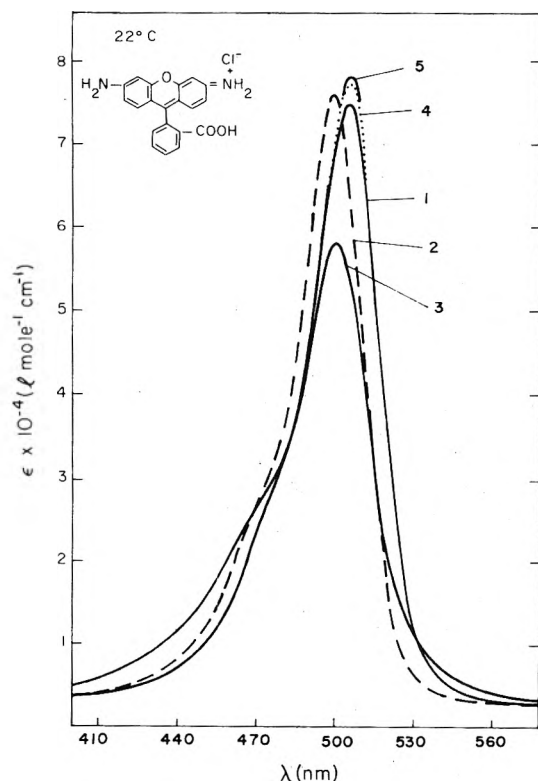
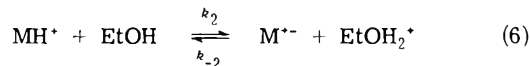
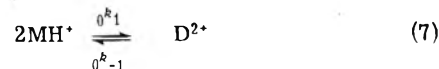


Figure 6. Absorption spectrum of Rhodamine 110 in ethanol at 22°C. The dye concentration is 10^{-4} M for curves 1 to 4 and 10^{-5} M for curve 5. The path length is 0.1 cm for curves 1 to 4 and 1 cm for curve 5: (curve 1) pure dye; (curve 2) 10^{-4} M NaOH; (curve 3) 10^{-1} M NaOH; (curves 4 and 5) 10^{-4} HCl. Comparison of curves 4 and 5 shows dimerization in an acidic medium, where the absorption maximum is at λ 505 nm. At this wavelength $\epsilon_d < 2\epsilon_m$ (see Figure 7), thus ϵ increases on dilution if two monomers are formed from one dimer.

are dealing with an (additional) acid-base equilibrium of the form



The very small equilibrium constant ${}_2K_{25^\circ} = 1.58 \times 10^{-14}$ (or ${}_2K_{25^\circ} = 2.68 \times 10^{-13}$ if the concentration of EtOH is included in the constant) indicates that the carboxylic proton is H bonded to the oxygen of the xanthene plane or to the $-\text{NH}_2$ group of another molecule. An increase of the H^+ concentration has little effect on equilibrium 6, but the dimerization equilibrium (${}_1K_{22^\circ} = 1.17 \times 10^{-4} \text{ M}^{-1}$) is



shifted to the right, as more H-bonded head-to-tail dimers are formed. The red-shifted dimer J bands of both Rhodamine 110 and Rhodamine B (Figure 7) also indicate a head-to-tail configuration. As a consequence, the relaxation times also become shorter in the acidic range, exceeding the capability of flow techniques.

The addition of OH^- ions shifts the acid-base equilibrium 6 to the right and the dimerization 7 to the left. At a sufficiently high OH^- ion concentration (0.1 M) in a 10^{-4} M dye solution there is not enough D^{2+} left in the equilibrium to do relaxation measurements. The large hypochromic effect that occurs simultaneously (curve 3 in Figure 6) is due to the small extinction coefficient of M^{*+} .

The kinetic experiments can be interpreted in terms of two coupled equilibria 6 and 7, where the two reciprocal relaxation times are given by

$$\tau_{1,2}^{-1} = \frac{\alpha_{11} + \alpha_{22}}{2} [1 \pm (1 - \beta)^{1/2}]$$

where

$$\alpha_{11} = k_2([\text{MH}^+] + [\text{EtOH}]) + k_{-2}([\text{M}^{*+}] + [\text{EtOH}_2^+])$$

$$\alpha_{12} = 2k_2([\text{MH}^+] + [\text{EtOH}])$$

$$\alpha_{21} = 2{}_0k_1[\text{MH}^+]$$

$$\alpha_{22} = 4{}_0k_1[\text{MH}^+] + {}_0k_{-1}$$

$$\beta = 4(\alpha_{11}\alpha_{22} - \alpha_{12}\alpha_{21})/(\alpha_{11} + \alpha_{22})^2$$

with brackets indicating equilibrium concentrations. Assuming k_{-2} to be diffusion controlled, $k_{-2} \gg {}_0k_1$, ${}_0k_{-1}$, and using the known values of ${}_1K_{22^\circ}$ and ${}_2K_{25^\circ}$, the following experimental conditions are established in a 10^{-4} M solution: $[\text{EtOH}] = 17 \text{ M}$, $[\text{MH}^+] \approx 10^{-5} \text{ M}$, $[\text{M}^{*+}] \approx [\text{EtOH}_2^+] \approx 5 \times 10^{-9} \text{ M}$, $k_{-2} \approx 10^9$, and $k_2 \approx 10^{-4}$. Using usual values for ${}_0k_1$ and ${}_0k_{-1}$ (see Table I) we obtain $\beta \ll 1$ and $\alpha_{22} \gg \alpha_{11}$. Thus, only one relaxation time is expected, $\tau_1^{-1} = \alpha_{22}$, as we observed (see eq 5).

Summary

Dimerization in aqueous solution is caused by the hydrophobic interaction of the alkyl substituents. The only member of the series lacking such substituents is Rhodamine 110, that on the other hand can readily form $-\text{COOH} \cdots \text{NH}_2-$ linked insoluble aggregates. The blue-shifted H bands of Rhodamine B, 3B, and 6G indicate parallel dimers, suggesting that only those collisions where two monomers approach one another from the unhindered side of the chromophore plane can lead to association. The monomer constituents in the dimer probably occupy positions that represent an inversion in a center of symmetry. Methyl

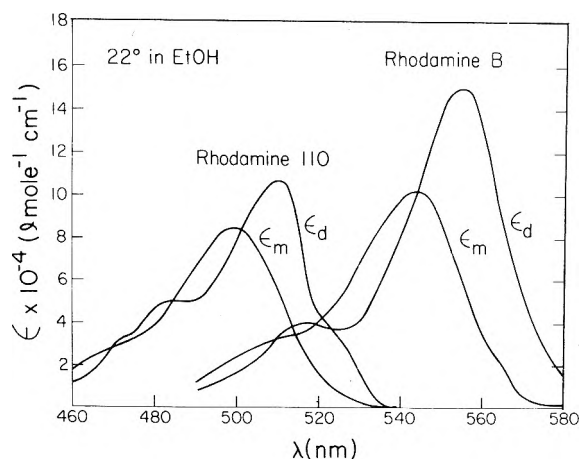


Figure 7. Resolved monomer and dimer extinction coefficients for ethanolic Rhodamine 110 and Rhodamine B at 22°.

substitution in the xanthene plane seems to be more important for aggregation than esterification of the carboxyl group. Rhodamine 6G's reaction rate(s) are too fast to be determined by flow methods.

Contrary to previous suggestions,^{3,11} we have shown using kinetic and spectroscopic arguments that Rhodamine B dimerizes in ethanol. The red-shifted J band of the dimer (Figure 7) indicates a head-to-tail configuration. Since the same is true only for Rhodamine 110, the unesterified -COOH group seems to be the crucial factor in forming the head-to-tail aggregates probably *via* hydrogen bond. However, a direct interaction between two carboxyl groups would not lead to significant color change for they are not part of the chromophore. The identical spectral behavior of the two dyes (ref 11, and our Figures 6 and 7), as well as the similarity of their rate parameters, supports the assumption that their dimer structures also resemble each other.

Since the change in enthalpy includes also the heat of solution of the monomer and dimer, which are not known, the determined ΔH values (Table I) cannot be interpreted in

terms of bond energy or heat of dissociation. The free enthalpy changes of dimerization ΔG_{295° for all four dyes are similar in both solvents, ranging between -4.3 and -6.1 kcal mol⁻¹. All the entropy changes ΔS_{295° are around 12 eu, with the exception of Rhodamine 3B in water (25 eu) and Rhodamine 110 in ethanol (28.8 eu). Since $\Delta H = \Delta G + T\Delta S$, the positive ΔH of these two dyes is due to the large entropy of dimerization of the dye-solvent system. A more detailed knowledge of the structures and the solvation equilibria involved is necessary for the unambiguous explanation of the entropy changes.

Acknowledgment. This work has been supported in part by the Research Corporation and the National Science Foundation. The authors are indebted to Dr. Drexhage for samples of Rhodamine 110 and 3B, as well as to R. J. Krusberg, R. E. Morton, R. Sexton, and M. W. Williams for technical assistance.

References and Notes

- (1) Abstracted in part from M. M. Wong's dissertation, to be submitted to the University of Georgia. Presented in part at the 166th National Meeting of the American Chemical Society, Aug 27-31, 1973, Chicago, Ill.
- (2) J. E. Selwyn and J. I. Steinfeld, *J. Phys. Chem.*, **76**, 762 (1972), and references therein.
- (3) K. H. Drexhage in "Dye Lasers," F. P. Schaefer, Ed., Springer-Verlag, New York, N. Y., 1973, Chapter 4.
- (4) (a) G. S. Levinson, W. T. Simpson, and W. Curtis, *J. Amer. Chem. Soc.*, **79**, 4314 (1957); (b) K. K. Rohatgi and G. S. Singhal, *J. Phys. Chem.*, **70**, 1695 (1966); (c) *ibid.*, **67**, 2844 (1963); (d) W. West and S. Pearce, *ibid.*, **69**, 1894 (1965); (e) K. Bergmann and C. T. O'Konski, *ibid.*, **67**, 2169 (1963).
- (5) M. M. Wong, R. A. Heckman, and Z. A. Schelly, *J. Phys. Chem.*, **77**, 1317 (1973).
- (6) R. G. Bates, M. Paabo, and R. A. Robinson, *J. Phys. Chem.*, **67**, 1833 (1963).
- (7) Z. A. Schelly, R. D. Farina, and E. M. Eyring, *J. Phys. Chem.*, **74**, 617 (1970); *Monatsh. Chem.*, **101**, 493 (1970).
- (8) M. M. Wong and Z. A. Schelly, *Rev. Sci. Instrum.*, **44**, 1226 (1973).
- (9) A. R. Monahan and D. F. Blossey, *J. Phys. Chem.*, **74**, 4014 (1970).
- (10) E. G. McRae and M. Kasha "Physical Processes in Radiation Biology," L. Angstein, B. Rosenber, and R. Mason, Ed., Academic Press, New York, N. Y., 1964, p 23.
- (11) J. Ferguson and A. W. H. Mau, *Chem. Phys. Lett.*, **17**, 543 (1972).
- (12) R. B. McKay and P. J. Hillson, *Trans. Faraday Soc.*, **61**, 1800 (1965).

Anaerobic Chemiluminescent Reaction of Aryl Grignard Reagents with Aryl Peroxides

Philip H. Bolton and David R. Kearns*

Department of Chemistry, University of California, Riverside, California 92502 (Received March 20, 1974)

Publication costs assisted by the U. S. Public Health Service

In this investigation we report a new anaerobic chemiluminescent reaction: the reaction of aryl Grignard reagents with benzoyl peroxide or *tert*-butyl peroxybenzoate. This reaction of the aryl Grignard reagents with the aryl peroxides exhibits a bright red chemiluminescence. The emitting species for this reaction has been identified as the triphenylmethyl radical.

Introduction

It has been known for some time that the reaction of certain Grignard reagents with molecular oxygen gives rise to the emission of light,¹ but there have been relatively few modern investigations of this phenomenon.^{2,3} In the course of our own studies of the oxygen induced chemiluminescence of Grignard reagents⁴ we discovered that the *anaerobic* reaction of aryl Grignard reagents with benzoyl peroxide or *tert*-butyl peroxybenzoate is highly chemiluminescent. The first study of the reaction of Grignard reagents with peroxides was described by Gilman and Adams,⁵ but they did not report that the reactions are chemiluminescent. More recently Lawesson and Yang⁶ examined the reaction of Grignard reagents with benzoyl peroxide and *tert*-butyl peroxybenzoate in greater detail and proposed a reaction scheme that accounts for the main products of the reactions, but did not observe any chemiluminescence. In an attempt to determine the origin of the red chemiluminescence which we observed we have reinvestigated the reaction of various aryl Grignard reagents with benzoyl peroxide and *tert*-butyl peroxybenzoate. On the basis of these studies we have concluded that the emission arises from the formation of electronically excited triphenylmethyl radicals.

Experimental Section

Preparation of Phenylmagnesium Bromide. Grignard reagents were prepared in the usual manner at about 0.1 M concentration under nitrogen with a 50% excess of magnesium. Mallinckrodt anhydrous diethyl ether, bromobenzene, and tetrahydrofuran (THF) were used without further purification. Baker and Adamson Grignard grade magnesium and doubly distilled magnesium (a gift from Dr. Harry Johnson) were heated to 120° before use to remove traces of water. Deuterated bromobenzene (99.5%) was obtained from Stohler Isotope Chemicals, Lot No. 5002.

Preparation of Reagents. Mallinckrodt benzophenone and Matheson Coleman and Bell *tert*-butyl peroxybenzoate were used without further purification. Triphenylmethyl radicals were prepared from Matheson Coleman and Bell triphenylcarbinol which was allowed to react with acetyl chloride followed by reaction with zinc dust.⁷ The overall yield of triphenylmethyl radical was low but adequate for the spectroscopic studies described below. No attempt was made to isolate the hydrocarbon dimer of the triphenylmethyl radical. Diphenylmagnesium was prepared free of halogen by allowing diphenylmercury (Alfa

Inorganics) to react with doubly distilled magnesium in diethyl ether or THF.

Spectroscopic Studies. Absorption Spectra. All absorption spectra were taken on a Cary 14 spectrometer. In obtaining the spectra of intermediates or products of the reaction of the Grignard reagents with the peroxy compounds an aliquot of the unreacted Grignard solution was used as the reference. In a typical experiment, 0.1 g of benzoyl peroxide or 0.1 g of *tert*-butyl peroxybenzoate was slowly added to 10 ml of 0.1 M Grignard solution.

An impurity in the Grignard grade magnesium gave rise to a misleading but reproducible result. The Grignard solutions which are originally a light brown color become red upon addition of the peroxy compound. Addition of excess peroxy compound causes the color of the solution to change from red to the yellow associated with the triphenylmethyl radical which the epr experiments described below clearly indicate as being present. The absorption spectra of the red species and triphenylmethyl radical are shown in Figures 1 and 2. We suspected that the red species was important in the chemiluminescent reaction. However, the red species was not formed when doubly distilled magnesium was used in the preparation of the Grignard reagent and yet the chemiluminescence intensity and spectral distribution were the same as when Grignard grade magnesium was used. In an attempt to identify this red species we allowed the triphenylmethyl radical to react with Grignard grade magnesium, but no red species was formed. This impurity induced species was identified as a halomagnesium diphenyl ketyl radical since it has an absorption spectrum identical with that of authentic halomagnesium diphenyl ketyl radical formed by the method of Gomberg and Bachmann.^{7,8}

Emission Spectra. The fluorescence spectra were taken using right angle excitation with the 447-nm line of a high-pressure mercury lamp. The fluorescence was focused onto the slits of a McPherson Model 2051 1-m monochromator and the output of a RCA 7625 photomultiplier was read out on a strip recorder. The fluorescence spectra were corrected for the spectral sensitivity of the monochromator and photomultiplier as well as the self-absorption of the solution. The fluorescence spectrum of the reaction products of benzoyl peroxide and phenylmagnesium bromide in diethyl ether and THF was found to be identical with the fluorescence spectrum of the triphenylmethyl radical. Furthermore, the fluorescence intensity of these reaction products was found to decrease with exposure to air. The decrease of the fluorescence intensity is approximately linear with the decrease in the epr signal of the triphenylmethyl radical

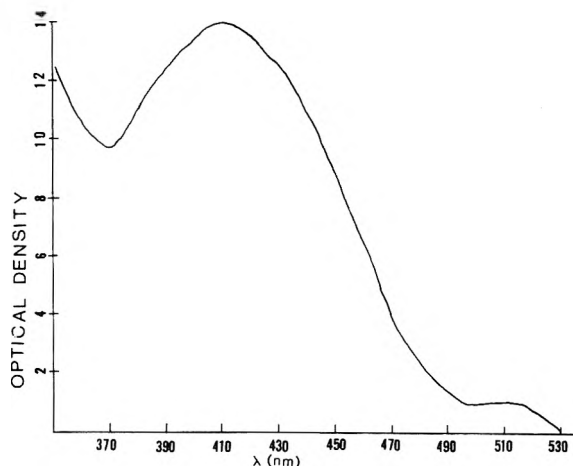


Figure 1. Absorption spectrum of 10^{-4} M triphenylmethyl radical in diethyl ether in a 1-cm cell. The extinction coefficient at 510 nm is 2000.

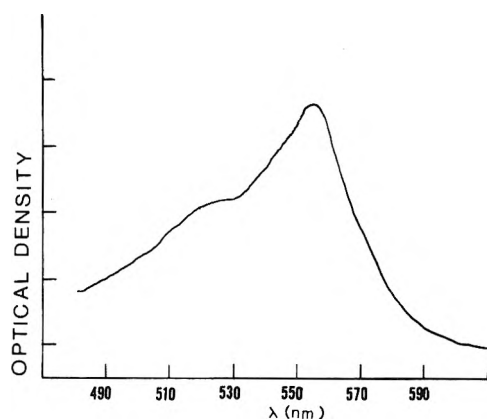


Figure 2. Absorption spectrum of the halomagnesium diphenyl ketyl radical formed by treating phenylmagnesium bromide from Grignard grade magnesium with benzoyl peroxide.

present in the reaction products and this provides further evidence that the emitting species is the triphenylmethyl radical. Due to the explosive nature of this reaction we could not construct a system which would produce a constant chemiluminescence. This restriction forced us to use the apparatus described below, rather than the monochromator-photomultiplier apparatus used in obtaining the fluorescence spectra. The chemiluminescent spectra were obtained through addition of 1 ml of a diethyl ether or THF solution of phenylmagnesium bromide to either a saturated solution of benzoyl peroxide, which is sparingly soluble in the solvents used, or to a dilute solution of *tert*-butyl peroxybenzoate in the same solvent as the Grignard. The peroxy solution was contained in a cylindrical cuvette (radius of 5 cm and volume 250 ml) with silvered walls. The light from the cuvette was focused on an EMI 9659 QB photomultiplier whose output was read out on a strip recorder. After the Grignard had been added to the peroxy solution a reading of the total chemiluminescent intensity I_0 was made. A series of Schott cut-off filters were then placed in the light path to give readings of the total chemiluminescent intensity occurring at wavelengths longer than the cut off of the filter. Readings of I_0 were alternated with the cut-off filter readings to assure that the total chemiluminescent intensity was decaying linearly with time. The ratio I/I_0 represents the percentage of the chemilumines-

cence occurring at wavelengths longer than the cut off of the filter so that the intensity occurring in a given band was calculated by subtracting I/I_0 of the corresponding next higher wavelength filter from the lower wavelength I/I_0 . This band intensity (usual band width 20 nm) was then corrected for photomultiplier response and transmittance of the filter. The spectral distribution of the chemiluminescence from the reaction of phenylmagnesium bromide and benzoyl peroxide is shown in Figure 3. Identical results were obtained from the reaction of phenylmagnesium bromide and *tert*-butyl peroxybenzoate and the spectral distribution of the chemiluminescence was found to be independent of the solvent. This technique also allowed us to measure the half-life of the chemiluminescence. Under the experimental conditions which the chemiluminescent spectral distribution was obtained the half-life in THF was 10 min and in diethyl ether 2 min for the reaction of benzoyl peroxide with phenylmagnesium bromide and for the reaction with *tert*-butyl peroxybenzoate the half-life was 16 min in THF and 3 min in diethyl ether.

Epr Spectra. Epr spectra were taken on a Varian Model V-4502 100-kHz epr spectrometer using an X-band bridge and a 0.15-mm quartz flat cell. In a typical experiment the samples were prepared in the same manner as in the absorption spectra experiments. Epr measurements were made on the reaction products of the reaction of phenylmagnesium bromide with the two peroxy compounds in both diethyl ether and THF solutions. In every case a strong epr signal ($g = 2$) was observed and a typical spectrum is shown in Figure 4 where it is compared with the epr spectrum of a reference sample of the triphenylmethyl radical. As long as the samples were kept sealed the epr signal did not decrease over a period of 1 month. Detuned epr spectra of the triphenylmethyl radical formed through the reaction of deuterated and protonated phenylmagnesium bromide with benzoyl peroxide and *tert*-butyl peroxybenzoate were obtained. The width of the envelope with the deuterated Grignard reagent was two-thirds that found with the protonated Grignard reagent as shown in Figure 5. The epr spectrometer was purposely detuned so as to obtain an accurate envelope width.

Results and Discussion

When concentrated solutions of phenylmagnesium bromide are mixed with solutions of benzoyl peroxide or *tert*-butyl peroxybenzoate there is a vigorous reaction accompanied by bright red chemiluminescence. (The reactions of the peroxy compounds with the Grignard reagents are extremely exothermic. Addition of liquid *tert*-butyl peroxybenzoate, for example, to a Grignard solution is explosive and due care must be exercised to prevent an explosion or ignition of the solution.) The spectral distribution of this red chemiluminescence is shown in Figure 3 where it is compared to the fluorescence spectrum of the triphenylmethyl radical.

The reactions of phenylmagnesium bromide, *p*-chlorophenylmagnesium bromide, and *p*-tolylmagnesium bromide with benzoyl peroxide and *tert*-butyl peroxybenzoate are all highly chemiluminescent. Reactions of diphenylmagnesium and aliphatic Grignard reagents with the peroxy compounds are not chemiluminescent, however.

In attempting to account for the origin of the chemiluminescence a number of possible emitting species were considered. After various reasonable alternatives had been eliminated we began to seriously consider the triphenyl-

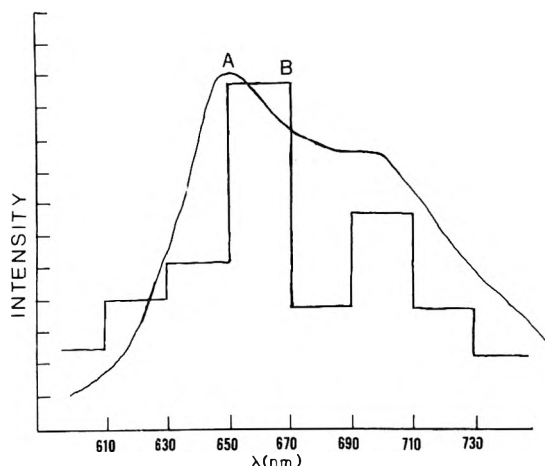


Figure 3. Fluorescence spectrum of 10^{-4} M triphenylmethyl radical, excitation 447 nm (A) in diethyl ether: chemiluminescence spectral distribution of the reaction of phenylmagnesium bromide with benzoyl peroxide in diethyl ether (B).

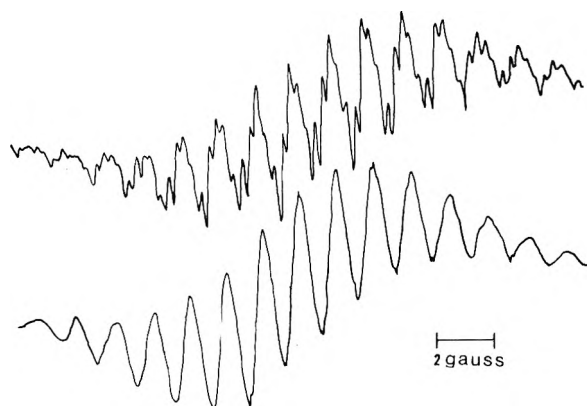


Figure 4. Epr spectrum of 10^{-4} M triphenylmethyl radical in diethyl ether (top). Epr spectrum of reaction products of phenylmagnesium bromide and benzoyl peroxide in diethyl ether solution (bottom).

methyl radical which the epr experiments had clearly demonstrated as being formed in the reaction (see Figure 4). The lower resolution in the epr spectrum of the reaction products is due to the use of a higher sensitivity of the epr spectrometer which causes a loss in resolution. The reaction product epr spectrum is superimposable on an epr spectrum of the triphenylmethyl radical obtained at comparable resolution. The fluorescence of the triphenylmethyl radical was found, within the experimental error of determining the chemiluminescence spectrum, to be identical with the chemiluminescence arising from the reaction of benzoyl peroxide or *tert*-butyl peroxybenzoate with phenylmagnesium bromide. Various fluorescent materials such as pentacene, rubrene, and Rhodamine G were added to the Grignard solution before reaction with the peroxy compounds, but in no case was there any detectable energy transfer. It should be noted, however, that the concentration of the added fluorescent materials was low, at most 10^{-3} M. A compound with the proper energy levels to observe energy transfer combined with high solubility in the solvents used and low reactivity with Grignard reagents could not be found. Lacking evidence to the contrary we presume that the triphenylmethyl radical is formed in an electronically excited state rather than being the recipient of energy transfer.

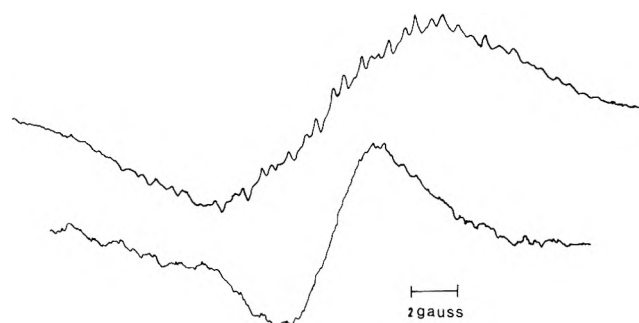
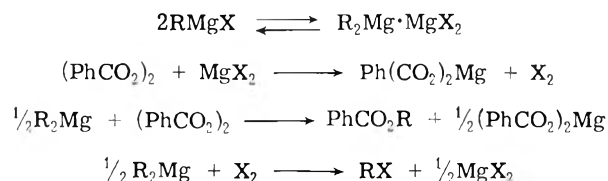


Figure 5. Detuned epr spectrum of reaction products from the reactions of protonated phenylmagnesium bromide with benzoyl peroxide in diethyl ether (top). Detuned epr spectrum of the reaction products of deuterated phenylmagnesium bromide with benzoyl peroxide (bottom).

To obtain information as to the mode of formation of the triphenylmethyl radical we examined the reaction of deuterated phenylmagnesium bromide with peroxy compounds. The epr envelope of the radical produced in this manner is two-thirds as wide as that produced in the reaction of the protonated Grignard (see Figure 5). This is taken as evidence that one of the phenyl rings of the triphenylmethyl radical is derived from the Grignard and the other two rings come from the peroxy compound.⁹ The production of the triphenylmethyl radical does not invalidate the reaction scheme of Lawesson and Yang⁶



since the yield of triphenylmethyl radical is quite small. The epr signal of the triphenylmethyl radical formed from the reaction of 0.1 M phenylmagnesium bromide with an excess of peroxy compound corresponds to about 10^{-4} M triphenylmethyl radical. However, the triphenylmethyl radical is in equilibrium with diamagnetic association compounds, $K \approx 20$,¹⁰ and therefore the yield of the triphenylmethyl radical and its diamagnetic association compound is about 1–5%.

This new chemiluminescent reaction, which is completely unrelated to the well-known oxygen-induced chemiluminescence of aryl Grignard reagents, illustrates one more of the many facets of Grignard reagents. The epr spectrum of the products of the reaction of phenylmagnesium bromide and peroxy compounds clearly demonstrate that the triphenylmethyl radical is formed in the reaction as shown in Figure 3. The fluorescence spectrum of the triphenylmethyl radical was found to be identical with the spectral distribution of the chemiluminescence within experimental error as shown in Figure 3. On this basis we have identified the emitting species of the chemiluminescent reaction as the triphenylmethyl radical. It is known that radicals are intermediates in many chemiluminescent reactions but it is very unusual for the radical to be the emitting species, especially in solution. Though the production of triphenylmethyl radicals appears to be a small side reaction with our conditions, further research might be able to improve the yield of both the triphenylmethyl radicals as well as the chemiluminescence.

Acknowledgments. The authors thank Dr. Harthmut Fuhr for his help in obtaining the chemiluminescence spectra, Dr. Harry Johnson for many interesting discussions, and Dr. A. H. Maki for help in interpreting the epr spectra. Support from the U. S. Public Health Service (Grant No. CA 11459) is gratefully acknowledged.

References and Notes

(1) F. McCapra, *Quart. Rev., Chem. Soc.*, 485 (1966).

- (2) T. Bremer and H. Friedmann, *Bull. Soc. Chim. Belg.*, **63**, 415 (1954).
 (3) R. L. Bardsley and D. M. Hercules, *J. Amer. Chem. Soc.*, **90**, 4545 (1968).
 (4) P. H. Bolton and D. R. Kearns, *J. Amer. Chem. Soc.*, **96**, 4651 (1974).
 (5) H. Gilman and C. E. Adams, *J. Amer. Chem. Soc.*, **47**, 2816 (1925).
 (6) S. O. Lawesson and N. C. Yang, *J. Amer. Chem. Soc.*, **81**, 4230 (1959).
 (7) M. Gomberg and W. E. Bachmann, *J. Amer. Chem. Soc.*, **49**, 236 (1927).
 (8) We thank the referee for suggesting this experiment.
 (9) A. Carrington and A. D. McLachlan, "Introduction to Magnetic Resonance," Harper and Row, New York, N. Y., 1967.
 (10) L. F. Fieser and M. Fieser, "Advances in Organic Chemistry," Reinhold, New York, N. Y., 1961, p 351.

Photolysis of Liquid Cyclohexane at 1634 Å and the Effect of the Addition of Carbon Tetrachloride and Sulfur Hexafluoride

J. Nafisi-Movaghar¹ and Yoshihiko Hatano*

Laboratory of Physical Chemistry, Tokyo Institute of Technology, Meguro-ku, Tokyo, Japan (Received September 11, 1973; Revised Manuscript Received June 3, 1974)

Photolysis of cyclohexane in a pure liquid state and in the presence of CCl_4 and SF_6 has been carried out at 1634 Å. The primary processes are molecular and atomic detachment of hydrogen from excited cyclohexane molecules leading to the formation of hydrogen, cyclohexene, and bicyclohexyl. The material balance between these products indicates the absence of others. Addition of CCl_4 (10^{-4} to 10^{-1} M) and SF_6 (10^{-4} to 6.5×10^{-2} M) results in the reduction in the yields of the photoproducts from cyclohexane. This is explained in terms of quenching of the excited state of cyclohexane by CCl_4 , $\text{C}_6\text{H}_{12}^* + \text{CCl}_4 \rightarrow \text{C}_6\text{H}_{12} + \text{CCl}_4^*$, and SF_6 , $\text{C}_6\text{H}_{12}^* + \text{SF}_6 \rightarrow \text{C}_6\text{H}_{12} + \text{SF}_6^*$, with the reaction rates $k = 2 \times 10^{11}$ and $1 \times 10^{11} \text{ M}^{-1} \text{ sec}^{-1}$, respectively. A chain reaction occurs in the photolysis of $\text{C}_6\text{H}_{12}\text{-CCl}_4$ mixtures leading to the formation of $\text{C}_6\text{H}_{11}\text{Cl}$, $\text{C}_6\text{H}_{11}\text{CCl}_3$, CHCl_3 , C_2Cl_6 , and probably HCl as additional products.

I. Introduction

The behavior of alkanes, pure and in the presence of additives, under high-energy and far-ultraviolet excitation, is still not fully understood.²⁻⁵ Cycloalkanes, especially cyclohexane, have received considerable attention among radiation chemists, photochemists, and photophysicists. Processes such as charge neutralization and transfer, radical reactions, and ion-molecule processes have been suggested to provide a framework for understanding the action of ionizing radiation.²

However, photochemical studies with photons of energies near to, or slightly above, the ionization threshold of cyclohexane indicate the importance of the contributions of excited cyclohexane molecules in the formation of the final products, common in both radiation and photochemistry from this compound.^{4,5} The recent development in the photophysics of alkanes,⁶ especially the low yield of fluorescence emission, is in accord with the assignment of the excited cyclohexane molecule as the main precursor of the final products. This view gains further support from new information about the excited state of cyclohexane, populated under pulse radiolysis and X-ray excitation.^{7,8}

However, the reaction sequences following the disappearance of the electronically excited species and the rela-

tive yields of the individual processes vary with the excitation energy and the state of aggregation of the system.^{5c} Further, polymer formation⁹ and the effect of the olefinic products on the rate of decay of the excited state and the quantum yield of fluorescence emission have been suggested, with the conclusion that necessary corrections should be made for these effects.^{6,8}

These complications necessitated further investigation of the photochemical processes in cyclohexane systems, which has been undertaken in the present work. Excitation was performed using the Br (1634 Å) emission line the energy of which is about 2 eV below the ionization potential of cyclohexane. Carbon tetrachloride and sulfur hexafluoride, commonly used as electron scavengers in radiation chemistry, were used as additives.

II. Experimental Section

Materials. Cyclohexane (Phillips Research Grade) was used as supplied. Impurities of less than 0.01%, about half of which was 2,4-dimethylpentane, were detected by gas chromatography using a flame ionization detector. Cyclohexene and other olefins were not detected. Further, upon radiolysis of the same supply performed in this laboratory,¹⁰ the *G* value of hydrogen did not change by treatment

on silica gel. Carbon tetrachloride (Merck, 99.8%) and sulfur hexafluoride (Matheson, >98%) were used without further treatment. Chloroform (Wako Junyaku, 99%), bicyclohexyl (K and K Laboratories, >99%), cyclohexene, cyclohexyl chloride, and hexachloroethane (all of Tokyo Kasei, >99%) were used as standards without purification. Ethylene (Takachiho, >99.9%) was checked by gas chromatography. About 0.03% ethane impurity was detected. It was used for actinometry as supplied. Bromine (Koso Kagaku, >99.9%) was purified by vacuum distillation over phosphorus pentoxide and sealed.

Light Source and Photolysis Cell. The photolysis apparatus is illustrated in Figure 1. The electrodeless discharge lamp¹¹ was constructed from an inner 34/35 standard taper joint with an upper tube of 1.5 cm o.d. The lower tube was joined, *via* a graded seal, to a quartz tube of 2 cm o.d., on one end of which a Suprasil quartz window of 1 mm thickness was attached. The full length of the lamp and the distance from the window to the ground glass were 35 and 3.3 cm, respectively. The other end of the lamp was provided with a side arm.

The lamp was evacuated to about 10^{-6} Torr at room temperature for 2 weeks and at *ca.* 300° for 1 week. After introducing 5 Torr of Ne the lamp was discharged for about 30 min and then evacuated. This cycle was repeated several times until the color of the discharge glow remained unchanged. Finally, bromine, through phosphorus pentoxide, and 2 Torr of Ne were introduced and the lamp was sealed. In order to avoid contamination of the lamp by grease etc. during the introduction of bromine, all the tubes leading to stopcocks were sealed. The discharge was initiated with a tesla coil and sustained by a stabilized microwave generator (Ito Chotanpa Co.) of 2450 MHz and 100 W. During the operation of the lamp the side arm was immersed in a Dry Ice-methanol slush. Lamp spectra, obtained by a vacuum uv spectrometer (JASCO Model VUV-1B), consisted of an intense line at 1634 Å and a very weak line at 1930 Å, the relative intensity of the latter being negligibly small. This weak emission, previously assigned as a carbon line due to possible contamination of the lamp by vacuum grease,¹² seems to be inherent in lamps containing Ne. A similar line is reported in Ne II emission.¹³ As mentioned above, contamination of the lamp by vacuum grease was avoided in the present work.

It was observed during the operation of the lamp that the intensity decreased gradually with time. This variation was due to the gradual collection of bromine in the side arm as the part of the lamp inside the cavity warmed, and hence, to the decrease in bromine pressure inside the lamp. This defect was rectified by keeping the lamp at a constant 200° prior to and during the operation, using heating tape. The lamp intensity under this condition remained constant (within 5%) for at least 60 min of continuous operation. The yield of hydrogen ($\phi(\text{H}_2) = 0.42$) from ethylene photolysis was used as an actinometer.¹⁴ The light intensity was 5.3×10^{-9} einstein/sec.

The photolysis cell was made of a Pyrex tube of 3.5 cm o.d., closed at one end and joined to the outer 34/35 standard taper joint at the other end. A grease trap, situated just below the ground glass, prevented contamination of solution by vacuum grease. The cell was 3 cm in length (exclusive of the joint and the trap), 53 ml in volume, and equipped with a vacuum stop cock on one side. The cell and the lamp were fitted together *via* the ground glass joint. The distance from the lamp window to the flat bot-

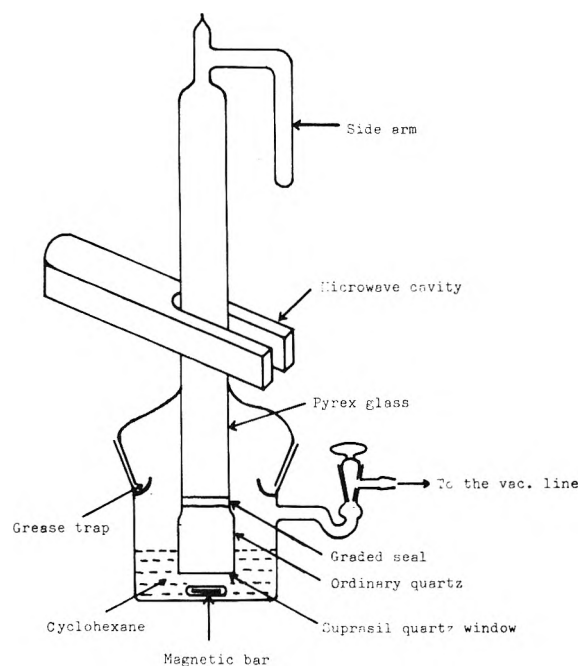


Figure 1. Photolysis apparatus.

tom of the cell was 1.2 cm. The window was covered with solution when 10 ml of the latter was introduced into the cell.

Sample Preparation and Photolysis. After introducing 10 ml of cyclohexane the cell was fitted to the lamp and connected to the vacuum line. Dissolved oxygen was removed by the freeze-thaw technique. Known amounts of CCl_4 and SF_6 were distilled into the cell and thoroughly mixed. The concentration of CCl_4 was checked by gas chromatography using a dimethylsulfolane column (4 m) at room temperature, and the concentration of SF_6 in the liquid was calculated¹⁵ from the Ostwald absorption coefficient of 1.25.

Photolysis was carried out at room temperature with stirring for 4 min. This was repeated about 10 times for cyclohexane both as a neat liquid and in the presence of additives. No appreciable change in the light intensity was observed, as confirmed by actinometry before and after each run.

Product Analysis. The noncondensable gases at -196° were collected and measured by means of a Teopler-McLeod system and identified by mass spectrometry.

Hydrogen chloride was estimated photometrically¹⁶ and by material balance.

All liquid products were analyzed quantitatively using Shimadzu gas chromatographs (Models GC-1C and GC-5A) equipped with flame ionization detectors. The columns used were as follows: for cyclohexene, a 3 mm by 4 m, 20% dimethylsulfolane on 60-80 mesh Neosorb NP at room temperature; for cyclohexyl chloride and chloroform, polyethylene glycol 6000, 3 mm by 2 m, 20%, on 60-80 mesh Celite 545 at 60°; for bicyclohexyl and trichloromethylcyclohexane, a 3 mm by 3 m, 0.1% Apiezon-L grease on Neosorb NGK at 90°; for hexachloroethane, the same column, but at 45°. The gas chromatograph was calibrated and the measurement of each product was carried out relative to its standard. No sample of trichloromethylcyclohexane was available. It was prepared¹⁷ by radiolysis of a $\text{C}_6\text{H}_{12}-\text{CCl}_4$ mixture (1:1). The retention time of the photoproduct

TABLE I: Photolysis of Cyclohexane in the Presence and Absence of Additives

Concn of additives ^a	Photolysis time, min ^c	Rate of product formation, $\mu\text{M}/\text{min}^b$							
		H ₂	C ₆ H ₁₀	C ₁₂ H ₂₂	C ₆ H ₁₁ Cl	HCl ^d	C ₆ H ₁₁ CCl ₃ ^e	CHCl ₃	C ₂ Cl ₆
O	81	0.320	0.276	0.048					
CCl ₄ (0.1 M)	82	0.214	0.201	0.024	0.695	<0.05	0.015	0.540	0.102
SF ₆ (0.065 M)	56	0.250	0.257	0.028					

^a Maximum concentrations at which the measurements were made. ^b The maximum estimated error is $\pm 5\%$. ^c Photolysis was carried out in two courses and the total photolysis time is listed. ^d HCl could not be detected photometrically indicating that its amount should have been less than ca. 4 μM , the lowest limit of sensitivity of this technique.¹⁶ It was, therefore, estimated. ^e No standard sample of this compound was available. Its value was, therefore, estimated from the relative peak areas on the chromatograms for photolyzed and radiolyzed samples, using $G(\text{C}_6\text{H}_{11}\text{CCl}_3) = 2$ for 1:1 mixture of C₆H₁₁-CCl₃.¹⁷

TABLE II: Product Distributions from Photolysis of Cyclohexane in the Presence and Absence of Additives^a

Concn of additives	H ₂	C ₆ H ₁₀	C ₁₂ H ₂₂	C ₆ H ₁₁ Cl	HCl	C ₆ H ₁₁ CCl ₃	CHCl ₃	C ₂ Cl ₆
O	1	0.86	0.15					
CCl ₄ (0.1 M)	1	0.94	0.11	3.25	<0.23	0.07	2.52	0.48
SF ₆ (0.065 M)	1	1.03	0.12					

^a The distributions are calculated (from Table I) relative to that of hydrogen in each system.

matched exactly that of the radiolysis product and, therefore, was assigned as trichloromethylcyclohexane. Quantitative measurement of this product was based on the reported G value.¹⁷

III. Results and Discussion

The noncondensable product at -196° from photolysis of cyclohexane, pure and in the presence of additives, was hydrogen. This was confirmed by mass spectrometric analysis. The liquid products in the case of pure cyclohexane were cyclohexene and bicyclohexyl. Additional products were formed in the presence of additives. These were identified and measured for the C₆H₁₂-CCl₄ system. The total amount of conversion in cyclohexane was less than 0.02%. This minimized the secondary effects arising from accumulation of the photoproducts.

The rate of formation of products and their distributions in all the system are given in Tables I and II, respectively.

Figure 2 shows the variation in the amount of hydrogen produced as a function of irradiation time for the photolysis of pure cyclohexane. Variations in the reciprocal amounts of hydrogen produced as a function of concentration of CCl₄ and SF₆ in the photolysis of mixtures of cyclohexane and these additives are presented in Figure 3.

Results obtained for pure cyclohexane and those in the presence of additives will be discussed separately in the following sections.

A. Pure Cyclohexane. Data presented in Table I show the material balance between the amount of hydrogen and the sum of the amounts of cyclohexene and bicyclohexyl produced in this system. This observation is similar to those reported previously^{5b-d,18} for the photolysis of cyclohexane with Xe and Kr resonance lamps, with the exception of degradation products which were not formed under the present experimental conditions. The formation of hydrogen-deficient product(s)¹⁹⁻²¹ and possibly polymeric species^{5a,22,23} have been suggested to account for the absence of material balance in both the radiation and the photochemistry of cyclohexane, and also for the variation of light intensity in the latter case.⁹ The material balance and the constant light intensity indicated that such products were not formed in the present system. This is expected, since the formation of these products is not favored in the liquid phase and under lower excitation energy.^{5c} The formation of C₆H₁₂⁺ ions and the subsequent reactions of

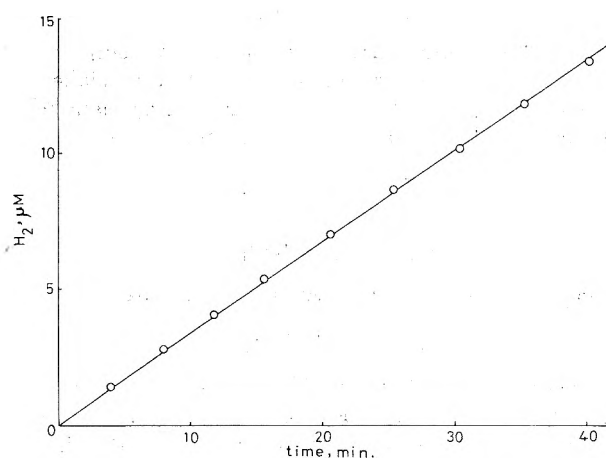


Figure 2. Variation in the amount of hydrogen produced as a function of the irradiation time for photolysis of cyclohexane as a neat liquid.

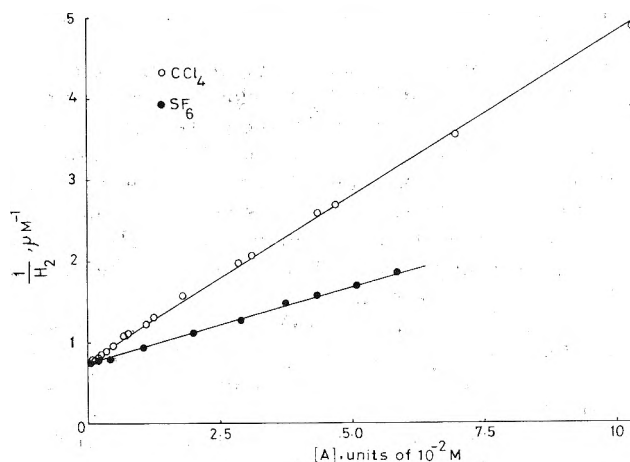
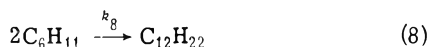
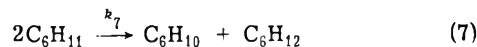
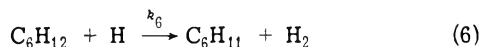
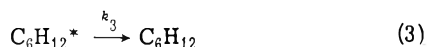
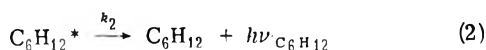
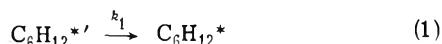
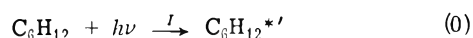


Figure 3. Variation in the reciprocal amount of hydrogen produced as a function of the concentration of additives, A, for the photolysis of cyclohexane.

these ions^{5a} are not probable since the photon energy at 1634 Å is about 2 eV below the ionization potential of cyclohexane.

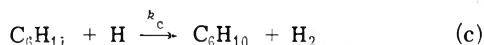
The following reaction scheme accounts adequately for the observed results.



where $\text{C}_6\text{H}_{12}^{*'}$ and $\text{C}_6\text{H}_{12}^*$ are the vibrationally excited species and the first excited singlet state of cyclohexane, respectively. On the basis of the kinetic treatment,^{5c,19,20} reactions a and b do not affect the observed results.



Reaction c, which was proposed in the photosensitized de-

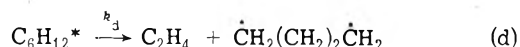


composition of cyclohexane,^{24,25} does not occur in the present system; inclusion of this process in the reaction scheme contradicts the material balance shown in Table I. This discrepancy may be explained in terms of the relatively high excitation energy in the present system and the low possibility of thermalization of the intermediates within the cage of the surrounding molecules.^{5c} We are, therefore, inclined to consider reactions 0-8 to account for the observed results.

The linearity of the plot in Figure 2 indicates that quenching of the excited state of cyclohexane by the photoproduct is not significant under the present experimental conditions. The quantum yield of hydrogen formation $\phi(\text{H}_2)_0 = 1.0 \pm 0.1$ was obtained from the slope of this plot and the light intensity. Even taking into account the quenching^{6a} effect of the photoproduct (C_6H_{10}), at the maximum conversion of 0.02%, does not alter the value of $\phi(\text{H}_2)_0$ by more than ca. 10%.

This value is similar to 1.0 (Yang, *et al.*^{5c}) and larger than 0.74 (Hentz and Rzad^{5b}) reported for the photolysis of cyclohexane at 1470 Å in the liquid and the gas phase, respectively.

To account for the difference between $\phi(-\text{C}_6\text{H}_{12}) = 1$ and $\phi(\text{H}_2)_0 = 0.74$, a nonhydrogen-producing process (reaction d) has been suggested^{5b} at 1470 Å, with consequent de-



composition of the biradical into two molecules of ethylene^{5a} or its polymerization.^{5b} In the absence of detectable amounts of these products and on the grounds of material balance, the occurrence of reaction d is not considered probable in the present system.

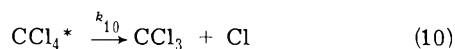
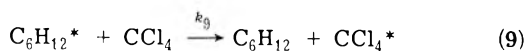
A decrease in the quantum yield of fluorescence with decreasing excitation wavelength has been observed and attributed, in part, to the presence of olefinic products which quench the fluorescence emission.^{6a} Also the effect of these products on the lifetime of the excited state has been argued similarly.^{6a,8} However, the small amounts of the total light absorbed in fluorescence measurements, which are usually carried out in a short time, do not seem to produce sufficient amounts of photoproducts able to affect the lifetime of the excited state and, hence, the fluorescence quantum yield. Similar values of ~0.3 nsec obtained for the lifetime of excited cyclohexane under pulse radiolysis⁷ and X-ray excitation⁸ is in accord with this view. Furthermore, the data reported recently^{6d} for a number of neat saturated hydrocarbons, including cyclohexane, under excitation at 1470 and 1650 Å indicate that the ratio of the fluorescence quantum yields $\beta_f = \phi_f(1470)/\phi_f(1650)$ is not affected considerably upon addition of oxygen (at 1 atm) and carbon tetrachloride (at $10^{-2} M$) as quenchers, whereas one would expect a substantial increase in β_f if quenching by photolysis products was important.^{6e} The implication is that the observed decrease in quantum yield of fluorescence with decreasing excitation wavelength is *not* principally due to the photolysis products quenching the emission but rather to nonunit efficiency for internal conversion from the state achieved by 1470-Å excitation to the state achieved by 1650-Å excitation.^{6f} An efficient competition of reaction d with internal conversion may serve, at least in part, to account for this effect. The relative yield of 0.5 for the formation of ethylene in the gas-phase photolysis of cyclohexane^{5a} under excitation with 1470 Å, and the fact that no fluorescence was observed under the same conditions, give some support to this view. At this point it must be noted that the quenching effect of the photoproducts can not be ignored at higher conversions.^{5c}

An accepted value for k_7/k_8 is 1.1.²⁶ We can estimate, from the yield of bicyclohexyl (Table I) that the hydrogen atom quantum yield, $\phi(\text{H})_0$, is about 0.3. This value is considerably higher than 0.07 reported by Hentz and Knight⁹ for the gas-phase photolysis of cyclohexane and 0.14 obtained by Yang, *et al.*,^{5c} in the liquid phase.

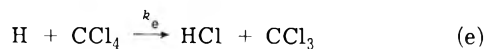
B. Cyclohexane in the Presence of Carbon Tetrachloride and Sulfur Hexafluoride. Relative yields of the chlorine containing products in Table II indicate the occurrence of a chain reaction in the cyclohexane-carbon tetrachloride system. Material balance is achieved between chlorine and trichloromethyl radical containing products. Similar results were obtained for radiolysis of this system by Henglein, *et al.*,¹⁷ and Stone, *et al.*²⁷ Data in Table I show that while the yields of products from cyclohexane are reduced in the presence of carbon tetrachloride and sulfur hexafluoride, material balance between the amount of hydrogen and the sum of the amounts of cyclohexene and bicyclohexyl is not disturbed within experimental error. On the other hand, it is evident from the values in Table II that while the relative yield of cyclohexene is not affected considerably, that of bicyclohexyl is reduced in the presence of additives. We interpret this variation in terms of scavenging of C_6H_{11} radicals by the additives which compete with reaction 8 and hence reduce the yield of bicyclohexyl. The effect on the yield of cyclohexene is not pronounced because of the relatively higher yield of reaction 4. We therefore conclude that the effect of the additives is mainly on the common precursor of the products, which is the excited state of cyclohexane. Fractions of the exciting light absorbed by sul-

for hexafluoride and carbon tetrachloride at the concentrations used in this experiment are negligible.²⁸

The following complimentary reactions account for the results obtained in the cyclohexane-carbon tetrachloride system.



Reaction e was suggested by Hardwick²⁹ and Henglein,²⁷ who estimated $k_e/k_6 = 140$.



However, this estimation seems to be incorrect in view of recently reported data; Stone and Dyne,^{27a} in the radiolysis of a $\text{C}_6\text{H}_{12}\text{-CDCl}_3$ system, observed that $G(\text{HD})$ was much less than the calculated value based on the above scheme. This has been further confirmed by esr studies^{27b} on the reactions of hydrogen atoms with carbon tetrachloride and cyclohexane in aqueous solutions which yielded $k_e/k_6 = 1.6$.

From the data obtained in the present work we are unable to decide about this reaction. However, HCl could not be detected photometrically¹⁶ indicating that its rate of production was less than $0.05 \mu\text{M}/\text{min}$. This is in accord with the material balance (see Table I) and, hence, supports our argument.

From the steady-state treatment of the results in reactions 0-15 one obtains

$$\frac{1}{[\text{H}_2]} = \frac{k_9}{I_T(k_4 + k_5)} [\text{CCl}_4] + \frac{\Sigma_2^5 k}{I_T(k_4 + k_5)} \quad (I)$$

where $[\text{H}_2]$ represents the amount of hydrogen produced, $\Sigma_2^5 k = k_2 + k_3 + k_4 + k_5$, I_T is the amount of light absorbed, and $[\text{CCl}_4]$ is the concentration of carbon tetrachloride. Equation I predicts a linear plot for $1/[\text{H}_2]$ vs. $[\text{CCl}_4]$. Such a variation is indeed observed (Figure 3) with the following values for the slope and intercept.

$$\text{slope} = k_9/I_T(k_4 + k_5) = 41 \times 10^6 M^{-2} \quad (II)$$

$$\text{intercept} = \Sigma_2^5 k/I_T(k_4 + k_5) = 0.73 \times 10^6 M^{-1} \quad (III)$$

It is evident from the form of eq I that

$$1/\text{intercept} = I_T \phi(\text{H}_2)_0 \quad (IV)$$

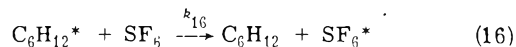
As mentioned in section II, irradiation was carried out for 4 min in each measurement and that $I = 5.3 \times 10^{-9}$ einstein/sec. Substitution of these values in eq III and IV yields $\phi(\text{H}_2)_0 = 1.1$ which agrees well with the value 1.0 obtained from the photolysis of pure cyclohexane and thus confirms the proposed mechanism.

From eq II and III one obtains the following ratio

$$\text{slope/intercept} = k_9(\Sigma_2^5 k)^{-1} = 56 M^{-1} \quad (V)$$

Substitution of the value $\Sigma_2^5 k = 3.6 \times 10^9 \text{ sec}^{-1}$, obtained by Beck and Thomas⁷ in the pulse radiolysis of cyclohexane, gives a value of $k_9 = 2 \times 10^{11} M^{-1} \text{ sec}^{-1}$ which is in good agreement with $3 \pm 1 \times 10^{11} M^{-1} \text{ sec}^{-1}$ obtained by these authors.

Treatment of the plot in Figure 3 for SF_6 in a manner similar to that for CCl_4 yields $\phi(\text{H}_2)_0 = 1.1$ and $k_{16} = 1 \times 10^{11} M^{-1} \text{ sec}^{-1}$, where k_{16} is the rate constant of the following reaction



Here again, agreement between $\phi(\text{H}_2)_0 = 1.1$ and that obtained from the photolysis of pure cyclohexane is excellent. A complete course of the reactions for the cyclohexane-sulfur hexafluoride system is not established. This is being currently considered. Some fluorine containing compounds have been reported for the photolysis of the *n*-hexane-sulfur hexafluoride system.³⁰ However, the occurrence of reaction 16 is obvious from the observed results. Comparison of the values of k_9 and k_{16} indicates that carbon tetrachloride is twice as good a quencher as sulfur hexafluoride.

From the foregoing discussion we conclude that the effects of carbon tetrachloride and sulfur hexafluoride are mainly due to the quenching of the excited state of cyclohexane and, to some extent, to the scavenging of cyclohexyl radicals produced in the system. A reasonable agreement between our results and that of Beck and Thomas⁷ and also the agreement between the values of 0.28 and 0.3 nsec obtained for the lifetime of the excited cyclohexane under the pulse radiolysis⁷ and X-ray excitation⁸ of cyclohexane, respectively, indicate that a similar mechanism (i.e., quenching of the excited state) is involved in all cases.

Values of k_9 and k_{16} are higher, by a factor of ca. 10, than those expected for a diffusion-controlled reaction. Similarly, a higher value of the rate constant has also been reported for the quenching of the excited state of decalin by carbon tetrachloride.⁸ Migration of excitation energy through the solvent molecules in a manner similar to that in aromatic solvents,^{31,32} may offer an explanation for this anomaly. As evidence for such migration in alkanes, Rothman, *et al.*,^{6d} have looked for a decrease in quenching efficiency upon dilution of decalin (the emitter) with pentadecane using carbon tetrachloride as a quencher. The quenching efficiency was not found to be affected by dilution. However, the exact state of affairs still remains obscure. Further work is certainly required to clarify the situation.

Acknowledgments. We thank Professor S. Lipsky for providing us with some absorption data, the members of Professor I. Tanaka's group of this Institute for their help in the preparation of the light source, and also Dr. M. H. Elnagdi, now at Cairo University, for his valuable suggestions in some chemical syntheses. J. N. M. acknowledges the tenure of a research scholarship of the Japanese Commission for UNESCO.

References and Notes

- (1) UNESCO Fellow (1972-1975).
- (2) (a) T. Gauman, Ed., "Aspects of Hydrocarbon Radiolysis," Academic Press, New York, N. Y., 1958; (b) P. Ausloos, Ed., "Fundamental Processes in Radiation Chemistry," Interscience, New York, N. Y., 1968.
- (3) J. R. McNesby and H. Okabe, *Advan. Photochem.*, **3**, 157 (1964).
- (4) P. Ausloos, *Mol. Photochem.*, **4**, 39 (1972).

- (5) (a) R. D. Doepker and P. Ausloos, *J. Chem. Phys.*, **42**, 3746 (1965); (b) R. R. Hentz and S. J. Rzed, *J. Phys. Chem.*, **71**, 4096 (1967); (c) J. Y. Yang, F. M. Servedio, and R. A. Holroyd, *J. Chem. Phys.*, **48**, 1331 (1968); (d) R. A. Holroyd, *Advan. Chem. Ser.*, No. **82**, 488 (1968); (e) P. Ausloos and S. G. Lias, *Annu. Rev. Phys. Chem.*, **22**, 85 (1971).
- (6) (a) F. Hirayama and S. Lipsky, *J. Chem. Phys.*, **51**, 3616 (1969); (b) F. Hirayama and S. Lipsky in "Organic Scintillators," D. L. Horrocks, Ed., Academic Press, New York, N. Y., 1970; (c) F. Hirayama, W. Rothman, and S. Lipsky, *Chem. Phys. Lett.*, **5**, 296 (1970); (d) W. Rothman, F. Hirayama, and S. Lipsky, *J. Chem. Phys.*, **58**, 1300 (1973); (e) C. Lawson, F. Hirayama, and S. Lipsky, "Molecular Luminescence," E. C. Lim, Ed., W. A. Benjamin, New York, N. Y., 1969, p. 837; (f) S. Lipsky, private communication.
- (7) G. Beck and J. K. Thomas, *J. Phys. Chem.*, **76**, 3856 (1972).
- (8) M. S. Henry and W. P. Helman, *J. Chem. Phys.*, **56**, 5734 (1972).
- (9) R. R. Hentz and R. J. Knight, *J. Phys. Chem.*, **72**, 4684 (1968).
- (10) Y. Hatano, K. Takeuchi, and S. Takao, *J. Phys. Chem.*, **77**, 586 (1973).
- (11) J. R. McNesby and H. Okabe, *Advan. Photochem.*, **3**, 157 (1964).
- (12) H. Akimoto, Ph.D. Thesis, Tokyo Institute of Technology, 1967.
- (13) A. R. Striganov and N. S. Sventitskii, "Tables of Spectral Lines of Neutral and Ionized Atoms," IFI-Plenum Data Corp., New York, N. Y., 1968.
- (14) L. C. Glasgo and P. Potzinger, *J. Phys. Chem.*, **76**, 138 (1972).
- (15) S. Sato, T. Terao, M. Kono, and S. Shida, *Bull. Chem. Soc. Jap.*, **40**, 1818 (1967).
- (16) D. M. Zall, D. Fisher, and M. Q. Garner, *Anal. Chem.*, **28**, 1665 (1956).
- (17) A. Henglein, E. Heckel, Y. Ojima, and G. Meissner, *Ber. Bunsenges. Phys. Chem.*, **67**, 988 (1964).
- (18) R. A. Holroyd, J. Y. Yang, and F. M. Servedio, *J. Chem. Phys.*, **46**, 4540 (1967).
- (19) W. G. Burns and J. R. Parry, *Nature (London)*, **210**, 814 (1964).
- (20) A. W. Boyd and H. W. J. Conner, *Can. J. Chem.*, **42**, 1418 (1964).
- (21) J. W. Falconer and M. Burton, *J. Phys. Chem.*, **67**, 1743 (1963).
- (22) W. A. Cramer, ref. 1, p. 166.
- (23) J. Blackford and P. J. Dyne, *Can. J. Chem.*, **42**, 1165 (1964).
- (24) W. A. Cramer, *J. Phys. Chem.*, **71**, 1112 (1967).
- (25) R. Hentz, J. Y. Chang, and M. Burton, *J. Phys. Chem.*, **69**, 2027 (1965).
- (26) W. A. Cramer, *J. Phys. Chem.*, **71**, 1171 (1967).
- (27) (a) J. A. Stone and P. J. Dyne, *Can. J. Chem.*, **42**, 669 (1964); (b) P. Neta, R. W. Fessenden, and R. H. Schuler, *J. Phys. Chem.*, **75**, 1654 (1971).
- (28) (a) L. W. Pickett, M. Muntz, and E. M. McPherson, *J. Amer. Chem. Soc.*, **73**, 4862 (1951); (b) E. D. Nostrand and A. B. F. Duncan, *ibid.*, **76**, 3377 (1954); (c) C. R. Zobel and A. B. F. Duncan, *ibid.*, **77**, 2611 (1955).
- (29) T. J. Hardwick, *J. Phys. Chem.*, **66**, 2246 (1962).
- (30) V. I. Pitchoozhkin, H. Yamazaki, and S. Shida, *Bull. Chem. Soc. Jap.*, **46**, 67 (1973).
- (31) J. B. Birks, "Photophysics of Aromatic Molecules," Wiley-Interscience, New York, N. Y., 1970.
- (32) J. Nafisi-Movaghar, J. B. Birks, and K. R. Naqvi, *Proc. Phys. Soc.*, **91**, 449 (1967).

Natural and Experimental Fluorescence Lifetimes of Benzene in Various Solvents

Menahem Luria, Mira Ofran, and Gabriel Stein*

Department of Physical Chemistry, Hebrew University, Jerusalem, Israel (Received December 29, 1972;

Revised Manuscript Received June 3, 1974)

Publication costs assisted by the Israel Academy of Sciences

Using a nanosecond flash lifetime apparatus the fluorescence lifetime of benzene was determined in a series of polar and nonpolar solvents (including light and heavy water) in the temperature range 6–48° and compared with calculated natural lifetimes. The apparent energy of activation of the nonradiative rate constant k_{nr} , leading to a decrease of fluorescence with increasing temperature, $E_a \sim 5.3$ kcal/mol, is largely independent of solvent, while k_{nr} itself is solvent dependent. The results are discussed also in relation to the photochemistry of benzene in polar and apolar solvents.

Introduction

The fluorescence of benzene in the gas phase, by excitation to the first singlet state ($^1B_{2u}$), has been the subject of many papers. Less work has been done on the fluorescence of benzene in solutions.

Investigations led to different quantum yields of the fluorescence in the gas phase in the range 0.18–0.4.^{1–7} Parmenter and White⁶ found that there is a dependence on pressure at very low pressures. Pressure dependence of the quantum yield ceases on approaching about 10 Torr.^{4,5} Noyes, Mulac, and Harter² determined that at pressures around 10 Torr the absolute value is 0.18 independent of pressure, at approximately 2530 Å.

Several workers have found, using different methods, experimental fluorescence lifetimes in the range of 60–80 nsec, independent of pressure up to 40 Torr.^{8–10} Selinger and Ware¹¹ have found that by excitation to a single vibronic level the fluorescence lifetime depended on pressure up to 0.1 Torr and depended also on the vibrational level to which the molecule was excited.

The fluorescence yield depends on the wavelength of the exciting light. Noyes, Mulac, and Harter² showed that below about 250 nm the gas-phase yield begins to decrease. Braun, Kato, and Lipsky obtained a decrease in solution¹² below about 230 nm.

In apolar solutions Ivanova, *et al.*,¹³ calculated the fluorescence lifetimes. Direct measurement of the experimental lifetime has been carried out by Berلمان¹⁴ in cyclohexane. Both found that there is significant quenching of the lifetime by oxygen at atmospheric pressure; the rate constant of quenching is close to diffusion controlled.¹³

Eastman¹⁵ investigated the effect of some solvents and of temperature on the quantum yield in solutions. Gregory and Helman¹⁶ determined the temperature dependence of the benzene monomer and excimer fluorescence in methylcyclohexane solutions.

In the present work we have measured fluorescence lifetimes of benzene in polar and apolar solvents, varying temperatures, exciting wavelength, and O₂ pressure in an attempt to try and understand the mechanism of radiative

and radiationless processes of the benzene molecule in solution. The results relate to our work¹⁷ on the photochemistry of benzene in aqueous solution on excitation into the ${}^1B_{2u}$ and ${}^1B_{1u}$ bands¹⁸ and in apolar solvents into the ${}^1B_{2u}$ band.¹⁹

Experimental Section

Apparatus. Absorption spectra were measured with a Cary 14 recording spectrophotometer.

Lifetime measurements were carried out with the aid of flash equipment similar to that described by Berlan.¹⁴ This equipment consisted of a nanosecond light pulser (TRW Instrument) with deuterium lamp (flash lifetime about 2 nsec), monochromator (Jarrel-Ash Model 82-410), oscilloscope (Tektronix 535A with a 1S1 Sampling unit), photomultiplier Philips (DUPV 56), a special measurement cell for fluorescence with a path length of 1 cm (made by Thermal Syndicate); a filter (Corning 0-53) to cut off the scattered light from the exciting source, a computer of average transients (TMC, CAT 400), and an X-Y recorder (Electro Instruments No. 520).

Static spectrophotofluorimetric measurements were carried out using a Turner 210 instrument, compensated both at the exciting and emitted wavelength.

Unless stated otherwise, experiments were carried out at $23 \pm 2^\circ$.

Materials and Solutions. Benzene was Fluka 99.93%. The water used was triple distilled. All other solvents were made by Fluka and were of spectrograde quality. These were tested to ensure that there was no fluorescence by excitation at wavelengths above 200 nm. To remove oxygen, solutions were treated through alternate freeze-thaw cycles until a pressure of less than 10^{-4} Torr of O_2 was present in the gas phase in equilibrium with the solution. Oxygen was introduced into the appropriate solutions after they had been evacuated. The solubility of oxygen was taken as 8% less than the values given by Bowen and Williams²⁰ at atmospheric pressure.

Calculation of Lifetimes. Natural lifetimes τ_0 were estimated by numerical integration of the absorption spectrum to the first singlet excited state in the range 271–225 nm. The spectrum was encoded point by point (about 300 points for the entire range) into punched cards for computation. The value of τ_0 was found using the Förster equation²¹

$$1/\tau_0 = \frac{8\pi 10^3 n^2 c \ln 10}{N_0} \int_{\nu_{00}}^{\nu'} \frac{(2\nu_{00} - \nu)^3}{\nu} \epsilon(\nu) d\nu$$

where n is the refractive index; c , the velocity of light; N_0 , Avogadro's number; ν , the frequency; ν_{00} , the frequency of the vibrational transition $0 \rightarrow 0$; ν' , the frequency at the high-energy limit of the band; and ϵ , the extinction coefficient.

The experimental lifetime was calculated with the aid of the convolution integral

$$R(t') = \int_0^{t'} Y(t)P(t' - t) dt$$

where $R(t')$ is the intensity of fluorescence at a particular time (t'); $Y(t)$, the response function of the system; and $P(t' - t)$, the fluorescence decay function of the system.

In all of the measurements the response of the system was exponential corresponding to first-order (or pseudo-first-order) decay

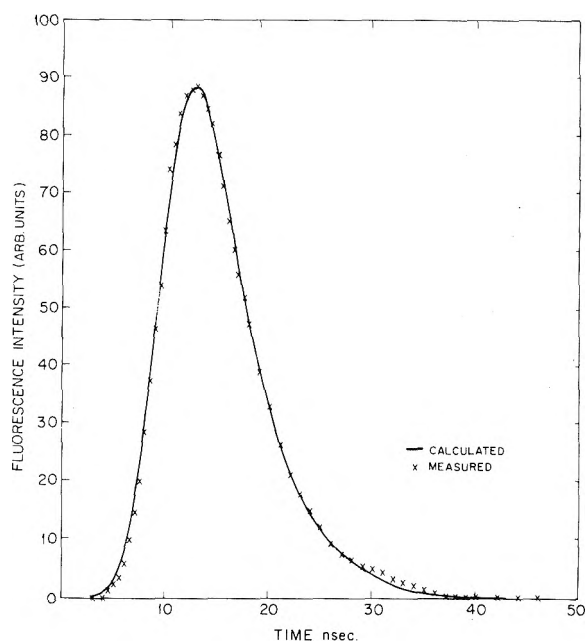


Figure 1. Experimental points and the calculated curve in the fluorescence lifetime measurements of benzene in cyclohexane in the presence of $1.5 \times 10^{-2} MO_2$, $T = 23 \pm 2^\circ$.

$$P(t' - t) = e^{-(t' - t)/\tau}$$

therefore

$$R(t') = e^{-t'/\tau} \int_0^{t'} Y(t)e^{t/\tau} dt$$

$Y(t)$ was determined graphically for each series of experiments using the lifetime flash system with a suitable reflecting mirror in place of the experimental solution.

The values of $R(t)$ and $Y(t)$ were fed into a 6400 CDC computer to determine the value of τ which would give the minimum deviation between the experimental and the calculated curves. One representative example of the good correspondence between calculated and measured results is shown in Figure 1.

Results

Our experimental results for the natural and experimental lifetimes of benzene in solutions at room temperature and some published results in the gas phase are shown in Table I. The absorption spectra in water and cyclohexane are compared in Figure 2.

It can be seen from Table I that there are differences between the extinction coefficients $\epsilon(\nu)$ in the various solvents. However the value of the integral appearing in the Förster equation,²¹ which is proportional to the area under the absorption curve, is almost the same for all solvents. The differences of the natural lifetimes in various solvents are only due to the differences in the refractive indices of the solvents.

Table I also shows that the experimental lifetimes are greatly influenced by the molecular nature of the medium. The lifetime is reduced by a factor of 15 going from an apolar solvent (cyclohexane or isooctane) to water. Differences in respective refractive indices do not greatly affect the experimental lifetimes (cyclohexane vs. isooctane). Viscosity too does not sharply affect experimental lifetimes (propylene glycol vs. ethanol).

In the case of some other solutes the differences in the

TABLE I

Solvents	Natural lifetimes ^a			Experimental lifetimes				
	$\epsilon, M^{-1} \text{ cm}^{-1}$ ($\pm 2\%$)	$\text{In}^c \times 10^{-14}$ ($\pm 3\%$)	τ_0, nsec ($\pm 3\%$)	τ, nsec	Quantum yield	$k_r \times 10^{-6}, \text{sec}^{-1d}$	$k_{nr} \times 10^{-7}, \text{sec}^{-1d}$	λ_{exc}, nm
Water	179	4.01	489	2.0 ± 0.2	0.0041	2.04	49.8	254
Heavy water	180	4.05	486	3.1 ± 0.3	0.0064	2.06	32.1	254
Acetonitrile	225	4.13	465	14.1 ± 0.5	0.032	2.15	7.8	254
Ethanol	242	4.13	455	10.9 ± 0.5	0.024	2.20	9.0	254
Propylene glycol	242	4.14	410	13.8 ± 0.5	0.030	2.44	7.0	254
Cyclohexane	247	4.11	413	29.5 ± 0.7	0.071	2.42	3.2	254
Isooctane	247	4.09	435	29.3 ± 0.7	0.067	2.30	3.2	254
Gas phase								
0.1 Torr			410	90 ± 4	0.22	2.4	0.87	266.2
			296	80 ± 3	0.27	3.4	0.91	259.0
			270	68 ± 2	0.25	3.7	1.1	253.0
Gas phase				72				Independent
50 Torr								of wave-
								length
								266.2–
								247.4 nm

^a Results taken from ref 7 and 11. τ_0 calculated by us from their results. ^b Extinction coefficient at the maximum of the A_1^0 band, λ_{max} varies slightly with solvent (~ 253 nm). ^c In represents the integral in the Förster equation. ^d $k_r = 1/\tau_0$; $k_{nr} = (1/\tau) - (1/\tau_0)$.

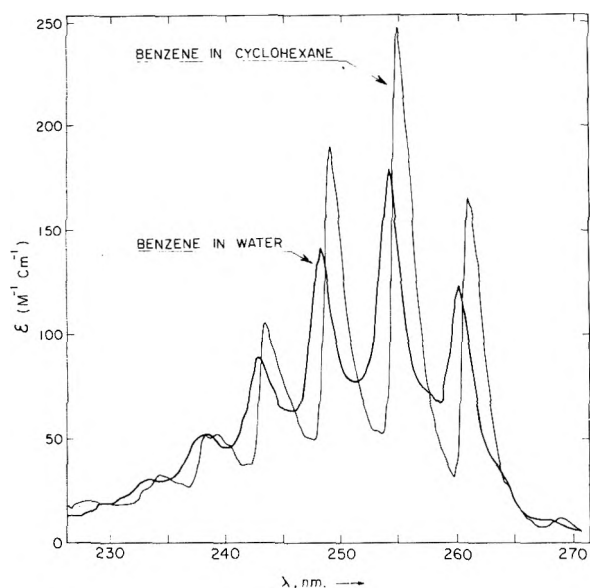


Figure 2. Absorption spectrum of benzene in water, ϵ_{254} 178, and in cyclohexane, ϵ_{254} 247.

experimental lifetimes in polar and apolar solvents are not so large. For example, in the case of β -naphthol τ (cyclohexane) = 14 nsec while τ (H_2O) = 8 nsec.²² The decrease of the experimental lifetime for benzene in H_2O is especially strong, indicating an efficient interaction between the excited benzene molecules and water. This is not in conflict with the known fact that the spectroscopic interaction between solvent molecules and benzene is weaker in water than in, e.g., cyclohexane.²³ The electronic transition occurs in $\sim 10^{-15}$ sec; the interaction of the water molecules with the benzene molecule excited above the fluorescent level lasts 10^{-12} sec, in competition with the internal conversion process.¹⁷ It can occur readily in $\sim 10^{-9}$ sec, interacting with the fluorescent level thus decreasing the experimental lifetime.

Spectroscopic data reveal little difference between the behavior of benzene in heavy or light water. We also found that there is no discernible difference in the photochemical

yields. There is, however, 50% difference between the experimental lifetimes, indicating that the processes responsible for the isotope effect have constants of the same order as the lifetimes. The values of τ , compared between ethanol and cyclohexane, indicate the effect of going from a polar hydroxylic to a nonpolar solvent.

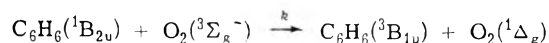
We carried out experiments in which the molecules were excited with excitation bands centered on different wavelengths. No dependence of experimental lifetimes on the wavelengths of the exciting light could be found using light centered at 260.5, 254.5, and 249 nm. These experiments on the effect of exciting wavelengths were carried out in water and in cyclohexane. No effect was found in either solvent.

From the results of Selinger and Ware¹¹ we calculated the natural lifetimes in the gas phase (Table I). It can be seen that on excitation to the lowest vibrational level in the gas phase the natural lifetime is similar to that in solution on excitation into the various bands. This further shows that in solution there is efficient vibrational relaxation in the $^1B_{2u}$ state before the emission of fluorescence, while in the gas phase emission occur before vibrational relaxation. On decreasing the exciting wavelength, we observed below ~ 240 nm an abrupt decrease in the fluorescence yield.

Variation of pH between 1 and 13 did not affect fluorescence in aqueous solution. The absorption²⁴ and emission spectra¹⁷ are independent of pH in this range. Although the H^+ and OH^- ions do not affect the radiative process in benzene, they do influence the photochemical processes.¹⁷

Effect of O_2 . Oxygen at 1-atm pressure did not affect the lifetime of benzene in water. This is as expected since $k(\text{C}_6\text{H}_6 + \text{O}_2) \sim 2 \times 10^{10} \text{ M}^{-1} \text{ sec}^{-1}$, $k_{rad} \sim 2 \times 10^{-6} \text{ sec}^{-1}$, and the oxygen concentration at 1 atm is $1.2 \times 10^{-3} \text{ M}$. In this case, the decrease of experimental lifetime would be less than 0.1 nsec and would not be observable with our experimental set-up.

The quenching of fluorescence by oxygen was measured in cyclohexane. Similar results were also obtained in hexane and isooctane. The probable quenching mechanism is²⁵



Plotting $1/\tau$ as a function of the oxygen concentration (Figure 3) gives a straight line with slope k . From Figure 3 we

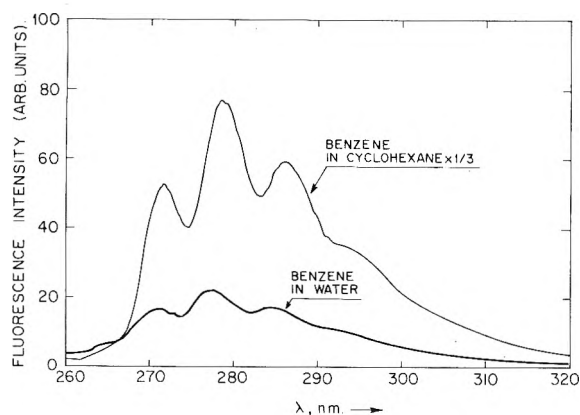


Figure 3. Fluorescence spectrum of benzene in water and in cyclohexane. The fluorescence in cyclohexane is measured on a scale reduced by a factor of 3.

see that $k = 1.85 \times 10^{10} M^{-1} \text{sec}^{-1}$. Plotting the Stern-Volmer constant $K_{sv} = \tau_0(1/[Q])(\tau_0/\tau) - 1$ as a function of $1/[O_2]$ also gives a straight line with zero slope (upper section of Figure 3), confirming Stern-Volmer kinetics.

The Role of Water and of Cyclohexane in Determining the Yield of the Fluorescent Level. Our photochemical experiments¹⁷⁻¹⁹ indicated that the influence of the solvent on the fluorescence yield may occur in two stages: first, in competition with the loss of excess vibrational energy, which occurs in $<10^{-9}$ sec from the vibrationally energy-rich primary spectroscopic state (resulting on light absorption) to the 0-0 vibrational fluorescent level of the ${}^1B_{2u}$ first singlet excited state; second, during the lifetime, $>10^{-9}$ sec, of the fluorescence emitting level. Solutions of benzene ($\sim 10^{-2} M$) in water or in cyclohexane, in the absence of O_2 , were now investigated both under steady illumination and in the flash-lifetime apparatus. In both solvents the exciting light was centered at 254 nm, in a relatively broad band, so that the areas under the two absorption curves were equal (Figure 2).

The fluorescence spectra under steady illumination are shown in Figure 4. From the areas under the curves we obtained the respective fluorescence yields by numerical integration using trapezoidal subdivisions over the wavelength range. The ratio cyclohexane:water was found to be 10:1.

Next, we similarly integrated the areas under the lifetime curves, thus obtaining again the respective fluorescent yields. The ratio cyclohexane:water was found to be 10:1.

The ratio between the experimental fluorescence lifetimes is $\sim 15:1$ (29.5 nsec in cyclohexane, ~ 2 nsec in water). Since in water there is 10 times less fluorescence obtained in 15 times less time, the rate of emission in water is a factor of $\frac{3}{2}$ greater than in cyclohexane. The rate of emission is proportional to the number of molecules reaching the fluorescent level, which is thus 1.5 times greater in water than in cyclohexane.

One possible explanation is that water is a slightly better medium for energy loss during fast internal conversion than cyclohexane, thus facilitating the formation of the lowest vibrational level from the nonrelaxed levels of the first excited singlet state, in competition with other processes occurring from the energy-rich nonequilibrium levels reached by light absorption. In cyclohexane the time of residence in energy levels above the lowest vibrational is longer, so that radiationless transitions from these may occur more effectively.

Though the agreement between results obtained from

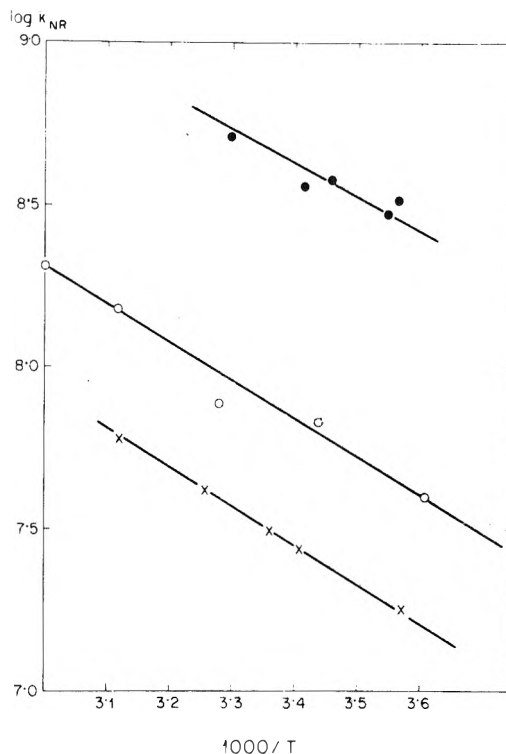


Figure 4. Dependence of the logarithm of the nonradiative rate constant $k_{nr} = 1/\tau - 1/\tau_0$ on the reciprocal of temperature according to the Arrhenius equation for solutions of benzene in (X) isooctane, (O) acetonitrile, and (●) D_2O .

fluorescence yields and lifetimes is good, the considerations in this section are qualitative rather than exact.

The Dependence of Fluorescence Lifetime on Temperature. Eastman¹⁵ has investigated the energy of activation of fluorescence intensity quenching in various solvents. Gregory and Helman¹⁶ have done the same in methylcyclohexane. Cundall and Pereira²⁶ have very recently reinvestigated these systems. To correlate our results with theirs we determined the fluorescence lifetimes in $1 \times 10^{-2} M$ solutions of benzene in isooctane over the range 6-48°. Above 2° at this concentration, excimer emission is not observed.¹⁵ Table II shows our results and the nonradiative rate constants calculated from $\tau/\tau_0 = \phi = k_r/(k_r + k_{nr})$, with the assumption that the radiative rate constant is unaffected by temperature. The standard deviation in determining τ was $\pm 2\%$.

Figure 5 shows $\log k_{nr}$ as a function of $1/T$, giving $E_a = 5.5 \pm 0.5$ kcal/mol for the activation energy. This is lower than the value obtained by Eastman¹⁵ in nonpolar hexane, but agrees well with the value found by Gregory and Helman¹⁶ in methylcyclohexane. Figure 5 also shows our results in acetonitrile, giving $E_a = 5.4$ kcal/mol. Our results in D_2O , also shown in Figure 5, are much less accurate since the lifetimes at higher temperatures are at the limit of our instrumental capacity. They yield $E_a \sim 5$ kcal/mol.

Discussion

The results on fluorescence lifetimes relate to the fate of the radiative level(s) of benzene, *i.e.*, the lowest vibrational level of the ${}^1B_{2u}$ first excited state (and also possibly levels close to it energetically, and in thermal equilibrium with it).

We find that the natural lifetime of benzene, calculated from its spectrum, is little affected by the nature of the sol-

TABLE II: Effect of Temperature on Fluorescent Lifetime in $1 \times 10^{-2} M$ Solutions of Benzene in Isooctane

$T, ^\circ K$	τ, nsec	$10^7 k_{nr}, \text{sec}^{-1}$
279	49.8	1.8
293	32.8	2.8
297	29.3	3.2
307	22.3	4.3
321	16.1	6.0

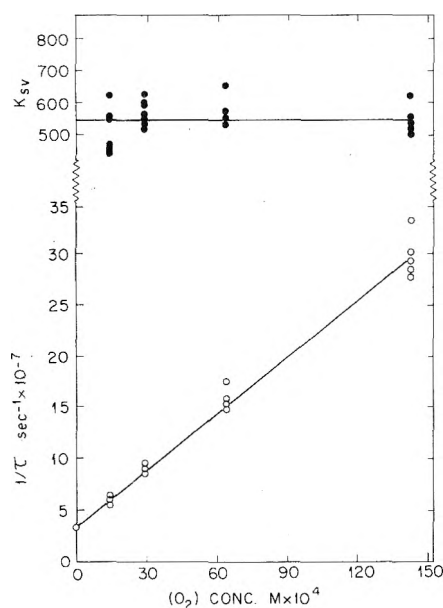


Figure 5. Quenching of fluorescence by O_2 . The lower line shows the reciprocal of the fluorescence lifetime against O_2 concentration, the upper line is a Stern-Volmer constant as a function of O_2 concentration.

vent. The experimental lifetime is strongly solvent dependent. The nonradiative rate constant, k_{nr} , calculated from the lifetime at a certain temperature increases with the polarity of the solvent in the series isooctane < acetonitrile < D_2O .

The apparent energy of activation E_a of the process characterized by the overall nonradiative rate constant appears to be independent of, or only weakly affected by, the nature of the solvent and thus a function of the properties of the benzene molecule itself.

Our present results on the temperature and solvent dependence of fluorescence lifetime of benzene correlate well with and extend some of the results in the literature.^{16,26,27} Cundall^{26,27} has in particular discussed the relationship of such results to the decay of the 1S state to the 1T state (and product(s) derived from it), as well as to the 0S ground state. We have shown, in an investigation of the photochemistry of benzene in aqueous solution,¹⁷ that the main photochemical product (a cyclopentadienyl derivative) is related to the isomerization reaction of excited benzene and originates in the energy-rich state preceding thermal equilibrium and preceding the formation of the fluorescent level. Thus this photochemistry arises in competition with internal conversion, thermalization, or a time scale of $\sim 10^{-12}$ sec. Our evidence for this was the following. Excitation at 228 nm is at a wavelength in the $^1B_{2u}$ lowest excited singlet state which conveys into the molecule sufficient excess vibrational energy so that the excited molecule does not convert internally to the fluorescent level effectively.

Photochemistry results, nevertheless quantitatively as in the region of the $^1B_{2u}$ band, above ~ 235 nm, where efficient fluorescence also occurs.

In two more recent investigations we have confirmed and extended these conclusions. We have shown in aqueous solutions of benzene¹⁸ that excitation into the $^1B_{1u}$ second excited singlet state at 214 nm also gives the photochemical product hydroxycyclopentadienyl aldehyde in somewhat higher yield as excitation over the $^1B_{2u}$ first excited singlet band. Yet the primary state resulting on absorption of 214-nm light does not effectively convert into the fluorescent level.

The use of aerated aqueous solutions enabled us to obtain an easily determined stable product. However this special feature of the strongly polar solvent allowed the possibility that the phenomenon is not general. We have now investigated the photochemistry of benzene in nonpolar (cyclohexane) solution¹⁹ and shown that the photochemical product of isomerization, benzvalene, arises here too from the prethermal equilibrium state. Its initial yield, $\sim 18\%$, is approximately equal to that of the product in oxygenated aqueous solutions, 19%.

Both in polar and nonpolar solvents the initial yield of the product was independent of temperature within experimental error. This fact indicates that in the case of the highly symmetrical benzene molecule, those nonsymmetrical vibrationally energy-rich electronic excited states, which are required for the isomerization, are not preferentially accessible by reversible thermal promotion from the fluorescent, e.g., zero vibrational state. The out-of-plane distortion of the strictly planar benzene molecule more readily occurs from the spectroscopically prepared state rich in nonsymmetrical vibrational energy.

According to our experiments, thermal promotion, leading to the depopulation of the fluorescent levels, does not efficiently lead to the photochemical isomerization pathway. It may lead to the pathway responsible for the abrupt decrease of fluorescence below ~ 240 nm, which, as we have shown, does not correlate with the preequilibrium photochemistry.

Thus for the special case of benzene, its high symmetry determines the accessibility of the photochemical path through light absorption preferentially.

That symmetry properties are paramount in determining the photochemical pathway, from the $^1B_{2u}$ or higher singlet states, is shown in our results on monofluorobenzene which is nontotally symmetrical in its ground state.²⁸ There the photochemical isomerization product appears to be more readily accessible through thermally promoted vibrational states.

Acknowledgment. This research was supported by the Israel Academy of Sciences. We thank Drs. R. B. Cundall and H. Lutz for valuable discussions and help, and Dr. W. A. Noyes, Jr., for important comments.

References and Notes

- (1) G. B. Kistiakowsky and C. S. Parmenter, *J. Chem. Phys.*, **42**, 2942 (1965).
- (2) W. A. Noyes, Jr., W. A. Mulac, and D. A. Harter, *J. Chem. Phys.*, **44**, 2100 (1966).
- (3) J. A. Poole, *J. Phys. Chem.*, **69**, 1343 (1965).
- (4) E. M. Andersen and G. B. Kistiakowsky, *J. Chem. Phys.*, **48**, 4778 (1968).
- (5) A. E. Douglas and C. W. Mathews, *J. Chem. Phys.*, **48**, 4788 (1968).
- (6) C. S. Parmenter and A. H. White, *J. Chem. Phys.*, **50**, 1631 (1969).

- (7) (a) C. S. Parmenter and M. W. Schuyler, *Chem. Phys. Lett.*, **6**, 339 (1970); (b) C. S. Parmenter, M. W. Schuyler, W. R. Ware, and B. K. Selinger, *ibid.*, **6**, 343 (1970).
 (8) G. M. Breuer and E. K. C. Lee, *J. Chem. Phys.*, **51**, 3130, 3615 (1969).
 (9) M. Nishikawa and P. R. Ludwig, *J. Chem. Phys.*, **52**, 107 (1970).
 (10) C. S. Burton and H. E. Hunziker, *J. Chem. Phys.*, **52**, 3302 (1970).
 (11) B. K. Selinger and W. R. Ware, *J. Chem. Phys.*, **52**, 5482 (1970); **53**, 3160 (1970).
 (12) C. L. Braun, S. Kato, and S. Lipsky, *J. Chem. Phys.*, **39**, 1645 (1963).
 (13) T. V. Ivanova, G. A. Mokeeva, and B. Y. Sveshnikov, *Opt. Spectrosc.*, **12**, 352 (1962).
 (14) I. B. Beriman, "Handbook of Fluorescence Spectra of Aromatic Molecules," Academic Press, New York, N. Y., 1965.
 (15) J. W. Eastman, *J. Chem. Phys.*, **49**, 4617 (1968).
 (16) T. A. Gregory and W. P. Helman, *J. Chem. Phys.*, **56**, 377 (1972).
 (17) M. Luria and G. Stein, *Chem. Commun.*, 1650 (1970); *J. Phys. Chem.*, **76**, 165 (1972).
 (18) Y. Ilan, M. Luria, and G. Stein, to be submitted for publication.
 (19) H. Lutz and G. Stein, **78**, 1909 (1974).
 (20) E. J. Bowen and A. H. Williams, *Trans. Faraday Soc.*, **37**, 765 (1939).
 (21) Th. Förster, "Fluoreszenz Organischer Verbindungen," Göttingen, 1951.
 (22) M. Ofan and G. Stein, unpublished results.
 (23) M. J. Mantione and J. P. Dandey, *Chem. Phys. Lett.*, **6**, 93 (1970).
 (24) D. G. Marketos, *Anal. Chem.*, **41**, 195 (1969).
 (25) A. Morikawa and R. J. Cvetanović, *J. Chem. Phys.*, **52**, 3237 (1970).
 (26) R. B. Cundall and L. C. Pereira, *J. Chem. Soc., Faraday Trans. 2*, **68**, 1152 (1972).
 (27) R. B. Cundall and D. A. Robinson, *J. Chem. Soc., Faraday Trans. 2*, **68**, 1145 (1972).
 (28) Y. Ilan, H. Lutz, and G. Stein, to be submitted for publication.

Photolysis of Benzene in Cyclohexane at 2537 Å

Hanspeter Lutz and Gabriel Stein*

Department of Physical Chemistry, The Hebrew University, Jerusalem, Israel (Received December 29, 1972; Revised Manuscript Received June 3, 1974)

Publication costs assisted by the Israel Academy of Sciences

Initial quantum yields of benzvalene formation in the 2537-Å photolysis of benzene in dilute cyclohexane solutions in the absence of oxygen were determined using an analytical method based on the reaction of benzvalene with bromine. The rate of formation of benzvalene is discussed in terms of a kinetic model which involves the reaction of triplet benzene with benzvalene. The initial quantum yield of benzvalene is 0.18. This value is nearly independent of temperature in the 9–50° range. The results are consistent with the view that benzvalene arises from the spectroscopically prepared higher vibronic state prior to vibrational relaxation to the fluorescent level.

Introduction

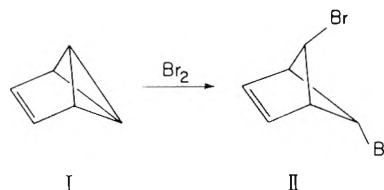
In recent years considerable experimental and theoretical effort has been directed to the study of the radiationless processes occurring in benzene. For this molecule, excited in dilute hydrocarbon solution to its $^1B_{2u}$ first excited singlet state, fluorescence and triplet state formation only account for about 30% of the total energy input.¹ It has been suggested that part of the electronic energy in excited benzene is converted into chemical potential by way of valence bond isomerization. Direct evidence for such chemical relaxation of electronic energy has been provided by the observation of benzvalene (I) in the 2537-Å photolysis of benzene in hexadecane solution.² Several authors have tentatively related this isomerization reaction producing benzvalene to the thermally activated fluorescence quenching of benzene.^{3–5} A difficulty with this interpretation is that no detailed studies of the kinetics of benzvalene formation and its temperature dependence have been reported. The quantum yield for formation of benzvalene in hexadecane solution at 2537 Å has been determined by gas chromatography to be 0.020.^{2,6} The yield of benzvalene was reported to increase with temperature, however, no quantitative results have been given. Another determination based on the photochemical rearrangement of benzene-*1,3,5-d*₃ in hexadecane solution at 2537 Å gave a value of 0.051 for the

quantum yield of the benzvalene intermediate assumed for this rearrangement.

In order to learn more about the mechanism of benzvalene formation and its relation to the spectroscopic properties of benzene we have undertaken a detailed study of the initial quantum yield of benzvalene formation in cyclohexane solution and its dependence on temperature. The amount of benzvalene formed in irradiated benzene solutions in the present study was determined by an analytical method based on the specific uptake of bromine by the benzvalene molecule.

The bromination of benzvalene has recently been studied in some detail by Rot₁ and Katz.⁷ These authors have observed that benzvalene (I) adds bromine, as shown in Scheme I, to form one single product, identified as 5,6-dibromobicyclo[2.1.1]hex-4-ene (II). The reaction has been shown to occur quantitatively. Interestingly, the olefinic

Scheme I



double bond, the usual site of electrophilic attack, remains unaffected during the bromination. We used this reaction to determine benzvalene in irradiated benzene solutions by measuring the amount of bromine consumed by the photolysis mixture and assuming that one molecule of photoproduct consumes 1 molecule of Br_2 . In our determination we used an ethanol solution of Br_3^- as brominating agent. The bromination was followed spectrophotometrically using the high absorption coefficient of the tribromide ion in the ultraviolet. In this way benzvalene concentrations as low as $10^{-5} M$ could be determined.

Benzvalene has been reported to be the only major photoproduct in the photolysis of benzene in dilute hydrocarbon solutions at 2537 \AA .² Fulvene, also reported to be formed, is a secondary product arising from benzvalene. Prolonged irradiation of very concentrated solutions of benzene in hexane results in a complex mixture of reaction products, most of them arising from reactions of the hexatrienyl radical.⁸ For the present study we accordingly assumed that the first stable photoproduct is only benzvalene. We report further support for this assumption. In order to obtain initial quantum yields for the benzvalene formation, we carried out the irradiations at low light intensities ($2 \times 10^{-6} \text{ einstein l}^{-1} \text{ sec}^{-1}$) and short irradiation times (up to 8 min). In addition, the benzene concentration was chosen sufficiently low ($0.01 M$) to avoid participation of singlet excimers in the photoreaction and prevent increase of triplet yield through excimer formation.⁹

Experimental Section

Benzene Fluka puriss (99.93%) thiophene free was used without further purification. The solvents, cyclohexane (Fluka) and ethanol (Fluka), were of spectroscopic grade.

The uv light source was a low-pressure mercury resonance lamp (Thermal Syndicate Ltd.). The 1849-\AA line of the lamp was eliminated by a filter containing KCl (75 g l^{-1}) with an optical path length of 1 cm . The light intensity was about $2 \times 10^{-6} \text{ einstein l}^{-1} \text{ sec}^{-1}$ at 2537 \AA .

In a typical experiment, 4 ml of a solution of $0.01 M$ benzene in cyclohexane was degassed by three freeze-pump-thaw cycles. The solution was irradiated at 2537 \AA in a 1-cm square silica cell. After completion of the irradiation, 4 ml of a solution of approximately $1\text{--}2 \times 10^{-4} M$ bromine in ethanol- KBr ($\text{KBr } 1 \text{ g l}^{-1}$) was added to the photolysis mixture. A blank was simultaneously prepared by treating a nonirradiated benzene solution with an equal volume of the bromination agent. For experiments at different temperatures, the photolysis mixture was brought to room temperature before adding bromine. The consumption of Br_3^- in the irradiated sample was followed against the blank as reference on a Cary 14 spectrophotometer with the recording wavelength fixed at 300 nm .

Results

In irradiated solutions of benzene added bromine is consumed rapidly. This is shown by Figure 1 (curve a) where the change in optical density at 300 nm due to the Br_3^- disappearance is plotted vs. the reaction time. In the range of the benzvalene concentrations obtained in our experiments the bromination went to completion within about 20 min of the reaction. Consequently, we have calculated the benzvalene concentration from the amount of bromine consumed after 20 min of the bromination reaction. Since the exact value of the extinction coefficient of the tribromide complex at 300 nm in a cyclohexane-ethanol mixture has not been reported, we calibrated our bromometric method

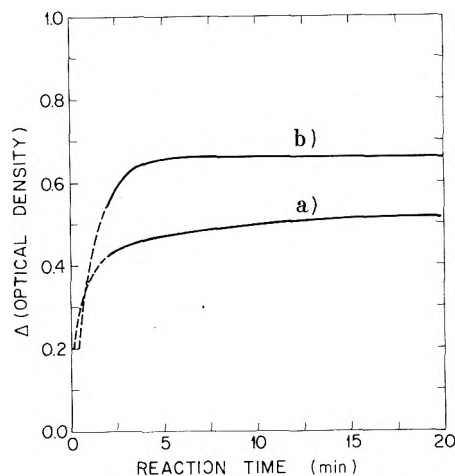
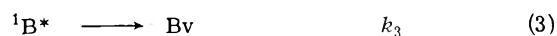
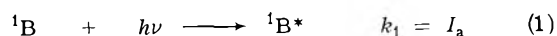


Figure 1. Change in optical density as a function of time for the reaction of brominating solution: (a) with a solution of $0.01 M$ benzene in cyclohexane irradiated at 2537 \AA with a dose of $1.74 \times 10^{-3} \text{ einstein l}^{-1}$ at 23° ; (b) with a solution of $9.64 \times 10^{-5} M$ cyclopentene in cyclohexane.

against a solution of cyclopentene as standard. We obtained a value of $13,700 M^{-1} \text{ cm}^{-1}$ for the extinction coefficient of Br_3^- at 300 nm in a 1:1 mixture of cyclohexane-ethanol. A typical curve showing the uptake of bromine by a solution of $9.64 \times 10^{-5} M$ cyclopentene in cyclohexane is given in Figure 1b. On the basis of the findings of Roth and Katz⁷ that 1 mol of bromine adds quantitatively to 1 mol of benzvalene, we equated the loss of Br_3^- to the concentration of benzvalene initially present in the irradiated solution. The detailed kinetics in the bromination system are likely to be complex.⁷ We have not established the nature of the product, but use the method as one giving a reproducible end point.

Figure 2 represents the concentration of benzvalene determined in the irradiated solutions by the above method as a function of light dose at three different temperatures. It is seen that initially, at low light doses, benzvalene is formed at a high rate, which decreases at higher light doses. In addition, it is seen that the overall yield of benzvalene increases with temperature. There is a large experimental error at low doses and much better reproducibility at higher ones.

We found that the experimental observations could be interpreted by the following reaction scheme for the benzvalene formation



Here, reaction 1 represents excitation to a higher vibrational level of the ${}^1\text{B}_{2u}$ electronic state. I_a is the absorbed light intensity. Process 2 represents all decay pathways, radiative and nonradiative, of the initially excited level other than benzvalene formation (reaction 3) and intersys-

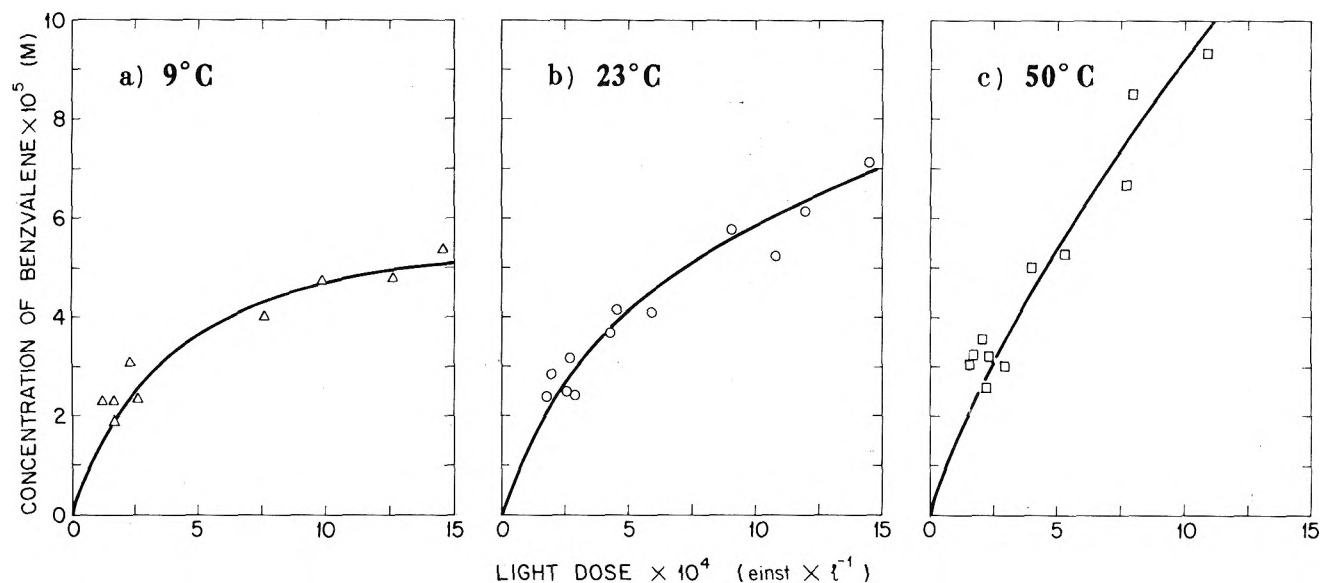


Figure 2. Formation of benzvalene in an oxygen-free solution of 0.01 M benzene irradiated at 2537 Å in cyclohexane as a function of light dose at 9, 23, and 50°. Curves are computer-drawn best fits to the experimental data using the kinetic scheme as described in the text.

tem crossing to $^3B^*$ (reaction 4). Expression 5 accounts for all decay processes of triplet benzene $^3B^*$ other than reaction 6, which represents the triplet sensitized disappearance of benzvalene.

Triplet sensitized disappearance of benzvalene has been observed by Kaplan and Wilzbach in the gas-phase photolysis of benzene at 2537 Å.¹⁰ These authors reported a marked enhancement of the benzvalene production when benzene vapor is irradiated at 2537 Å in the presence of added gases which quench triplet benzene and facilitate the vibrational relaxation of "hot" benzvalene. In the absence of triplet quenchers only traces of benzvalene were formed and no evidence for the formation of other photo-products which may arise from the triplet sensitized destruction of benzvalene has been reported. These observations are consistent with previous findings that benzene vapor is virtually inert to irradiation at 2537 Å.¹¹ We assume that such triplet sensitized disappearance of benzvalene also occurs in dilute hydrocarbon solutions.

According to the above reaction scheme the differential equation describing the formation of benzvalene is

$$d[Bv]/dt = I_a \phi_{Bv} - k_6 [^3B^*][Bv] \quad (7)$$

where ϕ_{Bv} is the initial quantum yield of benzvalene formation according to reaction 3.

Similarly, the kinetic equation expressing the benzene triplet state concentration takes the form

$$d[^3B^*]/dt = I_a \phi_T - k_5 [^3B^*] - k_6 [^3B^*][Bv] \quad (8)$$

here, ϕ_T represents the quantum yield of the intersystem crossing.

Since reaction 5 is fast (*vide infra*) we can use the stationary state hypothesis for the benzene triplet concentration and put the right-hand side of eq 8 equal to zero. The stationary concentration of $^3B^*$ is then given by

$$[^3B^*]_{\text{stationary}} = I_a \phi_T / (k_5 + k_6 [Bv]) \quad (9)$$

Introducing this result in eq 7 we obtain

$$\frac{d[Bv]}{dt} = I_a \phi_{Bv} - \frac{I_a \phi_T (k_6/k_5) [Bv]}{1 + (k_6/k_5) [Bv]} \quad (10)$$

This differential equation contains the two unknown parameters ϕ_{Bv} and (k_6/k_5) . In order to determine the values of these parameters eq 10 was solved analytically and the integrated function fitted to the experimental data on a 6400 CDC computer using a least-squares curve-fitting program. Values for the triplet quantum yield (ϕ_T) at the three temperatures of our experiments have been taken from data published by Cundall and Robinson.^{12,13} The full line curves given in Figure 2 are the computer drawn representations of the integrated functions which fit best to the experimental data sets obtained at 9, 23, and 50°, respectively. The corresponding adjusted parameters ϕ_{Bv} and (k_6/k_5) are given in Table I. Figure 3 shows the quantum yields of benzvalene as a function of light dose calculated from the data in Table I. It shows that the initial quantum yield of benzvalene formation does not depend on temperature. It appears that the observed temperature enhancement of benzvalene formation at finite doses can be fully ascribed to its triplet sensitized disappearance. The triplet sensitized destruction of benzvalene is expected to be reduced at higher temperatures since the triplet state is decreased with increasing temperature.

Discussion

Previous studies on the mechanism of benzvalene formation have indicated that benzvalene is not derived directly from the fluorescent state but that it must come, on a very short time scale, from upper vibrational levels of the $^1B_{2u}$ state.^{6,10} This conclusion has been drawn from the fact that the yield of benzvalene in the gas-phase photolysis of benzene increases with increasing energy of the exciting radiation while an opposite relationship is found for the fluorescence yield. That benzvalene does not arise from the lowest triplet state of benzene has been demonstrated by the observation of an increased benzvalene production in the presence of triplet quenchers.¹⁰

These conclusions derived from studies in the gas phase are consistent with our results in solution. Our experimental observation that the initial quantum yield of benzvalene is independent of temperature makes the possibility that the fluorescent level is responsible for the benzvalene formation less likely since the fluorescence yield decreases

TABLE I

Temp, °C	ϕ_T (ref 12, 13)	$\phi_{Bv}^{initial}$ (this work)	$(k_6/k_5), M^{-1}$
9	0.35	0.184	2.06×10^4
23	0.24	0.180	2.92×10^4
50	0.13	0.174	5.07×10^4

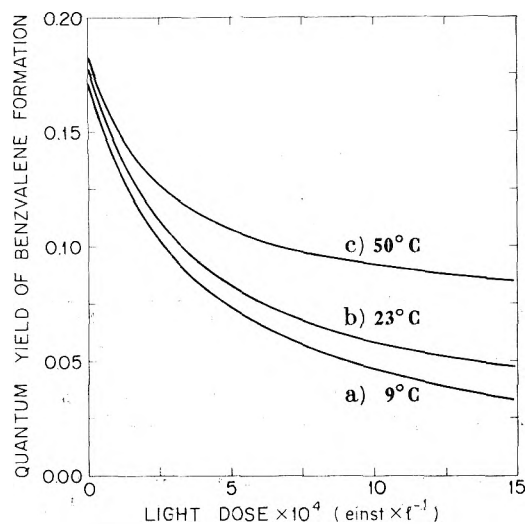


Figure 3. Quantum yields of benzvalene formation at 9, 23, and 50° as a function of light dose. Data calculated from computer-drawn best fit curves in Figure 2.

markedly with temperature.^{1,3-5,14,15} In addition, it appears that the overall benzvalene formation in cyclohexane is enhanced as the triplet formation is decreased at higher temperatures. The results derived from the bromination experiments shown in Figures 2 and 3 are subject to large experimental errors at low light doses and thus low bromine uptake. They are more accurate at higher doses. It is the good fit of the theoretical curves over the entire range and at three temperatures, using the same parameters, which gives support to the overall picture, though the extrapolated yields at zero dose may be subject to error.

The results of the present study correlate with the photochemical reactions occurring in oxygenated aqueous benzene solutions. The main photochemical product of the photooxidation of benzene in water,¹⁶ identified in alkaline solution as hydroxycyclopentadiene carboxaldehyde,¹⁷ has been shown to arise from addition of O₂ to a reactive intermediate which originates in the energy-rich state preceding thermal equilibrium and preceding the formation of the fluorescent level.^{18a} Evidence for the latter conclusion has been drawn from the fact that excitation at 229 and 214 nm gives the photooxidation product in slightly higher yield than excitation at 2537 or at 2650 Å.^{18a,19} Yet the primary state resulting on absorption at 229 or 214 nm does not efficiently convert into the fluorescent level.^{18a,20} The reactive intermediate was thought to be an isomer of ground-state benzene, *e.g.*, benzvalene, or the precursor from which this may arise.

Interestingly, the maximum quantum yield of the photooxidation product obtained in water solutions sufficiently saturated with oxygen is 0.19,^{18b} a figure very close to our value for the extrapolated initial quantum yield of benzvalene formation in cyclohexane. It appears that in water saturated with oxygen the precursor is efficiently trapped forming ultimately the oxidation product.^{18a} Similar quan-

tum yields in polar and nonpolar solvents indicate that the nature of the solvent has little or no effect on the formation of benzvalene. This result gives further support for the proposed mechanism in which benzvalene is formed in a pre-equilibrium state before solute-solvent interactions may occur. Since we postulate that benzvalene arises before interaction with the solvent, similar limiting initial yields would be expected in the gas phase. Noyes and Harter²¹ showed that, in the gas phase at pressures higher than 10 Torr the sum of ($\phi_F + \phi_T$), the quantum yields of fluorescence and triplet formation is about 0.80. This would then leave open the possibility of the quantum yield ϕ_{Bv} approaching 0.20.

As in our present case of the photoisomerization of benzene in cyclohexane the photooxidation of benzene in water has been found to be independent of temperature.^{18a,19} The temperature independent product yields observed in both cases indicate that for the highly symmetrical benzene molecule the energy-rich states responsible for the photoisomerization are less readily accessible by reversible thermal population from the fluorescent state. This would mean that benzvalene formation is not the result of the thermally activated quenching of benzene fluorescence. Other non-radiative relaxation processes must therefore be invoked to explain the inverse temperature dependence of the benzene fluorescence. A possible nonradiative channel from the ¹B_{2u} state is the thermally activated transition to a state such as that suggested by Callomon, Parkin, and Lopez-Delgado.²²

For the formation of benzvalene out of plane distortion of the benzene molecule is required. Benzene is planar in both the ground and fluorescent state.²³ The out of plane distortion in benzene appears to occur from electronic excitation into nontotally symmetrical vibrational levels above the fluorescent state, before relaxation. However, when a fluorine or methyl substituent is introduced in the benzene molecule, thus decreasing the symmetry, the photooxidation product in water appears to be accessible through thermally promoted vibrational states from the fluorescent level.²⁴

Table I gives the adjusted values for the ratio between the bimolecular rate constant for the triplet sensitized disappearance of benzvalene (k_6) and the rate constant for the unimolecular triplet decay (k_5). Assuming the reaction of triplet benzene with benzvalene to be diffusion controlled, the parameters in Table I allow an estimate of the lifetime of the benzene triplet in dilute cyclohexane solutions at the given temperatures. Using a value of $6.7 \times 10^9 M^{-1} \text{sec}^{-1}$ for the diffusion-controlled rate constant,²⁵ and the rate constant ratio, we get a triplet lifetime of about 4 μsec at 23°. This figure is in reasonable agreement with other estimates given in the literature. Sandros²⁶ estimated a triplet lifetime of 2 μsec and Lipsky²⁷ a value of 1 μsec in dilute cyclohexane solution. Recently, Cundall and Robinson¹³ presented evidence that the true triplet lifetime is in fact much shorter than these previously given estimates. If so, a longer lived species derived from triplet benzene would be responsible for the sensitized disappearance of benzvalene. However, further experimental details would be needed to explore this possibility.

Acknowledgment. We thank Professor H. J. G. Hayman for valuable advice and discussions. This work was supported by the Israel Academy of Sciences.

References and Notes

- (1) K. Sandros, *Acta Chem. Scand.*, **25**, 3651 (1971).
- (2) K. E. Wilzbach, J. S. Ritscher, and L. Kaplan, *J. Amer. Chem. Soc.*, **89**, 1031 (1967).
- (3) J. W. Eastman, *J. Chem. Phys.*, **49**, 4617 (1968).
- (4) W. P. Helman, *J. Chem. Phys.*, **51**, 354 (1969).
- (5) T. A. Gregory and W. P. Helman, *J. Chem. Phys.*, **56**, 377 (1972).
- (6) K. E. Wilzbach, A. L. Harkness, and L. Kaplan, *J. Amer. Chem. Soc.*, **90**, 1116 (1968).
- (7) R. J. Roth and T. J. Katz, *J. Amer. Chem. Soc.*, **94**, 4770 (1972).
- (8) K. H. Grellmann and W. Kühnle, *Tetrahedron Lett.*, 1537 (1969).
- (9) R. B. Cundall, L. C. Pereira, and D. A. Robinson, *Chem. Phys. Lett.*, **13**, 253 (1972).
- (10) L. Kaplan and K. E. Wilzbach, *J. Amer. Chem. Soc.*, **90**, 3291 (1968).
- (11) J. N. Pitts, Jr., J. K. Foote, and J. K. S. Wan, *Photochem. Photobiol.*, **4**, 323 (1965).
- (12) R. B. Cundall and D. A. Robinson, *Chem. Phys. Lett.*, **14**, 438 (1972).
- (13) R. B. Cundall and D. A. Robinson, *J. Chem. Soc., Faraday Trans. 2*, **68**, 1145 (1972).
- (14) R. B. Cundall and L. C. Pereira, *J. Chem. Soc., Faraday Trans. 2*, **68**, 1152 (1972).
- (15) R. B. Cundall and D. A. Robinson, *J. Chem. Soc., Faraday Trans. 2*, **68**, 1133 (1972).
- (16) E. Farenhorst, *Tetrahedron Lett.*, 4835 (1968).
- (17) M. Luria and G. Stein, *Chem. Commun.*, 1650 (1970).
- (18) (a) M. Luria and G. Stein, *J. Phys. Chem.*, **76**, 165 (1972); (b) submitted for publication.
- (19) Y. Ilan, M. Luria, and G. Stein, to be submitted for publication.
- (20) (a) C. L. Brauns, S. Kato, and S. Lipsky, *J. Chem. Phys.*, **39**, 1645 (1963); (b) M. D. Lumb, C. L. Braga, and L. C. Pereira, *Trans. Faraday Soc.*, **65**, 1992 (1969).
- (21) W. A. Noyes, Jr., and D. A. Harter, *J. Chem. Phys.*, **46**, 674 (1967).
- (22) J. H. Callomon, J. E. Parkin, and R. Lopez-Delgado, *Chem. Phys. Lett.*, **13**, 125 (1972).
- (23) T. M. Dunn in "Studies in Chemical Structure and Reactivity," J. H. Ridd, Ed., Methuen, London, 1966, p. 125.
- (24) H. Lutz, Y. Ilan, and G. Stein, to be submitted for publication.
- (25) P. J. Wagner and I. Kochevar, *J. Amer. Chem. Soc.*, **90**, 2232 (1968).
- (26) K. Sandros, *Acta Chem. Scand.*, **23**, 2815 (1969).
- (27) S. Lipsky, *J. Chem. Phys.*, **38**, 2786 (1963).

Ultrasonic Absorption in Aqueous Solutions of Calcium Acetate and Other Bivalent Metal Acetates

Gordon Atkinson,*¹ Mostafa M. Emara, and R. Fernández-Prini

Department of Chemistry, University of Oklahoma, Norman, Oklahoma 73069 (Received July 27, 1973; Revised Manuscript Received April 11, 1974)

Publication costs assisted by the National Science Foundation

Ultrasonic absorption measurements in aqueous solutions of calcium acetate in the concentration range 0.14–1.09 *M*, at various temperatures, show one relaxation for the low-concentration solutions and two for the high concentrations. On the basis of these measurements and analogous ones on Mg^{2+} , Ba^{2+} , and Ni^{2+} solutions, we conclude that the relaxations are due to the substitution of one or two waters in the inner coordination sphere of the Ca^{2+} ion by acetate. The scanty thermodynamic data available and the high concentration of some of the solutions hampered a thorough quantitative interpretation of the data. In magnesium and calcium acetate solutions more concentrated than 1.4 *M*, the ultrasonic absorption is not explicable in terms of discrete relaxation processes.

Introduction

Since Bazulin² measured ultrasonic absorption in aqueous zinc acetate solutions in 1939, many other acetate solutions have been studied by this technique. Stuehr and Yeager³ have summarized the results of ultrasonic investigations of aqueous acetate solutions. It may be concluded that (1) transition metal acetate solutions show an ultrasonic relaxation in the megahertz region due to a chemical process, (2) alkali metal acetate solutions show no significant excess sound absorption, (3) 0.05 *M* calcium acetate solutions were found by Kurtze and Tamm⁴ to show significant excess absorption with a relaxation frequency above 40 MHz, and (4) other processes such as acetate ion hydrolysis and acetic acid dimerization do not contribute significantly to sound absorption in metal acetate aqueous solutions.

We were particularly interested in studying alkaline earth acetate solutions, especially those of Ca^{2+} , so that the

results could be compared with those obtained in previous measurements of calcium and magnesium polycarboxylates.⁵ Furthermore, we felt that previous measurements in alkaline earth solutions had been affected by experimental artifacts.³ After the measurements reported here were completed, Purdie and Barlow⁶ published the results of ultrasonic measurements in aqueous magnesium and calcium acetate solutions. Their data, in general, agree with those presented here but are restricted to a narrower concentration range (<0.4 *M*) and a single temperature. In spite of the general data agreement, our analysis of our data, obtained over a much wider range of conditions, leads us to a significantly different interpretation. We attribute the observed single relaxation in dilute $Ca(Ac)_2$ solutions (<0.5 *M*) to the substitution of a water molecule in the inner hydration sphere of the Ca^{2+} ion by a single acetate ion. The second relaxation observed in $Ca(Ac)_2$ solutions at $C > 0.5$ *M* is attributed to the substitution of another water by a second acetate in the inner coordination sphere leading to

the uncharged $\text{Ca}(\text{Ac})_2$ complex. Unfortunately, it was necessary to use rather concentrated solutions in order to observe this second relaxation process. The general problems associated with concentrated electrolytes together with the lack of thermodynamic data at concentrations greater than 0.05 M have conspired against a thorough quantitative interpretation of the experimental results.

Experimental Section

Analytical reagent quality chemicals were employed without further purification. All solutions were made up with ion exchange purified water.

In the 10–190-MHz range ultrasonic absorption was measured using a conventional twin-crystal pulse apparatus.⁷ The measurements on the 0.427 M $\text{Mg}(\text{Ac})_2$ solution in the 2–20-MHz range were made using a differential cell technique.⁸ All measurements were made in thermostated cells with the temperature controlled to $\pm 0.1^\circ$.

Results

Magnesium and calcium acetate solutions were studied at various temperatures and concentrations. Using 2.57 M NaClO_4 as a solvent medium, ultrasonic absorption was measured in mixtures of NaAc with $\text{Ca}(\text{ClO}_4)_2$, $\text{Mg}(\text{ClO}_4)_2$, $\text{Ni}(\text{ClO}_4)_2$, and $\text{Ba}(\text{NO}_3)_2$. All the solutions containing Ca^{2+} and Ac^- showed excess absorption in the frequency range 10–190 MHz. This is illustrated for some cases in Figures 1 and 2 where α/f^2 (α is the ultrasonic absorption coefficient and f the frequency) is plotted against $\log f$. If the observed absorption were due to discrete relaxation processes, the experimental results should be representable by

$$\frac{\alpha}{f^2} = \sum_i \frac{A_i}{1 + (f/f_{r_i})^2} + B \quad (1)$$

where A_i is the absorption amplitude of the i th absorption and f_{r_i} is the relaxation frequency of the i th absorption. B is the background absorption usually considered that of the pure solvent. However, it also includes the absorption due to all processes with a relaxation frequency substantially higher than the measurement range.

The data obtained for solutions containing Ca^{2+} and Ac^- ions at concentrations less than 0.5 M show a single relaxation process. At higher concentrations two relaxations are needed to fit the data with the exception of 1.415 M $\text{Ca}(\text{Ac})_2$ at 10° . In this case the single band observed is too broad to fit a single discrete relaxation but cannot be realistically fitted to two discrete relaxations. This same peculiarity is also seen in the most concentrated $\text{Mg}(\text{Ac})_2$ solutions (see Figure 3).

Figure 4 shows the results for solutions of Ac^- ion with some other bivalent metal ions. It is noteworthy that for the Mg^{2+} and Ni^{2+} solutions, excess absorption is only apparent at the lowest frequencies measured indicating processes with relaxation frequencies much lower than for the Ca^{2+} solutions. Between 25 and 125 MHz, the $\text{Ba}(\text{Ac})_2$ solutions show no relaxations but do exhibit an absorption approximately 10% greater than the solvent background absorption.

In order to use eq 1 it is necessary to know or estimate the value of B . At the same molar concentration of M^{2+} ions, B is different in water and in 2.57 M NaClO_4 (see Figure 4 for an example). The background ultrasonic absorption of the solvent is due to classical and structural relaxations occurring at very high frequencies. Unfortunately, we do not have very good theory for structural relaxation.

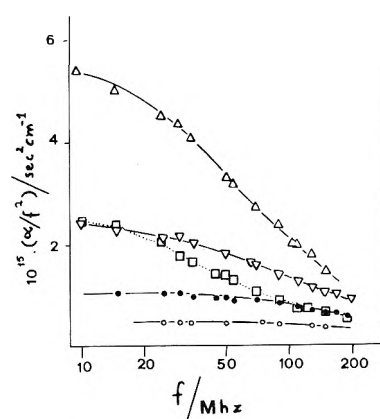


Figure 1. Ultrasonic absorption plotted against frequency for systems containing Ca^{2+} and acetate ions at 25° : O, 0.141 M $\text{Ca}(\text{Ac})_2$; ●, 0.397 M $\text{Ca}(\text{Ac})_2$; ▽, 0.698 M $\text{Ca}(\text{Ac})_2$; △, 1.088 M $\text{Ca}(\text{Ac})_2$; □, 2.57 M NaClO_4 , 0.70 M $\text{Ca}(\text{ClO}_4)_2$, 0.70 M NaAc .

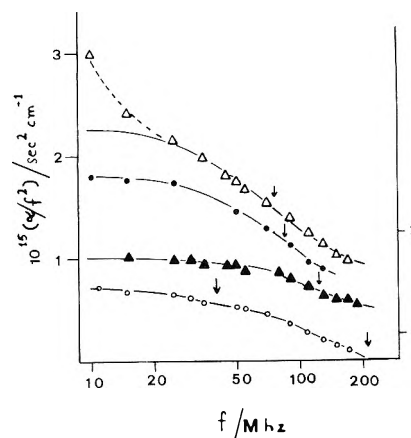


Figure 2. Ultrasonic absorption of calcium acetate solutions plotted against frequency at various temperatures: O, 0.70 M $\text{Ca}(\text{Ac})_2$ at 45.5° (right-hand ordinate axis); ▲, 0.397 M $\text{Ca}(\text{Ac})_2$ at 25.0° (left-hand ordinate axis); ●, 0.427 M $\text{Ca}(\text{Ac})_2$ at 10.0° (left-hand ordinate axis); △, 0.427 M $\text{Ca}(\text{Ac})_2$ at 2.5° (left-hand ordinate axis). Vertical arrows denote the position of the relaxation frequencies (cf. Table II).

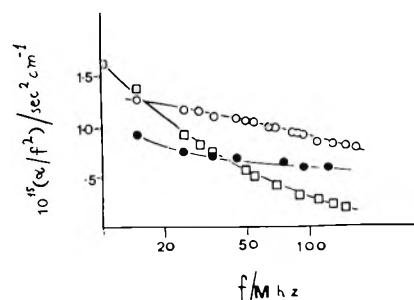


Figure 3. Ultrasonic absorption of concentrated alkaline earth acetate solutions plotted against frequency: ●, 1.986 M $\text{Mg}(\text{Ac})_2$ at 45° ; O, 1.986 M $\text{Mg}(\text{Ac})_2$ at 25° ; □, 1.415 M $\text{Ca}(\text{Ac})_2$ at 10° . (Ordinate scale reduced by a factor of 10.)

Davies and Litovitz⁹ have shown that it is proportional to the viscosity of the medium. It is also known that alkaline earth acetate solutions have rather high relative viscosities.^{10,11} Since our experiments do not extend to a high enough frequency to trust a measured B we have corrected the pure water background, $B_{\text{H}_2\text{O}}$, absorption using the ex-

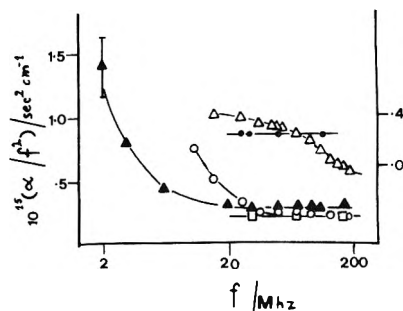


Figure 4. Ultrasonic absorption of solutions containing M^{2+} and acetate ions at 25° plotted against frequency: \square , 2.57 M NaClO_4 , 0.43 M NaAc , $0.43\text{ M Mg}(\text{ClO}_4)_2$; \circ , 2.57 M NaClO_4 , 0.43 M NaAc , $0.43\text{ M Ni}(\text{ClO}_4)_2$; \bullet , 2.57 M NaClO_4 , 0.43 M NaAc , $0.43\text{ M Ba}(\text{NO}_3)_2$ (right ordinate axis); \blacktriangle , $0.427\text{ M Mg}(\text{Ac})_2$; \triangle , $0.397\text{ M Ca}(\text{Ac})_2$.

perimentally determined relative viscosities of the solutions

$$B = B_{\text{H}_2\text{O}}(\eta/\eta_{\text{H}_2\text{O}})$$

Table I gives the relative viscosities and the corrected background absorptions for all the $\text{Ca}(\text{Ac})_2$ solutions measured. No relaxation was observed in 2.57 M NaClO_4 solutions containing $\text{Ca}(\text{ClO}_4)_2$ but no Ac^- ions. But when Ac^- was added, a relaxation was observed. Since the added Ac^- did not change the solution viscosity appreciably, it was possible to use the experimental α/f^2 for the solution not containing Ac^- as the B for the solution containing Ac^- .

Table II presents the results obtained by fitting the data using eq 1 and a least-squares program. For a single relaxation the fitting parameters are B , f_{r1} , and A_{r1} . When the excess absorption was small, it was necessary to fix B (noted in the table by putting the value in parentheses). In these cases the coincidence between the best B value and that calculated in Table I shows that our choice of B was sound. Whenever the data had to be fitted to a two-relaxation process, the B value was fixed. Measurements in $0.03\text{ M Ca}(\text{Ac})_2$ solutions gave the pure-solvent α/f^2 value within experimental error. Table II also shows that an increase in temperature produces the expected increase in relaxation frequency.

The ultrasonic absorption measured for other metal(II) acetate solutions could not be analyzed, either because the change of α/f^2 with frequency was too small (Ba^{2+}) or because the relaxation frequency clearly was below the lowest frequency measured (Mg^{2+} and Ni^{2+}). This is shown in Figure 4.

We are convinced that the observed excess absorption is not due to the sulfate ions, a common impurity in $\text{Ca}(\text{Ac})_2$, nor to OH^- ions produced by hydrolysis. Deliberate addition of these ions to the solutions does not substantially change the absorption.

Discussion

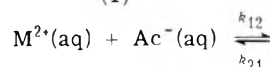
The present work shows that the excess ultrasonic absorption found in aqueous bivalent metal acetate solutions depends strongly on the nature of the metal. This is clearly illustrated in Figure 4 and agrees with previous work on such solutions. Maass¹² found relaxation frequencies between 7 and 20 MHz for copper(II), cadmium, and zinc acetate solutions, the value depending on the particular cation.

The simplest reaction scheme usually invoked for the encounter of oppositely charged ions is

TABLE I: Viscosities and Background Absorption of $\text{Ca}(\text{Ac})_2$ Solutions at Various Temperatures

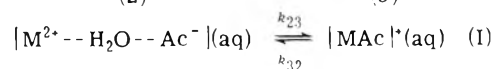
$T, ^\circ\text{C}$	C, M	η/η_0	$10^{17}B, \text{sec}^2 \text{cm}^{-1}$
2.5	0.141	1.134	56.7
	0.427	1.472	73.6
10.0	0.141	1.131	38.5
	0.427	1.443	49.1
	0.77	1.908	64.9
	1.415	3.621	123.1
25.0	0.141	1.118	28.0
	0.397	1.372	34.0
	0.698	1.756	43.9
	1.088	2.267	56.7
45.5	0.70	1.664	20.0
	1.09	2.247	27.0

(1)



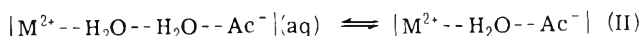
(2)

(3)



In the case of metal acetates, the observed relaxation (relaxation frequency f_{r1}) is due to the second step in scheme I for which the rate constants should depend on the nature of M^{2+} . This step corresponds to the substitution of an inner-sphere water molecule on M^{2+} by an acetate ion. In Table III the values of the relaxation frequencies, f_{r1} , found for the bivalent metal acetates in water are compared to the rate constant for the substitution of a water molecule in the inner coordination sphere of the M^{2+} ion, k_{23} . There is a clear correlation between the two values for each metal as would be expected if the second step of the reaction scheme I gave rise to f_{r1} in these solutions.

Purdie and Barlow⁶ measured ultrasonic absorption in aqueous magnesium and calcium acetate solutions up to 0.4 M . They assigned the observed relaxation to an intermediate association step of the type



However, this assignment would imply that the observed relaxation frequency would be cation independent, an assumption not borne out experimentally. Their data for aqueous CaAc_2 solutions agree fairly well with ours (see Table II). The interpretation, however, is different. They analyzed their data by fixing B to the solvent value. But due to the change of B with concentration, noted above, this tends to shift their relaxation frequencies above the correct values. In the case of $\text{Mg}(\text{Ac})_2$ solutions, the fitted values of A and f_{r1} obtained by Purdie and Barlow are not very meaningful since the excess absorption is always smaller than 30% of the background and changes very little with frequency.

The values of k_{23} and k_{32} corresponding to the reaction scheme I can be obtained by analyzing the $\text{Ca}(\text{Ac})_2$ solution data taken below 0.5 M . However, the scanty thermodynamic data and more complex relaxation process preclude quantitative analysis of data from the more concentrated solutions.

Reaction scheme I leads to the relaxation time equations^{3,4,12,13}

$$\begin{aligned} 2\pi f_{\text{r1}}' &= (1/2)[\Sigma + (\Sigma^2 - 4\Omega)^{1/2}] \\ 2\pi f_{\text{r1}}'' &= (1/2)[\Sigma - (\Sigma^2 - 4\Omega)^{1/2}] \end{aligned} \quad (2)$$

TABLE II: Ultrasonic Parameters for Aqueous Ca(Ac)₂ Solutions^a

A. Pure Water Medium							
<i>T</i> , °C	<i>C</i> , <i>M</i>	<i>f</i> _{T1} , MHz	10 ⁻¹⁷ <i>A</i> _I , sec ² cm ⁻¹	<i>f</i> _{TIII} , MHz	10 ⁻¹⁷ <i>A</i> _{III} , sec ² cm ⁻¹	10 ⁻¹⁷ <i>B</i> , sec ² cm ⁻¹	10 ⁻¹⁷ <i>σ</i> , ^b sec ² cm ⁻¹
2.5	0.141	87.7 ± 26.1	32.6 ± 6.1			59.4 ± 7.0	2.5
	0.427	73.8 ± 2.2	153.0 ± 2.9			73.0 ± 4.2	3.1
10.0	0.141	85.6 ± 12.4	28.0 ± 2.4			41.7 ± 2.8	1.3
	0.427	84.0 ± 3.3	132.7 ± 4.5			49.9 ± 5.1	1.6
	0.77	77.8 ± 5.3	279.7 ± 23.5	14.9 ± 4.4	186.7 ± 19.4	(64.9)	5.9
25.0	0.141	119 ± 18	15.1 ± 0.3			(28)	0.5
	0.367	129 ± 40	57 ± 14			38 ± 16	7 ^c
	0.397	124.6 ± 8.7	67.8 ± 4.4			34 ± 5	4.0
	0.698	122.5 ± 10.3	126.9 ± 15.6	34.1 ± 7.1	73.1 ± 18.8	(43.9)	2.9
45.5	1.088	114.2 ± 23.2	210.7 ± 69.5	36.8 ± 6.3	288.7 ± 63.8	(56.7)	7.1
	0.70	211.0 ± 1.5	101.9 ± 0.6	40.2 ± 1.0	25.9 ± 0.4	(20.0)	1.7
	1.09	187.9 ± 30.6	130.7 ± 26.1	57.7 ± 5.7	167.3 ± 24.7	(27.0)	4.1

B. 2.57 M NaClO ₄							
<i>C</i> (Ca ²⁺), <i>M</i>	<i>C</i> (Ac ⁻), <i>M</i>	<i>f</i> _{T1} , MHz	10 ⁻¹⁷ <i>A</i> _I , sec ² cm ⁻¹	<i>f</i> _{TIII} , MHz	10 ⁻¹⁷ <i>A</i> _{III} , sec ² cm ⁻¹	10 ⁻¹⁷ <i>B</i> , sec ² cm ⁻¹	10 ⁻¹⁷ <i>σ</i> , ^b sec ² cm ⁻¹
0.17	0.298	130.5 ± 13.0	35.0 ± 2.8			16.2 ± 3.0	1.1
	0.55	160.4 ± 1.2	35.4 ± 0.5	48.0 ± 0.6	41.4 ± 0.5	(17.3)	0.8
0.70	0.141	132 ± 29	16 ± 3			17.3 ± 3.2	0.8
	0.397	167.5 ± 3.8	35.7 ± 0.8	31.6 ± 0.6	59.8 ± 0.7	(19.8)	0.5
	0.70	164.1 ± 46.8	58.9 ± 17.2	34.6 ± 3.7	183.4 ± 14.7	(19.8)	4.2

^a A complete set of (α/f , f) data is available from G. A. on request. ^b Standard deviation of the fit. ^c Data from ref 6.

where

$$\Sigma = k_{12}L(\alpha) + k_{21} + k_{23} + k_{32}$$

$$\Omega = k_{12}L(\alpha)(k_{23} + k_{32}) + k_{21}k_{32} \quad (3)$$

$$L(\alpha) = \pi\gamma C_0 \left[1 + 2\alpha + (1 + \alpha) \left(\frac{\partial \ln \pi\gamma}{\partial \ln \alpha} \right)_{C_0} \right]$$

The overall association constant, K_A , is given by

$$K_A \pi\gamma = \frac{1 - \alpha}{(1 + \alpha)C_0} = K_{12}\pi\gamma(1 + K_{23}) \quad (4)$$

where C_0 is the stoichiometric concentration of $M(\text{Ac})_2$, K_{12} is the formation constant of the first step, K_{23} is the formation constant of the second step, and $\pi\gamma$ is the activity coefficient product.

Nancollas¹⁴ and Archer and Monk¹⁵ have reported the best values of the association constants of bivalent acetates in water. They found that up to 0.04 *M* only MAc^+ ion pairs are important in aqueous solution. Nancollas also measured the K_A at both 25 and 35° finding it little affected by temperature. Therefore, we shall assume the K_A 's at 10 and 25° to be the same. The Davies equation¹⁶ was used to calculate $\pi\gamma$ and its variation with α . This is above the normal range of validity but is still a reasonable approximation.

The first step in I, corresponding to the diffusion-controlled encounter of $M^{2+}(\text{aq})$ and $\text{Ac}^-(\text{aq})$ cannot be detected in these solutions. This is presumably because its relaxation frequency, f_{T1}' , is above our experimental frequency range and/or its relaxation amplitude is too small. The rate constants for this step can be calculated from the Debye-Smoluchowski equation. For this purpose the cation-anion approach distance is assumed to be 5 Å.

Table IV gives the values calculated for k_{12} and k_{21} and the values found for k_{23} and k_{32} using eq 2. The averages were obtained from the lower two concentrations at 10° and the three lower concentrations at 25° (Table II).

TABLE III: Observed Relaxation Frequency for $M(\text{Ac})_2$ Solutions and Characteristic Rate Constant for Water Substitution

Metal	<i>f</i> _{T1} , MHz	Source	<i>k</i> ₂₃ , ^a sec ⁻¹
Zn	8 × 10 ⁶	Ref 11	3 × 10 ⁷
Cd	(1.8-3.0) × 10 ⁷	Ref 11	<1 × 10 ⁸
Cu	2.0 × 10 ⁷	Ref 11	<1 × 10 ⁸
Ca	1.2 × 10 ⁸	This work	3 × 10 ⁸
Mg	<2 × 10 ⁶	This work	1 × 10 ⁶
Ni	<<1 × 10 ⁶	This work	1 × 10 ⁴

^a H. Diebler, *et al. Pure Appl. Chem.*, **20**, 93 (1969).

The average values of k_{23} are reasonably close to those estimated by Eigen and Maass¹⁴ for the rate constant of inner-sphere water substitution in $\text{Ca}(\text{H}_2\text{O})_n^{2+}$ by a multi-dentate ligand (*cf.* Table III). The difference between the two values is similar to that usually found in k_{23} as the ligand is changed.^{12,17}

Table IV also reports the values of $\Delta V_1''$ for these systems. These were calculated using Tamm's expressions.⁴ This ΔV does not correspond strictly to the volume change for the step (2) \rightleftharpoons (3) in reaction I but is related to it by the expression

$$\Delta V_1'' = \Delta V_{23} + \frac{k_{21}}{k_{12}L(\alpha) + k_{21}} \Delta V_{12} \quad (5)$$

Ultrasonic measurements give $(\Delta V_1'')^2$; hence the sign in Table IV has been assigned considering that the replacement of a water molecule in the inner coordination sphere of M^{2+} causes a positive ΔV . This is due to the increase in volume of the strongly electrostricted water molecule as it is released into the bulk water. The values of $\Delta V_1''$ in Table IV are quite reasonable when compared to the ΔV 's found for other M^{2+} -anion association processes.¹⁸

For solutions of $\text{Ca}(\text{Ac})_2$ with concentrations higher than 0.5 *M* or in 2.57 *M* NaClO_4 , a second relaxation appears at lower frequencies (Table II). This is attributable to the equilibrium

TABLE IV: Rate Constants and ΔV for $\text{Ca}(\text{Ac})_2$ Solutions

$T, ^\circ\text{C}$	$10^{-10}k_{12},$ $M^{-1} \text{sec}^{-1}$	$10^{-9}k_{21}, \text{sec}^{-1}$	$10^{-8}k_{23}, \text{sec}^{-1}$	$10^{-8}k_{32}, \text{sec}^{-1}$	C, M	$\Delta V_1', \text{cm}^3 \text{mol}^{-1}$
10.0	1.4	2.5	5.2 ± 1.0	3.8 ± 0.7	0.141	7.1^a
					0.427	7.8^a
	1.4	2.5	7.0 ± 1.0	3.3 ± 0.7	0.141	6.6^b
					0.427	7.6^b
25.0	2.2	3.7	6.3 ± 0.8	5.2 ± 0.7	0.141	6.2^a
					0.361	6.9^a
					0.397	7.0^a
	2.2	3.7	8.7 ± 1.4	4.6 ± 0.7	0.141	5.7^b
					0.361	6.7^b
					0.397	6.8^b

^a Using $K_A = 13.3 M^{-1}$, ^b Using $K_A = 17.5 M^{-1}$. The 0.361 M data are from ref 5.

(4)



(5)

(6)



Since the first step in (III) should also be diffusion controlled, we would not expect to observe it. So we believe that the low-frequency relaxation, f_{III} , probably arises from the step (5) \rightleftharpoons (6), the substitution of a second water in the inner coordination sphere of M^{2+} by a second acetate. This interpretation is supported by the fact that the f_{III} band also appears if a 0.17 M Ca^{2+} solution is treated with sufficient Ac^- (Table II).

For the solutions which have a $\text{Ca}(\text{Ac})_2$ concentration greater than 0.5 M and for these in 2.57 M NaClO_4 , there are no thermodynamic data so the rate constants and ΔV 's cannot be calculated.

In the most concentrated $\text{Ca}(\text{Ac})_2$ solutions the data can no longer be analyzed with eq 1 using one or two discrete relaxations. Instead relaxation bands are observed similar to those found in polyelectrolyte solutions.⁵ These bands correspond to a distribution of relaxation times. It is difficult to explain quantitatively why such a distribution should be observed. From a chemical point of view the distribution implies the existence of a set of kinetic events similar but not identical in their parameters. In the rather viscous most concentrated $\text{Ca}(\text{Ac})_2$ solutions this could be attributed to the slowing of the diffusion step and consequent breakdown of the Debye-Smoluchowski model. In the most concentrated solutions the most likely reaction partners are quite close together on the average and the

water structure is strongly affected by the ions. The ion atmosphere radius is very small at high concentrations and strongly affected by the formation of contact ion pairs. In general, then, the model visualized in the simple two-step association process no longer holds in the most concentrated solutions. The systems, indeed, behave more like the "wet" fused-salt systems examined by other workers¹¹ in recent years.

Acknowledgments. The authors gratefully acknowledge the support of the National Science Foundation (NSF Grant GP-33781X). We are grateful to Lic. M. Marano for assistance in the computer analysis.

References and Notes

- (1) To whom correspondence should be addressed.
- (2) P. Bazulin, *Zh. Eksp. Teor. Fiz.*, **9**, 1147 (1939).
- (3) J. Stuehr and E. Yeager in "Physical Acoustics," Vol. IIA, W. P. Mason, Ed., Academic Press, New York, N. Y., 1965, Chapter 6.
- (4) K. Tamm in "Handbuch der Physik," Vol. XI, S. Flugge, Ed., Springer, West Berlin, 1961.
- (5) G. Atkinson, E. Baumgartner, and R. Fernández-Prini, *J. Amer. Chem. Soc.*, **93**, 6436 (1971).
- (6) N. Purdie and A. J. Barlow, *J. Chem. Soc., Faraday Trans. 2*, **68**, 33 (1972).
- (7) R. Garnsey and D. W. Ebdon, *J. Amer. Chem. Soc.*, **91**, 50 (1969).
- (8) R. Corsaro, G. Atkinson, and B. R. Perlis, *Chem. Instrum.*, **2**, 389 (1970).
- (9) T. A. Litovitz and C. M. Davies in "Physical Acoustics," Vol. IIA, W. P. Mason, Ed., Academic Press, New York, N. Y., 1965, Chapter 5.
- (10) "International Critical Tables," Vol. V, McGraw-Hill, New York, N. Y., 1929.
- (11) W. B. Bonnor and C. G. Smith, *J. Chem. Soc.*, 1359 (1950).
- (12) G. Maass, *Z. Phys. Chem. (Frankfurt am Main)*, **60**, 138 (1968).
- (13) M. Eigen and K. Tamm, *Z. Elektrochem.*, **66**, 93 (1962).
- (14) G. H. Nancollas, *J. Chem. Soc.*, 744 (1956).
- (15) D. W. Archer and C. B. Monk, *J. Chem. Soc.*, 3117 (1964).
- (16) C. W. Davies in "Ion Association," Butterworths, London, 1962.
- (17) M. Eigen and G. Maass, *Z. Phys. Chem. (Frankfurt am Main)*, **49**, 163 (1966).
- (18) M. Eigen and K. Tamm, *Z. Elektrochem.*, **66**, 107 (1962).

Derivation of Rate Equations for Fischer Glycosidation of D-Glucose and Estimation of Rate Constants Using a Computer

Dwight F. Mowery, Jr.

College of Arts and Sciences, Southeastern Massachusetts University, North Dartmouth, Massachusetts 02747 (Received March 1, 1974)

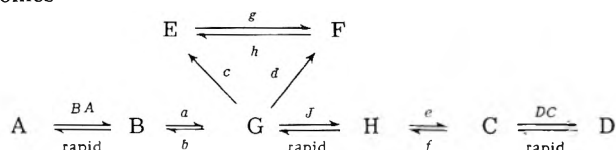
Integrated equations have been derived for the reaction mechanism proposed by Pater, Coelho, and Mowery¹ for the Fischer glycosidation of D-glucose and a computer program has been written for calculation of the expected per cent yield of each isomer at various time intervals as a function of the rate constants. Approximate rate constants for the reaction have been obtained by adjusting them until the theoretical yields at the timed intervals closely approximate the experimental yields.

Introduction

The mechanism proposed by Pater, Coelho, and Mowery¹ for the Fischer glycosidation of D-glucose in boiling methanol, using a strongly acidic ion-exchange resin as a catalyst, may be represented by the following scheme

$$\begin{array}{c}
 E \rightleftharpoons F \\
 \swarrow \quad \searrow \\
 A \rightleftharpoons B \rightleftharpoons G \rightleftharpoons H \rightleftharpoons C \rightleftharpoons D
 \end{array}$$

in which A represents α -D-glucose; B, β -D-glucose; C, methyl α -D-glucopyranoside; D, methyl β -D-glucopyranoside; E, methyl α -D-glucopyranoside; F, methyl β -D-glucopyranoside; G, the bicyclic cation protonated on the C₄ ring oxygen (formula 7 in ref 1); and H, the bicyclic cation protonated on the C₅ ring oxygen (formula 9 in ref 1). The reaction involves 16 rate constants or 8 rate constants and 8 equilibrium constants. Formulation of concentrations in terms of rate constants and time for this system with no approximations would involve a fifth-order determinant and solution of an equation of fifth power. Study of Table I, showing mole per cents of α and β -D-glucose, the two furanosides, and the two pyranosides obtained experimentally, reveals several things. First, the ratios of β - to α -D-glucose and methyl β -D-glucopyranoside to methyl α -D-glucopyranoside are essentially constant throughout the reaction at about 1.14 and 1.43, respectively. Second, the final equilibrium mixture contains negligible amounts of α - and β -D-glucose and α - and β -D-glucopyranoside. Third, the ratio of concentrations of α -D-glucopyranoside to β -D-glucose appears to be approaching a final equilibrium value of about 1.3. Fourth, the initial ratio of β - to α -D-glucopyranoside, obtained by extrapolation back to zero time, is about 1.4. Fifth, the final equilibrium mixture contains a ratio of methyl β -D-glucopyranoside to methyl α -D-glucopyranoside of 0.370. These facts indicate rapid equilibria between A and B and between C and D and essentially irreversible formation of E and F from G. A further assumption of a rapid equilibrium between G and H seems justified since this reaction involves only the shift of a proton from the C₄ to the C₅ ring oxygen. The reaction may therefore be simplified to include only eight rate constants, of which two may be directly related to two others. The scheme now becomes



in which $g/h = 0.370$, $d/c = 1.4$, $BA = CB/CA = 1.14$, $DC = CD/CC = 1.43$, and $J = CH/CG \approx 1.3(bf)/(ae)$. In these expressions CA, CB, CC, CD, CG, and CH represent moles per liter of the various substances. The last relationship results from the approximate ratio of 1.3 for CC/CB as equilibrium is approached. Because of the conditions under which the reaction was run, two stages must be considered. In the first stage, the boiling methanol is saturated with D-glucose (0.40 M) so that CA and CB ($CB = Q = 0.40 \times 1.14/2.14 = 0.213$ M) are constant and the concentrations of the intermediates and products increase from initial values of zero. In the second stage, the concentrations of all substances present except E and F, the two pyranosides, decrease to essentially zero so that the final equilibrium mixture contains 73 mol % α -pyranoside and 27 mol % β -pyranoside. During this stage the sum of concentrations of all species is calculated to be 1.11 M.

The derivations of the equations for calculating the concentrations of the various species as a function of time and the computer program written to perform this calculation and output the results in the form of Table I are available on microfilm.² The fixed quantities read into the computer are: overall sugar concentration, 1.11 M; D-glucose concentration in the saturated solution, 0.40 M; CD/CC , 1.43; g/h , 0.37; and $J = 1.3(bf)/(ae)$. Rate constant d is calculated by the computer as $1.4c$. The six rate constants a , b , c , e , f , and g were systematically varied until the best least-squares fit with the experimental data was obtained.

Results

It was found that c is related to a and b by the simple relationship, $c = 0.86b/a + 0.05$. The rate constants in hr^{-1} and natural logarithms were found as follows: a , 30 ± 5 ; b , $30(+10, -5)$; c , $0.9(+0.3, -0.1)$; d , $1.26(+0.42, -0.14)$; e , $50(+20, -10)$; f , $50(+20, -10)$; g , 0.11 ± 0.01 ; h , 0.29 ± 0.03 . The sum of the squares of the deviations of the calculated from the experimental mole per cents is 48. The range for each of these constants is roughly estimated as the maximum amount by which it may be varied which, with an optimum choice of values for the other constants, produces an increase in the sum of the squares of no more than about 10%. The computer yields a time of 12 min for complete solution of the D-glucose.

Conclusions and Projections

The agreement of the calculated and experimental mole per cents, shown in Table I, proves that a set of rate con-

TABLE I

Time, hr	Mole per cent ^a					
	A	B	C	D	E	F
0.083	31(32)	35(36)	13(12)	18(18)		3(2) ^b
0.167	26(25)	29(28)	16(18)	25(25)		4(4) ^b
0.25	19(19)	21(21)	20(22)	31(31)	4(3)	5(4)
0.50	14(15)	16(17)	23(22)	30(31)	8(7)	9(9)
1.00	11(12)	13(14)	20(18)	26(26)	15(15)	15(16)
2.00	8(8)	10(10)	12(12)	18(18)	28(27)	24(25)
4.00	4(4)	4(5)	5(6)	8(9)	46(45)	33(31)
8.00	1(1)	2(1)	2(2)	3(3)	61(63)	31(30)
12.00	0(0)	1(0)	0(1)	1(1)	71(70)	27(28)
24.00	0(0)	0(0)	0(0)	0(0)	73(73)	27(27)

^a Figures in parentheses are calculated by the computer program. The others are experimentally determined. ^b E and F were not resolved analytically in the samples taken at these time intervals and the figures calculated by the computer for E and for F were added together for comparison.

stants may be assigned upon the basis of the proposed mechanism of methyl glucoside formation.¹ In deriving the equations no allowance was made for variation of concentrations within the resin particles or transport of the reactant into and the products out of the resin. The primary objective was to determine whether satisfactory equations

could be derived. The next step in the investigation will be the determination of rate constants for the single-phase reaction, under identical conditions, using *p*-toluenesulfonic acid as a catalyst. A comparison of the two sets of rate constants should then show the direction and magnitude of the effect of the resin upon the reaction. Further experimental work designed to test the validity of the proposed mechanism, as applied to D-galactose, is also in progress.

Supplementary Material Available. Derivations for rate equations and the computer program will appear following these pages in the microfilm edition of this volume of the journal. Photocopies of the supplementary material from this paper only or microfiche (105 × 148 mm, 24× reduction, negatives) containing all of the supplementary material for the papers in this issue may be obtained from the Journals Department, American Chemical Society, 1155 16th St., N.W., Washington, D. C. 20036. Remit check or money order for \$3.00 for photocopy or \$2.00 for microfiche, referring to code number JPC-74-1918.

References and Notes

- (1) R. H. Pater, R. A. Coelho and D. F. Mowery, Jr., *J. Org. Chem.*, **38**, 3272 (1973).
- (2) See paragraph at end of text regarding supplementary material.

Stable Intermediates in Kinetic Models of Catalase Action

M. L. Kremer* and S. Baer

Department of Physical Chemistry, The Hebrew University, Jerusalem, Israel (Received September 24, 1973; Revised Manuscript Received May 20, 1974)

Publication costs assisted by the Central Research Fund of The Hebrew University

The peroxidatic model of catalase action (A) and one of its extensions (C) are discussed. A mathematical relation between the final concentration of the intermediate of model A and the initial peroxide concentration is derived. It is shown that the steady-state concentration is the upper limit of the possible final concentrations of the intermediate complex. In case C, which is a consecutive two-complex system, the first complex disappears at the end of the reaction while the second complex persists at infinite time. The terminal concentration of this complex may vary, depending on initial conditions and on the rate constants, between zero and the total enzyme concentration. Some aspects of the models relative to catalase kinetics are discussed.

Introduction

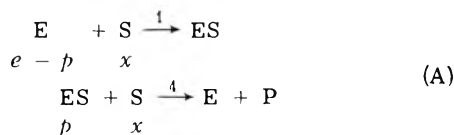
Both experimental and theoretical aspects of catalase kinetics drew considerable attention in the past. Theoretical treatments were, as a rule, confined to the steady state.¹ Many important results were, however, obtained under circumstances in which the system was removed from the steady state.² It is therefore of interest to investigate the mathematical properties of the kinetic equations of model systems under non-steady-state conditions. The analysis reveals many interesting features, all of which are, however, not yet accessible to experimental verification.

A complete integration of the rate equations is in general not possible. A discussion must thus rely largely on the

analysis of the differential rate equations themselves together with their numerical integration with the help of computers. In this connection the kinetics of the intermediates is of special interest as they exhibit, in some cases, characteristic behavior in that they do not disappear at the end of the reaction. In one particular case the intermediate accumulates in a two stage process, the second stage occurring at the end of the reaction when the concentrations of all other reacting species tend to zero.

The Peroxidatic Mechanism

The simplest mechanism for catalytic action has been proposed by Chance, *et al.*¹



E denotes catalase haematin and S hydrogen peroxide. ES is the enzyme substrate complex. Small type letters denote concentrations. e is the total concentration of catalase haematin.

The relative rate of formation of the intermediate and of peroxide (the latter is a negative quantity) is given by

$$\frac{dp}{dx} = \frac{-k_4 e + (k_4 - k_1)p}{k_1 e + (k_4 - k_1)p} \quad (1)$$

By integrating this expression between $t = 0$ and $t = \infty$ (corresponding to the limits $x_0, 0$ and $0, p_\infty$, respectively) we obtain

$$x_0 = \frac{1 - R}{1 + R} p_\infty - \frac{2R p^*}{1 + R} \ln \left(1 - \frac{p_\infty}{p^*} \right) \quad (2)$$

$R = k_4/k_1$. $p^* = e/(1 + R)$ is the steady-state concentration of ES. Equation 2 relates the final concentration of ES (p_∞) to the initial concentration of peroxide (x_0). It is seen that for $x_0 > 0$, p_∞ is positive, i.e., ES persists at the end of the reaction. Equation 2 also shows that p_∞ increases by increasing x_0 . The increase is, however, limited by the upper bound p^* . The dependence of p_∞ on x_0 at different R is shown in Figure 1. Both the shape of the curves and the upper limit depend on R . At low R (relatively low rate constant of reaction of ES with S), p^* is close to e and the curve approaches a straight line with a slope of unity. It corresponds to the quantitative formation of ES from its components. With increasing R , the peroxidatic step (reaction 4) becomes more important. As a consequence, p^* decreases and the line becomes curved (an increasing fraction of the peroxide is decomposed into oxygen and water).

In the course of a single run p increases monotonically toward its final limit. This behavior follows from the rate equation

$$dp/dt = x[k_1 e - (k_1 + k_4)p]$$

and from the condition $p \leq e/(1 + R)$. This time course of p is also known from analog and digital computer simulations of mechanism A.^{3,4}

The Two-Complex Mechanism

Mechanism A accounts for many aspects of catalase action.³ At high x_0 , however, an extension of this mechanism is necessary.^{5,6} One of these extensions involves the resolution of the formation of the active intermediate into two consecutive steps. Because of the interesting kinetic features of this system and because of its potential importance for the mechanism of the decomposition of H_2O_2 by iron centered catalysts in general, this mechanism will be examined in the following in some detail.⁷⁻¹⁰

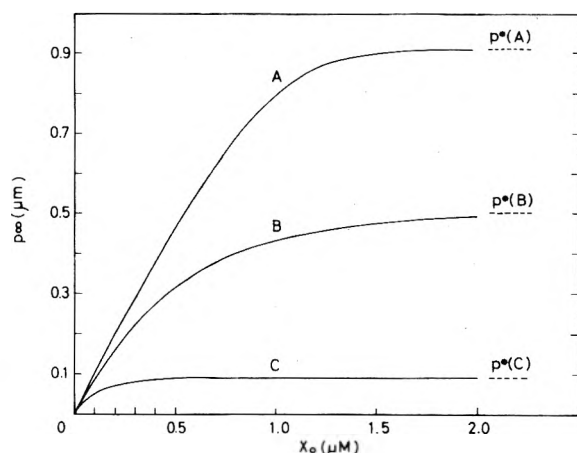
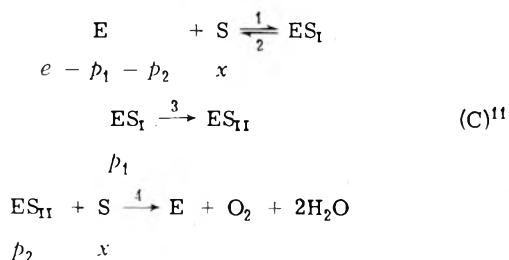


Figure 1. p_∞ as a function of x_0 : $e = 1 \mu\text{M}$, $R(\text{A}) = 0.1$, $p^*(\text{A}) = 0.909 \mu\text{M}$, $R(\text{B}) = 1$, $p^*(\text{B}) = 0.500 \mu\text{M}$, $R(\text{C}) = 10$, $p^*(\text{C}) = 0.091 \mu\text{M}$.

Considering the kinetics of the intermediates we find that p_1 exhibits "normal" behavior in the sense that it rises to a maximum then declines to zero. The kinetics of ES_{II} , on the other hand, is more complex. From the rate expressions for ES_I and ES_{II} we can derive the following relationship

$$\Delta = p_2 - p_2^* = - \frac{1}{k_4 x (x + K_M')} \left[\frac{k_3 dp_1}{k_1 dt} + (x + K_M) \frac{dp_2}{dt} \right] \quad (3)$$

$K_M = (k_2 + k_3)/k_1$; $K_M' = K_M + (k_3/k_4)$. p_2^* is the concentration of ES_{II} in the double steady state (both with regard to p_1 and p_2) and is given by

$$p_2^* = (k_3/k_4)e/(x + K_M') \quad (4)$$

Outside the steady state p_2^* is a quantity defined by eq 4. It follows from eq 3 that as long as p_2 is less than p_2^* , p_2 is increasing. (The expression in the bracket can be positive only for the combination $dp_1/dt > 0$ and $dp_2/dt > 0$, or for $dp_1/dt < 0$ and $dp_2/dt > 0$. The combination $dp_1/dt > 0$ and $dp_2/dt < 0$ is excluded because of the sequence of the intermediates.) It follows from the same argument that once p_2 has reached p_2^* , it cannot fall below it again. In this case the final value of p_2 cannot be lower than $(k_3/k_4)e/K_M'$.

Next we show that, under certain circumstances, p_2 can surpass p_2^* . We first assume that x_0 is sufficiently high that at some stage of the reaction a steady state is established ($p_2 = p_2^*$). As the reaction progresses and the peroxide is consumed, the steady state will ultimately be disturbed. Because of the sequence of the intermediates, first dp_1/dt will become negative. Assuming that $p_2 = p_2^*$ (p_2 cannot then be lower than p_2^*), it follows from eq 3 that dp_2/dt must be positive. Thus, in the late phase of the reaction, when the steady state breaks down, p_2 rises above its extrapolated steady-state level, which itself is increasing toward an upper limit. $p_{2\infty}$ will attain some value between $(k_3/k_4)e/K_M'$ and e . If x_0 is low, p_2 will tend, naturally, to lower limits. The entire range of possible final values of p_2 extends thus from 0 to e .

These conclusions are illustrated by some digital computer simulations shown in Figure 2. In the calculations e and x_0 were held constant. k_2 was put equal to zero. k_1 and k_4 were taken both as $1 \times 10^6 \text{ M}^{-1} \text{ sec}^{-1}$. k_3 was varied between 2 and $2 \times 10^6 \text{ sec}^{-1}$. For $k_3 = 2 \times 10^6 \text{ sec}^{-1}$, p_2 ap-

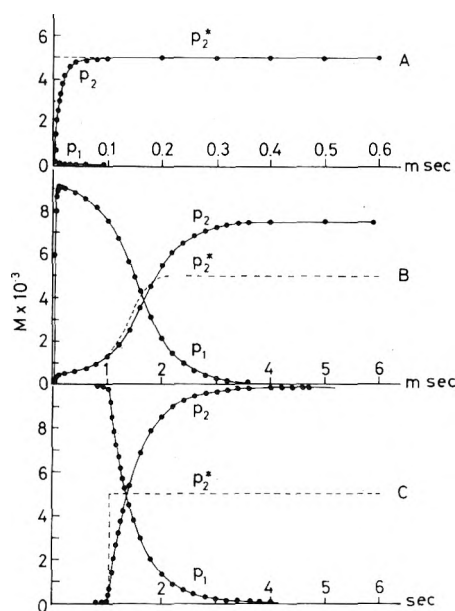


Figure 2. Digital computer simulations of mechanism C. Kinetics of the intermediate complexes for varying k_3 : $e = 1 \times 10^{-2} M$, $x_0 = 5 \times 10^{-2} M$, $k_1 = 1 \times 10^6 M^{-1} \text{sec}^{-1}$, $k_2 = 0 \text{sec}^{-1}$, $k_4 = 1 \times 10^6 M^{-1} \text{sec}^{-1}$, $k_3(A) = 2 \times 10^6 \text{sec}^{-1}$, $k_3(B) = 2 \times 10^3 \text{sec}^{-1}$, $k_3(C) = 2 \text{sec}^{-1}$. Broken lines denote the calculated steady-state concentrations of ES_{II} .

proaches closely the steady-state limit shown as a broken line (curve A). For $k_2 = 0$, this limit is the same for all values of k_3 and is given by $ek_1/(k_1 + k_4)$. For the given parameters it is $5 \times 10^{-3} M$. By decreasing k_3 , $p_{2\infty}$ exceeds the steady-state limit (curves B and C). At $k_3 = 2 \text{sec}^{-1}$, $p_{2\infty}$ becomes equal to $0.99e$ (curve C).

This behavior can be understood in the following way. The factor causing p_2 to exceed p_2^* is the negative value of dp_1/dt in the declining phase of p_1 . If the rate constant of the irreversible decomposition of ES_I (k_3) is high, p_1 remains low throughout the reaction ($|dp_1/dt| \ll |dp_2/dt|$, curve A). We obtain then the approximate relation

$$\Delta = p_2 - p_2^* = -\frac{1}{k_4} \frac{x + K_M}{x + K_M'} \frac{dp_2}{dt} \quad (3')$$

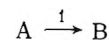
This equation implies that the system is self regulatory with respect to p_2 . For $p_2 < p_2^*$, p_2 increases, while for $p_2 > p_2^*$, it decreases: p_2 always tends to p_2^* . Since under the chosen conditions $x \ll K_M'$, p_2 approaches a constant value. By decreasing k_3 , p_1 becomes, temporarily, more substantial and causes, in its declining phase, an increase of p_2 to higher than steady-state levels (curves B and C). It is to be noted that in these cases also p_2^* varies during the reaction. It tends, however, always to the same final value.

It may appear paradoxical that a decrease of k_3 , i.e., a diminished rate of formation of ES_{II} , causes an accumulation of it at $t = \infty$. This contradiction is, however, only apparent. The main effect of k_3 in the later part of the reaction is on the relative concentrations of S and ES_I . As a low k_3 increases the ratio p_1/x , it increases the concentration of the species from which ES_{II} is formed (ES_I), and decreases the concentration of the species which decomposes it (S).¹³

Curve B shows a two stage formation curve of ES_{II} . In the first stage p_2 approaches its steady-state level. Then, as p_2^* increases, p_2 follows it and also surpasses it. In curve A only the first stage is seen. In curve C only the second is observable.

Discussion

The outstanding feature of both mechanisms A and C is the persistence of the active intermediate at infinite time. A similar case has been encountered before by Benson, who found that in the autocatalytic scheme

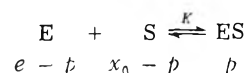


B did not disappear at the end of the reaction.¹⁴

Defining the degree of formation of ES, relative to its maximal value, $f = p_{\infty}/p^*$, we can write eq 2 in the form

$$\frac{x_0}{e} = \frac{f(1 - R) - 2R \ln(1 - f)}{(1 + R)^2} \quad (2')$$

Equation 2' shows apparent saturation at $p_{\infty} = p^*$. If ES is formed in an equilibrium reaction



saturation occurs naturally at $p_{eq} = e$. In this case we have the relationship

$$x_0/e = f + [f/(1 - f)](K/e) \quad (5)$$

The two modes of formation of ES can be distinguished from each other on the basis of the independence of the $x_0/e \dots f$ function of e , if eq 2' applies, and its dependence on it, if eq 5 is the appropriate one. (In the trivial case when $R = 0$ and $K = 0$, both equations degenerate into $x_0/e = f$.)

It has been observed experimentally that the intermediate of the catalase- H_2O_2 reaction disappeared in the final phase.² Taking mechanism A as a basis, Chance, *et al.*, considered the processes $ES \rightarrow E + S$ and $ES + AH_2 \rightarrow E + A + 2H_2O$ (5) as being responsible for the disappearance of ES. (Reaction 5 represents the peroxidation of a hydrogen donor AH_2 by ES.) Based on this extension of mechanism A, an approximate relation between the maximal concentration of ES (p_m) and x_0 was derived.¹ Using the symbols of the present paper it can be written in the form

$$x_0 = \frac{k_2 + k_5 a}{k_1} \frac{p_m}{e - (R + 1)p_m} - \frac{R - 1}{R + 1} p_m + \frac{2eR}{(R + 1)^2} \ln \frac{e}{e - (R + 1)p_m} \quad (6)$$

a denotes the (constant) concentration of the hydrogen donor. Computer calculations show that, by decreasing both k_2 and a , p_m is shifted to longer times. For $k_2 = 0$ and $a = 0$, t_m (t at $p = p_m$) becomes infinite and p_m can be identified with p_{∞} . Under these circumstances eq 2 and 6 become identical. For a finite a ($k_2 = 0$), $p_m < p_{\infty}$. Since, however, for all known donors, k_5 is much smaller, than either k_1 or k_4 , it can be shown that for not too high values of a (such as in the case of the "irremovable alcohol impurity" of catalase), p_m is very close to p_{∞} .¹⁵ Thus eq 2 is a good approximation to the experimental $p_m \dots x_0$ curve of catalase and H_2O_2 .³

Mechanism C is closely related to the peroxidatic mechanism. It can account, unlike mechanism A, for the zero-order term in the dependence of the steady-state rate of decomposition of H_2O_2 on x , when x is high.^{5,6} ES_{II} in mechanism C fulfills the same role as ES in mechanism A.

This similarity becomes apparent when the steady-state concentrations are considered. p_2^* is given by eq 4. For the case, $x \ll K_M'$ and $k_2 = 0$ it becomes, as elaborated above, $p_2^* = e/(1 + R)$. $R = k_4/k_1$. This expression is identical with that for p^* . The difference between p and p_2 appears in the final phase of the reaction; while the change of p is bound by its steady-state limit, p_2 can rise above it. This rise, however, may be very small, if k_3 is high.

Finally it should be remarked that both mechanisms A and C are catalytic schemes in which the catalyst is not freed at the end of the reaction. This fact requires a modification of the definition of a catalyst, it being a substance which accelerates a chemical transformation by reacting with the catalyzed system in a cyclic set of reactions which involve steps of both binding and releasing of the catalyst. It follows from the above considerations that there are catalytic systems which come to a rest in a state in which part or all of the catalyst is permanently bound.

References and Notes

- (1) B. Chance, D. S. Greenstein, and F. J. W. Roughton, *Arch. Biochem. Biophys.*, **37**, 301 (1952).
- (2) B. Chance, *Acta Chem. Scand.*, **1**, 236 (1947).
- (3) E. Zidoni and M. L. Kremer, *Arch. Biochem. Biophys.*, **161**, 658 (1974).
- (4) B. Chance, D. S. Greenstein, J. Higgins, and C. C. Yang, *Arch. Biochem. Biophys.*, **37**, 322 (1952).
- (5) Y. Ogura, *Arch. Biochem. Biophys.*, **57**, 288 (1955).
- (6) P. Jones and A. Suggett, *Biochem. J.*, **110**, 617 (1968).
- (7) M. L. Kremer and G. Stein, *Trans. Faraday Soc.*, **55**, 959 (1959).
- (8) P. Jones and W. F. K. Wynne-Jones, *Trans. Faraday Soc.*, **58**, 1148 (1962).
- (9) A. S. Brill in "Comprehensive Biochemistry," Vol. 14, M. Florkin and E. Stotz, Ed., Elsevier, Amsterdam, 1966, p 447.
- (10) M. L. Kremer, *Isr. J. Chem.*, **9**, 321 (1971).
- (11) The designation of mechanisms follows an order adopted in a previous article.¹²
- (12) M. L. Kremer, *Biochim. Biophys. Acta*, **198**, 199 (1970).
- (13) If $k_3 = 0$, there exists an equilibrium between E, S, and ES. For given k_1 and k_2 , the ratio p_1/x will be then highest. By increasing k_3 , the equilibrium will be disturbed and p_1/x will decrease.
- (14) S. W. Benson, "The Foundation of Chemical Kinetics," McGraw-Hill, New York, N. Y., 1960, p 44.
- (15) M.L. Kremer, to be submitted for publication.

Thermodynamics of Caffeine and the 1-1 Caffeine-Salicylate Complex in Water at 25°

J. H. Stern,* J. A. Devore, S. L. Hansen, and O. Yavuz

Department of Chemistry, California State University, Long Beach, California 90840 (Received April 1, 1974)

Enthalpies of solution of caffeine in pure water at 25° were determined over the range from 0.001 to 0.02 *m*. Below 0.01 *m* the enthalpies remain constant at $\Delta H_s^\circ = 3.60 \pm 0.06$ kcal/mol, while above 0.01 *m* they decrease markedly with increasing concentration indicating self-association as suggested by earlier studies. The value of ΔH_s° combined with the enthalpies of solution of caffeine in excess sodium salicylate (0.0100-0.1500 *m*) yield the enthalpy (-8.65 ± 0.10 kcal/mol), equilibrium constant (10.1 m^{-1}), free energy (-1.37 kcal/mol), and entropy (-24.5 gibbs/mol) of formation of the biochemically interesting 1-1 molecular complex caffeine-salicylate from aqueous caffeine and salicylate ion. Qualitative enthalpy data indicate similar complex formation of caffeine with *p*-aminobenzoic acid and sodium benzoate, while only electrolyte-nonelectrolyte interaction appears to occur with sodium citrate.

Introduction

Caffeine in pure water appears to exist as a monomer in very dilute solutions only. Various studies have indicated that complicated self-association effects appear to become important at concentrations above ca. 0.01 *m*.¹⁻³ In the presence of some aqueous aromatic acids and their anions, caffeine appears to form molecular complexes. Such systems have been studied by a solubility method at 15 and 30°, including caffeine in aqueous *p*-aminobenzoic acid, salicylic acid, sodium benzoate, and sodium salicylate.⁴ Cryoscopic^{5,6} and osmometric measurements¹ give supporting evidence for the existence of such complexes.

This contribution reports on enthalpies of solution of caffeine in pure water to final concentrations in the range from 0.001 to 0.020 *m*, and enthalpies of solution of caffeine in the presence of excess sodium salicylate (0.01-0.15 *m*). The data were analyzed assuming the formation of a 1-1 caffeine-salicylate complex to yield the enthalpy ΔH_1° , the equilibrium constant K_1 , the free energy ΔG_1° , and the en-

trophy of formation ΔS_1° of the reaction between aqueous caffeine and salicylate ion to form this complex. Qualitative results on enthalpies of solution of caffeine in aqueous *p*-aminobenzoic acid, sodium benzoate, and sodium citrate are also mentioned.

Experimental Section

Caffeine (Calbiochem, Grade A, Anhydrous) was recrystallized from benzene. Elemental analysis yielded the following results.

Anal. Calcd for caffeine: C, 49.48; N, 28.25; H, 5.19. Found: C, 49.47; N, 28.70; H, 5.25.

Sodium salicylate was Matheson Coleman and Bell AR Grade, and all solutions were prepared with distilled, deionized water. The calorimeter and general experimental procedure have been described elsewhere,^{7,8} with caffeine in sealed glass ampoules submerged and crushed in weighed quantities of 450 g (ca. 450 ml) of pure water or aqueous sodium salicylate.

TABLE I: Ethalpy of Solution of Caffeine in Pure Water at 25°

Moles of caffeine × 10 ³	ΔH _s , kcal/mol	Moles of caffeine × 10 ³	ΔH _s , kcal/mol
0.5989	3.42	3.079	3.61
0.5999	3.42	3.142	3.60
0.5541	3.83	3.142	3.49
0.5556	3.74	3.128	3.65
ΔH _s mean = 3.6 ± 0.1 ^a (0.001 <i>m</i>)		ΔH _s mean = 3.59 ± 0.03 (0.007 <i>m</i>)	
0.9351	3.51	4.576	3.49
0.8960	3.71	4.535	3.63
1.034	3.62	4.696	3.68
ΔH _s mean = 3.61 ± 0.06 (0.002 <i>m</i>)		ΔH _s mean = 3.60 ± 0.05 (0.010 <i>m</i>)	
1.336	3.63	6.899	3.41
1.380	3.67	6.685	3.60
1.338	3.59	6.773	3.38
1.374	3.40	6.775	3.40
		6.787	3.56
ΔH _s mean = 3.57 ± 0.06 (0.003 <i>m</i>)		ΔH _s mean = 3.42 ± 0.03 (0.015 <i>m</i>)	
2.194	3.69	9.078	3.33
2.285	3.68	9.078	3.33
2.099	3.50	9.050	3.33
2.214	3.66	9.098	3.41
ΔH _s mean = 3.63 ± 0.04 (0.005 <i>M</i>)		ΔH _s mean = 3.35 ± 0.02 (0.020 <i>M</i>)	
ΔH _s ^o = 3.60 ± 0.06 kcal/mol (average of ΔH _s mean at 0.001, 0.002, 0.003, 0.005, 0.007, and 0.010 <i>m</i>)			

^a Uncertainty intervals are standard deviations of the mean.

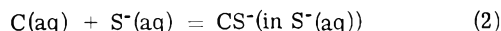
Results and Discussion

Enthalpies of solution of caffeine (ΔH_s) in pure water are shown in Table I and remain constant at 3.60 ± 0.06 kcal/mol (ΔH_s^o) below 0.01 *m*. The decrease in the enthalpy above this concentration indicates the exothermic effect of self-association, in agreement with earlier studies.

The heats of mixing *Q* (in calories) of aqueous caffeine with excess sodium salicylate for each run were obtained from

$$Q = Q' - n_1 \Delta H_s^o \quad (1)$$

where *Q'* is the measured heat of solution of *n*₁ moles of caffeine (*C*) (*ca.* 0.002 *m*) in aqueous sodium salicylate (*S*⁻). The value of ΔH_s^o in eq 1 is in calories/mole. Values of *Q* for each run at differing initial concentrations of *S*⁻ are shown in Table II. If it is assumed that only 1-1 caffeine salicylate (*CS*⁻) forms, then *Q* may be associated with the molal enthalpy ΔH₁^o of forming the complex according to the equation



For a given run *j* the tabulated heat of mixing *Q*_{*j*} is given by

$$Q^j = m_{\text{H}_2\text{O}}^j (CS^-) \Delta H_1^o \quad (3)$$

where *m*_{H₂O}^{*j*} is the mass of water in kilograms and (*CS*⁻) is the equilibrium concentration of the complex in moles/kilogram of H₂O as given by

$$(CS^-) = K_1 (C) (S^-) \quad (4)$$

For a given choice of *K*₁ (*m*⁻¹), the equilibrium concentrations of the species are computed for each calorimetric run. The set of heats of mixing *Q* are next curve fitted to eq 3 by the method of least squares to obtain ΔH₁^o and the proce-

TABLE II: Heats of Mixing Aqueous Caffeine with Aqueous Sodium Salicylate at 25°

<i>m</i> , sodium salicylate	<i>n</i> ₁ , moles of caffeine × 10 ³	- <i>Q</i> , cal/run
0.0100	0.8666	0.7167
	0.9614	0.8266
0.0250	0.9454	1.549
	0.9531	1.573
	0.9938	1.779
0.0500	0.9851	2.864
	1.003	2.978
	1.010	2.945
0.0750	0.9171	3.302
	0.9387	3.379
	0.9609	3.640
0.1000	0.9634	4.033
	0.9665	4.095
	0.9938	4.168
0.1250	0.8697	4.181
	0.9423	4.526
	0.9717	4.791
0.1500	0.8790	4.652
	0.9454	5.014
	0.9454	5.112

cedure is repeated until the value of *K* that minimizes the variance *U*, given by

$$U = \sum_j (Q_{\text{calcd}}^j - Q_{\text{expt}}^j)^2$$

is found. The computed value of ΔH₁^o is -8.65 kcal/mol with an estimated overall experimental error of ±0.10 kcal/mol, while *K*₁ is 10.1 *m*⁻¹. The free-energy change Δ*G*₁^o was calculated from Δ*G*₁^o = -*RT* ln *K*₁ and is -1.37 kcal/mol. The entropy change Δ*S*₁^o was obtained from Δ*S*₁^o = (1/*T*)(ΔH₁^o - Δ*G*₁^o) and is -24.5 gibbs/mol. It may be noted that the low concentrations of all solutes minimize uncertainties due to nonideal effects and formation of higher order complexes. Stabilization of this complex may occur *via* hydrogen bonding between the salicylate ion hydroxy hydrogen and the two nitrogens on the five-membered ring of caffeine, and by bonding between the six-membered rings of caffeine and salicylate ions, respectively.

Qualitative values of heats of solution of caffeine in aqueous *p*-aminobenzoic acid and sodium benzoate measured in this laboratory show similar behavior to that in sodium salicylate, pointing to complex formation.¹ In contrast, the heat of solution of caffeine in aqueous sodium citrate remains approximately constant with the concentration of this salt (*ca.* 0.1-0.20 *m*), and differs little (*ca.* 0.3 kcal/mol) from its heat of solution in pure water, indicating that only electrolyte-nonelectrolyte interactions occur.¹

Similar studies with other xanthines should be of interest, and calorimetric measurements with theophylline have been initiated.

Acknowledgment. The authors thank Professor Frank M. Goyan for fruitful discussions and the National Science Foundation for financial support (Grant No. GP 11271).

References and Notes

- (1) F. M. Goyan and H. N. Borazan, *J. Pharm. Sci.*, **57**, 861 (1968).
- (2) D. Guttman and T. Higuchi, *J. Amer. Pharm. Ass., Sci. Ed.*, **46**, 4 (1957).
- (3) S. J. Gill, M. Downing, and G. F. Sheats, *Biochemistry*, **6**, 272 (1967).
- (4) T. Higuchi and D. A. Zuck, *J. Amer. Pharm. Ass., Sci. Ed.*, **42**, 138 (1953).
- (5) M. Blake and L. E. Harris, *J. Amer. Pharm. Ass., Sci. Ed.*, **41**, 527 (1952); M. Donbrow and Z. Z. Jar, *J. Chem. Soc.*, 3845 (1963).
- (6) W. O. Emery and C. D. Wright, *J. Amer. Chem. Soc.*, **43**, 2323 (1921).
- (7) J. H. Stern and C. W. Anderson, *J. Phys. Chem.*, **68**, 2528 (1964).
- (8) J. H. Stern, J. P. Sandstrom, and A. Hermann, *J. Phys. Chem.*, **71**, 3623 (1967).

Heats of Mixing Aqueous Electrolytes. XI. The Charge-Asymmetric Limiting Law at Low Concentrations. Barium Chloride with Sodium Chloride and Sodium Sulfate with Sodium Chloride

R. B. Cassel and R. H. Wood*

Department of Chemistry, University of Delaware, Newark, Delaware 19711 (Received September 28, 1973; Revised Manuscript Received June 21, 1974)

The heats of mixing solutions of barium chloride with sodium chloride and sodium sulfate with sodium chloride have been measured in water at 25° at ionic strengths as low as $I = 0.02$ to 0.05 mol kg^{-1} . The solutions to be mixed have the same molal ionic strength (I). The data are a test of Friedman's limiting law for charged-asymmetric mixtures. The results show that the heats of mixing do change sharply below $I = 0.2 \text{ mol kg}^{-1}$ in the direction required by the limiting law. The results did not go to low enough concentrations to confirm the numerical value of the limiting law slope. In both systems the asymmetry of the heat of mixing curve *vs.* ionic strength fraction increased sharply at very low concentrations.

Introduction

The purpose of this paper is to present the results of a test of Friedman's limiting law for charge-asymmetric mixtures.¹⁻³ Previous results in this laboratory^{3,4} showed a trend toward higher positive values for the heat of mixing alkaline earth halides with alkali halides as the concentration was decreased to $0.5 I$. The results of Smith⁵ working with Young for Na_2SO_4 with NaCl showed a trend toward more negative values at low concentration contrary to the expectations of the limiting law. The present results extend the measurements on the two systems to an order of magnitude lower concentrations.

Experimental Section

Sodium chloride and sodium sulfate solutions were made up from Fisher certified ACS grade salts having total reported impurities of less than 0.01%. Barium chloride solutions were prepared from optronic grade ultrapure salt obtained from Alfa Inorganics specified to be 99.995% pure. Solutions were prepared by weight and checked by potentiometric titration or by conductivity and found to be within 0.1% of the calculated concentration. To double check certain unexpected results, duplicate solutions were prepared and assayed independently.

The calorimeter, a commercially available LKB batch microcalorimeter,⁶ has been described elsewhere.⁷ Because the purpose of this investigation is to explore low concentration limiting law behavior in experiments where heat effects will be very small, it was necessary to take extra precautions to reduce instrumental errors for low heat experiments. The largest source of (systematic) error for low heat measurements derives from the relatively large amount of heat ($600 \mu\text{cal}$) which is evolved during the rotation-mixing mode of the calorimeter which is essential to physically intermix the two solutions. This heat of intermixing has been shown⁸ to be highly sensitive to the weights of solution in the two compartments in the calorimeter cell. Since this heat of intermixing must be subtracted from the apparent heat of mixing, the blank experiment which follows the actual mixing experiment must duplicate as nearly as possible the physical intermixing in the original mix. This duplication can be best assured by the following loading procedure.^{8,9}

Loading Procedure. Approximately 5 g of solution A¹⁰ was loaded into the 4-ml side of the mixing cell which was either dry (in which case, $\text{wt}_B(\text{II}) = 0$) or contained $0.020 \pm 0.003 \text{ g}$ of the product of the previous mixing experiment run at the same ionic strength. The cell is then rotated as during the forthcoming mix and all but approximately $0.01 \pm 0.001 \text{ g}$ of the solution A which has spilled over into the 2-ml side is removed by syringe withdrawal and weighed. The net weights of component A and B in the 4-ml side are calculated (designated $\text{wt}_A(\text{II})$ and $\text{wt}_B(\text{II})$ in Table I). Approximately 2 g of the second solution (designated $\text{wt}_B(\text{I})$) is weighted into the 2-g side. This side also contains 0.01 g of component A ($\text{wt}_A(\text{I}) = 0.01 \text{ g}$) which was left on the walls. After waiting for thermal equilibrium, the chemical, electrical calibration, and blank intermixing heats are measured. When the solution is withdrawn to prepare for the next experiment, the volume withdrawn from each side of the cell will be the same as those loaded. This procedure minimizes the systematic error due to differences in the heats of intermixing.

Results and Discussion

The composition of the solutions in the calorimeter before mixing together with the experimental heats are given in Table I. The heat of mixing pure solutions of components A and B is represented by the equation²

$$\Delta_m H = -q = y_A(1 - y_A)I^2W[RTh_0 + (1 - 2y_A)RTh_1] \quad (1)$$

where y_A is the solute ionic strength fraction of component A (the component with the highest formula weight), q is the measured heat given off, W is the weight of water (in kg) in the final solution, RTh_0 and RTh_1 are parameters to describe the mixing, and I is the molal ionic strength. In fitting the actual calorimetric data in Table I, eq 1 was used to calculate q_I , q_{II} , and q_F (the heats of forming the initial solutions (I and II) and the final solution from the pure components). The calculated heat for the actual experiment is then $q_F - q_I - q_{II}$ and a least-squares procedure is used to adjust RTh_0 and RTh_1 to minimize the difference between experimental and calculated heats. The scatter of the experimental heat (q_{expt}) from the calculated

TABLE I: Calorimetric Data

<i>I</i>	Weights of solution, g				Heat, m cal ^c		<i>I</i>	Weights of solution, g				Heat, m cal ^c	
	<i>W</i> _{A(II)}	<i>W</i> _{B(II)}	<i>W</i> _{A(I)}	<i>W</i> _{B(I)}	- <i>q</i> _{expt}	- <i>q</i> _{calcd}		<i>W</i> _{A(II)}	<i>W</i> _{B(II)}	<i>W</i> _{A(I)}	<i>W</i> _{B(I)}	- <i>q</i> _{expt}	- <i>q</i> _{calcd}
BaCl ₂ (A) ^b -NaCl(B)						Na ₂ SO ₄ (A) ^b -NaCl(B)							
0.5	4.168	0.0	0.01	2.539	40.25	40.18	1.0	4.380	0.01	0.01	2.375	-43.26	-43.8
	3.927	0.01	0.01	2.110	34.93	35.78		4.131	0.01	0.01	2.209	-42.27	-40.96
	3.914	0.01	0.01	2.176	35.87	35.43		0.01	4.124	2.475	0.01	-46.24	-44.17
	3.848	0.01	0.01	2.196	34.70	35.42		0.01	4.099	2.301	0.01	-39.23	-42.07
	0.01	3.817	2.276	0.01	36.10	36.10	0.5	4.278	0.01	0.01	2.044	-9.36	-10.12
	0.01	3.845	2.194	0.01	36.14	35.36		4.253	0.01	0.01	2.234	-11.09	-10.72
	0.01	3.788	2.143	0.01	35.15	34.63		4.152	0.01	0.01	2.286	-10.19	-10.79
	0.01	3.820	2.115	0.01	33.16	34.44		4.152	0.01	0.01	2.007	-10.39	-10.99
0.2	3.764	0.0	0.01	2.375	7.048	6.997		0.01	4.141	2.306	0.01	-10.89	-10.86
	3.726	0.01	0.01	2.357	6.796	6.918		0.01	4.107	2.143	0.01	-10.82	-10.32
	3.715	0.01	0.01	2.264	6.718	6.727	0.2	4.026	0.0	0.01	2.406	-2.069	-2.342
	3.692	0.01	0.01	2.287	6.829	6.753		3.833	0.01	0.01	2.323	-2.492	-2.217
	0.01	3.774	2.255	0.01	7.431	7.364		3.774	0.01	0.01	2.472	-2.249	-2.226
	0.01	3.759	2.175	0.01	7.186	7.209		0.01	3.830	2.288	0.01	-1.340	-1.366
	0.01	3.811	2.091	0.01	7.021	7.094		0.01	3.786	2.257	0.01	-1.383	-1.332
	0.01	3.852	2.019	0.01	7.021	6.984		0.01	3.792	2.165	0.01	-1.243	-1.280
0.1	4.791	0.01	0.01	1.956	2.035	1.943	0.1	3.841	0.01	0.01	2.456	-0.560	-0.547
	3.898	0.0	0.01	2.192	1.978	2.007		3.702	0.01	0.01	2.004	-0.553	-0.566
	3.755	0.01	0.01	2.240	1.989	2.008		0.01	3.721	2.035	0.01	0.132	0.125
	3.731	0.01	0.01	2.289	1.968	2.034		0.01	3.769	1.992	0.01	0.138	0.142
	0.01	3.774	2.250	0.01	2.096	2.156	0.05	4.173	0.0	0.01	1.538	-0.170	-0.227
	0.01	3.831	2.088	0.01	2.174	2.078		3.823	0.01	0.01	2.290	-0.139	-0.155
	0.01	4.772	1.764	0.01	2.084	2.026		3.753	0.01	0.01	2.315	-0.180	-0.147
	0.0	4.274	1.730	0.01	1.862	1.932		3.744	0.0	0.01	2.260	-0.118	-0.156
0.05	4.248	0.01	0.01	1.858	0.498	0.505		3.734	0.01	0.01	2.165	-0.217	-0.157
	4.155	0.01	0.01	1.805	0.450	0.490		0.01	3.720	2.347	0.01	0.184	0.134
	4.076	0.01	0.01	1.968	0.526	0.529		0.01	3.728	2.221	0.01	0.200	0.146
	3.788	0.0	0.01	2.080	0.602	0.551		0.01	4.338	1.516	0.01	0.166	0.227
	0.01	3.873	2.341	0.01	0.792	0.750		4.317	0.01	0.01	1.542	-0.248	-0.231
	0.01	4.113	2.247	0.01	0.709	0.760							
	0.01	3.755	2.089	0.01	0.704	0.699							
	0.01	4.246	1.967	0.01	0.721	0.721							
0.02	4.114	0.01	0.01	1.884	0.119	0.121							
	3.926	0.01	0.01	2.292	0.130	0.146							
	3.88	0.01	0.01	2.291	0.164	0.146							
	0.01	4.099	2.120	0.01	0.191	0.198							
	0.01	3.936	2.099	0.01	0.200	0.193							

^a The weights of components A and B are designated by *W*_A and *W*_B, respectively. The 4-ml compartment of the calorimeter and the 2-ml compartment are designated by II and I, respectively. For example, in the second mixing experiment in Table I, a mixture containing 3.927 g of BaCl₂ solution (*I* = 0.5) and 0.01 g of NaCl solution (*I* = 0.5) was mixed with a mixture of 0.01 g of BaCl₂ solution (*I* = 0.5) and 2.110 g of NaCl solution (*I* = 0.5) absorbing 0.03493 cal. ^b Component A is the salt with the highest formula weight. ^c The experimental and calculated heat released by the system are designated by *q*_{expt} and *q*_{calcd}. Thus the BaCl₂-NaCl mixes were endothermic.

TABLE II: Mixing Parameters

	<i>I</i>	<i>RTh</i> ₀	<i>RTh</i> ₁
		cal kg mole ⁻²	cal kg mole ⁻²
BaCl ₂ (A)-NaCl(B)	0.5	105.6(16) ^a	0(7)
	0.2	127.7(12)	23(5)
	0.1	151.0(5)	20(14)
	0.05	189.0(10)	77(29)
	0.02	302.0(40)	176(131)
Na ₂ SO ₄ (A)-NaCl(B)	1.0	-30.3(25)	0
	0.5	-30.4(17)	0
	0.2	-32(4)	29(16)
	0.1	-17(2)	90(8)
	0.05	-1(12)	170(40)

^a The 95% confidence limits of the least significant digit is given in parentheses. For example, 105.6 ± 1.6 is written 105.6(16).

heat (*q*_{calcd}) indicates a precision of about 1% at high heats and about 30 μcal at low heats. The values for the parameters which best fit this data are given in Table II.

A plot of the present results together with the results of Wood and Ghamkhar⁴ at *I* = 0.5, 1, 2, and 3 for mixtures of barium chloride with sodium chloride is given in Figure 1. The agreement where the results overlap is quite good: 103.7 ± 1.0 vs. 105.6 ± 1.6 for the present results at *I* = 0.5.

Figure 2 gives a similar plot for the mixtures of sodium sulfate with sodium chloride. The independent results of Chen¹¹ working in this laboratory and Smith⁵ working with Young¹² are also shown in this plot. The results are in very good agreement at the higher concentrations. The only serious disagreement is at *I* = 0.2 where Smith's value is considerably lower than the present results. The estimated 95% confidence limits of the present results are shown in Figure 2 and it is quite possible that the disagreement at 0.2 *m* is within the combined experimental error of the two investigations.

Friedman's higher order limiting law^{1,2} for a mixture of a 2-1 with a 1-1 electrolyte (or a 1-2 with a 1-1 electrolyte) gives the following result³

$$h_0 = - (TA^2/3V) \left(\frac{1}{d} \frac{\partial d}{\partial T} - \frac{3}{D} \frac{\partial D}{\partial T} - \frac{3}{T} \right) \ln I \quad (2)$$

which depends only on temperature (*T*) and the following solvent properties: dielectric constant (*D*), density (*d*), specific volume (*V*), and a dimensionless Debye-Hückel limiting law parameter (*A* = 1.1723). For water at 25° eq 2 becomes³

$$RTh_0 = - 533 \log I \text{ (cal kg mol}^{-2}\text{)} \quad (3)$$

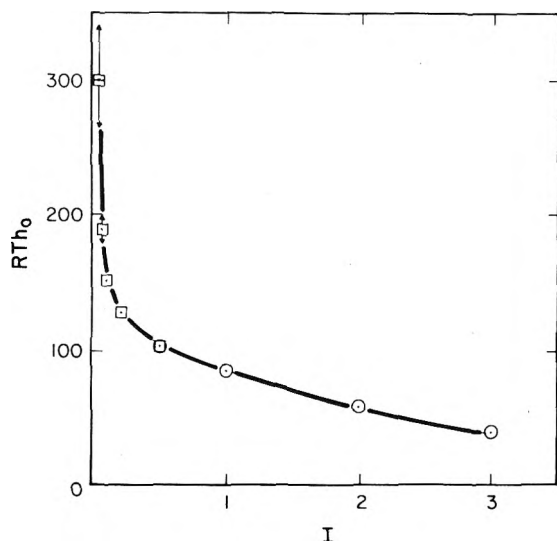


Figure 1. The value of RTh_0 for the $BaCl_2$ - $NaCl$ mixture is plotted vs. the total molal ionic strength: \odot indicates results of Wood and Ghamkhar (ref 4), \square indicates the present results.

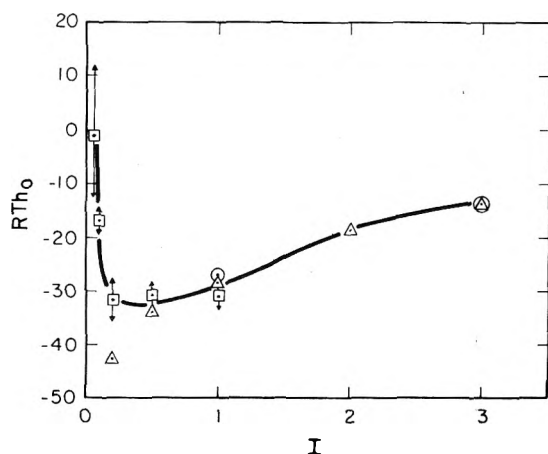


Figure 2. The value of RTh_0 for the Na_2SO_4 - $NaCl$ mixture is plotted vs. the total molal ionic strength: Δ indicates the results of Smith (ref 5) and of Wu, Smith, and Young at $I = 1.0$ (ref 12); \odot indicates the results of Chen (ref 11); and \square indicates the present results.

This limiting law predicts that as the concentration goes to zero RTh_0 will go to positive infinity with a slope vs. $\log I$ of -633 . The results in Figures 1 and 2 show an extremely sharp upturn to more positive values as the concentration gets smaller, as expected from this limiting law. However, an experimental verification of the theoretical slope in eq 2 is not possible at the present date. At $I = 0.07$ the slopes of both sets of data are an order of magnitude lower than the limiting law slope. For the mixture of barium chloride with sodium chloride, the results extend to $I = 0.02$ and the average slope from $I = 0.05$ to 0.02 is much larger. However it is still somewhat less than half of the theoretical slope. A plot of the present results vs. $\log I$ indicates that a smooth curve can be drawn through the present results with an approach to the limiting law slope below $I = 0.01$. Recent theoretical calculations for a mixture of magnesium chloride with sodium chloride¹³ show that the limiting law for the free energy corresponding to eq 2 is approached only at very low concentrations. Even at $I = 0.01$, the calculated

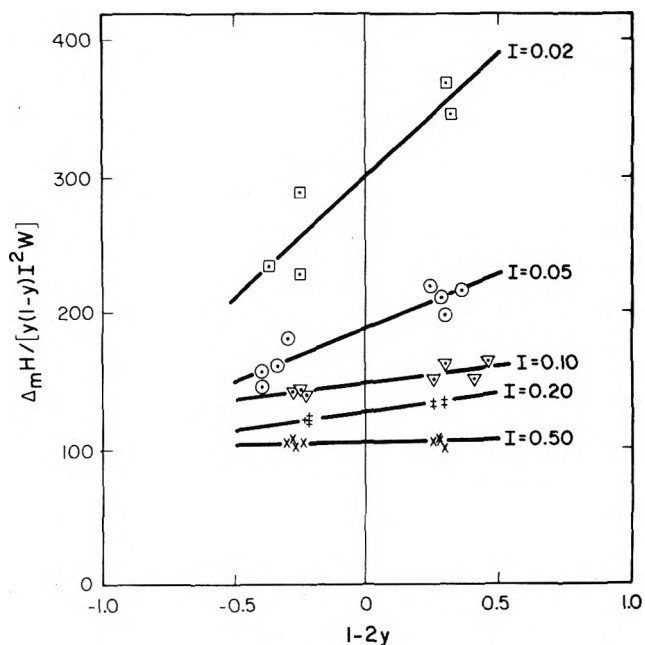


Figure 3. The value of $\Delta_m H / [y_A(1 - y_A)^2 W]$ for $BaCl_2(A)$ - $NaCl(B)$ is plotted vs. $(1 - 2y_A)$. The intercept at $(1 - 2y_A) = 0$ is RTh_0 and the slope is RTh_1 (see eq 1). The original data have been corrected to what would have been observed if the initial solutions contained pure A and B rather than a mixture of A and B. The correction is quite small.

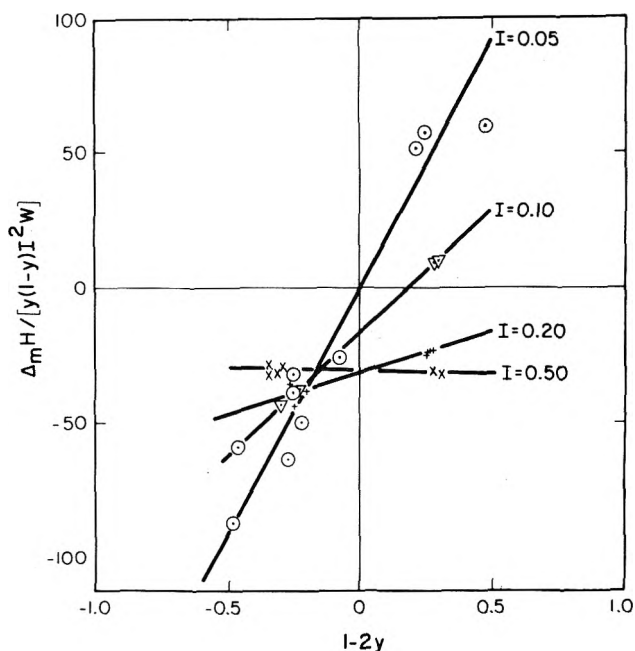


Figure 4. The value of $\Delta_m H / [y_A(1 - y_A)^2 W]$ for $Na_2SO_4(A)$ - $NaCl(B)$ is plotted vs. $(1 - 2y_A)$.

slope is only about one-fourth of the limiting law slope. The present results constitute an experimental verification of the Friedman's limiting law in the sense that this limiting law predicted the sharp upturn observed in Figures 1 and 2 and no other explanation for this sharp upturn is available. Since this limiting law has its origin in the $c \log c$ term for charge-asymmetric electrolytes² the present results are an experimental verification of this term.

There is one feature of the present results which is totally unexpected. Figures 3 and 4 show a plot of $\Delta_m H/y_A(1 - y_A)I^2W$ vs. $(1 - 2y_A)$ for both mixings. For this plot the experimental data were corrected to what would have been observed if the initial solutions contained pure component A and pure component B, respectively. This correction is quite small (less than 1 cal kg mol⁻²). According to eq 1 this plot should give a straight line, with the slope of this straight line equal to RTh_1 (the skew term) and an intercept at $1 - 2y = 0$ equal to RTh_0 . Both plots show slopes (RTh_1) that increase sharply as the concentration decreases. In addition, the value of RTh_1 is the same within experimental error for the two systems at the same concentration (see Table II).

At the time that these experiments were carried out Friedman had shown that charge asymmetric mixtures can give skew terms when strong three ion interactions are present, but that these interactions would give an RTh_1 that is proportional to the ionic strength.¹⁴ Thus, it was expected that the contributions of these terms to RTh_1 should get smaller as the concentration decreases. Recently, more refined hypernetted chain calculations of Krishnan and Friedman¹⁵ indicate a skew term increasing in magnitude with decreasing concentration. However the sign and magnitude of their results are not in agreement with the present experimental results.

Although the experiments are very difficult to carry out

at these low concentrations because of the extreme calorimetric sensitivity needed, the authors believe that the increase in RTh_1 is a real effect and not a systematic error in the experiments.

Acknowledgment. The authors are grateful for the support of this work by the Office of Saline Water, U. S. Department of the Interior.

References and Notes

- (1) H. L. Friedman, *J. Chem. Phys.*, **32**, 1134 (1960).
- (2) H. L. Friedman, "Ionic Solution Theory," Interscience, New York, N. Y., 1962, pp 244-246.
- (3) R. H. Wood, J. D. Patton, and M. Ghamkhar, *J. Phys. Chem.*, **73**, 346 (1969).
- (4) R. H. Wood and M. Ghamkhar, *J. Phys. Chem.*, **73**, 395E (1969).
- (5) M. B. Smith, Ph.D. Thesis, University of Chicago, 1942.
- (6) LKB Produkter AB, Fack, 161 25 Bromma 1, Sweden, Model 10700-2.
- (7) P. J. Reilly and R. H. Wood, *J. Phys. Chem.*, **76**, 3474 (1972).
- (8) A. S. Levine, Ph.D. Thesis, University of Delaware, June 1971.
- (9) J. S. Falcone, Jr., A. S. Levine, and R. H. Wood, *J. Phys. Chem.*, **77**, 2137 (1973).
- (10) Solution A is the solution of salt having the higher formula weight, solution B the solution of salt having the lower formula weight.
- (11) H. K. Chen, M.S. Thesis, University of Delaware, Newark, Del., June 1971.
- (12) Y. C. Wu, M. B. Smith, and T. F. Young, *J. Phys. Chem.*, **69**, 1868 (1965).
- (13) H. L. Friedman, A. Smithe-man, and R. DeSantis, *J. Solution Chem.*, **2**, 59 (1973).
- (14) Reference 3, p 231, or see P. J. Reilly and R. H. Wood, *J. Phys. Chem.*, **73**, 4292 (1969).
- (15) H. L. Friedman and C. V. Krishnan, **78**, 1927 (1974).

Charge-Asymmetric Mixtures of Electrolytes at Low Ionic Strength

Harold L. Friedman* and C. V. Krishnan

Department of Chemistry, State University of New York, Stony Brook, New York 11790 (Received March 28, 1974)

Publication costs assisted by the National Science Foundation

The limiting laws for the mixing coefficients g_1 (for the excess free energy) and h_1 (for the enthalpy) are derived from the cluster theory of ionic solutions. Both coefficients are found to be proportional to the square root of the ionic strength I near $I = 0$. The HNC approximation method is applied to models for several aqueous electrolyte mixtures at 25° in the range of I from 0.01 to 1.3 m. The computed g_1 and h_1 coefficients seem consistent with the limiting laws, which dominate the concentration dependence of g_1 and h_1 only at much smaller I . Although the calculated I dependence of these coefficients is quite striking, it is not consistent with the h_1 data of Cassel and Wood. It is remarkable that the HNC calculations fail to give satisfactory self-consistency tests at the level of the g_1 coefficients. This indicates the need of more powerful approximation methods for the calculation of g_1 and h_1 .

1. Introduction

The change in excess Gibbs free energy G^{ex} when pure solutions of electrolytes A and B, having the same molal ionic strength I , are mixed together at given T and P can be written in the form

$$\Delta_m G^{\text{ex}}(y, I) = y(1 - y)I^2WRT[g_0(I) + [1 - 2y]g_1(I) + [1 - 2y]^2g_2(I) + \dots] \quad (1.1)$$

where $y = y_A$ is the fraction of the mixture's ionic strength due to A and W is the mass (kg) of solvent in the mixture.

From eq 1.1 it is easy to derive corresponding equations for the other extensive thermodynamic variables. Thus for the enthalpy H one finds

$$\Delta_m H^{\text{ex}}(y, I) = y(1 - y)I^2WRT[h_0(I) + [1 - 2y]h_1(I) + [1 - 2y]^2h_2(I) + \dots] \quad (1.2)$$

where the mixing coefficients h_n are related to those for the free energy by the equation

$$h_n(I) = -T(\partial g_n(I)/\partial T)_{P,I} \quad n = 0, 1, 2, \dots \quad (1.3)$$

Cassel and Wood¹ have just reported values of h_1 for some charge-asymmetric common ion mixtures in which electrolyte A is 1,2 or 2,1 charge type while electrolyte B is 1,1. They report a strong increase in h_1 as I decreases below 0.1 m ; the effect is qualitatively the same for the two rather different mixtures which they studied. The insensitivity of the effect to the properties of the ions, aside from charges, suggests that it is a manifestation of the Coulomb interactions among the ions.

While the asymptotic behavior of $g_0(I)$ at small I , *i.e.*, the limiting law for g_0 , was worked out from the statistical mechanical theory of ionic solutions some time ago,²⁻⁴ the corresponding theory for g_1 appears not to have been developed. The limiting law behavior for such coefficients of ionic solutions is controlled by the coulombic interaction of the ions, so this a natural place to look for an explanation of the h_1 effect noted above. For this reason we have worked out the limiting laws for g_1 and h_1 for mixtures of this charge type as described in section 2.

Generally, even when the limiting law for a given solution coefficient is known, one does not know how small the ionic strength must be before the limiting law dominates the behavior of the coefficient. Thus, for aqueous solutions of simple electrolytes one must have $I < 0.1 m$ or even $I < 10^{-4} m$, depending on charge type, before the activity coefficient conforms closely to the Debye-Hückel limiting law. For another example, model calculations for MgCl_2 -NaCl mixtures show that only for $I < 10^{-4} m$ is the measurable coefficient

$$w_0(I) = \partial(Ig_0)/\partial I$$

close to its limiting law form.⁵ The model calculations reported in sections 3 and 4 show how g_1 and h_1 fall off from their limiting law behavior as I is increased.

The calculations in sections 2-4 yield thermodynamic functions in the so-called⁶ McMillan-Mayer (MM) system while the equations above, as well as the experimentally determined coefficients, hold in the Lewis-Randall (LR) system,⁶ the conventional system for ionic solution thermodynamics. Corresponding to eq 1.1 in the LR system is the following equation in the MM system

$$\Delta_m A^{\text{ex}}(y, I') = y(1 - y)I'^2 VRT[g_0'(I') + [1 - 2y]g_1'(I') + \dots] \quad (1.4)$$

where A^{ex} is the extensive excess Helmholtz free energy of the solution in osmotic equilibrium with solvent of specified activity (*i.e.*, the solvent is under a specified pressure P_0), V is the volume of the solution, and I' its molar ionic strength. Equation 1.4 refers to mixing at fixed P_0 and I' while y has the same meaning as in eq 1.1. The notation^{6,7} in eq 1.4, which is simpler than that originally introduced for this process,^{2,3} will be used below.

The relation between the g_1 and g_1' coefficients is given in section 5. In section 6 the results of the calculations are brought together and compared with the $h_1(I)$ data reported by Cassel and Wood.¹ The main conclusions of sections 3 and 6 are summarized in section 7.

2. Limiting Law for g_1' and h_1'

The excess Helmholtz free energy of a solution may be written^{3,7a}

$$-A^{\text{ex}}/VkT = \kappa^3/12\pi + s_2 + s_3 + s_4 + \dots \quad (2.1)$$

where we define

$$\kappa^2 = \lambda \sum_s \rho_s z_s^2 \quad (2.2)$$

$$\lambda = 4\pi e^2/\epsilon kT \quad (2.3)$$

and ρ_s is the particle number density of solute species s , z_s the charge (protonic units) on solute species s , e the electronic charge, ϵ the solvent's dielectric constant, and s_n is the contribution

$$\sum_{n_1+n_2+\dots+n} \rho_1^{n_1} \rho_2^{n_2} \dots B_{n_1, n_2, \dots}(\kappa)/n_1! n_2! \dots \quad (2.4)$$

from cluster integrals on n solute particles.

For our purpose we require the "moments" defined as follows³

$$\mu_n = \sum_s \rho_s z_s^n \quad (2.5)$$

We have special values

$$\mu_0 = \sum_s \rho_s \equiv \rho \quad (2.6)$$

$$\mu_1 = 0$$

$$\mu_2 = \kappa^2/\lambda \quad (2.7)$$

The effect of interest here especially involves μ_3 which vanishes for electrolytes of the NaCl or CaSO_4 type, but not for the types CaCl_2 or AlCl_3 .

The asymptotic κ dependence at small κ , *i.e.*, the limiting law form, has already been calculated³ for each s_n with results given here for the first few.⁸

$$s_2 = (\lambda^3/192\pi^2)\mu_3^2 \ln \kappa + O(\kappa^4) \quad (2.8)$$

$$s_3 = -(\lambda^5/8\kappa)\mu_3^2 \mu_4 i_3 + O(\kappa^5 \ln \kappa) \quad (2.9)$$

$$s_4 = (\lambda^6/16\kappa^3)\mu_3^4 i_4 + O(\kappa^6) \quad (2.10)$$

where^{8,9}

$$i_3 = 2.59_0 \times 10^{-4} \quad (2.11)$$

$$i_4 = 4.12_0 \times 10^{-5} \quad (2.12)$$

and where $O(f(\kappa))$ signifies a remainder R such that $R/f(\kappa)$ has a finite limit at $\kappa = 0$.

For a mixture of electrolyte A, here assumed to be either 2,1 or 1,2 charge type, with electrolyte B, here assumed to be 1,1 charge type, we find

$$\Delta_m \mu_3^2 = -(1 - Y^2)\mu_2^2/4 \quad (2.13)$$

$$\Delta_m(\mu_3^2 \mu_4) = -(1 - Y^2)(4 - Y)\mu_2^3/4 \quad (2.14)$$

$$\Delta_m \mu_3^4 = -(1 - Y^2)(7 - 4Y + Y^2)\mu_2^4/16 \quad (2.15)$$

where we define

$$Y = 1 - 2y_A \quad (2.16)$$

Now by combining these results with the following expression, derived from eq 2.1

$$-\Delta_m A^{\text{ex}}/VkT = \Delta_m s_2 + \Delta_m s_3 + \Delta_m s_4 + \dots \quad (2.17)$$

we can find the asymptotic form of $\Delta_m A^{\text{ex}}$ at low ionic strength. The result is most conveniently expressed in terms of the coefficients g_n' which appear in eq 1.4. Thus, we find, for mixtures of the specified charge type

$$I'^2 g_0' = -(\lambda^3/48\pi^2)\mu_2^2 \ln \kappa + O(\kappa^4) \quad (2.18)$$

$$I'^2 g_1' = -(\lambda^5/8\kappa)\mu_2^3 i_3 + (\lambda^6/16\kappa^3)\mu_2^4 i_4 + O(\kappa^6) \tag{2.19}$$

These results depend upon the charge type. Thus, for charge-symmetric mixtures (*i.e.*, A and B having the same charge type) we would have

$$\Delta_m \mu_n = 0 \quad n = 0, 1, 2, 3, \dots \tag{2.20}$$

and then g_n' is $O(\kappa^{2n})$.

By applying the thermodynamic equation (*cf.* eq 1.3)

$$h_n'(I') = -T(\partial g_n'(I')/\partial T)_{P_0, I'} \tag{2.21}$$

to eq 2.18 and 2.19 and noticing that (*cf.* eq 2.3)

$$\kappa = (\lambda\mu_2)^{1/2} \tag{2.22}$$

and

$$-\partial \ln \lambda / \partial \ln T = 1 + \partial \ln \epsilon / \partial \ln T \tag{2.23}$$

we find

$$h_0' = 3g_0'(1 + \partial \ln \epsilon / \partial \ln T) \tag{2.24}$$

$$h_1' = (9/2)g_1'(1 + \partial \ln \epsilon / \partial \ln T) \tag{2.25}$$

To express these limiting laws in practical units it is convenient to express ρ_s in particles per (ångströms)³ and λ in ångströms. Then the *molar* ionic strength is given by

$$I' = \mu_2 / (2 \times 6.025 \times 10^{-4}) \tag{2.26}$$

For water at 25° we have¹⁰

$$\partial \ln \epsilon / \partial \ln T = -1.371 \tag{2.27a}$$

$$\lambda = 4\pi \times 7.14 \text{ \AA} \tag{2.27b}$$

(*I.e.*, λ is 8π times the Bjerrum radius.¹⁰) The limiting law results for a mixture of A (1,2 or 2,1 charge type) with B (1,1 charge type) in water at 25° are

$$g_0' = 0.434 \ln I' = 1.000 \log I' \tag{2.28}$$

$$g_1' = 1.529\sqrt{I'} \tag{2.29}$$

$$h_0' = -0.48 \ln I' = -1.111 \log I' \tag{2.30}$$

$$h_1' = -2.55\sqrt{I'} \tag{2.31}$$

As usual,^{2,3} the logarithmic limiting laws are determined only up to a constant. Thus one really should write $\ln(\kappa/\kappa^*)$ in place of $\ln \kappa$ and $\ln(I'/I'^*)$ in place of $\ln I'$, where κ^* and I'^* are constants of suitable dimensions which otherwise are quite arbitrary.

The limiting laws for g_0' and h_0' , after consideration of the results of section 5, agree with those reported earlier on the basis of a less compact method of calculation from the same theory.^{2,3,5,11} The method used earlier would require the evaluation of ten different cluster integrals to calculate the s_3 contribution to g_1' . The number required to calculate the s_4 contribution is several times larger. Even when the integrals differ only in the charge and combinatorial factors it is difficult to evaluate g_1' by calculating so many integrals.

In systems in which $\mu_3 \neq 0$ one has μ_3 proportional to κ^2 for a variation at fixed y . For such a variation we see that s_4 like s_3 is proportional to κ^3 in the limiting law region, an observation which has been made before,³ but which is unexpected on the basis of intuitive considerations. As a consequence of this behavior of s_4 the limiting laws for g_1' and h_1' comprise contributions from the *fourth* as well as the third virial coefficients. Then one must assume that g_1' and h_1'

may also carry appreciable contributions from the fourth virial coefficients in solutions of ionic strength I' in the experimental range. These contributions may be responsible for the failure of the HNC approximation method in calculating g_1' as noted in section 3. Unfortunately, it would require a major effort to elucidate the behavior at larger I' by evaluating the cluster integrals more completely because of the very large number of integrals involved, as noted above.

3. HNC Calculations for the MnCl₂, LiCl Model

Calculations were made for models for MnCl₂, LiCl mixtures using the HNC approximation¹² and the computational methods described previously.^{5,12,13} The models studied here are specified in ref 5 and in Table I. The Gurney parameters in these models have been adjusted to give agreement with osmotic coefficient data for MnCl₂, LiCl, and their mixtures in water at 25°. ¹⁴ These procedures are described for another system in ref 5. The present calculations were made for another purpose, and will be described more completely elsewhere. Because they were made in double precision (16 decimal figures) and with a large number ($N = 1024$) of sampling points,¹² they are much more accurate and extensive than our usual calculations⁵ and, therefore, especially suitable for the calculation of g_1' . It seems appropriate to compare the results with the experimental results of Cassell and Wood because their results indicate that the main features are independent of the particular species of ions.

It is possible to calculate g_1' in several ways from the solute-solute pair correlation functions which are produced in the HNC calculations so we may test the calculations for self-consistency.¹⁵ These tests closely parallel those described earlier¹³ for w_p' so we only give the final expressions.

From eq 3.10 of ref 13 we find (in the present notation⁵ for the mixing coefficients while g_{A_y}, g_{B_y} are defined in ref 13)

$$g_1' - g_3' = -(1/6I'kT)(\partial(g_{A_y} - g_{B_y})/\partial Y)_{Y=0} \tag{3.1}$$

In the calculations made here g_3' is negligible.

From eq 3.11 and 3.12 of ref 13 we deduce

$$w_1' = \frac{\partial(I'g_1')}{\partial I'} = -\frac{1}{I'^2} \left(\frac{\partial}{\partial Y} \left[\frac{\Delta_m((1-\phi)\rho)}{y(1-y)} \right] \right)_{Y=0} \tag{3.2}$$

Equations 3.14 and 3.15 of ref 13 are in error; they should be replaced by

$$\frac{\Delta_m(\rho DEL/I')}{y(1-y)} = \frac{\partial}{\partial I'} (I'^2 w_0' + I'^2 w_1' Y + \dots) \tag{3.3}$$

from which we deduce

$$\frac{\partial}{\partial I'} (I'^2 w_1') = \left(\frac{\partial}{\partial Y} \left(\frac{\Delta_m(\rho DEL/I')}{y(1-y)} \right) \right)_{Y=0} \tag{3.4}$$

A fourth relation for g_1' can be derived by combining eq 3.2 and 3.10 of ref 13 to obtain

$$w_1' - w_3' = 2(g_1' - g_3') + \frac{1}{6I'} \left(\frac{\partial^2}{\partial Y^2} (g_{A_y} + g_{B_y}) \right)_{Y=0} \tag{3.5}$$

These relations may be applied to the results of model calculations made for a range of y and I' to see whether the

TABLE I: Description of Models^a

Model	A	B	C	D
r_1^* ^b	0.80 Å	0.80 Å	0.80 Å + d^c	0.80 Å + d
w_1^d	$2d$	$2d$	d	d
w_2	d	$2d$	d	$2d$
A_{11}^e	-52	-52	-120	-120
A_{12}	-78	-21.3	-81	-22
A_{22}	0	-10	0	-10
A_{13}	30	30	-101	-101
A_{23}	40	15	40	15

^a Species 1 is Mn^{2+} , species 2 is Li^+ , and species 3 is Cl^- . Aqueous solutions at 25°. For further description of the models and explanation of the notation see ref 5, where similar calculations for $MgCl_2, NaCl$ mixtures are described. ^b r_i^* is the radius parameter for species i . In these models $r_1^* = 0.60$ Å and $r_3^* = 1.81$ Å, the Pauling ionic radii. In models A and B Mn^{2+} has its Pauling radius while in models C and D it has the radius of an hydrated ion. ^c $d = 2.76$ Å, the diameter of a water molecule. ^d w_i is the thickness of the cosphere on species i . $w_3 = d$. ^e A_{ij} is the Gurney free-energy parameter in units of calories per mole of water displaced. In all these models $A_{33} = 0$.¹⁶

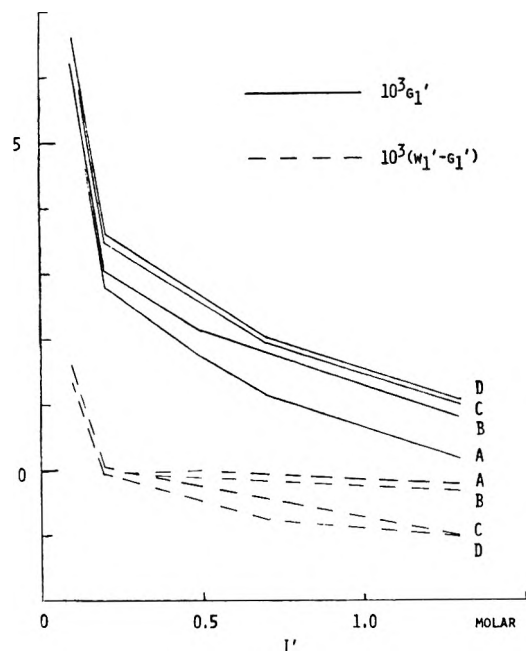


Figure 1. First-order mixing coefficients calculated for the models specified in Table I. The calculated points at $I' = 0.1, 0.3, 0.5, 0.7,$ and $1.3 M$ are connected by straight lines.

various ways of calculating g_1' and its derivatives with respect to I' are mutually consistent (cf. Rasaiah and Friedman¹⁵). Consistency is assured only if the solution of the HNC equation is accurate and the pair correlation functions given by the HNC approximation are accurate for the given model potential.

In the present calculations the self-consistency tests based upon g_1' fail badly. Typical results are given in Figure 1 where values of g_1' are obtained from eq 3.1 while values of w_1' are obtained from eq 3.2. For all these data we find approximately

$$\partial g_1' / \partial I' \approx -2 \times 10^{-3} / I'$$

Then, because we have (eq 3.2)

$$w_1' - g_1' = I' \partial g_1' / \partial I'$$

self-consistency requires that we find

$$w_1' - g_1' \approx -2 \times 10^{-3}$$

which is clearly in poor agreement with the calculations (Figure 1). The other self-consistency tests for g_1' also fail drastically.

The self-consistency tests of g_0' and w_0' work out satisfactorily for models A and B; the various methods of calculating w_0' agree within 30%. For models C and D, however, values of w_0' calculated in different ways are of the same sign and order of magnitude, but not much better than that. These aberrations led to the work reported here in which the HNC equation was solved much more accurately than in our usual practice^{5,12,13,16} but the improved accuracy did not improve the self-consistency tests significantly. This is what one would expect if the HNC approximation were not accurate enough to get self-consistency for a subtle coefficient such as g_0' or w_0' when some of the ions are as large as the Mn^{2+} is in models C and D.

Then the more complete failure of self-consistency for g_1' is not surprising. Moreover, this situation may be mainly due to fourth virial coefficient contributions in g_1' (cf. section 2).

As reported earlier, the self-consistency tests for w_0' were found to be quite satisfactory for a model for $LiCl, CsCl$ mixtures.¹³ From that report¹³ we can extract enough information to see that various ways of calculating g_1' from the data are fairly consistent. Thus we can conclude that the HNC approximation is markedly more satisfactory for a 1,1-1,1 mixture than for a 2,1-1,1 mixture.

For the rest we choose the g_1' coefficients calculated from the model by eq 3.1 as "best values" to be compared with experimental data and with the requirements of the limiting laws in Figure 2.

4. HNC Calculations for the $BaCl_2, NaCl$ Model

A few more HNC calculations (double precision and $N = 1024$) were made to see how the h_0' and h_1' coefficients which could be derived from the calculations compared with the limiting-law calculations on the one hand and the experimental data on the other.

The model studied was similar to model B in Table I but with radii appropriate to a $BaCl_2-NaCl$ mixture. Thus Ba^{2+} (species 1) and Na^+ (species 2) had cospheres with a thickness of two water molecules while Cl^- (species 3) had a cosphere one water molecule thick. All ions had Pauling radii. Parameters A_{11} and A_{13} were taken from ref 5. Parameters A_{22} and A_{23} were determined by fitting the model to the osmotic coefficient data of aqueous $NaCl$ at 25°; the fit was far better than that reported earlier¹⁶ for a model in which the cosphere on Na^+ was only one water molecule thick. The enthalpy data for the single electrolyte solutions^{10,17} at 25° were used to determine dA_{ij}/dT by comparing model calculations of the excess enthalpy^{15,16} with the experimental data. With all these parameters in hand,

TABLE II: Experimental and Model Values of Mixing Coefficients for Aqueous BaCl₂-NaCl at 25 °C

I', M	w_0^b	$w_0'(\text{HNC})$	$w_1'(\text{HNC})$	h_0^c	$h_1'(\text{HNC})$
0.5	0.0205 ± 0.006	0.0266	0.0008	0.177	0.182
0.1		0.0023	0.0078	0.253	0.252
0.02		-0.0631	0.0221	0.506	0.465

^a Ba²⁺ = 1, Na⁺ = 2, Cl⁻ = 3. At 25°, $A_{11} = -23$, $A_{12} = -19$, $A_{13} = 6$, $A_{22} = -17$, $A_{23} = 10$, $A_{33} = 0$, all in cal/mol.³ In the same order, $d(A_{ij}/T)/d(1/T) = -57, -5, -26, -17, -16, 0$ cal/mol. ^b Experimental, Robinson and Bowers.¹⁸ ^c Experimental, Cassel and Wood.¹

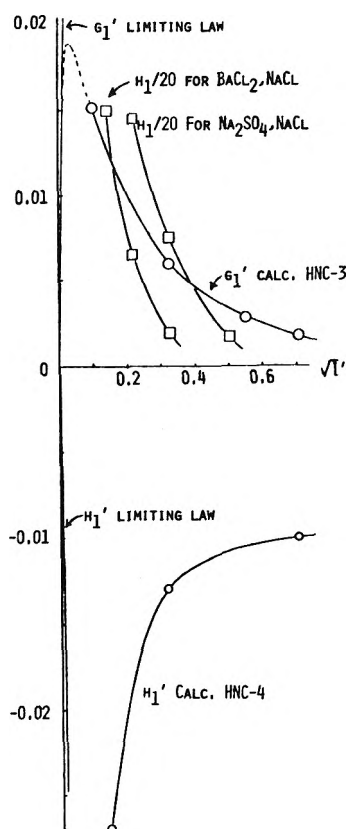


Figure 2. Comparison of the limiting law, the HNC model calculations from section 3 (HNC-3) and section 4 (HNC-4), and the enthalpy data of Cassel and Wood.¹ For the Cassel–Wood data it is $h_1/20$ which is actually plotted.

A_{12} and dA_{12}/dT were determined by fitting model calculations for the mixed electrolyte to experimental data^{1,18} for w_0 and h_0 for BaCl₂-NaCl mixtures at $I = 0.5 m$. The results are shown in Table II and Figure 2. It is remarkable that the computed values of h_0' at $I' = 0.1$ and $0.02 M$ are in good agreement with the experimental values, all the adjustable parameters having been fit by comparison with other data, as described above.

5. Relationship of g_1' to g_1 and h_1' to h_1

Proceeding from eq 45 of ref 6 we find the relation, asymptotically valid as $I' \rightarrow 0$

$$g_1' = V_w^0 g_1 + \frac{1}{2} g_0 (V_B^0 - V_A^0) I + \frac{1}{4} (V_B^0 - V_A^0)^2 I^2 / V_w^0 + \dots \quad (5.1)$$

where V_w^0 is the specific volume (liter/kg) of pure solvent and V_A^0 and V_B^0 are partial molar volumes at infinite dilution.⁶ Thus for aqueous solutions (because $V_w^0 \approx 1.0$ l./kg for water) the limiting law for g_1 is practically the same as for g_1' . From eq 5.1 we deduce

$$h_1' = V_w^0 h_1 - T g_1 \partial V_w^0 / \partial T + O(I \ln I) \quad (5.2)$$

so in aqueous solutions the limiting law for h_1 is very nearly the same as for h_1' .

At moderate concentrations, in all the cases of which we are aware, the difference in thermodynamic coefficients in the Lewis–Randall and McMillan–Mayer systems is modest; *i.e.*, the difference may not be negligible compared to experimental or calculational errors, but it does not make the coefficient in one system drastically different from the other.^{2–6} It seems likely that the same is true in the systems considered here and we shall so assume in the following section.

6. Collection of Various Results for g_1' and Related Functions

In Figure 2 values of g_1' from the HNC calculations are plotted together with the limiting law (section 2) to give an indication of the behavior of g_1' over the range $0 < I' < 0.5 M$ as predicted by theory. The predicted sharp maximum in a measurable solution function is quite remarkable.

Cassel and Wood's¹ data for h_1 are shown in the same figure, but it should be noticed that it is necessary to scale down their h_1 data by a factor of 20 so they would be comparable to the g_1' values in the figure. This feature suggests that their data and the HNC calculations are not mutually consistent. The same conclusion follows from the comparison of the experimental h_1 data and the HNC results for h_1' , also shown in Figure 2. Of course the significance of all these HNC results is not so clear because of the problems described in section 3, but it is interesting that the h_1' values from Table II, together with the limiting law, suggest that there is a sharp minimum in h_1' below $I' = 0.01 M$, corresponding to the maximum in g_1' .

Referring to Figure 2 we see that if there are no errors in the experiments or in the limiting-law theory then $h_1(I')$ has a minimum at very small I' and then a maximum at a larger value of I' that still is less than $0.02 M$. These extrema appear if we connect the h_1 limiting law line to the experimental data. While there is no precedent for such behavior of a measurable solution thermodynamic coefficient, neither can we say it is impossible.

7. Discussion

The calculations of g_1' reported here are especially important because they give evidence of the limited accuracy of the HNC approximation method as applied to models for simple aqueous solutions of moderate concentrations. This aspect of the work provides impetus for the development of even more powerful methods of calculating the equilibrium properties of hamiltonian models³ of electrolyte solutions.¹⁸ It may even have a beneficial effect in the important work of evaluating approximation methods if it directs emphasis away from intercomparison of osmotic coefficients and excess energies and toward the intercomparison of more sensitive thermodynamic functions. More-

over, the present work provides a textbook example of how one can go wrong in applying an approximation method without self-consistency tests; if we had calculated g_1' from the HNC correlation functions by only one route we would have had no clue as to the real difficulties.

For the rest the present results tend to emphasize the anomalous character of the $h_1(I)$ function found by Cassel and Wood¹ rather than to show how it can be understood in terms of ionic interactions in solution. This failure is especially surprising in view of the evidence (noted in section 1) that the large values of h_1 in dilute solutions arise from Coulombic interactions of the ions. It had seemed until now that contemporary theoretical methods give an accurate account of Coulombic interactions in ionic solutions and that the most important remaining problems relate to other terms in the interaction.

In conclusion it must be remarked that the theoretical difficulties encountered here do not tend to invalidate earlier calculations of less subtle thermodynamic coefficients by the HNC approximation method nor the conclusions about solution structure reached on the basis of comparing those calculations with experimental data. The excess free energy may be thought of as the primary quantity obtained by these calculations. The g_1 coefficient has the character of a third derivative of the excess free energy with respect to concentration; it is expected to be more difficult to evaluate than lower derivatives.

Acknowledgment. The support of the National Science Foundation is gratefully acknowledged. Also it is a pleasure to acknowledge the benefit of several helpful communications from Professor R. H. Wood.

References and Notes

- (1) R. B. Cassel and R. H. Wood, *J. Phys. Chem.*, **78**, 1924 (1974).
- (2) H. L. Friedman, *J. Chem. Phys.*, **32**, 1134 (1960).
- (3) (a) H. L. Friedman, "Ionic Solution Theory," Wiley-Interscience, New York, N. Y., 1962; (b) H. L. Friedman, *Mol. Phys.*, **2**, 190 (1959).
- (4) H. L. Friedman, "Computed Thermodynamic Properties and Distribution Functions for Simple Models of Ionic Solutions," in "Modern Aspects of Electrochemistry," Vol. 6, B. Conway and J. Bockris, Ed., Plenum Press, New York, N. Y., 1971.
- (5) H. L. Friedman, A. Smitherman, and R. DeSantis, *J. Solution Chem.*, **2**, 59 (1973).
- (6) H. L. Friedman, *J. Solution Chem.*, **1**, 418 (1972).
- (7) The mixing operator Δ_m is more completely defined in eq 2 and 3 of ref 6 as well as eq 18.1 and 18.10 of ref 3a or eq 2.3 and 2.6 of ref 2.
- (7) (a) The quantity here represented by s is represented in the earlier work³ by an upper-case German S.
- (8) Reference 3a, eq 17.7, 17.52-17.59, Table 15.1. Equation 2.9 differs by a factor of -3 from the corresponding equation in ref 3a, which is in error. (The combinatorial coefficients in these equations were calculated by specializing a general equation in ref 3b which seems to be correct.) We have also

$$\kappa^2 i_3 = \triangle, \quad \kappa^3 i_4 = \square + \frac{2}{3} \boxtimes$$

where the graphs represent integrals in the usual way.³ The bonds of the graphs are q functions; $q(r) = e^{-\kappa r}/4\pi r$. The first and third integrals were evaluated numerically by Haga.⁹ We have verified his result for i_3 . The other is rather difficult.
- (9) E. Haga, *J. Phys. Soc. Jap.*, **8**, 714 (1953).
- (10) H. S. Harned and B. B. Owen, "Physical Chemistry of Electrolyte Solutions," 3rd ed, Reinhold, New York, N. Y., 1958.
- (11) R. H. Wood, J. D. Patton, and M. Ghamkar, *J. Phys. Chem.*, **73**, 346 (1969).
- (12) J. C. Rasaiah and H. L. Friedman, *J. Chem. Phys.*, **48**, 2742 (1969).
- (13) H. L. Friedman and P. S. Ramanathan, *J. Phys. Chem.*, **74**, 3756 (1970).
- (14) We are grateful to Dr. R. F. Platford for communicating w_0 data for these mixtures in advance of publication.
- (15) J. C. Rasaiah and H. L. Friedman, *J. Chem. Phys.*, **50**, 3965 (1969).
- (16) P. S. Ramanathan and H. L. Friedman, *J. Chem. Phys.*, **54**, 1086 (1971).
- (17) V. B. Parker, *Nat. Ref. Data Ser., Nat. Bur. Stand.*, No. 2 (1965).
- (18) R. A. Robinson and V. E. Bowers, *J. Res. Nat. Bur. Stand., Sect. A*, **69**, 19 (1965).
- (19) Other approximation methods currently under development are described in a review by J. C. Rasaiah, *J. Solution Chem.*, **2**, 301 (1973).

The Lithium–Lithium Hydride System

Ewald Veleckis,* Erven H. Van Deventer, and Milton Blander

Chemical Engineering Division, Argonne National Laboratory, Argonne, Illinois 60439 (Received February 22, 1974; Revised Manuscript Received June 17, 1974)

Publication costs assisted by Argonne National Laboratory

Equilibrium hydrogen pressures (P_{H_2}) of lithium–lithium hydride mixtures sealed in iron capsules were measured over the following temperature–pressure–composition ranges: 710–903°, 0.5–760 Torr, and 0.5–99 mol % LiH. The isotherms show the phase diagram to consist of two homogeneous terminal solutions separated by a miscibility gap whose boundaries range from 25.2 and 98.4 mol % LiH at 710° to 45.4 and 85.5 mol % LiH at 903°. The data were fitted by a consistent thermodynamic treatment using the Margules forms for the activity coefficients. For each homogeneous solution region, this treatment yielded analytical expressions for the chemical potentials and activity coefficients of each species. The data show strong positive deviations from ideality of the solute species, especially in the LiH-rich solutions, where they may be related to the associative tendency of the lithium atoms. For dilute solutions of LiH in lithium, the ratio $N_{LiH}/(P_{H_2})^{1/2} = K'$ is given by $K'(\text{atm}^{-1/2}) = \exp(-6.498 + 6182T^{-1})$, where N_{LiH} is the mol fraction of LiH and T is the Kelvin temperature. For dilute solutions of Li in liquid LiH, the distribution of lithium between the gas and the solution phases is heavily weighted in favor of the latter, reflecting strong interactions between Li atoms and liquid LiH. The standard free energy of formation of liquid LiH is given by ΔG_f° (kcal/mol) = $13.47 \times 10^{-3}T - 16.55$.

Introduction

In many respects alkali–alkali hydride systems resemble alkali–alkali halide systems, which are much studied examples of metal–salt interactions.¹ Experimentally, the hydride systems offer an advantage in that one may obtain their thermodynamic properties by measuring equilibrium hydrogen pressures through membranes that are permeable to hydrogen only. A study of the Li–LiH system is particularly attractive because of the simplicity of the electronic structures of Li^+ and H^- ions, because most of the important features of its phase diagram lie in easily accessible ranges, and because studies of isotopic substitution of both lithium and hydrogen are feasible. In addition to this fundamental interest, the solution properties of Li–LiH, Li–LiD, and Li–LiT systems are important to the controlled thermonuclear research (CTR) program in which liquid lithium is a prime candidate for use as the breeder blanket fluid in fusion reactors.

The existing phase diagram and thermodynamic information on Li–LiH, Li–LiD, and Li–LiT systems has been reviewed by Messer.² For the Li–LiH system, Hill³ obtained a single P_{H_2} vs. N_{LiH} isotherm at 700°, Perlow⁴ extended this work by obtaining isothermal data at 770 and 825°, and Heumann and Salmon⁵ remeasured the 700° isotherm. The solid LiH–liquid Li equilibrium was studied by Messer, *et al.*,⁶ by the method of thermal analysis. From graphical representations² of the combined P_{H_2} vs. N_{LiH} data, it is apparent that the scatter in the data and an insufficient number of isotherms make it difficult to extract meaningful thermodynamic information, particularly in the dilute solution regions, where the disagreements result in crossing isotherms which also fail to pass through the origin. The same difficulties are found in the Li–LiD and Li–LiT systems, which were also briefly examined by Heumann and Salmon.⁵

Because of these shortcomings, we are conducting experimental studies to remeasure with improved precision the

chemical activities and phase equilibria in the condensed systems Li–LiH, Li–LiD, and Li–LiT. The results obtained for the Li–LiH system are presented here.

Experimental Section

Apparatus. The experiments were carried out in a modified Sieverts' apparatus (shown in Figure 1) which consisted of three main sections designed for (a) gas purification, (b) gas metering, and (c) equilibration of the gas with an encapsulated Li–LiH melt.

In the first section, gases were purified by passing them through appropriate getters: liquid-nitrogen-cooled silica-gel for helium (the calibrating gas), and a hot titanium metal sponge for hydrogen. The titanium sponge, in conjunction with a 1-l. bulb, also served as a reservoir for large amounts of pure hydrogen needed for the experiments. A mercury bubbler protected against overpressure resulting from accidental overheating of the H_2 -saturated sponge.

The gas metering section consisted of a water-thermostated (35°) bulb having a calibrated volume (~500 cm^3) between mark a and the three-way stopcock S, a mercury leveling bulb, and three pressure gauges in the ranges 0–20 (± 0.05), 0–200 (± 0.1), and 0–800 (± 0.2) Torr for determining gas pressures in the calibrated bulb. The gauges were frequently calibrated vs. a mercury manometer.

The equilibration section, which extends from mark b to the sample volume, was comprised of (1) a double-walled fused-silica tube which contained the sample, (2) a partially thermostated manifold, and (3) three low-volume, high-precision gauges calibrated to within 0.05 Torr. Double-walled construction of the reaction tube was necessary because hydrogen has an appreciable permeability through fused silica at higher temperatures. [The permeation loss of hydrogen from a single-walled fused-silica tube was found to be high enough (0.5 standard $cm^3/hr atm$ at 815°) to cause substantial errors in the data.] Hydrogen losses were minimized by automatically controlling, *via* a capaci-

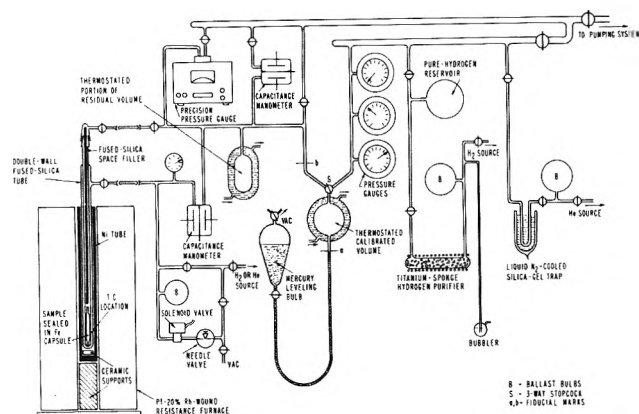


Figure 1. Apparatus for studying the Li-LiH system.

tance manometer, the hydrogen pressure in the annular space of the double-walled tube at the same value as that of the inner chamber.

The ambient temperature of the residual gases in the equilibration section was maintained uniform by (a) insulating the glass parts in the immediate vicinity of the furnace and (b) thermostating (at 35°) a major portion of the residual volume. A fused-silica rod space filler was placed inside the fused-silica tube to reduce the hot portion of the residual volume and to limit convection currents.

The sample was heated by a Pt-20% Rh-wound, single-zone Marshall tubular furnace (1.5-in. i.d., 20-in. long) in conjunction with a West SCR stepless temperature controller. The controller maintained temperatures constant to within 1° for periods greater than 1 hr. Temperatures were measured with three Pt-Pt-10% Rh thermocouples placed radially at 120° angles in the annular space of the tube at the sample level. The thermocouples were calibrated *in situ* against a standard thermocouple which was placed in an unsealed iron capsule filled with lead metal substituting for lithium.

Containment of Lithium. Because of the high volatility and reactivity of alkali metals, there are problems associated with open-cell techniques.⁷ Consequently, in this study, lithium was contained in closed capsules (2.25-in. long, 0.5-in. diameter cylinders with 0.015-in. wall) made of Armco iron tubing. Iron was selected on the basis of its corrosion resistance toward lithium,⁸ relatively high hydrogen permeability,⁹ and low hydrogen solubility.¹⁰ To facilitate the loading of lithium, the ends of the capsules were made in the shape of a funnel with the stems facing outward. Before loading, the capsules were heated in hydrogen and then degassed at 850–900°.

The capsules were filled with lithium according to the following procedure. A glass stopcock was attached, *via* a glass-to-metal seal, to the top funnel stem and a 5- μ m porosity stainless-steel filter was attached to the bottom stem of a capsule. The assembly was placed in a high-purity helium atmosphere glove box (~1 ppm of nitrogen and oxygen) and the bottom half of the capsule was filled by (a) immersion of the filter end in a pot of molten lithium and (b) application of gentle suction through the stopcock. The capsule was then cooled to room temperature and the bottom funnel stem was closed by a heli-arc weld. After removal from the glove box, the capsule was evacuated to 10^{-6} Torr and, after flattening part of the top funnel stem, the glass portion was sealed with a flame. The capsule was then sealed and cut *in vacuo* at the flattened portion by electron-beam welding.

Each loaded capsule was tested for leaks and degassed by heating at ~900° *in vacuo*. (The capsule used for the measurements at 710° was degassed at ~700°). Care was taken not to exceed the α - γ transformation point of iron (910°). New capsules required 2–3 days for degassing; used capsules, already containing hydrided lithium, required about 2 weeks.

The evacuated space of the capsule (2–4 cm³) is expected to be filled with lithium vapor which may react with hydrogen to form gaseous LiH.¹¹ Below the monotectic temperature (685°), condensation of solid hydride on the capsule walls could inhibit hydrogen diffusion; above this temperature, however, LiH is liquid and should be adequately drained from the capsule walls. Accordingly, all the experiments but one were conducted at temperatures above the monotectic.

Procedure. For each hydridation experiment, a new Armco iron capsule containing approximately 2 g of pure, degassed lithium was placed in the double-walled tube. The tube was connected to the apparatus, evacuated, and heated to the temperature of the experiment. The effective volume of the equilibration section of the apparatus was then determined by filling it several times with known amounts of helium and measuring the pressure each time. Helium was selected as the calibrating gas because its thermal conductivity is most nearly equal to that of hydrogen. After the calibration, the helium was pumped off.

Hydrogen was then added to the sample in 20 to 30 portions. The size of these portions was varied in such a way as to aid in the delineation of an isotherm. Thus, at the very low and the very high hydrogen concentrations, where the isotherm is steep, small additions (2–6 mmol of H₂) were used, whereas, in the extensive plateau portions, the additions were quite large (20–25 mmol of H₂). For each addition, the amount of hydrogen was measured in the calibrated bulb. The contents of the bulb were then quantitatively transferred into the equilibration section by flooding the bulb with mercury up to the mark b. Successive portions of hydrogen were added using this procedure until the equilibrium hydrogen pressure approached 1 atm. Equilibrium was considered established when the recorded pressure *vs.* time charts showed no further pressure changes (± 0.01 Torr) for at least 6 hr. The validity of this criterion for equilibrium was confirmed by our observation of a correspondence between the observed kinetics of hydrogen uptake and equations derived from a diffusion model. According to Heumann and Salmon,⁵ the rate of hydrogen uptake by lithium sealed in iron capsules (same wall thickness as in our work) was very nearly equal to that expected for hydrogen diffusion through iron. They allowed 8–12 hr for each equilibration. The amount of lithium used in the present work was ~50 times larger and the time required to reach equilibrium was 12–48 hr, depending on the quantity of hydrogen added, on the temperature, and on the equilibrium hydrogen pressure.

During the course of experiments, several desorption measurements were carried out as a test of thermodynamic reversibility. This was accomplished by removing a measured amount of hydrogen (by Toepler pumping) and measuring the pressure after the reestablishment of equilibrium.

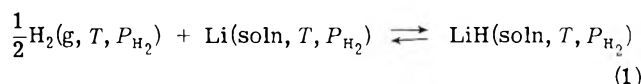
The concentration of hydrogen in lithium resulting from each hydrogen addition was calculated from the weight of lithium and from the total hydrogen added which was corrected for the amounts of hydrogen remaining in the resid-

ual volume, in the vapor space inside the capsule, and dissolved in iron. The latter two amounts combined were less than 0.04% of the total hydrogen content. The fraction of hydrogen remaining in the residual volume ranged from ~6% at 10 Torr to ~15% at 760 Torr.

Materials. Lithium metal ingots, packed under argon and having a stated purity of 99.98%, were purchased from the Foote Mineral Co. The major metallic impurities were found to be sodium (79 ppm) and potassium (35 ppm). The measured $^6\text{Li}/^7\text{Li}$ atom ratio was 0.0815 ± 0.0007 , in good agreement with the accepted value for natural lithium.

Analysis of Data

If we assume that hydrogen in the condensed phase is in the form of a hydride, then the equilibrium reaction between gaseous hydrogen and liquid lithium may be written as



The equilibrium constant, K , for this reaction is given by

$$K = N_2\gamma_2/N_1\gamma_1(P_{\text{H}_2})^{1/2} \quad (2)$$

where the subscripts 1 and 2 refer to Li and LiH, respectively, the N 's are the mole fractions of the components in the condensed phase, the γ 's are the corresponding activity coefficients, P_{H_2} is the equilibrium hydrogen pressure in atmospheres, and T is the Kelvin temperature. Equation 2 can be rewritten in the form

$$\ln [(P_{\text{H}_2})^{1/2} N_1/N_2] = -\ln K + \ln (\gamma_2/\gamma_1) \quad (3)$$

According to Margules, the activity coefficients of the components in a binary solution may be represented by a power series in N .¹² When the series are truncated at their cubic terms, the activity coefficients are consistently given by

$$\ln \gamma_1 = \alpha N_2^2 + \beta N_2^3 \quad (4)$$

and

$$\ln \gamma_2 = \left(\alpha + \frac{3}{2}\beta\right) N_1^2 - \beta N_1^3 \quad (5)$$

Substitution of eq 4 and 5 into eq 3 yields a second-order power series for $\ln [(P_{\text{H}_2})^{1/2} N_1/N_2]$ vs. N_2 , *i.e.*

$$\ln [(P_{\text{H}_2})^{1/2} N_1/N_2] = -\ln K + \alpha(1 - 2N_2) + (1/2)\beta(1 - 3N_2^2) \quad (6)$$

At the extreme limits of the composition range, $N_2 \rightarrow 0$ and $N_2 \rightarrow 1$, eq 6 becomes

$$\lim_{N_2 \rightarrow 0} \ln [(P_{\text{H}_2})^{1/2}/N_2] = -\ln K + \alpha + (1/2)\beta \quad (7)$$

and

$$\lim_{N_2 \rightarrow 1} \ln [(P_{\text{H}_2})^{1/2} N_1] = -\ln K - \alpha - \beta \quad (8)$$

The data from the hydridation experiments consist of sets of isothermal pressure-composition values.¹³ A convenient method of graphical representation of these data is to project each set of isothermal values on the square root of hydrogen pressure vs. composition plane. Six isotherms (at

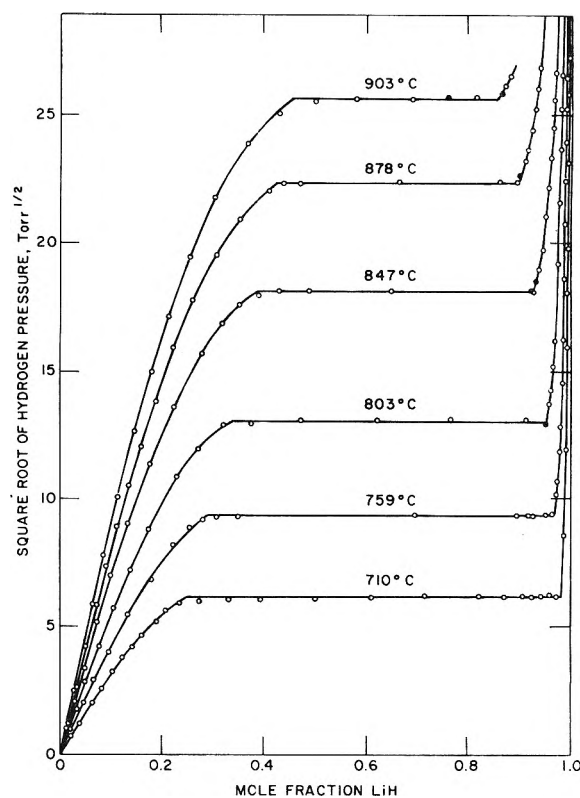


Figure 2. Projection of the hydridation data on the square root of hydrogen pressure vs. composition plane for the system Li-LiH. Solid points indicate desorption measurements.

710, 759, 803, 847, 878, and 903°) were obtained for the system Li-LiH and are exhibited in this manner in Figure 2.

The pressure-composition data obtained from the hydridation experiments were corrected for (1) the average temperature of the isotherm to which the data belonged, (2) the initial hydrogen concentration in lithium, and (3) the stoichiometry of LiH. The nature of these corrections is described below.

(1) Because of the temperature fluctuations in the furnace, each datum point on an isotherm was recorded at a slightly different temperature (WITHIN $\pm 1^\circ$). Therefore, each pressure reading was corrected to the average temperature for that isotherm. The corrections were based on the temperature coefficients calculated, as a function of composition, from all six isotherms.

(2) According to eq 7, plots of $\ln [(P_{\text{H}_2})^{1/2} N_1/N_2]$ vs. N_2 should intersect the ordinate at finite values. Figure 3a shows such plots for the first rising portions of the isotherms. In all cases, as $N_2 \rightarrow 0$, the curves tended to bend sharply upward. The most plausible explanation of this behavior is that, due to incomplete degassing, some residual hydrogen is retained in the encapsulated lithium at the start of the experiments. This assumption is supported by the fact that the effect was larger for the first isotherm (at 710°) for which the lithium sample was degassed less completely, at a lower temperature (700°), and for a shorter time.

The data were corrected by applying increments, ϵ , to the N_2 's in eq 6. The increments represent the estimated initial mole fraction of LiH in lithium. For each isotherm, the value of ϵ was selected such that a least-squares fit of $\ln [(P_{\text{H}_2})^{1/2}(1 - N_2 - \epsilon)/(N_2 + \epsilon)]$ vs. $(N_2 + \epsilon)$ showed a minimum in the sum of the squared residuals. The resulting

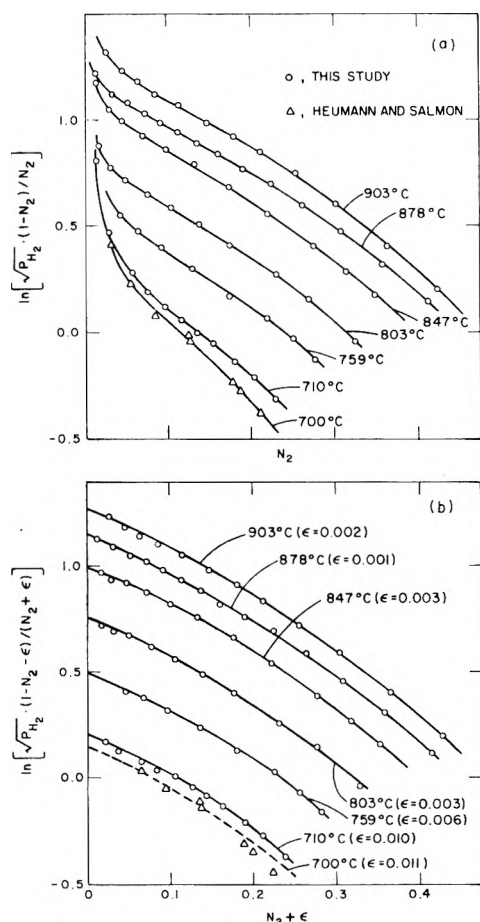


Figure 3. Effect of residual hydrogen concentration, ϵ , on the shape of isotherms in the dilute region of the Li-LiH system: (a) original data, (b) data corrected for ϵ .

curves and the corresponding ϵ values are shown in Figure 3b.

This corrective procedure was also applied to the hydridation data (at 700°) of Heumann and Salmon⁵ which show a similar upward trend in the dilute region (Figure 3a). After the correction ($\epsilon = 0.011$), their data agree reasonably with the values extrapolated from ours (dashed curve in Figure 3b).

One may speculate about the sources of the residual hydrogen. One possibility is the retention of hydrogen by the lithium during its manufacture. This could not be confirmed because of the difficulties associated with the vacuum fusion analysis of liquid lithium. Another source of hydrogen could be the presence of adsorbed water on the surfaces in the vicinity of the iron capsule. Calculations show that owing to the equilibria $\text{Fe} + \text{H}_2\text{O} \rightleftharpoons \text{FeO} + \text{H}_2$ and $3\text{Fe} + 4\text{H}_2\text{O} \rightleftharpoons \text{Fe}_3\text{O}_4 + 4\text{H}_2$, the partial pressures of water necessary to produce the requisite residual hydrogen concentration are, on the average, only 6×10^{-4} Torr ($\epsilon = 0.001$) and 6×10^{-2} Torr ($\epsilon = 0.01$) at 700° and 8×10^{-3} Torr ($\epsilon = 0.001$) and 8×10^{-1} Torr ($\epsilon = 0.01$) at 900°. These results also stress the importance of prolonged high-temperature degassing of encapsulated lithium prior to an experiment.

(3) When the data of the second rising portions of the isotherms are plotted as $1/(P_{\text{H}_2})^{1/2}$ vs. N_1 , the extrapolated $[1/(P_{\text{H}_2})^{1/2} \rightarrow 0]$ least-squared curves did not intersect the abscissa at exactly $N_1^0 = 0$, as required by eq 8, but rather at $N_1^0 = -0.013$ (at 710°), -0.007 (759°), -0.016 (803°), -0.008 (847°), -0.014 (878°), and -0.007 (903°). Because

in the case of lithium a stoichiometric hydride is expected, the slight bias in N_1^0 was attributed to errors accumulated in numerous hydrogen additions during the experiment. A correction was applied by multiplying all N_2 's of an isothermal data set by its respective normalization factor, $1/(1 - N_1^0)$. (If LiH was found to be nonstoichiometric, it would be simple to adjust our data to take this finding into account.)

Results

Each of the isotherms comprises two rising portions that are separated by a horizontal line. The composition ranges of the first and second rising portions correspond to homogeneous phases; the constant-pressure plateau defines the two-phase coexistence region. This shape of the isotherms supports the expected¹ analogy between the Li-LiH system and the alkali-alkali halide systems. The temperature-composition phase diagrams of the latter systems¹⁴ consist of a monotectic horizontal above which there is a closed region of coexistence of two liquids and below which a solid salt containing very small amounts of metal is in equilibrium with a solution of salt in the liquid metal. A monotectic horizontal for the Li-LiH system has been reported⁶ at $685 \pm 1^\circ$.

The desorption data are also shown in Figure 2. No evidence of hysteresis was observed, thus confirming the reversibility of the hydrogen-lithium reactions. Because of the particular apparatus used, the hydrogen pressures were limited within the range 0.5–760 Torr. The error in the individual pressure measurements was estimated to be $\pm 0.5\%$, resulting primarily from the fluctuations in the ambient temperature of the residual volume.

An attempt was made to determine an isotherm at 653°, *i.e.*, below the monotectic temperature. For the first rising portion of this isotherm, hydrogen absorption rates were similar to those observed at the higher temperatures; however, when the pressure plateau was approached, hydrogen uptake was slowed down to impractical levels, probably owing to a coating of solid LiH on the inside walls of the capsule. The experiment was discontinued and only an approximate value (15.5 ± 1.5 mol % LiH) could be estimated for the solubility of solid LiH in liquid lithium.

The miscibility gap data are presented in Table I. Items in Table I are discussed below.

Plateau Dissociation Pressures. A review of the literature data on the plateau pressures, P_{H_2} , for the Li-LiH system has been made elsewhere.² The results obtained in this study, combined with the six pieces of data reported by Heumann and Salmon⁵ (at 728, 728.5, 756, 774, 785, and 804°), may be represented by

$$\ln P_{\text{H}_2} (\text{Torr}) = 21.128 - 17,186T^{-1} \quad (9)$$

with an uncertainty of only 1.5% (at the 95% confidence level) in the predicted value of P_{H_2} . [The seventh datum point (at 700°) of Heumann and Salmon fell outside the error band and was omitted from the least-squares analysis.] Statistical F tests showed that both sets of data originated from the same population. The data of older work² appear to be less reliable and are excluded.

Miscibility Gap Limits. The lower limit, $N_2'(\text{satd})$, represents the solubility of LiH in liquid lithium; the upper limit, $N_2''(\text{satd})$, that of lithium in liquid LiH. The logarithms of both limits are shown as functions of temperature in Figure 4; they may be represented by

TABLE I: Miscibility Gap Data of the System Li-LiH

T, °C	Plateau pressure, ^a Torr	Miscibility gap limits ^a		Activity coefficients ^b			
		N ₂ '(satd)	N ₂ ''(satd)	γ ₁ '(satd)	γ ₂ '(satd)	γ ₁ ''(satd)	γ ₂ ''(satd)
710	38.5	0.252	0.984	1.084	4.02	49.7	1.002
759	88.3	0.285	0.971	1.122	3.35	28.6	1.006
803	171.4	0.332	0.957	1.169	2.87	17.6	1.013
847	329.2	0.386	0.923	1.230	2.47	10.1	1.032
878	500.2	0.418	0.888	1.283	2.23	6.80	1.059
903	658.8	0.454	0.855	1.333	2.06	5.05	1.090

^a Observed data from which eq 9-11 were derived. ^b Calculated from eq 19-22 with N₂(satd) values derived from eq 10 and 11.

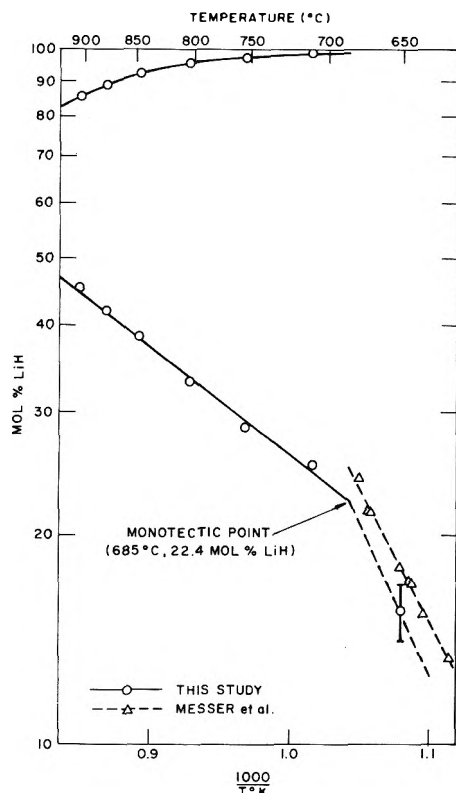


Figure 4. Temperature dependence of the miscibility gap boundaries for the Li-LiH system.

$$\ln N_2'(\text{satd}) = 2.235 - 3,576T^{-1} \quad (10)$$

and

$$\ln N_2''(\text{satd}) = -36.5585 + 1.10246 \times 10^5 T^{-1} - 1.11116 \times 10^8 T^{-2} + 3.74082 \times 10^{10} T^{-3} \quad (11)$$

The errors estimated for $N_2'(\text{satd})$ and $N_2''(\text{satd})$ were ± 0.01 and ± 0.005 , respectively.

An extrapolation was made into the region below the monotectic temperature (685°) by connecting the monotectic point (22.4 mol % LiH according to eq 10) with our approximate single solubility value for the solid LiH. This value, together with the freezing points of mixtures of LiH and lithium, measured in the range 624-679° by thermal analysis,⁶ is also shown in Figure 4. There is an apparent discrepancy between the two sets of data. Because of the relative steepness of the freezing-point curve, the thermal values may not be as reliable as desired. Need for further work in this area is indicated.

Discussion

Because of the width and the asymmetry of the miscibility gap in the Li-LiH system, it is difficult to find continu-

ous functions of the activity coefficients that would simultaneously satisfy the data for both terminal solutions. As an alternative, we chose to obtain activity coefficient expressions separately for each terminal solution.

Two conditions must be met in this data treatment: (1) the same equilibrium constant must govern both regions, and (2) the chemical activities of a component must be the same on both sides of the miscibility gap, *i.e.*, $N_1'(\text{satd})\gamma_1'(\text{satd}) = N_1''(\text{satd})\gamma_1''(\text{satd})$ and $N_2'(\text{satd})\gamma_2'(\text{satd}) = N_2''(\text{satd})\gamma_2''(\text{satd})$, where the single and double prime superscripts refer to the first and the second terminal solutions, the designation (satd) indicates the value at the miscibility gap boundary, and standard states of Li and LiH are the pure liquid phases. In spite of the relatively small scatter in the data, it was not possible to meet these conditions exactly at each datum point. Instead, a statistical treatment was sought.

The equilibrium constant, K , was regarded as an adjustable parameter, subject to the constraint

$$K = \frac{N_2''(\text{satd})\gamma_2''(\text{satd})}{N_1'(\text{satd})\gamma_1'(\text{satd})[P_{\text{H}_2}(\text{plateau})]^{1/2}} \quad (12)$$

which resulted from the combination of eq 2 and the above equalities. In eq 12 the γ 's are subscripted to refer to those solution components which are at higher concentrations at the miscibility gap boundaries. This choice of γ 's is convenient because their values are never far removed from unity and can be more precisely determined from the data (see, *e.g.*, Table I). Next, eq 6 was transformed into two linear equations, one for each terminal solution

$$Z_{ij}' = A_1'Y_{ij}' + B_1'X_i'Y_{ij}' + A_2'W_{ij}' + B_2'X_i'W_{ij}' \quad (13)$$

and

$$Z_{ij}'' = A_1''Y_{ij}'' + B_1''X_i''Y_{ij}'' + A_2''W_{ij}'' + B_2''X_i''W_{ij}'' \quad (14)$$

where the indices i and j refer to temperature and concentration, respectively, and the symbols are defined as follows: $Z_{ij} = \ln [K_i(P_i)^{1/2}(N_1/N_2)_{ij}]$, $Y_{ij} = (1 - 2N_2)_{ij}$, $W_{ij} = (1 - 3N_2^2)_{ij}$, $X_i = (1/T)_i$, $\alpha_i' = A_1' + B_1'X_i$, $\beta_i' = A_2' + B_2'X_i$, $\alpha_i'' = A_1'' + B_1''X_i$, $\beta_i'' = A_2'' + B_2''X_i$.

With the use of an initial estimated value of the equilibrium constant, the eight A and B parameters in eq 13 and 14 were evaluated by the method of least squares from 118 pieces of observed pressure-temperature-composition data of the terminal solution regions. Improved values of K were then calculated from the resulting A and B parameters using eq 12. Generally, K converged after five iterations.

The final $\ln K$ vs. $1/T$ points, when plotted, exhibited only a very slight deviation from linearity and therefore

could be represented by the equation

$$\ln K \text{ (atm}^{-1/2}\text{)} = -6.780 + 8328T^{-1} \quad (15)$$

with an error of only 0.5% (95% confidence level) in the mean value of K . The corresponding expression for the standard free energy of formation of liquid LiH, $\Delta G_f^\circ = [\mu_{\text{LiH}}^0(l, T, P_{\text{H}_2}) - \mu_{\text{Li}}^0(l, T, P_{\text{H}_2}) - \frac{1}{2}\mu_{\text{H}_2}^0(g, T, 1 \text{ atm})]$, is given by

$$\Delta G_f^\circ \text{ (kcal/mol)} = 13.47(\pm 0.17) \times 10^{-3}T - 16.55(\pm 0.18) \quad (16)$$

ΔG_f° values calculated from eq 16 (e.g., -3.07 kcal/mol at 1000°K , -0.38 at 1200°K) are slightly lower than the independently determined values listed in the JANAF tables¹⁵ (-2.859 at 1000°K , -0.288 at 1200°K).

Final values of the parameters in eq 13 and 14, calculated with K 's represented by eq 15, are $A_1' = -0.2295$, $A_2' = -0.1039$, $A_1'' = 25.127$, $A_2'' = -29.669$, $B_1' = 986.5^\circ\text{K}$, $B_2' = 2,308^\circ\text{K}$, $B_1'' = -30,699^\circ\text{K}$, $B_2'' = 39,285^\circ\text{K}$.

Using these parameters one can numerically express the change in the chemical potential of the reaction in eq 1 as a function of temperature and concentration. Since this change in the chemical potential is defined by $[\mu_{\text{LiH}}(\text{soln}, T, P_{\text{H}_2}) - \mu_{\text{Li}}(\text{soln}, T, P_{\text{H}_2}) - \frac{1}{2}\mu_{\text{H}_2}^0(g, T, 1 \text{ atm})] = RT \ln (P_{\text{H}_2})^{1/2}$, we have from eq 6, for the first terminal solution

$$\ln (P_{\text{H}_2})^{1/2} = \ln (N_2/N_1) + 6.498 + 0.4589N_2 + 0.1558N_2^2 - (1/T)(6182 + 1973N_2 + 3462N_2^2) \quad (17)$$

and, for the second terminal solution

$$\ln (P_{\text{H}_2})^{1/2} = \ln (N_2/N_1) + 11.322 - 38.753N_1 + 44.504N_1^2 - (1/T)(16,914 - 56,457N_1 + 58,928N_1^2) \quad (18)$$

where P_{H_2} is the equilibrium hydrogen pressure in atmospheres.

Equations 17 and 18 can be used to construct any isotherm within the temperature range of this study. For that purpose, the plateau pressures and the miscibility gap boundaries are given by eq 9–11. When the isotherms are calculated at the experimental temperatures of this study and are then superimposed on the data points (in a plot similar to that of Figure 2), the agreement is excellent at 710 , 759 , 803 , and 847° , whereas at 878 and 903° , some deviations occur in the plateau region, caused mainly by a larger scatter in the plateau pressure values at these temperatures. The largest deviations occur at 903° , near the lower boundary of the miscibility gap, but even here they amount to less than 3%. Such a deviation would correspond to an uncertainty in temperature of less than 2° .

Equations 17 and 18 were also used to obtain the temperature and composition of the consolute point by equating to zero the first derivatives with respect to N and solving the resulting equations. The calculations yielded (to five significant figures) 1000° and 60.0 mol % LiH. The former value is in good agreement with the consolute temperature reported by Heumann and Salmon (997°).⁵

The activity coefficients of Li and LiH in the first (γ_1' , γ_2') and in the second (γ_1'' , γ_2'') terminal solutions were obtained from the A and B parameters and from eq 4 and 5. Thus

$$\ln \gamma_1'/N_2^2 = (-0.2295 - 0.1039N_2) + (1/T)(986.5 + 2308N_2) \quad (19)$$

$$\ln \gamma_2'/N_1^2 = (-0.3853 + 0.1039N_1) + (1/T)(4448 - 2308N_1) \quad (20)$$

$$\ln \gamma_1''/N_2^2 = (25.127 - 29.669N_2) - (1/T)(30,699 - 39,285N_2) \quad (21)$$

$$\ln \gamma_2''/N_1^2 = (-19.377 + 29.669N_1) + (1/T)(28,228 - 39,285N_1) \quad (22)$$

Activity coefficients, calculated from eq 19–22 for concentrations corresponding to the miscibility gap boundaries, are listed in Table I. Their values indicate that the positive deviations from ideality in the LiH-rich solutions are much larger than those in the Li-rich solutions, as would be expected from the direction of the asymmetry of the miscibility gap. It is also interesting to note that according to eq 20 the excess entropy, $\Delta S^E = -R[\partial(T \ln \gamma)/\partial T]$, of LiH in the Li-rich solutions is small (0.3 – 0.6 eu at 800°). Although this is common in binary molten-salt solutions,¹⁶ the result is surprising because of the relatively large differences in bonding characteristics between Li and LiH. In contrast, the excess entropy (calculated from eq 21) of Li in the LiH-rich solutions (4 – 9 eu at 800°) appears to be unusually large. This may be related to an apparent tendency for the alkali metals, especially lithium, to associate in solutions.¹⁴

Additional important thermodynamic information that has bearing on the fundamental interactions between Li and LiH in solutions can be obtained by considering two limiting cases.

Dilute Solutions of LiH in Liquid Lithium. From the condition $N_2 \rightarrow 0$, it follows that $N_1\gamma_1 \rightarrow 1$, $\gamma_2 \rightarrow \gamma_2^*$, and eq 2 reduces to

$$K = K'\gamma_2^* \quad (23)$$

Here, γ_2^* is the activity coefficient of LiH at infinite dilution. It corresponds to the change in state $RT \ln \gamma_{\text{LiH}}^* = [\mu_{\text{LiH}}^*(T, P_{\text{H}_2}) - \mu_{\text{LiH}}^0(l, T, P_{\text{H}_2})]$ where $\mu_{\text{LiH}}^*(T, P_{\text{H}_2})$ is the chemical potential of LiH in a standard state defined in terms of an infinite dilution of LiH in Li, and $\mu_{\text{LiH}}^0(l, T, P_{\text{H}_2})$ is the chemical potential of pure liquid LiH. $K' = N_2/(P_{\text{H}_2})^{1/2}$ is a temperature-dependent constant¹⁷ corresponding to the change in state $RT \ln K' = -[\mu_{\text{LiH}}^*(T, P_{\text{H}_2}) - \mu_{\text{Li}}^0(l, T, P_{\text{H}_2}) - \frac{1}{2}\mu_{\text{H}_2}^0(g, T, 1 \text{ atm})]$.

Numerically, γ_{LiH}^* may be evaluated¹⁸ by applying the condition $N_1 = 1$ to eq 20. K' is then calculated according to eq 23. Thus

$$\ln K' \text{ (atm}^{-1/2}\text{)} = -6.498 + 6182T^{-1} \quad (24)$$

The knowledge of P - T - C relations in dilute solutions (<1 ppm) of hydrogen isotopes in liquid lithium is important in the CTR program. For dilute solutions, the hydrogen pressures calculated from eq 24 very well approximate those obtained from the more complex eq 17. For example, in the temperature range of this study, the difference in the hydrogen pressures calculated from the two equations is $<1\%$ for $N_{\text{LiH}} = 0.01$ and $<0.1\%$ for $N_{\text{LiH}} = 0.001$.

Dilute Solutions of Li in Liquid LiH. For the second terminal solution region, as $N_1 \rightarrow 0$, $N_2\gamma_2 \rightarrow 1$, and $\gamma_1 \rightarrow \gamma_1^*$, eq 2 becomes

$$K = K''/\gamma_1^* \quad (25)$$

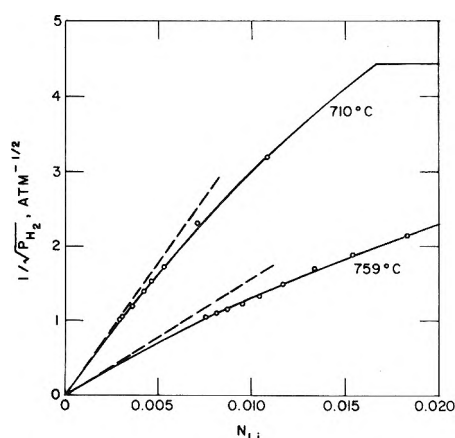


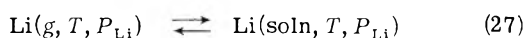
Figure 5. Portions of two lowest temperature isotherms showing the approach to a limiting law in the Li-rich solutions: (O) experimental points, (—) isotherms calculated from eq 18, (---) limiting slopes calculated from eq 26.

where γ_{Li}^* is the activity coefficient of lithium at infinite dilution defining the change in state $RT \ln \gamma_{Li}^* = [\mu_{Li}^*(T, P_{H_2}) - \mu_{Li}^0(l, T, P_{H_2})]$, and $K'' = 1/[N_1(P_{H_2})^{1/2}]$ is a constant analogous to K' . In terms of the chemical potentials, K'' corresponds to $RT \ln K'' = -[\mu_{LiH}^0(l, T, P_{H_2}) - \mu_{Li}^*(T, P_{H_2}) - \frac{1}{2}\mu_{H_2}^0(g, T, 1 \text{ atm})]$. When the values of γ_{Li}^* are evaluated¹⁸ from eq 21 (at $N_2 = 1$), those of K'' may be obtained from eq 25. Thus

$$\ln K'' (\text{atm}^{-1/2}) = -11.322 + 16,908T^{-1} \quad (26)$$

According to the definition of K'' , a plot of $1/(P_{H_2})^{1/2}$ vs. N_{Li} should approach linearity, as $N_{Li} \rightarrow 0$. In Figure 5 we present such plots at the two lowest temperatures of this study, 710 and 759°. It is evident that the experimental points support the limiting linearity requirements; however, because of the data normalization discussed above, a positive proof must await more detailed data in this terminal region.

Further useful thermodynamic information for solutions in this region is obtained by considering the following equilibrium



As $N_{Li} \rightarrow 1$ and $\gamma_{Li} \rightarrow 1$, the equilibrium constant and the corresponding change in the chemical potentials are given by

$$K_h = \frac{N_{Li}}{P_{Li}} = \exp \left[-\frac{\mu_{Li}^*(T, P_{Li}) - \mu_{Li}^0(g, T, 1 \text{ atm})}{RT} \right] \quad (28)$$

where P_{Li} is the partial pressure of lithium in the vapor phase, K_h is Henry's law constant, $\mu_{Li}^*(T, P_{Li})$ is the standard chemical potential of lithium defined at infinite dilution, and $\mu_{Li}^0(g, T, 1 \text{ atm})$ is the standard chemical potential of lithium vapor. No direct measurements for P_{Li} are available but, since $a_{Li} = N_{Li}\gamma_{Li} = P_{Li}/P_{Li}^0$, it can be replaced by the product $P_{Li}^0 N_{Li}\gamma_{Li}$. Thus

$$\ln K_h (\text{atm}^{-1}) = -\ln (P_{Li}^0 \gamma_{Li}^*) = -6.994 + 9986T^{-1} \quad (29)$$

where P_{Li}^0 , the vapor pressure of pure liquid lithium, is given¹⁹ by $\ln P_{Li}^0 (\text{atm}) = 11.536 - 18,572T^{-1}$, and γ_{Li}^* is obtained from eq 21 (with $N_2 = 1$).

A more useful way of describing the equilibrium reaction in eq 27 is in terms of the Ostwald coefficient, λ , defined by

$$\lambda = (C_{\text{soln}}/C_g) = \exp \left[-\frac{\mu_{Li}^*(T, P_{Li}) - \mu_{Li}^0(g, T, P_{Li} = R'Td_{LiH}/M_{LiH})}{RT} \right] \quad (30)$$

where C_{soln} and C_g are the concentrations (in mol/cm³) of lithium in the solution and in the ideal vapor phase, respectively, $R' = 82.06 \text{ cm}^3 \text{ atm/deg mol}$ is the gas constant, d_{LiH} is the density²⁰ of liquid LiH, and M_{LiH} is the molecular weight of LiH. The standard chemical potential $\mu_{Li}^0(g, T, P_{Li} = R'Td_{LiH}/M_{LiH})$ corresponds to 1 mol of ideal lithium vapor at temperature T and in a volume equal to the molar volume of solvent LiH. This standard state differs from $\mu_{Li}^0(g, T, 1 \text{ atm})$ in eq 28 in that it eliminates the physically unimportant contribution arising from differences in the molar volumes of the two phases. Thus, the quantity $RT \ln \lambda$ in eq 30 can be interpreted as the standard free energy of vaporization of lithium from the solution phase into the same volume of the vapor phase and is a direct measure of the interaction of Li atoms with molten LiH. The quantities K_h and λ are related by $\lambda = K_h R'Td_{LiH}/M_{LiH}$ and, according to eq 29

$$\ln \lambda = \ln (d_{LiH} T) - 4.659 + 9986T^{-1} \quad (31)$$

Topol²¹ has estimated values of $RT \ln \lambda$ for 34 molten metal-metal chloride solutions at $\sim 1000^\circ \text{K}$. For the alkali metal systems he obtained 20, 10, 11, and 10 kcal/mol for the Li-LiCl, Na-NaCl, K-KCl, and Rb-RbCl systems, respectively. From eq 31 for the Li-LiH system we obtain 23.1 kcal/mol, a value similar to Topol's estimate for Li-LiCl. The standard entropy and enthalpy of vaporization of lithium from LiH solutions, calculated at 1000°K by differentiating eq 31 with respect to temperature, are respectively -4.9 eu and 18.2 kcal/mol .

A large positive value of the free energy of vaporization indicates that the distribution of lithium between the gas and the molten hydride phase is heavily weighted in favor of the latter and reflects very strong interactions between lithium and LiH. This is in contrast to the solutions of noble gases in sodium²² and in molten fluorides,²³ where the Ostwald coefficients are small ($\lambda \approx 10^{-3}$) and therefore the distribution of the noble gas is strongly shifted in favor of the gas phase.

The results obtained in this study appear to be more precise than those of previous work. Several factors might have contributed to the improved precision: (a) the use of a larger quantity of lithium, (b) the absence of gases other than hydrogen in contact with lithium, (c) the prevention of hydrogen leakage from the reaction tube (double-walled construction), (d) the stabilization of hydrogen pressures by thermostating a major portion of the residual volume, (e) the thermostating of the calibrated volume for hydrogen metering, (f) the use of pure hydrogen generated by thermal decomposition of TiH₂, (g) the length of the equilibration times, and finally (h) the corrections for the initial concentration of hydrogen in the sample.

A similar investigation of the Li-LiD system is in progress.

Acknowledgments. We thank F. J. Karasek for manufacturing the Armco iron tubing and Dr. H. M. Feder, Dr. V. A. Maroni, and Professor S. E. Wood for helpful discussions.

sions. This work was performed under the auspices of the U. S. Atomic Energy Commission.

Supplementary Material Available. Tabular results of the measurements will appear following these pages in the microfilm edition of this volume of the journal. Photocopies of the supplementary material from this paper only or microfiche (105 × 148 mm, 24× reduction, negatives) containing all of the supplementary material for the papers in this issue may be obtained from the Journals Department, American Chemical Society, 1155 16th St., N.W., Washington, D. C. 20036. Remit check or money order for \$3.00 for photocopy or \$2.00 for microfiche, referring to code number JPC-74-1933.

References and Notes

- (1) W. M. Mueller, J. P. Blackledge, and G. G. Libowitz, "Metal Hydrides," Academic Press, New York, N. Y., 1968.
- (2) C. E. Messer, "A Survey Report on Lithium Hydride," AEC Research and Development Report No. NYO-9470, 1960.
- (3) L. O. Hill, Ph.D. Dissertation, University of Chicago, 1938.
- (4) M. R. J. Perlow, Ph.D. Dissertation, University of Chicago, 1941.
- (5) F. K. Heumann and O. N. Salmon, "The Lithium Hydride, Deuteride, and Tritide Systems," USAEC Report No. KAPL-1667, 1956.
- (6) C. E. Messer, E. B. Damon, P. C. Maybury, J. Mellor, and R. A. Seales, *J. Phys. Chem.*, **62**, 220 (1958).
- (7) S. A. Meacham, E. F. Hill, and A. A. Gordus, "The Solubility of Hydrogen in Liquid Sodium," Atomic Power Development Associates, Inc., Report No. APDA-241, 1970.
- (8) M. F. Amateau, "The Effect of Molten Alkali Metals on Containment Metals and Alloys at High Temperatures," Defense Metal Information Center, Report No. DMIC-169, 1962.
- (9) R. W. Webb, "Permeation of Hydrogen Through Metals," Atomic International, Report No. NAA-SR-10462, 1965.
- (10) P. D. Blake, M. F. Jordan, and W. I. Pumphrey, *Iron Steel Inst., Spec. Rep.*, **73**, 76 (1962).
- (11) H. R. Ihle and C. H. Wu, "Mass-Spectrometric Knudsen Effusion Measurements of Vapor Species in the System Lithium-Hydrogen," Report No. EUR-4938, p 89, from the 7th Symposium on Fusion Technology, Grenoble, France, Oct 1972.
- (12) See, e.g., J. H. Hildebrand and R. L. Scott, "The Solubility of Nonelectrolytes," 3rd ed, Reinhold, New York, N. Y., 1950, p 34.
- (13) See paragraph at end of text regarding supplementary material.
- (14) M. A. Bredig in "Molten Salt Chemistry," M. Blander, Ed., Interscience, New York, N. Y., 1964, p 386.
- (15) "JANAF Thermochemical Tables," Dow Chemical Co., Midland, Mich., Sept 30, 1967.
- (16) L. S. Hersh and O. J. Kleppa, *J. Chem. Phys.*, **42**, 1309 (1965); K. Hagemark, D. Hengstenberg, and M. Blander, *J. Chem. Eng. Data*, **17**, 216 (1972).
- (17) The constant K' is essentially the same as the Sieverts' law constant, K_s , which is defined as

$$K_s = \frac{N_H}{(P_{H_2})^{1/2}} = \exp \left\{ - \left[\mu_H^*(T, P_{H_2}) - \frac{1}{2} \mu_{H_2}^0(g, T, 1 \text{ atm}) \right] / RT \right\}$$
 where $N_H = N_{LiH} / (1 + N_{LiH})$ is the atom fraction of H in lithium. For the cases where $N_{LiH} \ll 1$, K' becomes identical with K_s .
- (18) An equivalent way of defining the limiting activity coefficients is provided by eq 4 and 5. They give $\ln \gamma_2^* = \alpha' + (\frac{1}{2})\beta'$ and $\ln \gamma_1^* = \alpha'' + \beta''$.
- (19) H. W. Davison, "Compilation of Thermophysical Properties of Liquid Lithium," NASA Report No. TN D-4650, 1968.
- (20) The density of liquid LiH has been derived from unstated sources at six temperatures (700–950°) in F. H. Welsh, "Properties of LiH. III. Summary of GE-ANPD Data," Report No. XDC-61-5-67, 1961. These data fit the equation $d_{LiH}(g/cm^3) = 5.572 - 14.547 \times 10^{-3}T + 14.116 \times 10^{-6}T^2 - 4.593 \times 10^{-9}T^3$, where T is the Kelvin temperature.
- (21) L. E. Topol, *J. Phys. Chem.*, **69**, 11 (1965).
- (22) E. Veleckis, S. K. Dhar, F. A. Cafasso, and H. M. Feder, *J. Phys. Chem.*, **75**, 2832 (1971).
- (23) G. M. Watson, R. B. Evans, W. R. Grimes, and N. V. Smith, *J. Chem. Eng. Data*, **7**, 285 (1962).

Metal Ion Association in Alcohol Solutions. IV. The Existence of an Inner-Sphere Complex between Erbium(III) and Perchlorate

Herbert B. Silber

Department of Chemistry, University of Maryland Baltimore County, Baltimore, Maryland 21228 (Received June 5, 1974)

An ultrasonic relaxation investigation of erbium(III) perchlorate solutions in aqueous methanol revealed the existence of inner-sphere perchlorate complexes below water mole fractions of 0.9. The rate constant for the formation of the inner-sphere complex at 25° is $(1.2 \pm 0.2) \times 10^8 \text{ sec}^{-1}$.

The use of LiClO_4 or NaClO_4 as nonassociating "inert" electrolytes to maintain constant ionic strength in electrochemical, thermodynamic, and kinetic studies is a common technique. If an inner-sphere metal ion-perchlorate complex exists, the experimental observations can be erroneous because reactions of a solvated metal ion need not be the same as those of a metal ion-ligand complex.¹ This problem becomes more acute in solutions of lower dielectric constant than water where increased ionic association would be expected.

We have chosen to determine if an inner-sphere perchlorate complex can be detected in a test system utilizing

Er(III) , a lanthanide ion. There are several reasons for choosing this system. First, there exist kinetic differences in the association reactions of the lanthanides with murexide when the inert electrolyte is KNO_3 or NaClO_4 ,^{2,3} and the nitrates are known to form inner-sphere complexes in aqueous solutions.⁴⁻⁶ Second, kinetic studies of lanthanide complexation are starting to appear in alcohols using NaClO_4 as the "inert" electrolyte.⁷ Third, pmr measurements have been carried out on lanthanide perchlorate systems to determine the cation solvation number, but these studies cannot detect perchlorate binding.^{8,9} Fourth, we have successfully used the ultrasonic relaxation technique

in aqueous methanol solutions of ErCl_3 to detect inner-sphere complexation which was absent in the aqueous solutions.¹⁰ We now report measurements on $\text{Er}(\text{ClO}_4)_3$ which have led to surprising results.

Experimental Section

The erbium perchlorate solutions were made from the oxide (American Potash & Chemical Corp.), which was dissolved in aqueous perchloric acid. For stock solutions containing the minimum amounts of water the $\text{Er}(\text{ClO}_4)_3$ solutions were heated until a slurry formed; methanol was added; and the process repeated several times. Whenever possible the stock solutions were made in an aqueous medium, heating only to allow the oxide to react, and then diluting with the appropriate volume of methanol. Karl Fischer titrations were used to determine the water content in the solvent systems containing only a small quantity of water.

The ultrasonic relaxation apparatus and technique employed were similar to those described earlier.^{6,10} For a system undergoing chemical relaxation, the measured sound absorption, α/f^2 , fits a standard curve defined by

$$\alpha/f^2 = B + \sum_i \frac{A_i}{1 + (f/f_{R_i})^2} \quad (1)$$

where f is the frequency, f_{R_i} is the relaxation frequency of each independent chemical relaxation step, A_i is the amplitude of the relaxation, and B is the experimental background which is characteristic of the solvent medium. The difference between the solution absorbance and that of the solvent is described in terms of the excess absorbance, μ , defined as

$$\mu = (\alpha/f^2 - B)fc \quad (2)$$

where c is the sound velocity in the solution.

All calculations were carried out on a Wang 700 programmable calculator. The equilibrium analysis was obtained with a Cary 17 spectrophotometer. All temperatures were at 25°.

Results

No excess absorbance was observed over the frequency range 10–230 MHz for a 0.200 M $\text{Er}(\text{ClO}_4)_3$ solution in water, indicating that any complexes that exist would be of the outer-sphere type. Solutions of 0.200 M $\text{Er}(\text{ClO}_4)_3$ in aqueous methanol exhibited an excess absorbance. When the data were calculated assuming only a single relaxation, the calculated solvent background varied between 37 and 63×10^{-17} nepers $\text{cm}^{-1} \text{sec}^2$. In the absence of $\text{Er}(\text{ClO}_4)_3$, or in the presence of NaClO_4 , the solvent background was measured to be 25×10^{-17} nepers $\text{cm}^{-1} \text{sec}^2$, in agreement with the literature results for aqueous methanol solutions.¹¹ As in aqueous solutions^{4–6} and for ErCl_3 in aqueous methanol,¹⁰ the abnormally high background is interpreted in terms of an additional high-frequency reaction step being present in these systems. Thus, all the ultrasonic relaxation data were calculated in terms of our double relaxation program. The variation in excess absorbance maximum, defined as

$$\mu_{\max_i} = f_{R_i} A_i (c/2) \quad (3)$$

and that of the relaxation frequency with water mole fraction, $X_{\text{H}_2\text{O}}$, are shown in Figure 1. As in the case of $\text{Er}(\text{NO}_3)_3$ and ErCl_3 we believe that the data contained in Figure 1 can be used to describe the nature of the lanthanide complexes existing in these solutions.

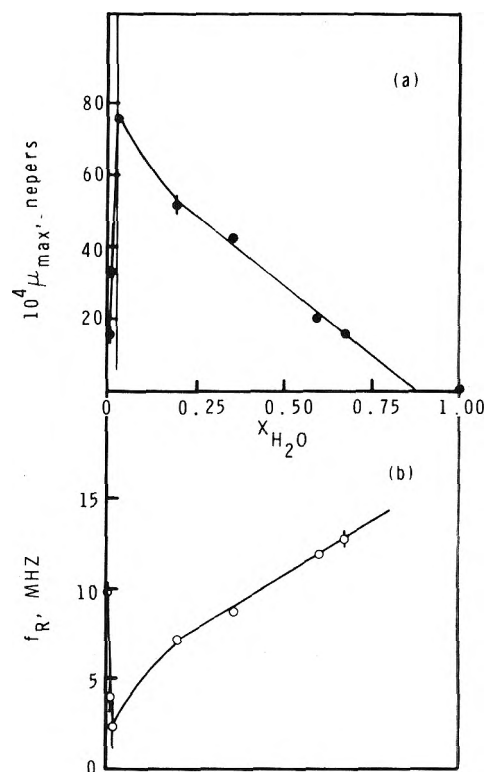


Figure 1. Variation in μ_{\max} and f_R for erbium perchlorate in aqueous methanol at 25°. The relaxation frequencies below 10 MHz are those calculated from the computer program and are only an estimate.

Although we believe the similarity of these results with those of the chloride and nitrate in aqueous methanol,¹⁰ as well as the nitrates^{4–6,12} and sulfates^{5,6,13–15} in water, indicate that the low-frequency relaxation corresponds to the formation of inner-sphere complexes, other data are necessary for confirmation. Our approach is to choose one reference solvent composition, selected such that the low-frequency relaxation is greater than 10 MHz (the low-frequency limit of our apparatus); to obtain relaxation data as a function of concentration; to establish that the concentration data fit the relaxation equations derived for our assumed complexation mechanism; and lastly to determine the ErClO_4^{2+} association constant in an independent study. Our reference solvent was 50% water by volume, corresponding to a water mole fraction of 0.69.

The usual procedure in ultrasonic analysis is to determine a complex formation constant *via* conductivity measurements and then to convert these to activities of all of the reacting species.^{4–6,13–15} Even in aqueous solutions this procedure cannot be followed exactly since at the high concentrations necessary for the ultrasonic measurements, the activities of lanthanide species are neither known nor calculable by a vigorous procedure. Hence, variations of the Davies equation are used to estimate the activity coefficients. In the case of the lanthanide sulfates in water, the major sources of error between different studies was the method of estimating the outer-sphere association constants and was not the choice of activity coefficients or the measurements of relaxation frequencies.^{13–15} In mixed solvents the estimation of activities for high concentrations of unsymmetrical electrolytes compounds these difficulties. However, we have previously shown that in the aqueous lanthanide sulfate systems, the complex formation rate

TABLE I: Kinetic and Equilibrium Data for the $\text{Er}(\text{ClO}_4)_3$ Solutions in 50% Aqueous Methanol at 25°

$\text{Er}(\text{ClO}_4)_3, M$	0.100	0.200	0.300	0.400	0.500
	Equilibrium Data				
$[\text{Er}^{3+}]$	0.050	0.070	0.081	0.088	0.093
$[\text{ErClO}_4^{2+}]$	0.050	0.131	0.219	0.312	0.407
$[\text{ClO}_4^-]$	0.250	0.469	0.681	0.888	1.09
$\theta(c)$	0.300	0.539	0.761	0.976	1.19
$\phi(c)$	0.217	0.333	0.413	0.475	0.523
	Double Relaxation Data, $B = 25 \times 10^{-17}$ nepers $\text{cm}^{-1} \text{sec}^2$				
$10^{17} A_{12}^a$	15.2 ± 1.2	13.8 ± 1.0	14.3 ± 1.5	15.1 ± 1.1	13.9 ± 0.8
f_{R12}, MHz	165 ± 22	209 ± 30	191 ± 36	276 ± 58	298 ± 47
$10^{17} A_{III}^a$	112 ± 19	163 ± 7	216 ± 6	287 ± 5	340 ± 3
f_{R111}	9.0 ± 1.4	12.1 ± 0.6	13.6 ± 0.5	14.2 ± 0.3	16.0 ± 0.2

^a Units are nepers $\text{cm}^{-1} \text{sec}^2$.

constant is relatively insensitive to the choice of the stability constant¹⁵ and in aqueous methanol reasonable kinetic results were obtained for ErCl_3 when a spectrophotometric technique was used to estimate the complexation constants in terms of concentrations, and then the relaxation equations were modified to eliminate the activities.¹⁰ This latter method was used in this study and the details are not repeated here.^{10,16} The absorption data at 380 nm deviated from Beer's law and the complexation constant

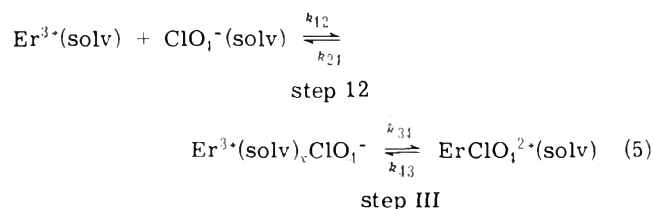
$$K_f = [\text{ErClO}_4^{2+}]/[\text{Er}^{3+}][\text{ClO}_4^-] \quad (4)$$

was determined to be 4 at 25° assuming only the 1:1 complex is formed. This number appears reasonable because the excess absorbance in 50% aqueous methanol was somewhat lower than for lanthanide complexes where K_f , obtained by conductivity, varied from 7 to 17.^{6,10}

Ultrasonic absorption data were obtained on five $\text{Er}(\text{ClO}_4)_3$ solutions in 50% aqueous methanol. These results are summarized in Table I along with the equilibrium data and concentration parameters to be derived in a later section.

Discussion

We will assume for the present that the low-frequency relaxation corresponds to the formation of an inner-sphere complex between erbium and perchlorate. The high-frequency relaxation corresponds to the formation of a solvent-separated outer-sphere complex. The two-step association mechanism will be



Here solv represents the solvation shell surrounding the ions in this medium and consists of methanol and/or water molecules. The formation constant reported is analogous to those obtained by conductivity measurements in that the complex corresponds to the combination of inner- and outer-sphere complexes. If $K_{12} = k_{12}/k_{21}$ and $K_{III} = k_{34}/k_{43}$, then

$$K_f = K_{12}(1 + K_{III}) \quad (6)$$

If step 12 is more rapid than step III, Tamm has shown that the two relaxation times, τ_i , are given by¹⁷

$$\tau_{12}^{-1} = 2\pi f_{R12} = k_{21} + k_{12}\theta(c) \quad (7)$$

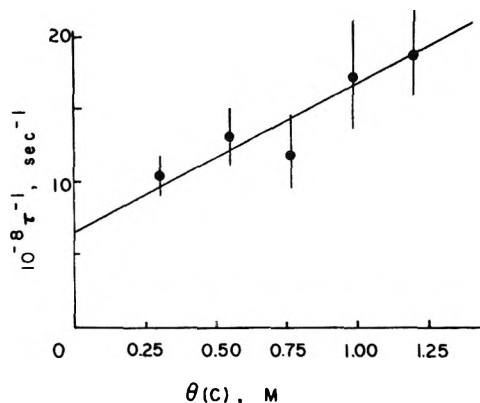


Figure 2. Relaxation data for the formation of the outer-sphere erbium perchlorate complex.

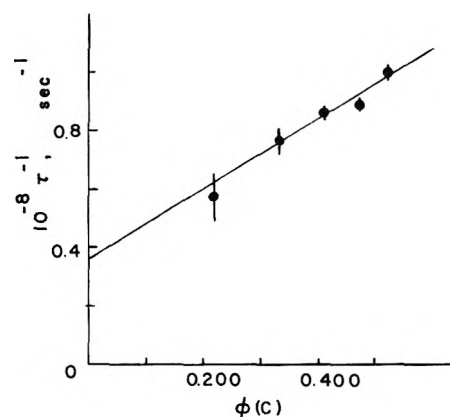


Figure 3. Relaxation data for the formation of the inner-sphere erbium perchlorate complex.

$$\tau_{III}^{-1} = 2\pi f_{R111} = k_{43} + k_{34}\phi(c) \quad (8)$$

where $\theta(c)$ in this case is

$$\theta(c) = [\text{Er}^{3+}] + [\text{ClO}_4^-] \quad (9)$$

and

$$\phi(c) = \theta(c)/[K_{12}^{-1} + \theta(c)] \quad (10)$$

The numerical values of $\theta(c)$ and $\phi(c)$ are summarized in Table I. Figures 2 and 3 are plots of the high- and low-frequency relaxation times as functions of the appropriate concentration-dependent terms. The low-frequency relaxation for the 0.100 M solution was calculated to be below the experimental frequency range, and hence this solution was not actually used in any of the kinetic calculations.

When the relaxation data for the high-frequency relaxation process are calculated as a function of $\theta(c)$, a straight-line can be drawn through the data. According to the proposed mechanism of eq 5, this relaxation step corresponds to the formation of the outer-sphere erbium-perchlorate complex. The fit of the data for this step is no worse than in the aqueous NdNO_3^{2+} system where a mechanism similar to eq 5 is valid.⁶ The rate constants for this step are $k_{12} = (1.0 \pm 0.4) \times 10^9 \text{ M}^{-1} \text{ sec}^{-1}$ and $k_{21} = (6.5 \pm 3.5) \times 10^8 \text{ sec}^{-1}$. These results are similar to those for the formation of the outer-sphere ErCl_2^+ complex in aqueous methanol, where k_{12} was calculated to be $(2.3 \pm 1.2) \times 10^9 \text{ M}^{-1} \text{ sec}^{-1}$ and $(1.8 \pm 2.8) \times 10^9 \text{ M}^{-1} \text{ sec}^{-1}$ in solutions containing 1.5 and 2.9% water, respectively. The ErCl_2^+ k_{21} results were $(8.1 \pm 1.7) \times 10^8 \text{ sec}^{-1}$ and $(2.0 \pm 0.6) \times 10^9 \text{ sec}^{-1}$ and K_{12} was 2.8 and 0.94 in the 1.5 and 2.9% aqueous solutions. The calculated K_{12} for ErClO_4^{2+} is 1.6, in close agreement with the chloride results.

Further evidence for our proposed mechanism comes from the examination of the low-frequency data in Figure 3. The experimental fit of this data is one of the best ever achieved in this laboratory in lanthanide complexation systems. As in previous studies, we believe that a better estimate of K_{12} comes from the low-frequency relaxation data, and the results are analyzed accordingly.¹⁵ The rate constants which we ascribe to the formation of an inner-sphere erbium perchlorate complex in 50% aqueous methanol at 25° are $k_{34} = (1.2 \pm 0.2) \times 10^8 \text{ sec}^{-1}$ and $k_{43} = (3.6 \pm 0.9) \times 10^7 \text{ sec}^{-1}$. This yields a K_{III} of 3.3 and a K_{12} of 0.9, in close agreement to the step 12 results. The kinetic results in the chloride system are $k_{34} = (1.0 \pm 0.4) \times 10^8 \text{ sec}^{-1}$ and $k_{43} = (5.9 \pm 1.1) \times 10^7 \text{ sec}^{-1}$ for the 1.5% water solutions, and $k_{34} = (7.7 \pm 4.1) \times 10^7 \text{ sec}^{-1}$ and $k_{43} = (6.7 \pm 1.7) \times 10^7 \text{ sec}^{-1}$ for the 2.9% water solutions.¹⁰ Although there is no *a priori* reason why all the respective rate constants should be equal, all of the lanthanide complex formation rate constants in water are similar for those ligands which react *via* eq 5. Thus, the experimental data support the assumption that the relaxations correspond to the formation of both outer- and inner-sphere complexes.

Using this mechanism, the variation in f_R and μ_{max} for 0.200 M $\text{Er}(\text{ClO}_4)_3$ will be examined as a function of $X_{\text{H}_2\text{O}}$ for the low-frequency process. Above $X_{\text{H}_2\text{O}} = 0.04_4$ the f_R variation with $X_{\text{H}_2\text{O}}$ is typical of lanthanide complexation reactions in aqueous alcohols, where the complex formation rate constant is independent of the alcohol composition as long as water is present.^{7,10} The only kinetic change observed as water is added to the alcohol solutions of the rare earths is to increase the dissociation rate constant, and hence to increase f_R according to eq 8. This explanation is different from the results reported for the association reaction between Zn^{2+} and SO_4^{2-} studied by ultrasonic relaxation in aqueous glycol mixtures.¹⁸ In the range of $X_{\text{H}_2\text{O}}$ of 0.50–1.0, f_R varied between 20 and 80 MHz, a larger but similar variation to that in lanthanide systems. However, the ZnSO_4 data were interpreted in terms of the loss of water from the inner coordination shell of Zn^{2+} being rate determining. The entire variation in f_R was accounted for by the effect of viscosity and dielectric constant upon the activity coefficients for the different compositions. The different interpretations for the increasing f_R 's with $X_{\text{H}_2\text{O}}$ for Zn^{2+} and the lanthanides should not be surprising, since cation solvent exchange is not rate determining for lanthanide systems.¹⁵

The data which are more difficult to interpret occur

below $X_{\text{H}_2\text{O}} = 0.04_4$. This same f_R variation occurred in the ErCl_3 solutions of low water content and was explained using an earlier temperature jump relaxation study on lanthanide acetate complexes.^{10,19} In the acetate system, the rate constants for the formation of the 1:1 dysprosium acetate complex were found to be similar to those of other Dy(III) reactions. However, in the presence of excess acetate the bis complex is formed with larger rate constants and a much larger τ^{-1} , compared to when only the 1:1 complex is present. If we assume that the bis(perchlorate) complex is stable in anhydrous alcohol we would expect an abnormally high f_R , as is observed in Figure 1. As water is added, the concentration of bis complex decreases, and this is reflected in a lower value of f_R . Near $X_{\text{H}_2\text{O}} = 0.04_4$, the bis complex is no longer stable and the relaxation frequency is that observed for 1:1 complexes. As additional water is added, f_R increases as already described.

In aqueous $\text{Er}(\text{ClO}_4)_3$ solutions outer-sphere complexes predominate, while in methanol both outer- and inner-sphere complexes can be detected. Since μ_{max} for the low-frequency relaxation is proportional to the square of the reaction volume change, ΔV^2 , times the concentration of inner-sphere complexes, a monotonic decrease in μ_{maxIII} is expected with increasing $X_{\text{H}_2\text{O}}$ due to the decreasing concentrations of inner-sphere complexes. Furthermore, since at least one solvent molecule is lost from the cation solvent shell, ΔV for solvent exchange is about 40 cm^3/mol for methanol exchange and 18 cm^3/mol for water exchange. In ErCl_3 a smooth decrease in μ_{maxIII} with increasing water mole fraction was observed, which is the expected behavior for the shift in distribution from inner- to outer-sphere complexes. In addition, this smooth decrease indicates that there is no marked preference for water over methanol in the inner solvation shell because a sharp drop in μ_{max} would be observed if water was preferentially bound to the cation. The $\text{Er}(\text{ClO}_4)_3$ results are clearly different with μ_{maxIII} increasing as water is added to methanol, reaching a maximum value around $X_{\text{H}_2\text{O}} = 0.04_4$, and then decreasing to zero where essentially no inner-sphere complexes are present. The question must be raised about whether this variation is an experimental artifact, arising from a variation in μ_{max} with solvent composition alone, or is caused by five of seven f_R values being below the low-frequency range of the apparatus. Although similar maxima in μ_{max} with $X_{\text{H}_2\text{O}}$ curves occur in the absence of salts with the higher alcohols plus water, they are not present when the alcohol is methanol.¹¹ Ultrasonic measurements made on NaClO_4 solutions and $\text{Ca}(\text{ClO}_4)_2$ solutions²⁰ in aqueous methanol did not possess this maximum. Hence, our results cannot be attributed to the solvent system or solvent plus nonassociating salt. To test whether the μ_{maxIII} variation is an artifact of the four-parameter non-linear least-squares fit of eq 1 for the absorption data, we have plotted the measured ultrasonic absorption, α/f^2 , as a function of $X_{\text{H}_2\text{O}}$ at 10, 15, and 70 MHz, shown in Figure 4. The 10- and 15-MHz data are typical of those at all frequencies below 65 MHz and a maximum occurs around water mole fraction 0.2. This α/f^2 maximum below 65 MHz is similar to that observed in the erbium nitrate case at all frequencies.¹⁰ Above 65 MHz there is a monotonic decrease in α/f^2 with $X_{\text{H}_2\text{O}}$, a result which is similar to that observed at all frequencies for erbium chloride solutions. Although the maximum does not occur at the same water mole fraction for the μ_{maxIII} and α/f^2 plots, there can be no doubt that the effect is real.

The high-frequency α/f^2 variation with $X_{\text{H}_2\text{O}}$ varies in

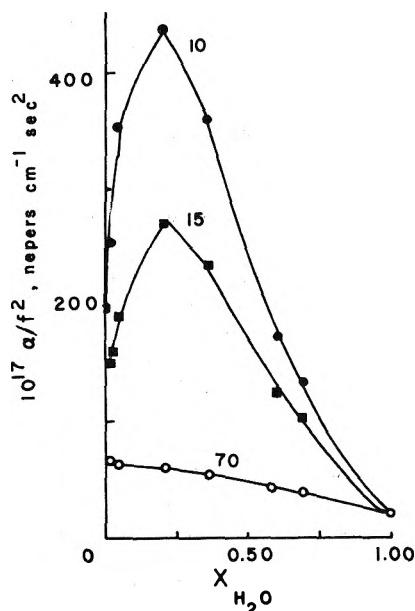


Figure 4. Ultrasonic absorption for selected frequencies as a function of water mole fraction.

the manner expected for electrostatic complexes as the water content and solvent dielectric constant increase. Since the absorbance data in this range are related to outer-sphere complexes, this indicates that as water is added to methanolic solutions of erbium perchlorate, the outer-sphere complex concentration must be decreasing. The low-frequency data reflects differences with solvent composition for the formation of inner-sphere complexes. The existence of a maximum in α/f^2 or μ_{maxIII} must mean that at least one additional process occurs in the region of this maximum compared to the remainder of the solvent compositions. As in the case of the nitrate,¹⁰ this could most easily be explained by a change in solvation number occurring between $X_{\text{H}_2\text{O}}$ of 0.04 and 0.2. This solvation number change involving an equilibrium between two forms of solvated cations has often been postulated to exist in aqueous solutions of the lanthanides. This apparent solvation number change may be a result of crowding in the solvation shell of the inner-sphere erbium perchlorate complex or it may indicate a shift from bidentate to monodentate perchlorate association. This study cannot distinguish between these possibilities.

In addition to confirming the existence of inner-sphere complexes between Er(III) and perchlorate, this study demonstrates the unusually high selectivity of ultrasonics to distinguish between inner- and outer-sphere complexes. Although optical spectroscopic measurements have indicated the existence of a perchlorate complex with Ce(III) in water, which was assumed to be outer sphere,²¹ and with Fe(III) in aqueous methanol,²² these spectral measure-

ments cannot distinguish between the two types of complexes. At 25° and 2.0 M ionic strength, a solvent extraction technique was used to determine a stability constant of about unity for perchlorate association with Am(III) and due to the low value of the constant the association was assumed to be outer sphere.²³ In a recent ultrasonic investigation of Ni(II), Cu(II), and Zn(II) association with perchlorate in acetonitrile, the inner coordination shell was found to be composed of acetonitrile molecules, and hence outer-sphere perchlorate complexes were established.²⁴ We have recently measured the ultrasonic association between Ca(II) and perchlorate in aqueous methanol and found that essentially only outer-sphere complexes are formed.²⁰ These studies should be extended to other cation systems, such as Mg(II), to determine if inner-sphere perchlorate complexes are unique to the lanthanides; are unique to some metal ions forming electrostatic complexes; or if, under certain conditions, inner-sphere perchlorate complexes can be formed with most cations in aqueous alcohols.

Acknowledgment. We are indebted to the University of Maryland for a research grant which made this investigation possible.

References and Notes

- (1) See, for example, K. Kustin, R. F. Pasternack, and E. M. Weinstock, *J. Amer. Chem. Soc.*, **88**, 4610 (1966); R. G. Wilkins, *Accounts Chem. Res.*, **3**, 408 (1970).
- (2) G. Geier, *Ber. Bunsenges. Phys. Chem.*, **69**, 617 (1965).
- (3) H. B. Silber, R. D. Farina, and J. H. Swinehart, *Inorg. Chem.*, **8**, 819 (1969).
- (4) R. Garnsey and D. W. Ebdon, *J. Amer. Chem. Soc.*, **91**, 50 (1969).
- (5) D. P. Fay, D. Litchinsky, and N. Purdie, *J. Phys. Chem.*, **73**, 544 (1969).
- (6) H. B. Silber, N. Scheinin, G. Atkinson, and J. J. Grecsek, *J. Chem. Soc., Faraday Trans. 1*, **68**, 1200 (1972).
- (7) J. L. Bear and C. T. Lin, *J. Inorg. Nucl. Chem.*, **34**, 2368 (1972).
- (8) A. Fratiello, V. Kubo, S. Peak, B. Sanchez, and R. E. Schuster, *Inorg. Chem.*, **10**, 2552 (1971).
- (9) A. Fratiello, V. Kubo, and G. A. Vidulich, *Inorg. Chem.*, **12**, 2066 (1973).
- (10) J. Reidler and H. B. Silber, *J. Inorg. Nucl. Chem.*, **36**, 175 (1974); *J. Chem. Soc., Chem. Commun.*, 354 (1973); *J. Phys. Chem.*, **78**, 424 (1974).
- (11) C. J. Burton, *J. Acoust. Soc. Amer.*, **20**, 186 (1948); L. R. O. Storey, *Proc. Phys. Soc. (London)*, **B65**, 943 (1952).
- (12) G. S. Darbari, F. Fittipaldi, S. Petrucci, and P. Hemmes, *Acustica*, **25**, 125 (1971).
- (13) N. Purdie and C. A. Vincent, *Trans. Faraday Soc.*, **63**, 2745 (1967).
- (14) M. F. Farrow and N. Purdie, *J. Solution Chem.*, **2**, 513 (1973).
- (15) H. B. Silber, *J. Chem. Soc., Chem. Commun.*, 1970 (1971); J. Reidler and H. B. Silber *J. Phys. Chem.*, **77**, 1275 (1973).
- (16) F. J. C. Rossotti and H. Rossotti, "The Determination of Stability Constants," McGraw-Hill, New York, N. Y., 1961, p 276.
- (17) K. Tamm, "Dispersion and Absorption of Sound by Molecular Processes," D. Sette, Ed., Academic Press, New York, N. Y., 1963, pp 175-222.
- (18) F. Fittipaldi and S. Petrucci, *J. Phys. Chem.*, **71**, 3414 (1967)).
- (19) M. Doyle and H. B. Silber, *J. Chem. Soc., Chem. Commun.*, 1067 (1972).
- (20) H. B. Silber, *FEBS Lett.*, **41**, 303 (1974).
- (21) L. J. Heidt and J. Berestecki, *J. Amer. Chem. Soc.*, **77**, 2049 (1955).
- (22) G. Wada and A. Endo, *Bull. Chem. Soc. Jap.*, **45**, 1073 (1972).
- (23) P. A. Baisden, G. R. Choppin, and W. F. Kinard, *J. Inorg. Nucl. Chem.*, **34**, 2029 (1972).
- (24) A. Diamond, A. Fanelli, and S. Petrucci, *Inorg. Chem.*, **12**, 611 (1973).

Predicted Properties of the Superheavy Elements. III. Element 115, Eka-Bismuth^{1a}

O. L. Keller, Jr.,* ^{1b} C. W. Nestor, Jr.,

Oak Ridge National Laboratory, Oak Ridge, Tennessee 37830

and Burkhard Fricke

Gesellschaft für Schwerionenforschung, Darmstadt, BRD, Germany (Received April 29, 1974)

Publication costs assisted by Oak Ridge National Laboratory

Element 115 is expected to be in group V-a of the periodic table and have most stable oxidation states of I and III. The oxidation state of I, which plays a minor role in bismuth chemistry, should be a major factor in 115 chemistry. This change will arise because of the large relativistic splitting of the spherically symmetric $7p_{1/2}$ shell from the $7p_{3/2}$ shell. Element 115 will therefore have a single $7p_{3/2}$ electron outside a $7p_{1/2}^2$ closed shell. The magnitude of the first ionization energy and ionic radius suggest a chemistry similar to Tl^+ . Similar considerations suggest that 115^{3+} will have a chemistry similar to Bi^{3+} . Hydrolysis will therefore be easy and relatively strongly complexing anions of strong acids will be needed in general to effect studies of complexation chemistry. Some other properties of 115 predicted are as follows: ionization potentials I 5.2 eV, II 18.1 eV, III 27.4 eV, IV 48.5 eV, $0 \rightarrow 5^+$ 159 eV; heat of sublimation, 34 kcal (g-atom)⁻¹; atomic radius, 2.0 Å; ionic radius, 115^+ 1.5 Å, 115^{3+} 1.0 Å; entropy, 16 cal deg⁻¹ (g-atom)⁻¹ (25°C); standard electrode potential $115^+|115$, -1.5 V; melting and boiling points are similar to element 113.

Introduction

Interest in superheavy elements remains high as new heavy-ion beams are being developed at the Super HILAC accelerator at Berkeley and construction proceeds on the UNILAC in Darmstadt. For over 1 year the Dubna heavy-ion accelerator group has been carrying out reactions that might produce superheavy elements. The recent Russian attempt to use the reaction of ^{76}Ge with ^{232}Th to reach elements in the island of stability was unfortunately unsuccessful.² This suggests that the discovery of superheavy elements will probably be difficult, since the germanium plus thorium reaction was expected to be one of the more favorable cases.³ Chemical separations methods may now take on added importance in the search since they might offer much higher reliability and sensitivity than physical and nuclear methods. This was the case in the discovery of fission, for example.⁴

Element 115, eka-bismuth, is a particularly interesting case scientifically since its chemistry will be strongly altered by relativistic effects.⁵ There is, in fact, no element like 115 available to us in the present periodic system. An approach involving careful comparisons with the periodic table and analogies based on relativistic Hartree-Fock (rel HF) and relativistic Hartree-Fock-Slater (rel HFS) calculations appears to be best under these circumstances. Our predictions therefore involve first calculating electronic energy levels, ionization potentials, promotion energies to excited states, and atomic and ionic radii. The rel HFS programs were those of Oak Ridge and Fricke that we have used previously.^{6,7} The relativistic Hartree-Fock program was very kindly made available to us by Desclaux.⁸

All three atomic calculational methods gave results which were close to each other. Further properties were estimated by combining the calculated quantities with valence bond theory or other general theories and by extrapolations in the periodic system. We first of all present in the following paragraphs our calculational results. These will

then be combined in the following sections to arrive at specific predictions on the chemical properties of element 115.

Ionization Energies

Calculated and experimental ionization energies of the Group V-a elements are given in Table I. The difference, Δ , between the experimental and rel HFS results were used to estimate an "experimental" value for the ionization potentials of 115 and its ions. For comparison we give in Table II the rel HFS and experimental values for the ionization energies of the group III-a elements, Pb, and Po.

Atomic and Ionic Radii

In our considerations of chemical and physical properties the atomic and ionic radii are of considerable importance. Stabilization of an ion in a solution or crystal is dependent on the magnitude of decrease in the ionic radius with increase in its ionization (charge) since the radius strongly influences solvation and lattice energies. The atomic radii, on the other hand, are important for considerations involving valence bond theory. As pointed out by Pauling⁹ and by Drago,¹⁰ metallic atoms with a large volume have weaker covalent bonding because the valence electrons are spread over a larger space so that less overlap with the orbitals of anions results. Calculated atomic radii of the group V-a elements along with their empirical values as given by Slater¹¹ are given in Table III. Values for Tl, Pb, and Po are also given for comparison. The average radius of the outermost electronic shell, $\langle r \rangle$, was calculated both by the rel HF and rel HFS methods for As, Sb, Bi, and 115. The results of the two methods are very similar. Also the radius of maximum radial charge density for the outermost shell, r_{max} , is given. The latter is preferred by Slater¹¹ for comparison with his empirical atomic radii. In Figure 1 we plot Slater's atomic radii and the calculated r_{max} for the group V-a elements vs. row of the periodic table. The reproduction of the trend of the empirical radii by the calculations is obviously excel-

TABLE I: Ionization Energies of Group V-a Elements

Z	Ion	Ionization energies, eV			$\Delta(\text{exptl} - \text{rel HFS})$
		rel HF	rel HFS	Exptl	
15	P		8.6	10.484	1.9
	P ⁺		18.0	19.72	1.7
	P ²⁺		28.5	30.156	1.6
	0 → 5 ⁺		169.8	176.72	6.9
33	As	8.44	8.00	9.81	1.8
	As ⁺	17.0	17.1	18.63	1.6
	As ²⁺	27.6	27.0	28.34	1.4
	As ³⁺		49.6	50.1	0.5
51	0 → 5 ⁺	162.5	164.2	169.5	5.3
	Sb	7.49	7.05	8.639	1.6
	Sb ⁺	15.4	15.5	16.5	1.0
	Sb ²⁺	24.6	24.1	25.3	1.2
83	0 → 5 ⁺	142.4	144.6	150.5	5.9
	Bi	6.58	6.09	7.287	1.2
	Bi ⁺	15.5	15.7	16.68	0.94
	Bi ²⁺	24.8	24.5	25.56	1.1
115	0 → 5 ⁺	143.7	146.3	150.8	4.5
	115	4.79	4.70	(5.2)	(0.5)
	115 ⁺	17.70	17.4	(18.1)	(0.7)
	115 ²⁺	27.3	26.5	(27.4)	(0.9)
	115 ³⁺		48.0	(48.5)	(0.5)
	0 → 5 ⁺	155	155	(159)	(4)

TABLE II: Ionization Potentials of Group III-a, Pb, and Po (eV)

	rel HFS	Exptl	Δ
Ga	5.02	6.00	0.98
	20.21	20.51	0.30
	30.50	30.70	0.20
0 → 3 ⁺	55.73	57.21	1.48
In	4.88	5.785	0.90
	18.41	18.86	0.45
	27.56	28.03	0.47
0 → 3 ⁺	50.85	52.67	1.82
Tl	5.24	6.106	0.87
	19.90	20.42	0.52
	29.30	29.8	0.5
0 → 3 ⁺	54.4	56.3	1.90
113	6.51	(7.4)	(0.9)
	22.78	(23.3)	(0.5)
	32.47	(33.0)	(0.5)
0 → 3 ⁺	61.76	(63.7)	(1.9)
Pb	6.4	7.415	1.0
	14.0	15.028	1.0
	31.6	31.93	0.3
Po	7.2	8.43	1.2
	14.8		
	26.8		

TABLE III: Slater Atomic Radius

Z	Element	rel HF, (r)	Atomic radius		Slater atomic radius
			rel HFS, (r)	rel HFS, (r _{max})	
15	P		1.21	0.98	1.00
33	As	1.35	1.31	1.07	1.15
51	Sb	1.57	1.52	1.27	1.45
83	Bi	1.72	1.67	1.41	1.60
115	eka-Bi	2.07	2.00	1.77	(2.0)
81	Tl		1.80	1.42	1.90
82	Pb		1.58	1.22	1.80
84	Po		1.52	1.21	1.90

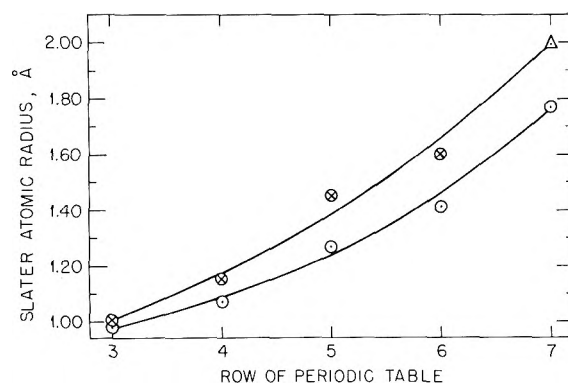


Figure 1. Slater atomic radii of group V-a elements (⊗), extrapolated atomic radius of element 115 (Δ) and maximum radial charge density in the outermost shell computed by rel HFS.

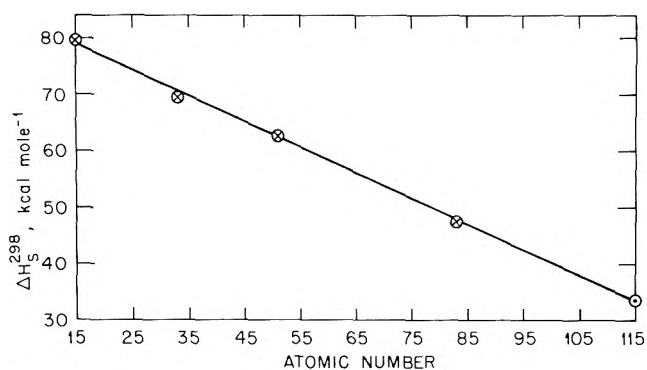


Figure 2. Heat sublimation of element 115.

lent, so we can use the plot of r_{max} with confidence as a guide in extrapolating to the value of 2.0 Å for the atomic radius of 115. This value is the same as our calculated values of $\langle r \rangle$.

In Table IV the computed values of $\langle r \rangle$ and r_{max} are given for the +1 and +2 or +3 ions of thallium, lead, bismuth, polonium, 113, and 115. Empirical ionic radii from Shannon and Prewitt¹² are given in the last column for the known ions. By comparison of the calculated radii with the elements whose radii are known, we estimate the radii of Bi⁺, Po²⁺, 113⁺, 113³⁺, 115⁺, and 115³⁺. The ionic radius of 115⁺ as derived in this way (1.5 Å) is found to be close to that of Tl⁺ and Bi⁺. The ionic radius of 115³⁺ (1.0 Å) is found to be close to that of Bi³⁺, but somewhat larger than Tl³⁺.

Heat of Sublimation

The heat of sublimation, ΔH_s^{298} , was obtained by extrapolation of the values¹³ for P, As, Sb, and Bi vs. atomic number, Z . As shown in Figure 2, ΔH_s^{298} for 115 is 34 kcal (g-atom)⁻¹. David¹⁴ extrapolated $\log \Delta H_s^{298}$ vs. $\log Z$ to obtain 35 kcal (g-atom)⁻¹. These simple extrapolations^{6,14} also yield 34 kcal (g-atom)⁻¹ for the ΔH_s^{298} of element 113. Since 115 and 113 are close together in the periodic system and both have a single 7p electron outside of closed shells, it is not surprising that their heats of sublimation would be similar. The higher first ionization potential of element 113 (Tables I and II) and its possibly smaller atomic radius might indicate that it would have a higher heat of sublimation than 115. The results obtained by extrapolation indicate a higher polarizability of 115 than 113 to counteract

TABLE IV: Radii of Ions of Tl, Pb, Bi, Po, 113, and 115 (Å)

Z	Ion	rel HFS (calcd)		Ionic radius ^a
		$\langle r \rangle$	r_{\max}	
81	Tl ⁺	1.23	1.11	1.50
	Tl ³⁺	0.69	0.60	0.88
82	Pb ⁺	1.43	1.18	
	Pb ²⁺	1.12	0.99	1.18
83	Bi ⁺	1.33	1.19	(1.5)
	Bi ³⁺	1.04	0.97	1.02
84	Po ⁺	1.41	1.18	
	Po ²⁺	1.18	1.03	(1.2)
113	113 ⁺	1.16	1.05	(1.4)
	113 ³⁺	0.82	0.72	(1.0)
115	115 ⁺	1.25	1.12	(1.5)
	115 ³⁺	1.01	0.95	(1.0)

^a Estimated values in parentheses. Empirical values from ref 12.

the ionization energy and possible radius differences. The rather high promotion energy of 7.4 eV from the 7s²7p ground state of element 113 to the 7s7p² trigonally hybridized valence state is an indication of a low polarizability compared to element 115 whose promotion energy from the 7p²_{1/2}7p_{3/2} state to the 7p_{1/2}7p²_{3/2} state is calculated to be 4.8 eV (Table V where 115 is included under group III-a for tabular convenience).

The melting point and boiling point of 115 can be expected to be close to the values for 113 given in paper I of this series.⁶

Excited State Energies

For 115(V) the promotion energy to the trigonal-bipyramidal sp³d valence state is needed. The promotion energies for the group V-a elements from the s²p³ ground state to the sp³d valence state are therefore also given in Table V. The rather high promotion energy for 115(V) of 18.4 eV compared to the value for Bi(V) of 15.5 eV indicates that the group valence will be even less important for eka-bismuth than for bismuth.

The Nature of the 115⁺ Ion

We expect that the chemistry of 115⁺ will be found more analogous to Tl⁺ than any other ion in the periodic system. This prediction is based on the values we have obtained for its ionization energy, ionic radius, and polarizability. The background for these conclusions follows.

The ground-state electronic configuration of element 115 is 7s²_{1/2}7p²_{1/2}7p_{3/2}. The presence of the 7p²_{1/2}7p_{3/2} ground-state configuration of 115 invites comparison to the s²p ground state of the group III-a elements. This is true because the 7p_{1/2} orbital is spherically symmetric (Figure 3) in the relativistic limit and is therefore rather like an s orbital. Most particularly, the 7p²_{1/2} shell is closed analogous to an s² closed shell. Thus the 7p_{3/2} electron is the first electron added outside closed shells and as a result its ionization energy is rather low (5.2 eV). The situation with respect to ionization energy is found to be similar to Tl which has a 6p_{1/2} electron outside of closed shells and has a first ionization energy of 6.1 eV.

A second important determining factor in the chemistry of 115⁺ will be its ionic radius compared to its atomic radius. A large decrease in radius indicates stabilization for the oxidation state involved. This stabilization is due to the accompanying increase in solvation or lattice energy. The decrease in radius on ionizing the 7p_{3/2} electron to form 115⁺

TABLE V: Promotion Energies^a

	ΔE , eV
I Group III-a (s ² p → sp ²)	
Ga	6.4
In	5.5
Tl	6.3
113	7.4
115 (7p ² _{1/2} 7p _{3/2} → 7p _{1/2} 7p ² _{3/2})	4.8
II Group V-a (s ² p ³ → sp ³ d)	
P	15.8
As	16.4
Sb	14.2
Bi	15.5
115	18.4
III Tl ⁺ (6s ² _{1/2} → 6s _{1/2} 6p _{1/2})	7.0
Bi ⁺ (6s ² _{1/2} 6p ² _{1/2} → 6s ² _{1/2} 6p _{1/2} 6p _{3/2})	2.2
Po ²⁺ (6s ² _{1/2} 6p ² _{1/2} → 6s ² _{1/2} 6p _{1/2} 6p _{3/2})	3.1
113 ⁺ (7s ² _{1/2} → 7s _{1/2} 7p _{1/2})	6.9
115 ⁺ (7s ² _{1/2} 7p ² _{1/2} → 7s ² _{1/2} 7p _{1/2} 7p _{3/2})	5.6

^a Differences of total energies by rel HFS.

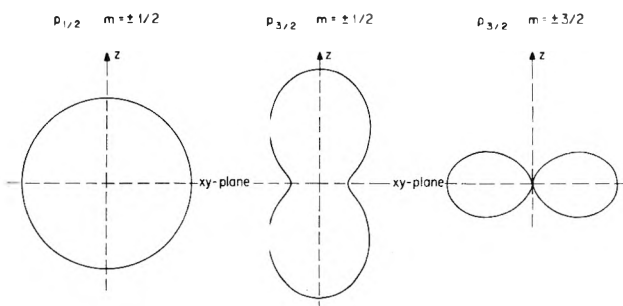


Figure 3. Angular distributions of relativistic p orbitals.

with a 7p²_{1/2} outer shell is 0.5 Å, quite comparable to the change of 0.4 Å in going from Tl to Tl⁺. In the case of Bi⁺ the decrease is only about 0.1 Å. This small decrease in radius coupled with the higher first ionization energy of 7.3 eV explains why Bi⁺ is not found in aqueous solutions (although it is found in molten salt media¹⁶). Tl⁺ is, of course, stable in aqueous solutions. At bismuth the relativistic effects have not become large enough to allow the two electrons in the 6p_{1/2} orbital to form a strongly closed shell. For this reason, 115⁺ is found to be more analogous to Tl⁺ than to Bi⁺ in its ionization potential and ionic radius.

There is, however, a further question about 115⁺, and this concerns how strong a “b” metal character it will have.¹⁵ Tl⁺ is intermediate in its behavior between Cu⁺, Ag⁺, and Au⁺ and the alkali metals.¹⁷ In analogy to the “b” cations, Tl⁺ forms an insoluble chloride, bromide, iodide, sulfate, and sulfide. On the other hand, Tl⁺ resembles the alkali metals in forming a soluble cyanide, hydroxide, carbonate, and oxalate. In contrast to Cu⁺, Ag⁺, and Au⁺, Tl⁺ forms only weak complexes with anions such as Cl⁻, Br⁻, and I⁻. It is for this reason, for example, that TlCl is not made more soluble¹⁸ by excess HCl whereas AgCl dissolves.

Dunitz and Orgel¹⁹ found a rough correlation between d-s separation energies and the tendency of d¹⁰ ions to distort or to show covalency effects in their bonding. The d-s separation energies for the “b” type ions Cu⁺, Ag⁺, and Au⁺ are 2.7, 4.8, and 1.9 eV, respectively.⁷ Of course, their radii would be expected to have an importance as well. The Slater atomic radii¹¹ are Cu (1.35 Å), Ag (1.60 Å), and Au (1.35 Å). The energies of separation in Tl⁺, Bi⁺, and 115⁺ between the ground and first excited states are given in

TABLE VI: Standard Electrode Potential for the 115⁺|115 Couple^{a,b}

ΔH_s^{298}	Ionization energy	$\Delta H_{\text{hyd}}(115^+(\text{aq}))$	$\bar{S}^\circ_{115^+(\text{aq})}$	$\bar{S}^\circ_{115(\text{s})}$	$-T\Delta S$	E°
1.5	5.2	-3.22	13.4×10^{-4}	6.9×10^{-4}	+0.4	-1.5

^a All quantities in appropriate units with energies in eV. ^b $0.5S^\circ_{\text{H}_2(\text{g})} = 6.8 \times 10^{-4} \text{ deg}^{-1}$. ΔH for reaction $0.5\text{H}_2(\text{g}) \rightarrow \text{H}^+(\text{aq}) + \text{e}^-$ is taken as 4.6 eV.

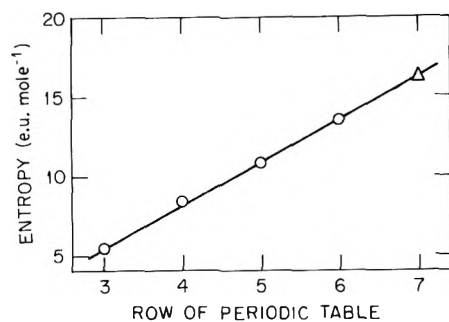


Figure 4. Entropy of elemental 115 (298°K).

Table V (where the values of Po^{2+} and 113^+ are also given for comparison). The calculated energies are Tl^+ (7.0 eV), Bi^+ (2.2 eV), and 115^+ (5.6 eV). 115^+ is thus seen to be intermediate between Tl^+ and Ag^+ in its promotion energy, but the much larger atomic radius of 115 (2.0 Å) will weaken covalent bonding effects in 115^+ as it does in Tl^+ (atomic radius = 1.90 Å).

Also the large ionic radius of 115^+ of 1.5 Å (Table IV) is similar to that of Tl^+ (1.5 Å), so the polarizing power of 115^+ on anions is expected to be weak as well.

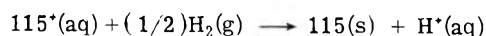
The conclusion we reach then is that the ionic picture of bonding is applicable to 115^+ to a degree that is similar to that found for Tl^+ .

Smith and Davis²⁰ have already pointed out expected relationships between Bi^+ and 115^+ with emphasis on spectroscopic and polycationic features.

Standard Electrode Potential of the 115⁺|115 Couple

For the cations of an ionic nature it is found that a calculation based on the Born-Haber cycle yields a reasonably quantitative value for the standard electrode potential.¹⁷ In paper I of this series,⁶ it was found that the Born-Haber cycle approach plus the inclusion of the entropy term gave quantitative agreement for the $\text{Tl}^+|\text{Tl}$ couple. We therefore expect a similar calculation to be helpful in interpreting the chemistry of 115^+ .

Electrode potentials are usually related to the standard $\text{H}^+(\text{aq})|\frac{1}{2}\text{H}_2(\text{g})$ couple whose potential is set equal to zero. We therefore consider the change in state for reduction of the aqueous metallic cation, $115^+(\text{aq})$, to the metal, $115(\text{s})$



The change in Gibbs free energy for this one electron reaction is related to the reduction potential and to the enthalpy and entropy by the equation

$$\Delta G = -E^\circ = \Delta H - T\Delta S \text{ (units in eV)}$$

The enthalpy change can be obtained using the Born-Haber cycle.⁶ The entropy change requires obtaining the elemental entropy of 115 metal by extrapolation as shown in Figure 4. The entropy of the aqueous metal ion can be calculated using the equation of Powell and Latimer.^{6,21} The results are given in Table VI. The $115^+|115$ couple is found to have the standard electrode potential -1.5 V com-

pared to the $\text{Tl}^+|\text{Tl}$ couple of -0.34 V and the $113^+|113$ couple of +0.6 V. (Please note that in paper I the so-called "american convention" on sign was used so that the couple referred to an oxidation potential.)

The Chemistry of the 115⁺ Ion

The 115^+ ion emerges as being more like the Tl^+ ion than any other species. It may even be still more ionic in its nature since the $115^+|115$ couple is calculated to be more negative, although this calculation cannot be taken too literally. Nonetheless, as for Tl^+ , the complexing ability of 115^+ can be expected to be low with such anions as the halides, cyanide, and ammonia. Hydrolysis should not be a problem for 115 in the oxidation state of I, and the hydroxide, carbonate, oxalate, and fluoride should be soluble. The sulfide should be insoluble and the chloride, bromide, iodide, and thiocyanate only slightly soluble. Excess HCl will not affect the solubility of $(115)\text{Cl}$ appreciably, for example. 115^+ should be more similar to Tl^+ in this respect than to Ag^+ .

The Chemistry of 115³⁺

The other possible oxidation state of element 115 is +3. We have not found it possible to predict the relative stabilities of the +1 and +3 states. In fact, their relative stabilities may well depend strongly on the state of complexation or hydrolytic conditions. As one might expect from simple extrapolation in the periodic table, we shall find that 115^{3+} is analogous to Bi^{3+} .

The sum of the first three ionization energies of Bi is 49.53 eV, of Tl^{3+} 56.3 eV, and of 115^{3+} (51 eV) (Table I). The ionization energy of 115^{3+} is therefore close to Bi^{3+} , but quite a bit below Tl^{3+} . Furthermore, the ionic radius of 115^{3+} is found to be close to that of Bi^{3+} (1.0 Å) but somewhat larger than that of Tl^{3+} (0.88 Å) (Table IV). On this basis 115^{3+} would be predicted to be more similar to Bi^{3+} than to Tl^{3+} . However the differences between the chemistry of Bi^{3+} and Tl^{3+} are more of degree than of kind, Bi^{3+} being a relatively weak "b" cation whereas Tl^{3+} is "super b."

In the first aqueous chemical studies of 115^{3+} hydrolysis should be avoided in order to obtain the more regular behavior usually associated with complex ion chemistry. In this connection, it should be remembered that mostly only the anions of strong acids are able to compete with hydrolysis in Bi^{3+} and Tl^{3+} aqueous chemistry. In their studies, Graner and Sillen²² found that 0.05 M Bi^{3+} hydrolyzes below an acidity of 0.5 M in 3 M perchlorate. Ahrlund and Grenthe²³ worked at an acidity of 1 M in their studies of the chloride, bromide, and iodide complexes of bismuth. They still found BiOCl and BiOBr precipitating in the absence of extra halide. Tl^{3+} behaves similarly except that its complexation powers are stronger. Ahrlund and Johansson²⁴ studied the chloride and bromide complexes of Tl^{3+} at an acidity of 3 M. Woods, Gallagher, Hugus and King²⁵ worked at an acidity of 0.5 and 3 M in their determinations of the association of Cl^- with Tl^{3+} . A helpful study has been done on this whole question by Biedermann and

Spiro.²⁶ These various studies suggest that the first ion-exchange or solvent-extraction studies of 115^{3+} should be tried at a concentration of around 3 M of a complexing acid such as HCl and/or a suitably high concentration of a relatively strongly complexing anion such as Cl^- .

In the general chemistry of 115^{3+} we expect a behavior similar to Bi^{3+} . The trichloride, tribromide, and triiodide of 115^{3+} will probably be soluble, and they may show a tendency to hydrolyze to form salts analogous to BiOCl and BiOBr . The trifluoride should be insoluble like BiF_3 . Bismuth shows slight amphoteric character and thallium shows essentially none; so 115^{3+} is not expected to be amphoteric to any degree. Like Tl_2S_3 and Bi_2S_3 , $(115)_2\text{S}_3$ will be insoluble. The sulfate and nitrate will be soluble in the respective acids and the phosphate will be insoluble.

Acknowledgment. We gratefully acknowledge the continued interest and encouragement furnished by Glenn T. Seaborg to all of us working in the field of superheavy elements. We are particularly indebted to G. Pedro Smith for most illuminating discussions.

References and Notes

- (1) (a) Research sponsored by the U. S. Atomic Energy Commission under contract with the Union Carbide Corporation. (b) Address correspondence to this author at Oak Ridge National Laboratory, Oak Ridge, Tenn. 37830.
- (2) Yu. Ts. Oganessian, "Synthesis of Superheavy Elements," Proceedings of International Conference on Nuclear Physics, Munich, Aug 27-Sept 1, 1973.
- (3) W. J. Swiatecki and C. F. Tsang, Nuclear Chemistry Annual Report No. LBL-666, Lawrence Berkeley Laboratory, 1971.
- (4) O. R. Frisch and John A. Wheeler, *Phys. Today*, **20**(7), 43 (1967).
- (5) B. Fricke and J. T. Waber, *Actinides Rev.*, **1**, 433 (1971).
- (6) O. L. Keller, J. L. Burnett, T. A. Carlson, and C. W. Nesstor, Jr., *J. Phys. Chem.*, **74**, 1127 (1970).
- (7) O. L. Keller, Jr., C. W. Nesstor, Jr., T. A. Carlson, and B. Fricke, *J. Phys. Chem.*, **77**, 1806 (1973).
- (8) J. P. Desclaux, private communication.
- (9) L. Pauling, *J. Phys. Chem.*, **58**, 662 (1954).
- (10) R. S. Drago, *J. Phys. Chem.*, **62**, 353 (1958).
- (11) J. C. Slater, Quantum Theory of Molecules and Solids, Vol. 2, McGraw-Hill, New York, N. Y., 1965.
- (12) R. D. Shannon and C. T. Prewitt, *Acta Crystallogr., Sect. B*, **25**, 925 (1969).
- (13) D. R. Stull and G. C. Sinke, "Thermodynamic Properties of the Elements," American Chemical Society, Washington, D. C., 1956.
- (14) F. David, "Prediction of the Oxidation-Reduction Properties of the Superheavy Elements 8s, 7p and 6d," Institut de Physique Nucléaire, Division de Radiochimie, RC-71-06, 1 Oct 1971.
- (15) See S. Ahrland, J. Chatt, and N. R. Davies, *Quart. Rev. Chem. Soc.*, **12**, 265 (1958), for a discussion of the a/b classification of cations. A related scheme, based on the terminology "hard" and "soft," is given by R. G. Pearson, *J. Amer. Chem. Soc.*, **85**, 3533 (1963).
- (16) N. J. Bjerrum, H. L. Davis, and G. Pedro Smith, *Inorg. Chem.*, **6**, 1603 (1967).
- (17) C. S. G. Phillips and R. J. P. Williams, "Inorganic Chemistry," Oxford University Press, London, 1966, 2 volumes.
- (18) T. E. Alekseeva, N. F. Arkhipova, and V. A. Rabinovich, *Russ. J. Inorg. Chem.*, **17**, 140 (1972).
- (19) J. D. Dunitz and L. E. Orgel, *Advan. Inorg. Radiochem.*, **2**, 1 (1960).
- (20) G. P. Smith and H. L. Davis, *Inorg. Nucl. Chem. Lett.*, **9**, 991 (1973).
- (21) R. E. Powell and W. M. Latimer, *J. Chem. Phys.*, **19**, 1139 (1951).
- (22) F. Graner and L. G. Sillen, *Acta Chem. Scand.*, **1**, 631 (1947).
- (23) S. Ahrland and I. Grenthe, *Acta. Chem. Scand.*, **11**, 1111 (1957).
- (24) S. Ahrland and L. Johansson, *Acta Chem. Scand.*, **18**, 2125 (1964).
- (25) J. M. Woods, P. K. Gallagher, Z. Z. Hugus, Jr., and E. L. King, *Inorg. Chem.*, **3**, 1313 (1964).
- (26) G. Biedermann and T. G. Spiro, *Chem. Scr.*, **1**, 155 (1971).

Aerodynamic Drag on Bursting Bubbles

G. Frens

Philips Research Laboratories, Eindhoven, The Netherlands (Received September 10, 1973; Revised Manuscript Received June 4, 1974)

Publication costs assisted by Philips Research Laboratories

It is shown how aerodynamic drag affects the bursting rate of thin liquid films. Drag coefficients for low Reynolds number ($1 < \text{Re} < 100$) are obtained from experiments with bursting soap films and compared with literature data. Bursting experiments with the very thin ($\delta < 10$ nm) equilibrium soap films of the common and of the Newton types are discussed. It is found that the differences in bursting rate between films of the two types cannot be interpreted as drag effects alone. This points to different structural properties of the common and of the Newton films.

Introduction

The rate of expansion of a hole in a thin liquid film depends on the mass and on the surface tension of the film. In theory it is given by "Culick's velocity"¹

$$U = (2\sigma/\rho\delta)^{1/2} \quad (1)$$

where σ is the surface tension, ρ the density, and δ the thickness of the film. In the derivation of eq 1 the effects of aerodynamic drag are neglected, as are also those of changes in surface tension of the film near the hole, which may originate in the bursting process.

Such a lowering of the surface tension near the hole occurs when the surfaces of the film are covered with surfactant monolayers—as in soap films.²⁻⁷ Frankel and Mysels³ have treated this case—always neglecting drag effects. They showed that eq 1 gives the maximum velocity of the hole. Surface tension variations give rise to a small retardation of the perimeter of the hole and to the formation of an aureole. The aureole is a region of thickening film which expands in front of the hole.

The shape of the aureole depends on the relation between the surface tension and the area per molecule or surfactant in the monolayer. From an analysis of aureole pro-

files one can in principle obtain the equation of state for the supersaturated monolayer near the hole.^{4,6}

The experiments with bursting soap films have consistently shown that there is a difference between the real velocity V of the rim of the hole and the theoretical value U . The difference is a small constant percentage for relatively thick films ($\delta > 200$ nm) but increases considerably ($V < U$) as the films become thinner. This observation, in combination with the theory for the aureole, has led to the speculation that the surface properties of the films are influenced by the film thickness.²

When it was found that the difference between U and V depends on the composition of the atmosphere around the film,^{4,5} it became clear that the discrepancy between theory and experiment should, at least partly, be ascribed to aerodynamic drag. The drag effect has to be included in the theory before the surface properties of very thin films can be obtained from bursting data. Mysels and Vijayendran⁵ have done the relevant experiments, but their interpretation of the data seems dubious. Below we will first develop an aerodynamic model for the bursting process. The model will be compared with the experimental results and the implications for the surface properties of different types of soap films will be discussed.

Theory

Figure 1 depicts a model for a bursting liquid film. It is a perpendicular cross section through a flat film with a circular hole in it. The hole is expanding; the material which formerly filled the hole is now present in a toroidal rim between the hole and the yet undisturbed film. No force from the hole counteracts the surface tension of the film. This keeps the hole growing, and as it grows the rim consumes the film. In this model the force F on the rim is equal to 2σ , and $d(mV)/dt = V^2\rho\delta$, with m as the mass per unit length of the rim. Conservation of momentum and neglecting drag forces lead then directly³ to eq 1 with the rim velocity $V = U$.

In the same model we can incorporate the aerodynamic drag by writing

$$F - D = \frac{d}{dt}(mV) \quad (2)$$

The drag force D is given by

$$D = (1/2)C_D dS V^2 \quad (3)$$

d is the density of the atmosphere. S is the projected area of the rim perpendicular to the direction of the motion. Per unit length it is equal to the rim diameter. The drag coefficient C_D depends on the shape of the moving object (sphere, cylinder, etc.) and on the Reynolds number Re . The radius of the hole is much larger than the other rim dimensions, so that the rim can locally be described as a cylinder.

From these equations one obtains

$$V = \left(\frac{2\sigma}{\rho\delta + (1/2)C_D dS} \right)^{1/2} \quad (4)$$

analogous with the derivation of eq 1, but with drag effects included.

With eq 4 it is possible to compute the rim velocity V for different films, atmospheres, hole sizes, etc., provided that C_D is known. However, C_D depends on Re , and there are not many literature data for C_D of cylinders at a low Re . The relation between C_D and Re can be determined direct-

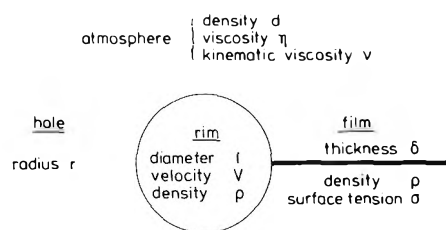


Figure 1. Model of a bursting soap film of thickness δ and surface tension σ . A rim (diameter l and density ρ) moves with a velocity V in an atmosphere with a viscosity η and a density d .

ly from bursting experiments by fitting computed curves for V with experimental data for thick films, bursting in different atmospheres. We will describe this procedure below.

There are some useful approximations for small drag, *i.e.*, when the films are not very thin. Eliminating $\rho\delta$ between (1) and (4) one obtains

$$V = U(1 + KU^2)^{-1/2} \approx U(1 - (1/2)KU^2) \quad (5)$$

where $KU^2 = \frac{1}{2}C_D dS(\rho\delta)^{-1}$. Now consider the Reynolds number $Re = Vld\eta^{-1}$ for films of different δ which burst in the same atmosphere. η is the viscosity of the atmosphere, ηd^{-1} is called the kinematic viscosity ν . For small drag V is almost proportional with $\delta^{-1/2}$. But the rim diameter l is of course proportional with $\delta^{1/2}$. For holes of equal size in not too thin films Re is therefore independent of the film thickness and depends only on such bulk properties as the kinematic viscosity of the surrounding atmosphere. The drag coefficient C_D is constant for a given Reynolds number. It is therefore also constant for thick films of different δ in the same atmosphere.

For films of equal δ in different atmospheres the differences in Re and C_D are due to differences in ν . For two atmospheres with equal ν (*e.g.*, H_2 and He) the C_D 's are equal again, and differences between the rim velocities which are caused by drag are then proportional with the density d of the atmospheres.

Aureoles

Frankel and Mysels³ derived that Culick's velocity U is the maximum velocity of the rim. They found that the rim velocity at zero drag is smaller, if only slightly, when the rim is preceded by an aureole. They also showed that as long as the surface properties of the film remain unchanged—but always neglecting drag—the retardation due to the aureole is a constant fraction of U and independent of δ . This conclusion is corroborated by the experiment. In very thick films, where drag is relatively unimportant, the rim velocity is slightly smaller than but very near U and almost independent of the properties of the surrounding atmosphere.⁴⁻⁶

The geometry of a rim with an aureole in front of it would seem to complicate the aerodynamic situation considerably. But the aureole is very thin and the average velocity of the aureole surface relative to the surrounding atmosphere is only a few per cent of that of the much thicker rim. In our model we will therefore neglect the drag on the aureole and describe the effects of the atmosphere in terms of drag on the toroidal rim alone.

The diameter l of a rim which is preceded by an aureole is smaller than that of the rim of a hole of equal size, in a film of equal thickness, but without an aureole. From the

data of ref 6 it follows that the rim contains approximately one-third of the hole material, so that the effect of the aureoles in these soap films is a reduction of the rim diameter to half its original value. We have used this value in the calculation of the drag on the rim in the soap films described in ref 5 and 6. One might prefer a description of the drag on the rim and its aureole in terms of a rim with an "effective" diameter. Then, using literature data for the relation between C_D and Re it would be possible to determine this effective diameter from the experiments by using eq 4. With this procedure one finds that the effective diameter is approximately 0.5 times the diameter of a rim without an aureole. This value is so close to the actual diameter of a rim with an aureole that it can be considered experimental proof for the validity of neglecting the drag on the aureole altogether.

But in principle it is only for simplification that we neglect the aureole. This assumption is not critical for the line of reasoning in this paper, and a model with an effective diameter is equally valid.

Experimental Data

Several authors³⁻⁸ have determined bursting rates, and we refer to their original publications for experimental details. The "two-hole method"⁶ is considered the best way of measuring velocities in bursting films. It has been used^{4,5} for experiments in atmospheres other than air. In the experiments of ref 4-6 the radius of the hole R was always approximately 1 cm. This radius enters into our theory through the rim diameter, but only as $R^{1/2}$, and in the experiments we have found no effect of R over the small range of R available.

Throughout this paper we have plotted rim velocities V as a function of Culick's velocity U instead of the film thickness. This method of representation was introduced⁵ as a means for comparing results with films of different compositions and thus with different surface tensions.

Although the data in Figure 2 are plotted in this way, they relate to films of one composition (*i.e.*, solution 1 of ref 6) but with different thicknesses and bursting in air. These data were obtained in the course of the work for ref 6 but they were not published there. For $\delta \approx 800$ nm (a thick film on which the drag is small) the rim moved with a velocity $V \approx U \approx 10^3$ cm sec⁻¹. For the rim of these thick films bursting in air this corresponds to a Reynolds number $Re = 23$.

The experimental points for atmospheres other than air (Figure 4) are taken from ref 5. We consider these the best available experimental data for films bursting in other atmospheres.

Results and Discussion

A small object has a small Reynolds number, even if it moves at a fairly high speed. Such is the case in bursting soap films where $1 < Re < 100$ despite velocities of the order of 10^3 cm sec⁻¹. As a test of our model we have compared the drag coefficients which follow from soap film experiments with literature data obtained on slowly moving cylinders of much larger size.

The drag coefficient C_D is constant as long as Re is constant. Such is the case for films bursting in the same atmosphere, as long as the drag is relatively small—*i.e.*, for thick films. With eq 4 one can compute how the rim velocity V is affected by air drag for different assumed values of C_D and different film thicknesses. Comparing the computed curves with experimental data one can then determine the real C_D

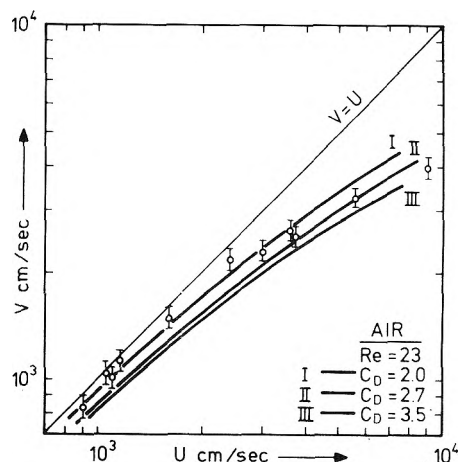


Figure 2. Rim velocity in air as a function U : top line, Culick's velocity for zero drag; lines I-III, computed curves for different values of C_D and a radius of the hole of 1 cm.

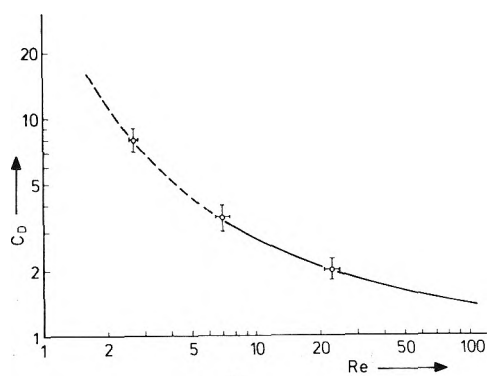


Figure 3. Drag coefficient C_D as a function of the Reynolds number: dashed line, values extrapolating from data at higher Re .⁹

as the C_D value which gives the best fit with experimental results for fairly thick films. This procedure is illustrated by Figure 2. In these experiments it appears that $C_D = 2.0$ for $Re = 23$.

Drag effects increase from H_2 to He to air to Ne when films of equal thickness burst in the different atmospheres.^{4,5} The kinematic viscosities of these atmospheres are $\nu = 1.1, 1.1, 0.15,$ and 0.38 , respectively, and Reynolds numbers for thick films are 2.7, 2.7, 23, and 7, respectively. In the way described above we have determined C_D values at these Reynolds numbers. $C_D = 8.0, 8.0, 2.0,$ and 3.5 are the "best" values for the drag coefficient of cylinders at these respective Re values, as obtained from experiments with bursting bubbles. In Figure 3 these are compared with literature data.⁹ The quantitative fit between the results from completely different experiments can be considered experimental proof for our model where drag on the aureole is neglected relative to drag on the rim.

On this basis we can then undertake the interpretation of experimental data concerning the drag on not so thick films bursting in different atmospheres. The experimental points of Figure 4 are mostly from experiments with very thin films, where large drag effects are expected. We will first compare these data with the "thick-film approximation" which is obtained when Re and C_D are given the (constant) values obtained with thick films. In Figure 4 this leads to the drawn lines. Theory and experiment fit fairly well together, but the experimental points deviate from the

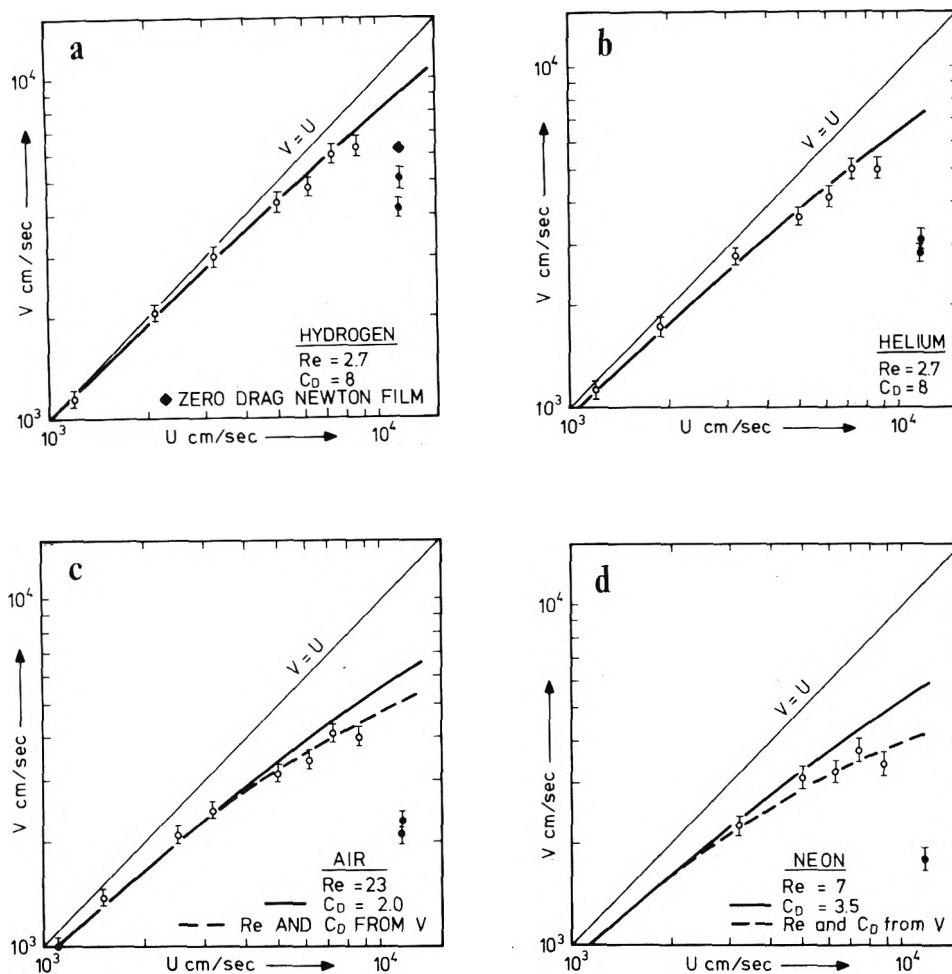


Figure 4. Rim velocity for equilibrium films of different thicknesses in different atmospheres.

approximate theory when the drag effects are large (*i.e.*, for thin films and for heavy atmospheres).

This deviation between the experimental data and the theoretical curve is solely due to the change of Re with δ which cannot be neglected for these thin films. For air and for Ne atmospheres where the deviations are largest we have computed the relation between V and U when C_D is no longer constant. Instead we have used $C_D = f(Re)$ as given by Figure 3. This leads to a complete fit between the theory and the experimental results, shown by the dotted lines in Figure 4c and 4d.

We note that this agreement on the basis of Figure 3 is not a trivial result. Figure 3 was obtained by comparing films in different atmospheres and in the limit of small drag. In Figures 4c and 4d this result is used to compute the behavior of thin films of different thicknesses, but all in one atmosphere, under conditions with relatively large drag effects. That complete agreement between theory and experiment is the result gives proof of the internal consistency of the aerodynamic analysis. There appears to be no effect of the film thickness on the surface properties of these films. All retardation is due to drag.

Another prediction of the theory is also borne out by the experimental data. The retardation Δ of the rim should be proportional to the density of the atmosphere when films have the same thickness and the surrounding atmospheres have equal kinematic viscosities. For H_2 and He atmospheres these conditions are fulfilled when U is equal, and

indeed $\Delta_{He} = 2.2\Delta_{H_2}$ with $d_{He} = 0.180$ and $d_{H_2} = 0.083$ g l.⁻¹

Newton Films

Newton films are a special kind of soap films, which are obtained when soap films with a high electrolyte content drain to equilibrium due to capillary suction and gravity. Newton films are thinner than the equilibrium films resulting from drainage of soap films of a lower salt concentration. There is some evidence^{10,11} that a Newton film is not simply a very thin soap film but that it is a separate structure, different in its properties from a common soap film. In a bursting Newton film it is found that the hole is not smoothly circular but that it has a scalloped appearance.²

In their study of bursting films Mysels and Vijayendran have disregarded the physical differences between a Newton film and a common soap film. Including data for Newton films in their analysis they postulated that one mechanism is responsible for the retardation of the rim in both types of film. The rim velocity in a Newton film is only half the velocity of the rim of the hole in the thicker common equilibrium film when the two films burst in the same atmosphere. Instead of attempting to invent an explanation for this observation they assumed that it had to be due to atmospheric drag and then determined a "purely empirical" relationship for the difference between U and V . This was done by fitting a curve through the experimental data, and these included the data on Newton films.

The outcome of this procedure is shown in their Figure 3, but close inspection shows that the agreement between a fitted curve and the experimental points belonging to it is bad, except for the thinnest (Newton) and the thickest films. It is easily seen that this bias on the extremes is due to the curve-fitting procedure which is illustrated by their Figure 4. Had they fitted their curves in a correct, nonlogarithmic, way and only through the experimental points for one (the common) type of film, then they would have obtained an empirical relation for U and V which closely confirms the predictions of the aerodynamic theory (cf our Figure 4). But in that case they would have found that the experimental bursting rate of a Newton film is much lower than the extrapolated value of V for a common soap film of comparable thickness and surface tension.

The bursting Newton film is indeed affected by aerodynamic drag, for V differs in different atmospheres. From data for different atmospheres it is easy to calculate the rim velocity of a Newton film at zero drag (Figure 4a). This calculated rim velocity is considerably smaller than Culick's velocity U , which is always given by eq 1. From the difference between U and the bursting rate at zero drag it must be concluded that some effect other than drag is responsible for the slow speed of the rim in a bursting Newton film.

Rim velocities smaller than U are known from experiments on the bursting of films with rigid surfaces.² It is therefore tempting to relate the observations on the Newton films, with their peculiar bilayer structure, to those on rigid films. The wide aureoles which are characteristic for Newton films are not just extensively dragged out aureoles

which may be compared to those of thicker films. Their width represents a genuine difference in the surface tension-surface area relationship (*i.e.*, surface elasticity) between Newton type and common soap films. According to ref 3 this would result in different values for V —even without drag—and all of them would be smaller than U . But it seems also possible that the retardation of the rim in Newton films and in rigid films has a kinetic origin and that the transformation of the two-dimensional structure in the surface into three-dimensional rim material is the rate-determining process.

Acknowledgment. This paper originates from a difference of opinion between Dr. K. J. Mysels and the author concerning the interpretation of the experiments described in ref 5. The author thanks Drs. Mysels and Vijayendran for making their data available prior to publication and also for the friendly if highly critical discussion concerning the manuscripts of the papers.

References and Notes

- (1) R. E. G. Culick, *J. Appl. Phys.*, **31**, 1128 (1960).
- (2) W. R. Mc Entee and K. J. Mysels, *J. Phys. Chem.*, **73**, 3018 (1969).
- (3) S. P. Frankel and K. J. Mysels, *J. Phys. Chem.*, **73**, 3028 (1969).
- (4) G. Frens, K. J. Mysels, and B. R. Vijayendran *Spec. Discuss. Faraday Soc.*, **1**, 12 (1970).
- (5) K. J. Mysels and B. R. Vijayendran, *J. Phys. Chem.*, **77**, 1692 (1973).
- (6) A. T. Florence and G. Frens, *J. Phys. Chem.*, **76**, 3024 (1972).
- (7) I. Liebman and H. E. Perlee, *Science*, **616**, 373 (1968).
- (8) W. E. Ranz, *J. Appl. Phys.*, **30**, 1950 (1959).
- (9) L. Rosenhead, Ed., "Laminar Boundary Layers," Clarendon Press, Oxford, 1963, p 106.
- (10) D. den Engelsens and G. Frens, *J. Chem. Soc., Faraday Trans. 1*, **70**, 237 (1974).
- (11) J. A. de Feyter Thesis, Utrecht, 1973.

Fluorescence Quenching of the Indole Ring System by Lanthanide Ions

Robert W. Ricci* and Kurt B. Kilichowski

Department of Chemistry, College of the Holy Cross, Worcester, Massachusetts 01610 (Received March 11, 1974)

A 100-fold difference in efficiency was found among the lanthanides in their ability to quench indole fluorescence in aqueous solution. The order of quenching efficiency was $\text{Eu(III)} > \text{Yb(III)} > \text{Sm(III)} > \text{Tb(III)} > \text{Gd(III)} > \text{Ho(III)} \approx \text{Dy(III)}$. The quenching appears to be predominately dynamic in nature judged from the facts that (a) the quenching rate decreased with increasing solution viscosity and (b) the lanthanides continued to quench indole fluorescence even after being strongly complexed with EDTA. The quenching abilities of the lanthanides parallel their polarographic reduction potentials as well as their ability to capture solvated electrons in aqueous solution. These correlations suggest that quenching is occurring through a mechanism involving electron transfer from the excited indole ring to the lanthanide.

Introduction

There is much interest in the use of lanthanide ions as spectroscopic probes of biomolecules. For example, Luk¹ has studied the effect of lanthanide ions on the fluorescent properties of the metal-binding protein transferrin while others have employed the lanthanides as perturbative agents in absorption² and nmr³ spectroscopy of proteins.

Lamola and Eisinger⁴ recently reported that Eu(III) and Tb(III) quench the fluorescence of the amino acid tryptophan at rates approaching a diffusion-controlled limit but did not postulate a mechanism to account for the effect. In addition to the lanthanide ions, several studies have appeared upon the general phenomenon of fluorescence quenching of biomolecules by many cations and anions. Mercury ion quenching of the indole ring system has been

reported by Chen.⁵ The quenching in this case appears to be due to ground-state complexation. Steiner and Kirby⁶ reported on many anion and cation quenchers of the indole fluorophore and suggested that the process was taking place at least partly *via* electron transfer from the electronically excited indole ring to the quencher. In addition, iodide,⁷ nitrate,⁸ hydrogen, and hydroxide ions⁹ all appear to quench the indole fluorophore but the mechanism, in most cases, has not been proven. The riboflavin system has also been found to be readily quenched by transition metal ions although in this case the quenching appears to be occurring by more than one mechanism.¹⁰

In view of the sustained interest in the use of lanthanide ions as fluorescence quenchers and as probes in fluorescence spectroscopy, we undertook a study into the nature of the fluorescence quenching of the biologically important indole ring system by lanthanides.

In the absence of ground-state complexation, fluorescence quenching of biomolecules normally requires collisional interaction; such quenching obeys the Stern–Volmer relationship

$$(Q_f^0/Q_f - 1) = k_q \tau [Q] \quad (1)$$

where Q_f^0 and Q_f represent respectively the fluorescence yield in the absence of quencher and in the presence of the quencher at concentration $[Q]$; k_q is the rate constant for quenching, and τ the measured lifetime of the fluorophore in the absence of quencher. By graphing the left hand side of eq 1 *vs.* $[Q]$ a linear plot is obtained. If τ is known, k_q can be obtained directly from the slope.

Experimental Section

a. Materials. DL-Tryptophan, *N*-acetyltryptophanamide HCl (NATA), and DL-tryptophan ethyl ester were obtained from Sigma Chemical and used without further purification. Indole (Aldrich Chemical Co.) was purified by sublimation. The lanthanides (Alfa Inorganics) were obtained as the hydrated chlorides (99.9% pure). All other materials were reagent grade.

b. Method. Fluorescence measurements were made on an instrument which employed a Bausch and Lomb high-intensity mercury light source for excitation. The monochromatized exciting light was focused into a light-tight, dual cell, thermostated sample compartment; the light emission was observed at right angles to excitation using a Beckman prism monochromator and a 1P28 photomultiplier. The tube output was amplified and displayed on a strip-chart recorder. In no case did the shape of the fluorescence envelope appear to be altered by the quencher. Under these conditions the quenching studies could be carried out by measuring the fluorescence at the wavelength of maximum intensity. The temperature of the quartz sample cells was controlled to within 0.1° by means of a hollow metal jacket through which thermostated water was circulated. Fluorescence intensity variations due to long-term fluctuations in lamp intensity were corrected with the use of a fluorescent standard while short-term fluctuations were electronically filtered.

The samples were excited at 300 nm and the fluorescence was measured in the region of 350 nm depending upon the individual fluorophore. Absorption spectra were taken on a Beckman DK-2A. Care was exercised to ensure that the exciting light was being absorbed only by the fluorophore (>98% in all cases). Reabsorption of the emitted light was negligible in all cases.

TABLE I: Quenching of Indole Fluorescence by Lanthanide Ions^a

Ion	K_{SV}, M^{-1}	$k_q \times 10^{-9}, M^{-1} \text{sec}^{-1}$	M	$k_{ec} \times 10^{-10}, M^{-1} \text{sec}^{-1}$	$-E_{1/2}^b$	Z
Eu(III)	22	4.50	7	6.1 ^c	0.67 ^b	63
Yb(III)	7.8	1.60	2	4.3 ^c	1.40 ^b	70
Sm(III)	5.2	1.06	6	2.5 ^c	1.68 ^b	62
Gd(III)	0.49	0.10	8	0.055 ^c	1.77 ^b	64
Tb(III)	0.74	0.15	7	0.037 ^c	1.79 ^b	65
Ho(III)	<0.25	<0.05	5	0.24 ^c	1.79 ^b	67
Dy(III)	<0.25	<0.05	6	0.046 ^c	1.80 ^b	66
Cu(II)		10.0 ^d	2	2.9 ^f	0.02 ^c	29
Pb(II)		3.10 ^d	1	3.9 ^f	0.40 ^c	82
Cd(II)		0.54 ^d	1	5.2 ^f	0.60 ^c	48
Mn(II)		0.38 ^d	6	0.0077 ^f	1.51 ^c	25

^a pH 5.0 aqueous solution, temperature 24°. ^b W. Noddack and A. Brull, *Angew. Chem.*, **50**, 362 (1937). ^c I. M. Kolthoff and J. J. Lingane, "Polarography," 2nd ed, Interscience, New York, N. Y., 1952. Supporting electrolyte 0.1 M KCl, except for Cu²⁺ (1 M HNO₃). ^d Reference 6. ^e Reference 16. ^f Reference 20.

c. Solutions. The concentrations of stock lanthanide solutions were determined from their uv absorption spectra and known molar extinction coefficients.¹¹ Sodium acetate–acetic acid buffer solutions were used to regulate the pH of the solutions. The buffer did not alter the fluorescent properties of the fluorophore.

Results and Discussion

Indole, in aqueous solution, has a fluorescence yield of 0.23 at 25° and a fluorescent maximum at 350 nm. The fluorescence lifetime in the absence of quencher is 4.9×10^{-9} sec.¹² Addition of lanthanide quenchers has no discernable effect on the shape of the indole fluorescence envelope.

Table I summarizes the results of indole fluorescence quenching by several lanthanide ions. The Stern–Volmer constants K_{SV} 's were obtained from eq 1. Lanthanide concentration ranged from 0 to 0.20 M. A 100-fold difference in quenching efficiencies among the lanthanides was found. Eu(III), the most efficient quencher, approached the diffusion-controlled limit of $2.5 \times 10^{10} M^{-1} \text{sec}^{-1}$ as estimated by the Smoluchowski relationship¹³

$$k_{diff} = 8.8 \times 10^{14} (D_a + D_b) \quad (2)$$

where D_a and D_b are diffusion coefficients for Eu(III) and indole as determined from the Stokes–Einstein equation

$$D = 2.2 \times 10^{13} / R \quad (3)$$

R for Eu(III) was taken as 0.950 Å¹⁴ while R for indole estimated as 4 Å. The transition metal ion quenching data obtained by Steiner and Kirby⁶ are also shown in Table I. The comparisons are not entirely valid since they employed acetyltryptophan and tryptophanamide as the fluorophore rather than indole. Nonetheless, the data can be compared in a qualitative fashion insofar as it is the indole ring which is being quenched in each case. The fluorescence quenching of six indole fluorophores by both Eu(III) and Eu(EDTA)⁻ are shown in Table II.

Several mechanisms could account for lanthanide quenching of the indole ring system fluorescence. They include ground-state complex formation in which quenching occurs by virtue of the formation of a nonfluorescent complex between indole and lanthanide. This mechanism does not require collisional interaction of lanthanide and indole during the excited lifetime of the indole since they are already coupled when excitation occurs. Dynamic mecha-

TABLE II: Fluorescence Quenching of the Indole Fluorophore by Europium (III)^a

Fluorophore	τ , nsec	$k_q \times 10^{-9}$, $M^{-1} \text{sec}^{-1}$	
		Eu(III)	EuEDTA ⁻
Indole	4.9 ^b	4.5	9.0
Indole-3-acetic acid	8.7 ^d	11.5	11.5
Tryptophan	3.3 ^b	8.0	18.0
Tryptophanamide	1.4 ^c	4.0	16.9
N-Acetyltryptophanamide	3.8 ^c	4.5	13.3

^a Aqueous solution pH 4.5 buffered with acetic acid-sodium acetate buffer (0.03 M), temperature 24°. ^b Reference 12. ^c I. Weinryb and R. Steiner, *Biochemistry*, **1**, 2488 (1968). ^d E. Kirby and R. F. Steiner, private communication.

nisms in which quenching occurs through a bimolecular interaction between quencher and fluorophore during the latter's excited lifetime include enhancement of intersystem-crossing rates by a heavy-atom effect or by interaction with unpaired electrons of the quencher and quenching following electron or proton transfer.

Conformity to the Stern-Volmer equation is not sufficient evidence for a dynamic quenching mechanism since ground-state quenching also results in a linear Stern-Volmer plot but with a slope equal to the association constant for the complex (assuming that the complex is nonfluorescent). On the other hand, ground-state complexation, unlike dynamic quenching, should result in a significant change in the uv absorption spectrum of indole. Studies revealed, however, that the uv absorption spectrum of the indole-quencher mixture was identical with the sum of an indole and quencher uv absorption spectra measured separately. Furthermore, if complex formation were occurring in the ground state to yield a fluorescent complex one would expect its fluorescence properties to be different from that of uncomplexed indole. However, no change in the shape of the fluorescence envelope was noted when quencher was added to indole.

The lanthanide ions form relatively few complexes in solution due partly to the unavailability of f orbitals to form covalent bonds and partly to the lanthanides' relatively large radii which reduce electrostatic forces of attraction.¹⁴ Complexing occurs mostly with polyfunctional organic acids and halogenated ketones. Nonetheless, since ground-state complexing of the lanthanides with proteins and metal-binding enzymes appears to be well established,^{2,3} an additional series of studies was carried out in order to establish if the fluorescence quenching of the indole ring was due to ground-state complexation under the conditions of our experiments.

Dynamic quenching approaching the diffusion-controlled limit, unlike ground-state quenching, is strongly dependent upon the viscosity of medium, and the quenching constant can be related to a simplified form of the Smoluchowski equation¹³

$$k_{dc} = 8RT/3000\eta \quad (4)$$

where R is the gas constant, T the absolute temperature of the medium, and η the viscosity. Figure 1 illustrates a test of eq 4 using NATA as fluorophore. Excellent conformity was found with Eu(III) as quenchers when the viscosity of the solvent was varied by altering the temperature between 278 and 323 °K. A comparable decrease in Eu(III) quenching rate was observed when the viscosity of a NATA solution was increased by adding glycerin. In a few cases, notably with tryptophan, a small positive deviation from eq 4

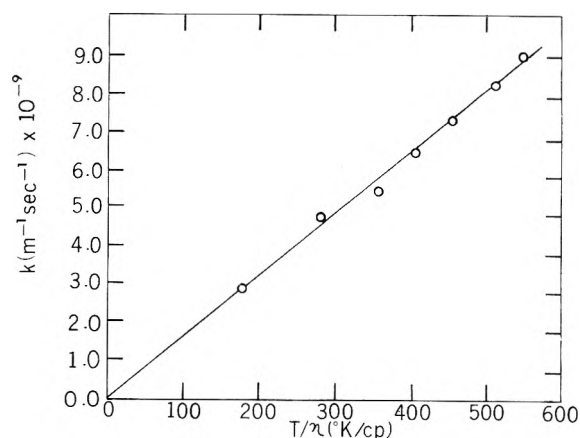


Figure 1. Eu(III) quenching of *N*-acetyltryptophanamide fluorescence as a function of temperature and viscosity.

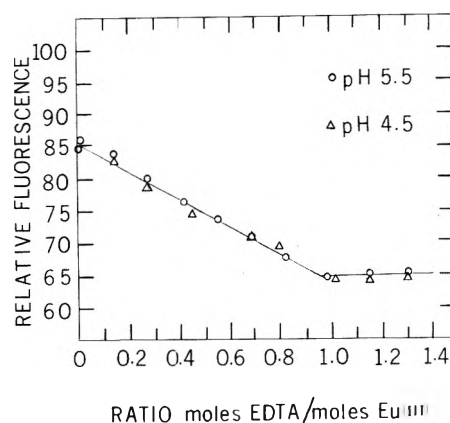


Figure 2. Effect of EDTA on Eu(III) quenching of NATA fluorescence.

was noted at higher temperature, indicating perhaps some quenching through ground-state complexing.

Indole, which lacks a localized pair of nonbonded electrons, would not be expected to form highly stable complexes with the lanthanides. Furthermore, even if it should form a weak complex with the lanthanides, it could be readily displaced by a more strongly coordinating multidentate ligand. Thus, the presence of such a firmly held ligand on the lanthanide would further ensure that quenching occurred through a dynamic mechanism. To investigate this possibility, EDTA was chosen as the chelate since it forms a very stable complex with the lanthanides while only slightly modifying their uv absorption properties. Figure 2 illustrates the effect of EDTA on the quenching efficiency of Eu(III). An aqueous solution of NATA ($Q_f^0 = 100$ units) was partially quenched ($Q_f = 85$ units) with 0.013 M Eu(III). Addition of EDTA resulted in further quenching and the decrease in fluorescence intensity continued until 1:1 molar ratio of EDTA:Eu(III) was reached after which increasing the amount of EDTA had little effect on the NATA fluorescence. From this data we infer that the complexed Eu(III) species being formed is the more efficient quencher, Eu(EDTA)⁻. The EDTA ligand alone has no quenching effect on NATA fluorescence as seen from the fact that the addition of EDTA beyond a 1:1 Eu:EDTA molar ratio resulted in no further quenching.

Studies of the effect of viscosity on the quenching ability of Eu(EDTA)⁻ showed that the quenching is also dynamic in nature. Quenching data for Eu(III) and Eu(EDTA)⁻ for

several indole compounds are summarized in Table II. One conclusion is unmistakable. $\text{Eu}(\text{EDTA})^-$ is a more efficient quencher of the indole fluorophore than $\text{Eu}(\text{III})$.

To summarize the above studies we conclude that the predominant mechanism for quenching is dynamic in nature though the possibility for small amounts of parallel quenching by ground-state complexing can not be entirely excluded.

Dynamic quenching of fluorescence by metal ions is a well-established phenomenon.¹⁵ In general, paramagnetic transition ions produce the greatest effect suggesting that one possible quenching mechanism may be paramagnetic enhancement of the intersystem crossing rates in the organic fluorophore. This does not appear to be the case with the lanthanide ions. Inspection of Table I shows no correlation between k_q and the electronic multiplicity of the ions. ($\text{Eu}(\text{III})$ and $\text{Yb}(\text{III})$, the two most efficient quenchers, differ in multiplicity by 5 units.) Similarly, $\text{Cu}(\text{II})$ has a multiplicity of 2 while the relatively poor quencher $\text{Mn}(\text{II})$ has a multiplicity of 5.

Quenching through enhancement of intersystem crossing rates through a heavy-atom effect does not appear to be an important mechanism. The lanthanides are all approximately of the same atomic number yet they still show a 100-fold difference in quenching rates. Further, $\text{Cu}(\text{II})$ and $\text{Pb}(\text{II})$ are both efficient quenchers and yet they differ in atomic number by almost a factor of 3.

While the quenching efficiencies does not appear to be related to the electronic multiplicity, the electron structure of the quencher may be a clue to the quenching mechanism. $\text{Eu}(\text{III})$ and $\text{Yb}(\text{III})$ have $4f^{13}$ and $4f^6$ electronic subshells, respectively. In each case, the addition of one electron results in a stable filled and half-filled $4f$ subshell. Also, in the case of the efficient quencher $\text{Cu}(\text{II})$ the addition of one electron results in a stable filled $3d$ subshell. These observations suggest that the quenching mechanism may involve the electron-accepting ability of the metal ion.

The polarographic reduction potential measures the electron-accepting ability of the species being reduced at an electrode surface. If fluorescence quenching is occurring through either complete or partial transfer of an electron from an excited π orbital of the indole fluorophore to the metal ion, one might expect a correlation between k_q and the polarographic reduction potential of the metal ions. An examination of Table I reveals that this does appear to be the case both with the lanthanide and the $2+$ transition ions.

Thomas, Gordon, and Hunt¹⁶ through flash photolysis techniques have measured the ability of several $3+$ lanthanide ions to capture free, solvated electrons in aqueous media. In Table I are listed the rate constants for hydrated electron capture for those ions studied. Clearly, the more efficient the lanthanide is in capturing hydrated electrons, the better it acts as a quencher of indole fluorophore emission. On the basis of these correlations, it would not be unreasonable to postulate that the lanthanide ions are quenching through a mechanism involving electron transfer from the excited indole ring to the lanthanide. Detection of a transient indole cation radical would constitute unequivocal evidence for this mechanism. Such a detection was not possible in the present study though Grossweiner

and Joschek¹⁷ have reported the detection of both solvated electrons and the indole cation during flash photolysis studies of the indole ring compounds even in the absence of quenchers.

Fluorescence quenching through electron transfer has been studied in some detail by Weller¹⁸ and Mataga.¹⁹ Weller has shown, for example, that quenching efficiency by acridine amines and perylene amines increases with decreasing ionization potential of the amine. In these cases electron transfer is from fluorophore to quencher. Two mechanisms may account for fluorescence quenching by intermolecular electron transfer. In one case the quencher and fluorophore undergo a strong interaction forming an encounter complex in which chemical interaction may be significant. In the extreme, this leads to exciplex formation of a charge-transfer nature. The exciplex may further revert to a solvated ion pair or even dissociate to form solvated ion radicals in solvents of high dielectric constant. On the other hand, it also appears possible for electron transfer to take place over longer distances which preclude the possibility of strong chemical interaction between quencher and fluorophore.

In these "weak interaction" cases quenching leads directly to solvated dissociated ion radicals. It is difficult to conclude which mechanism is operating in the case of lanthanide quenching of indole fluorescence, although some evidence presented here favors the second mechanism. In one respect, a strong covalent interaction of the indole π cloud with the lanthanide would be precluded by the relative inaccessibility of lanthanide $4f$ suborbital buried in an inner valence shell. Also, complexing the lanthanide with EDTA, a bulky ligand, actually increases its quenching efficiency though exciplex formation would appear to be even less favorable than for the aqueous complex. Presumably, the greater quenching efficiency of the EDTA complex is related to the ease with which the EDTA ligand can channel electrons to the central metal ion.

References and Notes

- (1) C. K. Luk, *Biochemistry*, **10**, 2838 (1971).
- (2) F. C. Wedler and V. D'Aurora, private communication.
- (3) R. A. Dwek and R. E. Richards, *Eur. J. Biochem.*, **21**, 204 (1971).
- (4) A. A. Lamola and J. Eisinger, "Molecular Luminescence," E. C. Lim, Ed., W. A. Benjamin, New York, N. Y., 1969, p 801.
- (5) R. F. Chen, *Arch. Biochem. Biophys.*, **142**, 552 (1971).
- (6) R. F. Steiner and E. P. Kirby, *J. Phys. Chem.*, **73**, 4130 (1969).
- (7) S. S. Lehrer, *Biochemistry*, **10**, 3254 (1971).
- (8) M. N. Ivokova, N. S. Vedenkina, and E. A. Burshtein, *Mol. Biol.*, **5**, 168 (1971).
- (9) A. White, *Biochem. J.*, **71**, 217 (1959).
- (10) A. W. Varnes, R. B. Dodson, and E. L. Wehry, *J. Amer. Chem. Soc.*, **94**, 946 (1972).
- (11) P. K. Gallagher, *J. Chem. Phys.*, **41**, 3061 (1964).
- (12) R. W. Ricci, *Photochem. Photobiol.*, **12**, 67 (1970).
- (13) C. A. Parker, "Photoluminescence of Solutions," Elsevier, Amsterdam, 1968, p 74.
- (14) F. A. Cotton and G. Wilkinson, "Advanced Inorganic Chemistry," Interscience, New York, N. Y., 1962, Chapter 31.
- (15) E. L. Wehry, "Practical Fluorescence," G. C. Guilbault, Ed., Marcel Dekker, New York, N. Y., 1973, p 120.
- (16) J. K. Thomas, S. Gordon, and E. J. Hunt, *J. Phys. Chem.*, **68**, 1524 (1964).
- (17) L. I. Grossweiner and H. I. Joschek, *J. Amer. Chem. Soc.*, **88**, 3261 (1966).
- (18) A. Weller, "Fast Reactions and Primary Processes in Chemical Kinetics," S. Claesson, Ed., Almqvist and Wiksell, Stockholm, 1967, p 413.
- (19) N. Mataga and O. Tanimoto, *Theor. Chim. Acta*, **15**, 111 (1969).
- (20) J. H. Baxendale, E. M. Fielden, C. Capellos, J. M. Francis, J. V. Davies, M. Ebert, C. W. Gilbert, J. P. Keene, E. J. Land, A. J. Swallow, and J. M. Nosworthy, *Nature (London)*, **201**, 468 (1964).

Electron Paramagnetic Resonance Spectra of Tetrachloromanganate(II) in Molten Tetrabutylammonium Tetrachlorocadmiate

Myron Ira Pollack and Benson R. Sundheim*

Department of Chemistry, New York University, New York, New York 10003 (Received March 6, 1974)

Publication costs assisted by New York University

The spin-spin interaction between tetrachloromanganate ions in molten tetrabutylammonium tetrachloromanganate solutions in molten tetrabutylammonium tetrachlorocadmiate has been studied as a function of temperature and mole fraction of manganese. The density and viscosity of the mixtures as well as the interdiffusion coefficient of Mn/Cd were also determined. The results suggest that the value of the anion-anion pair distribution function at (or near) contact is depressed substantially below that expected for a random distribution.

Intermolecular magnetic perturbations between molecular and/or ionic species can be used to study transport properties in liquids. The dipole-dipole interaction between paramagnetic species provides a time-dependent contribution to the Hamiltonian which appears in the transverse relaxation time and affects the line width of the esr spectrum. Similarly, the lifetime of excited states whose return to the ground state is spin forbidden is thought to be sensitive to magnetic perturbations which may relieve the selection rule. Fluorescence and phosphorescence quenching have long been used to study diffusion reactions at short times and distances and have recently been reported for fused tetrabutylammonium tetrahalomanganates.¹ Therefore, it seemed particularly interesting to examine the same system by magnetic resonance in order to compare and contrast the results. In addition, some questions of local structure of a fused salt appear in an interesting way.

We report here on a study of the spin-spin interaction between tetrachloromanganate ions in molten tetrabutylammonium tetrachloromanganate. The paramagnetic tetrachloromanganate ion is replaced isomorphously by a diamagnetic tetrachlorocadmiate ion. The latter may be used to change the concentration of the tetrachloromanganate ion without changing the structure of the solution. ESR spectra are reported as functions of temperature and mole fraction of manganese. In addition, the density and viscosity of the mixtures were determined as well as the interdiffusion coefficient of Mn/Cd.

Experimental Section

The epr spectra were measured in a Varian V-4502 spectrometer operated at X-band with 100-kHz field modulation. The variable temperature control was supplied with the instrument and maintained the temperature of the sample in the range up to 300° with an accuracy of $\pm 3^\circ$ and a precision of $\pm 2^\circ$. This was accomplished by the use of dry nitrogen gas as the heat transfer medium together with a platinum resistance thermometer serving as a sensor for the controller. The temperature settings were calibrated with an iron-constantan thermocouple placed in an otherwise empty sample tube. Sample tubes were constructed from 3-mm o.d. Pyrex tubing which was sealed under vacuum after loading with the sample.

The manganese and cadmium salts were synthesized and purified as required by conventional techniques.² As a check, their optical absorption spectra, melting points, and ultimate analyses were determined and found to be satisfactory. Mixtures were prepared by weighing the various components together and melting them under vacuum. Very low concentrations were obtained by serial dilution. Viscosities of the solutions used were determined in a Cannon-Ubbelohde semimicroviscometer. It was mounted in a constant temperature bath and maintained under a stream of dry nitrogen during the measurements. Density measurements were carried out by a floating bob technique using a Cahn recording electrobalance. Diffusion coefficients were obtained by the diffusion out of a capillary method.³ Here the $(\text{Bu}_4\text{N})_2\text{MnCl}_4$ was taken to be the active material and was loaded by a vacuum filling technique into a 4-cm long uniform-bore capillary tube which was closed at one end. This tube was then introduced with stirring into a bath of the inactive material, $(\text{Bu}_4\text{N})_2\text{CdCl}_4$, and allowed to diffuse for given amounts of time.³ Tubes were withdrawn at regular intervals and analyzed for manganese.

The spectrum of high-spin Mn(II) ions in solution is expected to display 30 allowed transitions conforming to the selection rules $\delta m_s = \pm 1$ and $\delta m_l = 0$ among the 36 energy levels produced by the $5/2$ electron and the $5/2$ nuclear spin. The line positions for these transitions are given to the fourth order in perturbation theory by the following well-known expression⁴

$$H(m_s, m_l) = H_0 - Am_l - \frac{A^2 C_2}{2H_0} - \frac{A^4 C_4}{8H_0^3}$$

where $H_0 = h\nu/g\beta$, $C_2 = (35/4) - m_l^2 + m_l(2m_s - 1)$, and $C_4 = (4m_s^3 - 6m_s^2 + 4m_s - 1)(25.25m_l - m_l^3) + (3m_s^2 - 3m_s + 1)(m_l^4 - 43.5m_l^2 + 149.6875) + (2m_s - 1)(43.5m_l^3 - 350.625m_l) - (25.25m_l^4 - 350.625m_l^2 - 1644.45)$. Each value of m_l has five electron spin transitions associated with it, each occurring at a slightly different field. The relative intensities then occur in the ratios 5:8:9:8:5. Synthetic curves of the first derivative spectra were constructed under the assumptions that the individual lines were either Lorentzian or Gaussian. The experimental line width was determined by comparing the theoretical and experimental curves. In all cases the Lorentzian line shape gave the better fit and hence was used throughout.

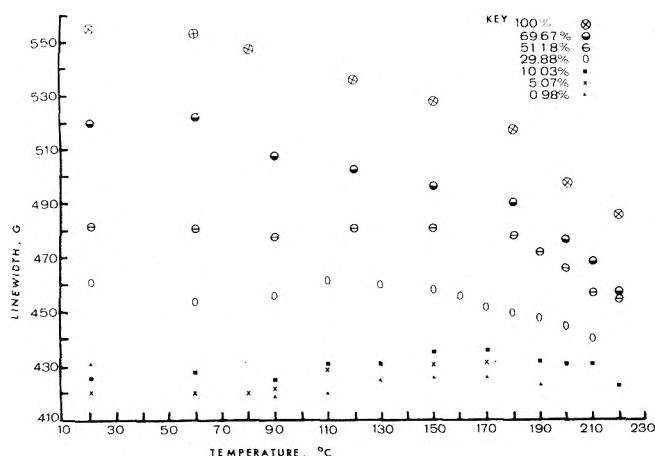


Figure 1. Dependence of overall line width on the concentration and temperature for various mole per cent solutions of $(\text{Bu}_4\text{N})_2\text{MnCl}_4$ in $(\text{Bu}_4\text{N})_2\text{CdCl}_4$.

The dependence of the overall line width (peak-to-peak on first derivative representation) on the concentration and dependence for various mole per cent solutions of tetrabutylammonium tetrachloromanganate in tetrabutylammonium tetrachlorocadmate is given in Figure 1.

In the most dilute solution studied, where the concentration-dependent part of the line width is expected to make a negligible contribution, the line width is approximately 34 G. As the concentration is raised to 10 mol %, a concentration-dependent contribution of about 6 G appears, increasing to approximately 85 G in the pure tetrabutylammonium tetrachloromanganate (at a molarity of 1.45 at 138°). The concentration-independent part was found to be independent of temperature as well.

The density of tetrabutylammonium tetrachlorocadmate was found to be essentially linear as a function of temperature in the range 117.5–169.4° and is well represented by $d = -5.268 \times 10^{-4}T(^{\circ}\text{C}) + 1.146$. The density of tetrabutylammonium tetrachloromanganate is well represented by the equation $d = -5.268 \times 10^{-4}T(^{\circ}\text{C}) + 1.057$. It was assumed that the density of a mixture of these two could be represented by simple linear combination of the separate densities.

The viscosity of tetrabutylammonium tetrachlorocadmate was well represented by the equation $\log \eta = 2.77 \times 10^{-5}/T(^{\circ}\text{K}) - 4.44$. The viscosity of tetrabutylammonium tetrachloromanganate is well represented by the equation $\log \eta = 2.75 \times 10^{-5}/T(^{\circ}\text{K}) - 4.45$. These two equations are valid over the range 120–190°. The viscosity of a mixture was obtained by taking linear combinations of the logarithms of the separate viscosities. This procedure was checked by direct determination of the viscosity of a 51.8 mol % mixture of tetrabutylammonium tetrachloromanganate and tetrabutylammonium tetrachlorocadmate. The interpolation procedure was found to be satisfactory.

The average of the four determinations of the diffusion coefficient of tetrabutylammonium tetrachloromanganate into tetrabutylammonium tetrachlorocadmate at 138° was found to be $2.23 \times 10^{-6} \text{ cm}^2/\text{sec}$.

Discussion

Looking first at the concentration-dependent part of the line width, we note that in concentrated solutions dipole interactions between the complex ions are to be expected. Hinckley and Morgan⁵ found that in aqueous solutions of

$\text{Mn}(\text{ClO}_4)_2$ in the same concentration range the dipole-dipole interaction was the predominant intermolecular relaxation process.

If we assume that the interaction between the two complexes is diffusion controlled, a bimolecular rate constant can be calculated using a simplified model for the transport process which views the interacting particles as hard spheres. The rate constant for such diffusion-controlled processes given by $k = 2\pi\rho D$, where ρ is the distance between centers upon collision and D is the sum of the self-diffusion coefficients of the two interacting particles. Here we take $\rho = 2(\text{ionic radius of } \text{Cl}^- + \text{Mn-Cl bond distance})^{7,8} = 8.36 \times 10^{-8} \text{ cm}$, and $D = 2(\text{self-diffusion coefficient of } \text{MnCl}_4^{2-}) = 4.4 \times 10^{-6} \text{ cm}^2/\text{sec}$. From these figures we deduce that $k = 1.39 \times 10^9 \text{ M}^{-1} \text{ sec}$. Multiplying this by the molarity, 1.44, we obtain an overall rate constant of $2 \times 10^9 \text{ sec}^{-1}$. This corresponds to 714 G as the expected width of each hyperfine component if each encounter terminated the spin state of the colliding particle. The overall line width observed at this temperature (which is the envelope of six hyperfine lines) is about 530 G. Therefore, we must assume either that not every encounter is successful or that the number of encounters cannot be calculated so simply. If the former is assumed, a probability factor must be employed.^{9,10} Previous applications of this idea to Mn(II) normally have been made in the exchange-narrowed region. Our high concentration results are not in the exchange-narrowed region (although we observed only a single line here) since the line width is still increasing rather than decreasing with concentration.

If we turn to the 10 mol % solution with an overall line width of 435 G and a hyperfine line width (fourth line from the low-field side) of 40 G, the concentration-dependent part is about 6 G and the above theory predicts a line width of 71 G if all encounters are successful. That is, a probability factor of approximately 0.08 is required.

An alternative and more plausible explanation is that the layer structure^{11,12} of the fused salt causes the rate of encounter to be much reduced below that expected for structureless systems. That is, the experiment reveals that the value of the anion-anion pair distribution function at (or near) contact is depressed by a factor of about 12 below that expected for a random distribution.

As the concentration of the paramagnetic complex is reduced by the replacement of diamagnetic tetrabutylammonium tetrachlorocadmate for tetrabutylammonium tetrachloromanganate the probability of Mn(II)-Mn(II) contact is reduced, but considerable additional broadening remains, probably due to ligand-hyperfine interaction.

Let us estimate the volume of MnCl_4^{2-} from crystal radius measurements and compare this result with a similar calculation from liquid density data. For the crystal measurements, we assume the complex to be spherical, and, hence, the apparent molar volume V is given by $V = 4\pi r^3 N/3 = 4\pi(4.2 \times 10^{-8})^3(6.02 \times 10^{23})/3 = 187 \text{ cm}^3/\text{mol}$. The apparent ionic volume may be calculated from the liquid density.^{2,13-15} We take the volume of MnCl_4^{2-} to be equal to the volume of $(\text{Bu}_4\text{N})_2\text{MnCl}_4$ minus twice the volume of $(\text{Bu}_4\text{N})\text{Cl}$ plus twice the volume of Cl^- . For the Cl^- we take half of the molal volume of KCl as an approximation, obtaining $V = (2 \times 349) - 636 + 49 = 111 \text{ cm}^3/\text{mol}$. The discrepancy between these two very approximate values (187 vs. 111) apparently reflects a deviation in the structure from the close packing of spheres. It suggests that the complex must fit itself into or in between the bulky tet-

trabutylammonium ions and hence is not free to rotate in solution. As a consequence of this hindered motion, anisotropic interactions are not expected to be averaged out in solution and, depending on the rate of rotation, may provide a relaxation mechanism which leads to line broadening. Further support for restricted motion comes from the relatively high viscosities encountered in these systems.

It is interesting to compare these results with those obtained from phosphorescence lifetimes.¹ Lifetimes of the order of 2–5 μ sec were obtained for the ${}^4T_1 \rightarrow {}^6S_0$ transition in tetrabutylammonium tetrachloromanganate and these did not change with concentration. By contrast, this study shows that about 1000 anion-anion collisions, sufficient to affect the spin transverse relaxation time, take place during a phosphorescence lifetime but do not play any role in shortening that lifetime. Further studies on this system will be reported shortly.

Acknowledgment. It is a pleasure to acknowledge sup-

port from the National Science Foundation (Grant No. GP 14615).

References and Notes

- (1) B. R. Sundheim, E. Levy, and B. Howard, *J. Chem. Phys.*, **57**, 4492 (1972).
- (2) M. I. Pollack, Ph.D. Dissertation, New York University, 1973.
- (3) L. Yang and M. T. Simnad in "Physicochemical Measurements at High Temperatures," J. O'M. Bockris, J. L. White, and J. C. MacKenzie, Ed., Academic Press, New York, N. Y., 1959, Chapter 14.
- (4) F. K. Hurd, M. Sachs, and W. D. Hershberger, *Phys. Rev.*, **93**, 373 (1954).
- (5) C. C. Hinckley and L. O. Morgan, *J. Chem. Phys.*, **44**, 898 (1968).
- (6) R. M. Noyes, *Progr. React. Kinet.*, **1**, 129 (1961).
- (7) G. H. Aylward and T. J. V. Findlay, "SI Chemical Data" Wiley, New York, N. Y., 1971, p 6.
- (8) M. T. Vala, C. J. Ballhausen, R. Dingle, and S. L. Holt, *Mol. Phys.*, **23**, 217 (1972).
- (9) T. B. Swanson, *J. Chem. Phys.*, **45**, 179 (1966).
- (10) G. E. Pake and T. R. Tuttle, Jr., *Phys. Rev. Lett.*, **3**, 423 (1959).
- (11) L. V. Woodcock and K. Singer, *Trans. Faraday Soc.*, **67**, 12 (1971).
- (12) L. V. Woodcock, Ph.D. Thesis, University of London, 1970.
- (13) T. R. Griffiths, *J. Chem. Eng. Data*, **8**, 568 (1963).
- (14) J. E. Lind, Jr., H. A. A. Abdel-Rehim, and S. W. Rudich, *J. Phys. Chem.*, **70**, 3610 (1966).
- (15) E. R. Van Artsdalen and I. S. Yaffe, *J. Phys. Chem.*, **59**, 18 (1955).

Structure and Texture of a Crushed Na-Y Zeolite

Bernard Moraweck, Pierre Gallezot, Albert Renouprez,* and Boris Imelik

Institut de Recherches sur la Catalyse, 69100, Villeurbanne, France (Received April 29, 1974)

Publication costs assisted by the Centre National de la Recherche Scientifique

The structure and texture of a crushed Na-Y zeolite have been investigated by X-ray techniques, ir spectroscopy, and adsorption measurements. The grinding treatment produces a progressive breakdown of the crystal structure and porous framework. This transformation to the amorphous state is explained by a local overheating of the sample.

Introduction

Synthetic Y zeolites are crystalline aluminosilicates with an open three-dimensional framework of alumina and silica tetrahedra.¹ They are now widely used as adsorbents and catalysts because of their high and polar internal surface, accessible only to molecules small enough to diffuse through the pore system. Moreover, zeolites exhibit a remarkable stability and may undergo a great deal of modifications such as dealumination, cation exchange, and cation reduction, which improve their potentialities.

However, little is known about the mechanical strength of these materials, which are involved in industrial applications and often undergo severe treatments.

The purpose of this paper is to investigate the changes occurring in the texture and structure of a Na-Y zeolite during grinding.

Experimental Section and Results

A 2–3-g sample of a Linde Na-Y zeolite was grinded in an agate crusher for successive 0.5-hr periods. The pressure

on the pestle was 7 kg. In all the cases, the powder was completely amorphous after 10 hr.

X-Ray Diffraction. The breakdown of the Na-Y zeolite produced by crushing the sample was followed by X-ray diffraction. The patterns were recorded with a Siemens goniometer using monochromatized Cu $K\alpha_1$ radiation. A pattern was taken every 0.5 hr during the grinding and the intensities of the different lines were adjusted to the same scale with the help of an internal standard. The intensities of several reflections (normalized to 1) are plotted in Figure 1 as a function of the grinding time. These results and particularly the required time for a total vanishing of the diffraction lines depend on several parameters, including the crusher features and the amount of powder.

However it turns out that (i) the line intensities undergo a fast decrease during the first hour of grinding, (ii) the curves have the same shape, *i.e.*, the long-range order in the different crystallographic planes decreases simultaneously, without anisotropic effect, and (iii) the shape of the different lines is not altered by crushing.

X-Ray Small-Angle Scattering. The experiments were performed with a small-angle goniometer² which permits a

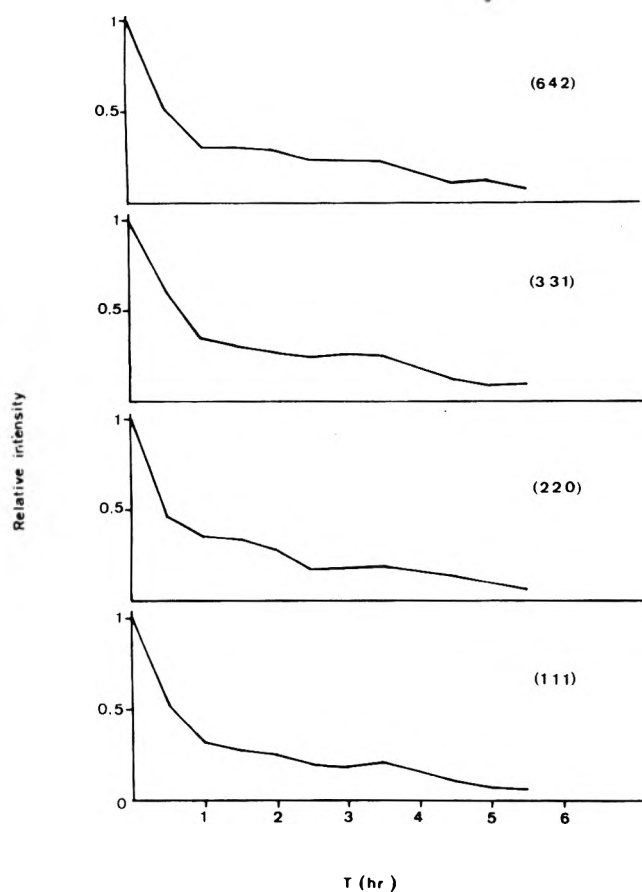


Figure 1. Variations of X-ray diffraction line intensities as a function of grinding time, for different (hkl) values.

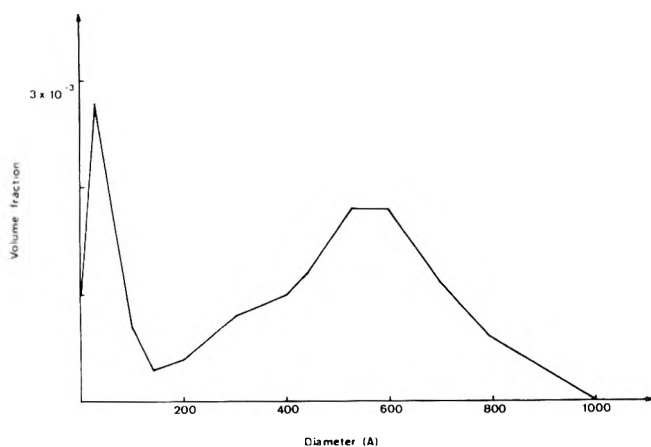


Figure 2. Particle size volume distribution as a function of the diameter (sample crushed for 10 hr).

resolution of 2500 Å. The multiple scattering treatment was performed³ and led to the values of the specific surface areas, to the porosity, and to distribution curves of particle (or pore) diameters.

The scattering produced by the initial Y zeolite is very weak. This result, at first sight surprising, is due to the regular arrangement of the pore system: the calculated area is 15 m²/g, whereas the BET area is 800 m²/g. The 2000-Å particles have a geometrical area of 10–12 m²/g and the porosity of these particles (5 mm³/g) represents 3–5 m²/g.

TABLE I: X-Ray Small-Angle Scattering Parameters

Sample	Surface area, m ² /g	Porosity, mm ³ /g	Pore diameter, Å	Particle diameter, Å
Na-Y zeolite	15	5	30	2000
Crushed 10 hr	64	10	30	500
Heated at 1000°	24	1	150	500–2000

The sample crushed for 10 hr has a specific area of 64 m²/g. The particle distribution curve shows a well-defined maximum at 500 Å (Figure 2). At the same time the porosity of these particles has increased to 10 mm³/g which corresponds to 10 m²/g.

This sample was compared to a zeolite heated in air at 1000°. In that case the area is 24 m²/g; some 500–1000-Å particles appear but the porosity of these crystallites is only 1–2 mm³/g. These results are summarized in Table I. The BET areas corresponding to the grinded and to the heated samples are respectively 25 m²/g and less than 1 m²/g. This means that most of the pores are closed.

Infrared Measurements. Infrared transmission spectra of the zeolite were recorded with a Perkin-Elmer Model 125 spectrometer. It was checked that the pressure required to obtain the ir wafers does not change the X-ray crystallinity of a reference sample. The ir spectra recorded in the 1300–200-cm⁻¹ region may be used to detect changes in the framework structure.⁴ In addition to internal vibrations of the T-O₄ tetrahedra, there are vibrations related to external linkages between tetrahedra which are sensitive to the framework structure. Thus the two broad bands occurring near 560 and 380 cm⁻¹ are related to double 6-ring of tetrahedra and 12-ring of tetrahedra, respectively (breathing motion of pore openings). The bands corresponding to the internal vibrations of the T-O₄ tetrahedra are still detected (although broadened) on the spectra of the crushed zeolite but the 6- and 12-ring vibrations have disappeared. This clearly indicates that the structure of the Y zeolite no longer exists. Similar effects occur in the case of thermally decomposed Y zeolite.⁴

Adsorption Capacity Measurements. In order to measure the water adsorption capacity, the zeolite samples were activated at 400° under vacuum for 6 hr and then allowed to equilibrate in water vapor at saturation (25°) until a limit value of weight uptake was observed.

This water adsorption measurement is well suited to determine the intracrystalline void volume⁵ and thus to determine if a variation of this volume follows the structure breakdown. Typically, a Faujasite-type zeolite adsorbs as much as 0.35 g of water/g.⁴ The 8 hr crushed Na-Y zeolite loses only 0.03 g/g during evacuation and reabsorbs the same amount of water. This sharp loss of adsorption capacity indicates that most of the microporous network of the crushed zeolite has been destroyed so that water molecules (and molecules of larger size) are no longer able to penetrate inside the solid.

Discussion

We have shown that the grinding of a Na-Y zeolite for 6–10 hr causes a breakdown of the crystal structure. But this transformation appears to be a rather complex phenomenon: (i) the former 2000-Å crystallites have been broken into 500-Å particles; (ii) no long- or medium-range order remains in such a particle; however, as the shape of the diffraction lines are not altered by a partial crushing, it can be assumed that this order disappears suddenly in one

particle but not in the whole sample at the same time; (iii) the pores are completely destroyed and the T-O₄ units lie in an ill-defined close-packed arrangement.

The question arises as to the reason for such a destruction. The analogy with the case of the heated sample suggests the possibility of a thermal effect: the shearing stress due to the crushing may well induce local increase of temperature which, step by step, may break some of the covalent linkages between the tetrahedra and provoke the structure breakdown.

In order to support this hypothesis, test experiments were performed. A mixture of sodium oxalate (decomposition temperature 270°) and Na-Y zeolite was grinded for 3

hr; its X-ray pattern indicates that the salt is completely decomposed. The same experiment performed with a mixture of zeolite and anatase (TiO₂) has shown that the transformation into the rutile form is also complete. So, during the crushing, the temperature reached is higher than 600°.

References and Notes

- (1) J. V. Smith, *Advan. Chem. Ser.*, **No. 101**, 171 (1971).
- (2) A. J. Renouprez, H. Bottazzi, D. Weigel, and B. Imelik, *J. Chim. Phys. Physicochim. Biol.*, **62**, 131 (1965).
- (3) H. Brusset and J. R. Donati, *J. Appl. Crystallogr.*, **2**, 55, (1969).
- (4) E. M. Flanigen, H. Khatami, and H. A. Szymanski, *Advan. Chem. Ser.*, **No. 101**, 201 (1971).
- (5) D. W. Breck and R. W. Crose, *Advan. Chem. Ser.*, **No. 121**, 319 (1973).

Thermodynamic Properties of Systems with Specific Interactions Calculated from the Hard-Sphere Equation of State. I. Binary Systems with One Inert Component

Aleksander Kreglewski* and Randolph C. Wilhoit

Thermodynamics Research Center, Department of Chemistry, Texas A & M University, College Station, Texas 77843

(Received February 19, 1974)

Publication costs assisted by Texas A & M University

Two theories of intermolecular forces, the theory of Balescu and the theory of Rowlinson, were extensively tested by comparisons with the excess functions (G^E , H^E , V^E , C_p^E) and the gas-liquid critical temperatures ($T^c(\varphi)$) of 77 binary systems involving either one or two inert components. The tests were based on the hard-sphere equation of state and carried out *without the aid of a reference substance*. For several reasons Rowlinson's theory is superior, however, the liquid-vapor equilibrium diagrams can be correlated equally well by both theories. The prediction of such diagrams may easily be accomplished in the frames of Balescu's theory. The terms ΔG^c and ΔH^c which correct G^E and H^E , respectively, for the effect of clustering in the vicinity of critical solution temperature T^{cs} were derived from the theory of Fixman. ΔH^c is negative and may become large near T^{cs} . An empirical correction for the Helmholtz free energy due to large size differences of the components is found to vary with $(kT)^{-1/2}$. The knowledge of only one term, η/kT , that is determined from G^E or $T^c(\varphi)$, is required to correlate all the excess functions in case of weak specific interactions between the molecules of one of the components, while two (η/kT and $(\nu/kT)^2$) are required in case of such interactions of moderate strength. The average values of η/k and ν/k for 32 compounds, based on Balescu's theory, are tabulated.

In this work we have tested two theories of temperature-dependent interactions in mixtures of fluids on the basis of the hard-sphere equation of state. The basic relations were summarized previously (method A).¹ The van der Waals parameter a_m of an m -component mixture is now expressed by a more simple but equally accurate relation that has some theoretical justification

$$a_m = 4.7R \left[\sum_{i=1}^m (V_i^*)^{2/3} x_i \right]^2 \left[\sum_i \sum_j q \epsilon_{ij} \varphi_i \varphi_j \right] \quad (1)$$

where R is the gas constant, V_i^* is the corrected liquid molar volume at the reduced temperature $T/T^c = 0.6$ and evaluated from the formerly given relation,¹ and x_i and φ_i are the mole and the surface fractions of the i th component, respectively, ϵ_{ij} is the minimum potential energy for

interaction of equivalent surfaces between molecules of components i and j , and q is a proportionality constant. For brevity, we substitute in all relations

$$q \epsilon \equiv T^c / (V^*)^{1/3} \quad (2)$$

where T^c is the gas-liquid critical temperature. For the pure compound "i," a_m becomes $a_i = 4.7RT_i^c V_i^* = 4.7Rq \epsilon_{ii} (V_i^*)^{4/3}$. In the following discussion the symbols ϵ , χ , η , Δ , and ν represent quantities associated with the interactions between two molecules. The subscripts ii and jj on these symbols indicate interactions between two similar molecules, and the subscript ij indicates an interaction between two different kinds of molecules. Subscripts are omitted from equations which apply to either kind of interaction.

Previously,¹ a_m was assumed to be independent of the temperature and equal to the value at the critical point (a_m^c). We now assume a more general relation

$$\epsilon = \epsilon^0(1 + \chi)$$

$$\chi = (\Delta/kT)^{1/2} + (\eta/kT) + (\nu/kT)^2 \quad (3)$$

The terms in $T^{-1/2}$ and T^{-2} appear in the specific cases only, considered below. The leading term, η/kT , is treated differently according to the two theories,²⁻⁴ published about 20 years ago.

Balescu⁴ developed a theory in which ϵ^0 represents the contribution of London forces, treated as independent of the temperature, whereas η/k is that due to dipole-dipole (or, more generally, multipole) interactions.

Previously,^{1,5} we have treated the London forces as independent of the temperature and found that the following rule holds remarkably well

$$\epsilon_{ij}^0 = 2[(1/\epsilon_{ii}^0) + (1/\epsilon_{jj}^0)]^{-1} \quad (4)$$

We wish to emphasize again that this rule has a theoretical foundation only for interactions between equal surfaces (or segments of equal size, as in Flory's theory of chain molecules) and only if the polarizability α is a common function of V^* , say, $\alpha = aV^* + b$, where a and b are constants⁶ (in this case the α 's and the σ 's in the general London formula cancel). Although Fender and Halsey⁷ and recently Lin and Robinson⁸ found empirically that this rule holds for total pair potentials \bar{u}_{ij} for mixtures of the rare gases, their tests were based on the assumption that the collision diameter $\sigma_{ij} = (\sigma_{ii} + \sigma_{jj})/2$. This assumption yields much more negative V^E than Lebowitz's exact relations¹ and V^E is equal to $2B_{ij} - B_{ii} - B_{jj}$, where B 's are the second virial coefficients used in these tests. Moreover, σ is a function of $u(r)/kT$. For these reasons B_{ij} is not suitable for testing a combining rule for \bar{u}_{ij} or ϵ_{ij}^0 . Earlier Kreglewski and Stryjek made this same mistake and arrived at an inaccurate combining rule. The problem is discussed in ref 6. We recall that the proper test of eq 4 was made a few years ago⁵ by evaluation of $T^c(\varphi)$ of numerous systems.

For interactions between equivalent surfaces, following Balescu's theory, η_{ij} is proportional to $\mu_i^2\mu_j^2/\epsilon_{ij}^0$ (or $Q_i^2Q_j^2/\epsilon_{ij}^0$, where μ and Q are the dipole and the quadrupole moments, respectively) and therefore

$$\eta_{ij} = (\eta_{ii}\eta_{jj})^{1/2}(\epsilon_{ii}^0 + \epsilon_{jj}^0)[2(\epsilon_{ii}^0\epsilon_{jj}^0)^{1/2}]^{-1} \quad (5)$$

Hence, when one of the components, e.g., i , is an inert component, then $\eta_{ii} = \eta_{ij} = 0$. The values of ϵ^0 of the pure components are obtained by combining eq 2 and 3

$$q\epsilon^0 = T^c[(V^*)^{1/3}(1 + \chi^c)]^{-1} \quad (6)$$

where χ^c is the value of χ at $T = T^c$.

It is sometimes stated that large values of the excess Gibbs energy of mixing G^E or enthalpy of mixing H^E point to "unusually weak" $i + j$ interactions. It suffices, however, to assume that for one of the components $\eta_{ij} > 0$ to obtain a large value of G^E . This value of η_{ij} should also reflect the temperature dependence of the configurational energy U' of the pure j th component. In fact, we find that, for example, fluoroalkanes exhibit a stronger dependence of U' on the temperature than do alkanes. Hence, if $\eta_{ii} = 0$ (alkanes treated as inert components) then for fluoroalkanes $\eta_{ij} > 0$. Unfortunately, the values of η_{ij} found from dU'/dT are not accurate enough and must be found from a property of the mixture, G^E or $T^c(\varphi)$.

Cook, Rowlinson, and Sutton² introduced the concept of noncentral forces that appear to vary with T^{-1} and account for orientation-dependent interactions between nonspherical molecules. Rowlinson³ found that the respective parameter δ^c at the critical point is simply related to the acentric factor: $\omega = 2.40\delta^c$. On the other hand, $2\delta^c = \eta_n/kT^c$, where η_n is the parameter in eq 3 with the subscript n indicating that it refers to the concept of noncentral forces; therefore

$$\eta_n/k = 0.833\omega T^c \quad (7)$$

According to this theory, ϵ^0 represents only this part of London energy that is independent of the temperature. In attempting to apply the concept of noncentral forces, we encounter the problem of combining rules for ϵ_{nij}^0 and η_{nij} . For ϵ_{nij}^0 we applied eq 4 because it holds for mixtures of Ar, Kr, and CH_4 ⁵ where $\omega \approx 0$ and $\eta_n \approx 0$. However, at least two alternatives remain for η_{nij} . If η_{nii} and η_{njj} are calculated from eq 7, then in presence of specific interactions in the j th component, η_{nij} appears to be "unusually weak." For example for benzene mixtures with numerous inert solvents we obtain $\eta_{nij} \approx 0.96(\eta_{nii}\eta_{njj})^{1/2}$. The second alternative follows from the well-known fact that even weakly associated substances have more negative second virial coefficients than those calculated from the acentric factors. Thus, for such substances $\eta_n/k = 0.833\omega T_0^c + \eta_s/k$, where η_s is a correction due to multipole (specific) interactions and T_0^c is a hypothetical critical temperature due to London forces only. η_{sij} is analogous to η_{ij} in Balescu's theory and can be evaluated from eq 5. If $\eta_{sii} = 0$ (inert component), then also $\eta_{sij} = 0$ and a large value of G^E is due to a large value of η_{sij} . However, the combining rule for the "inert" contribution to η_n (eq 7) is unknown. For this reason, we have limited the comparisons with experimental data to a few cases in which Rowlinson's theory yields distinctly different results than does Balescu's theory.

Balescu's theory, due to its simplicity and the available combining rules, offers a convenient basis for a treatment of complex mixtures in which $i + i$, $j + j$, and $i + j$ specific interactions may simultaneously occur and which will be considered in part II. Below, we apply the theory to a few systems with specific $j + j$ interactions only. Most of the systems considered here exhibit deviations from any theory of random mixtures due to certain effects that have to be taken into account.

Ordering Effects in Binary Mixtures with One Inert Component. Two kinds of such ordering effects may be roughly distinguished: (a) clustering in the vicinity of the critical solution temperature T^{cs} , (b) strongly localized attraction of two or more molecules of the same kind, usually called *association*. This effect can be classified as *weak* or *moderate* for the kinds of molecules considered in this paper.

The system $n\text{-C}_6\text{H}_{14} + n\text{-C}_6\text{F}_{14}$ offers a convenient example of the effect of clustering on the excess functions. The values of G^E and H^E were determined at 308 K (Table III) close to $T^{cs} = 295.85$ K determined by Gaw and Scott.⁹ At the gas-liquid critical point the system is practically a random mixture. In Figure 1 several calculated curves are compared with the T^c data. The method of evaluation of critical constants is outlined elsewhere.^{5,6} Since the temperature varies along the T^c line, χ^c in eq 6 was evaluated by taking $T = T_i^c$ for the pure components, whereas in terms involving Δ_{ij} , η_{ij} , or ν_{ij}/kT , T was set equal to $(T_i^c + T_j^c)/2$. Curve 1 was evaluated from η_{ij} fitting G^E at 308 K only. The values of G^E appear to be slightly larger than for

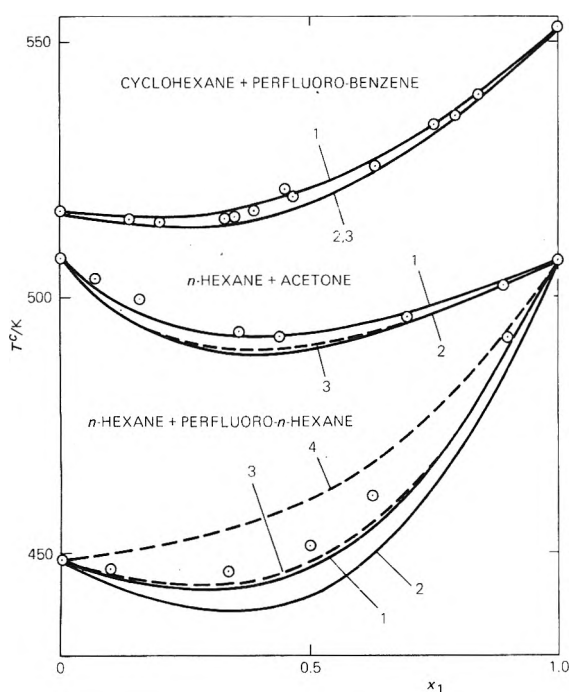


Figure 1. Gas-liquid critical temperatures of the systems: (a) cyclohexane + perfluorobenzene, (b) *n*-hexane + acetone, and (c) *n*-hexane + perfluoro-*n*-hexane. x_1 is the mole fraction of the inert component. The experimental points were determined by (a) Powell, Swinton, and Young,¹³ (b) W. B. Kay, *J. Phys. Chem.*, **68**, 827 (1964), and (c) A. H. N. Mousa, W. B. Kay, and A. Kreglewski, *J. Chem. Thermodyn.*, **4**, 301 (1972). The full and the dashed curves were calculated from Balescu's and Rowinson's theory, respectively, with parameters fitting (1) G^E only, (2) G^E , (3) G^E and H^E (noncentral), and (4) H^E only. The values of the parameters are given under Figure 3 ($\Delta G^E = \Delta H^E = 0$ at the gas-liquid critical point).

a random mixture (curve 1 lies below the T^c data), whereas those for H^E must be much smaller than for random mixture (curve 4 lies above the T^c data). Curves 2 and 3 are discussed later.

A few years ago, Fixman¹⁰ derived a relation for the heat capacity in the vicinity of T^{cs}

$$C_p = C_0 + D_0(T - T^{cs})^{-1/2} \quad (8)$$

at constant, critical composition, where D_0 is a constant. The heat capacity C_0 is the value of C_p in absence of any ordering effects, *i.e.*, for an ideal mixture, and does not appear in the "excess" functions of clustering (superscripts *c*). We assume that the functions derived from eq 8 are symmetrical with respect to φ_i , *i.e.*, they will be multiplied by $4\varphi_i\varphi_j$. Equation 8 suggests that the enthalpy of clustering is $\Delta H^c/(4\varphi_i\varphi_j) = 2D_0(T - T^{cs})^{1/2} - B$. Dimensional considerations require that B be proportional to $(T^{cs})^{1/2}$. Therefore

$$\Delta H^c/(4\varphi_i\varphi_j) = 2D_0(T - T^{cs})^{1/2} - B_0(T^{cs})^{1/2} \quad (9)$$

where B_0 is a constant.

Since $[\partial(\Delta G^c/T)/\partial T]_p = -\Delta H^c/T^2$, we obtain for the "excess" Gibbs energy of clustering

$$\frac{\Delta G^c}{4\varphi_i\varphi_j} = \frac{\Delta H^c}{4\varphi_i\varphi_j} - \frac{2D_0T}{(T^{cs})^{1/2}} \times \left[\arctan\left(\frac{T}{T^{cs}} - 1\right)^{1/2} + ET \right] \quad (10)$$

where E is a constant. ΔH^c is negative at $T = T^{cs}$ and, according to eq 9 changes sign and becomes positive at T/T^{cs}

$\geq [B_0/(2D_0)]^2 + 1$. Since a positive value of ΔH^c is meaningless, the value of ΔG^c and ΔH^c above this T/T^{cs} must be neglected. The condition that ΔG^c be simultaneously zero at this T/T^{cs} requires that $E = [2D_0/(T^{cs})^{1/2}] \arctan(B_0/2D_0)$. Therefore

$$\frac{\Delta G^c}{4\varphi_i\varphi_j} = \frac{\Delta H^c}{4\varphi_i\varphi_j} - \frac{2D_0T}{(T^{cs})^{1/2}} \times \left[\arctan\left(\frac{T}{T^{cs}} - 1\right)^{1/2} - \arctan\left(\frac{B_0}{2D_0}\right) \right] \quad (11)$$

Fixman obtained a rather uncertain theoretical value of D_0 ; this value was used. The value of B_0 was obtained by fitting to the observed values of G^E and H^E of the *n*-C₆H₁₄ and *n*-C₆F₁₄ system. The values are $D_0 = 75$; $B_0 = 68$ J mol⁻¹ K^{-1/2}.

In this model, D_0 is a universal constant. We further assume that $\Delta G^c/(T^{cs})^{1/2}$ and $\Delta H^c/(T^{cs})^{1/2}$ conform to a certain principle of corresponding states and therefore B_0 is a universal constant. Equation 9 implies that ΔH^c at equal T/T^{cs} is proportional to $(T^{cs})^{1/2}$.

The value of T^{cs} is often unknown and in this paper we used uniformly predicted values except for perfluoroalkane systems. Becker and Kiefer¹¹ derived from a lattice theory for several coordination numbers

$$T^{cs} \approx G_{cs}^E/(0.55R) \quad (12)$$

where G_{cs}^E is the value of G^E at the critical solution point. The value of G_{cs}^E may be estimated by an iteration from a value of G^E measured at a certain T from the relation

$$G_{cs}^E \approx G^E[1 + \ln(T/T^{cs})] \quad (13)$$

The effect of association on the excess functions varies with T less rapidly than ΔH^c or ΔG^c . According to Saroléa,¹² the effect on G^E is small, but it may lower considerably H^E . If the London energies of the two components are equal and $\eta_{ii} = 0$ (inert solvent), then the contribution to the excess entropy¹² is equal to $-3R[(\eta_{ij} - \frac{1}{2}\eta_{jj})/(kT)]^2$. We have retained the temperature dependence of the correcting term in accordance with Saroléa's theory and expressed it by $(\nu_{ij}/kT)^2$ in eq 3. Although ν_{ij} refers to mixed $i + j$ interactions, we assume that ν_{ij} depends only on the nature of specific interactions in component j and is independent of the inert solvent i that merely serves as a diluting medium. Therefore, ν_{ij} is coupled with η_{jj} .

As in the case of clustering, we find that the $T^c(\varphi)$ curve of the *n*-C₆H₁₄ + (CH₃)₂CO system calculated from η_{jj} fitted to G^E data only (curve 1 in Figure 1) conforms to the experimental data. The curve obtained for η_{jj} fitting H^E data only is not shown but it lies far above the experimental points for T^c . In general, in the presence of ordering effects (clustering, association) H^E and TS^E decrease much below the values for a random mixture, whereas G^E is distorted to a lesser extent.

We note that an attempt to test the theory of noncentral forces was made earlier.¹³ However, the authors assumed that $T^c(x)$ of the *c*-C₆H₁₂ + C₆F₆ system depends on only one parameter, e_{12} , treated as independent of the temperature, whereas the excess functions depend on e_{12} and $(2\delta_{12} - \delta_{11} - \delta_{22})$, where the δ 's vary with T^{-1} . Since the δ 's obviously do not vanish at $T = T^c$, the test is not conclusive. We confirm, however, that the theory as well as Balescu's theory are valid for this system (Figure 1).

The relations for the excess functions were summarized elsewhere.¹ They remain the same for the hard-sphere term

TABLE I: The Effect of Size Differences of the Components for Systems with Parameters $u_{ij} = u_{ji} = 0$, $\Delta_{ij} > 0$, $u_{ij} > 0$, and $v_{ij} = v_{ji} = 0$

System	T	$\frac{u_{ij}}{k}$	Calculated values				Observed values		
			$\frac{\Delta_{ij}}{k}$	G^E	H^E	V^E	G^E	H^E	V^E
Methane +	115.8	0	0	240	120	-1.1	310 ^a		-1.1
2-methylpentane									
Methane +	155	0	0	310	-100	-4.5			-3.6
2-methylpentane									
Cyclopentane +	298	0	1.40	(-210)	160	-0.3	-208	212	0.046
OMCTS ^b									
n-Hexane +	293	0	0.002	(-65)	130	0.8	-65	129	-0.48
n-Hexadecane									
n-Hexane +	333	0	0.002	-90	60	0.7	-84	10	-0.97
n-Hexadecane									
n-Hexane +	373	0	0.002	-100	-40	-0.1			-0.6
n-Hexadecane									
Methane + propane	100	0	0.004	(190)	90	-0.6	100	113	
2,2,4-Trimethylpentane +	293	0	0	-20	80	0.5	0	230	-0.49
n-Hexadecane									
n-Hexane +	293	0	0	-20	70	0.4	-25	46	-0.31
n-Dodecane									
Cyclopentane +	298	0	0	-10	-0.1		2	-40	-0.283
cyclohexane									
Cyclopentane +	288	0	0.017	(10)	40	-0.2	12 ^c	-7 ^c	-0.268 ^d
2,3-dimethylbutane									
Cyclopentane +	298	0	0.017	10	40	-0.2	13 ^c	-2 ^c	-0.269 ^d
2,3-dimethylbutane									
Cyclopentane +	308	0	0.017	10	40	-0.2	13 ^c	4 ^c	-0.268 ^d
2,3-dimethylbutane									
2,3-Dimethylbutane +	288	0	0	190	160	-0.9	184 ^d	185 ^d	-0.623 ^d
cyclohexane									
2,3-Dimethylbutane +	298	0	0	190	160	-1.0	184 ^d	176 ^d	-0.700 ^d
cyclohexane									
2,3-Dimethylbutane +	308	0	0	190	150	-1.2	184 ^d	161 ^d	-0.828 ^d
cyclohexane									
n-Hexadecane +	298	1	0.30	(-120)	340	1.0	-118 ^e	397 ^f	
carbon tetrachloride									
n-Hexadecane +	328	1	0.30	-160	320	1.3	-182 ^e		
carbon tetrachloride									
n-Octane +	298	1	0.018	(95)	290	0.1	95 ^f	356 ^f	
carbon tetrachloride									
n-Heptane + benzene	333	11	0.02	(300)	840	0.4	30 ^h	900 ⁱ	0.59 ^h
n-Octane + benzene	298	11	0.04	(330)	940	0.6	331 ^j		0.71 ^k
n-Hexadecane + benzene	298	11	0.54	(91)	1000	1.3	91 ^l		
n-Hexadecane + benzene	328	11	0.54	4	900	1.7	1 ^m		

^aUnless otherwise indicated, the references to observed values are given in ref. 1.

^bOMCTS = octamethylcyclotetrasiloxane

^cM. B. Ewing and K. N. Marsh, *J. Chem. Thermodyn.*, **5**, 659 (1973).

^dM. B. Ewing and K. N. Marsh, *J. Chem. Thermodyn.*, **5**, 651 (1973).

^eD. V. S. Jain and B. S. Lark, *J. Chem. Thermodyn.*, **5**, 455 (1973).

^fValues of H^E at 300 K; D. V. S. Jain, O. P. Yadav, and S. S. Gill, *Indian J. Chem.*, **9**, 339 (1971).

^gD. V. S. Jain, V. K. Gupta, and B. S. Lark, *Indian J. Chem.*, **9**, 465 (1971).

^hB. Brown and A. H. Ewald, *Aust. J. Sci. Res., Ser. A*, **4**, 198 (1955).

ⁱC. P. Brown, A. R. Mathieson, and J. C. Thynne, *J. Chem. Soc.*, 4141 (1955).

^jD. V. S. Jain, V. K. Gupta, and B. S. Lark, *J. Chem. Thermodyn.*, **5**, 451 (1973).

^kK. R. Harris and P. J. Dunlop, *J. Chem. Thermodyn.*, **2**, 805 (1970).

TABLE II: Excess Functions of the Binary Systems with Parameters $u_{ij} = u_{ji} = v_{ij} = v_{ji} = 0$, $\Delta_{ij} > 0$, $u_{ij} > 0$, and $v_{ij} = 0$

System	T	$\frac{u_{ij}}{k}$	Calculated values				Observed values		
			$\frac{\Delta_{ij}}{k}$	G^E	H^E	V^E	G^E	H^E	V^E
Benzene									
+ 2-methylpentane	303	0	11	(470)	1030	0.1	463 ^a	1020 ^a	0.53 ^a
+ 2,2-dimethylbutane	303	0	9.5	(480)	1000	0.1	484 ^a	980 ^a	0.85 ^a
+ 2,3-dimethylbutane	303	0	10	(435)	950	0.1	435 ^a	900 ^a	0.81 ^a
+ neopentane	273	0	6	(570)	920	-1.2	570 ^b		-0.5 ^b
+ cyclohexane	273	0	16	(390)	980	0.6	387 ^c		
+ cyclohexane	313	0	15	(300)	780	0.7	300 ^d	790 ^d	0.64 ^d
+ cyclohexane	343	0	15	(430)	910	0.1	431 ^e		0.66 ^e
+ n-hexane	273	-0	8	(390)	910	0.1	399 ^f	870 ^f	0.40 ^f
+ n-hexane	298	-0	8	(390)	850	0.1	382 ^g		
+ cyclopentane	308	0	13	(260)	640	0.4	272 ^h		
Toluene									
+ n-hexane	293	0	7	(340)	650	-0.2	350 ⁱ	460 ⁱ	
+ 3-methylpentane	303	0	7.5	(340)	660	-0.3	342 ^j	640 ^j	0.21 ^j
+ n-pentane	298	0	9	(360)	620	-0.7	360 ^k		0.32 ^k
+ cyclohexane	293	0	(11)	240	(590)	0.4	600 ^l		0.6 ^l
+ methylcyclohexane	298	0	8	220	(520)	0.4	521 ^m		0.37 ^m
m-Xylene									
+ cyclohexane	303	0	16.8	(350)	850	0.6	352 ⁿ		
+ cyclohexane	313	0	16.8	335	820	0.6	330 ^o		
+ cyclohexane	323	0	16.8	320	780	0.6	320 ^p		
m-Xylene									
+ cyclohexane	303	0	14.3	(280)	700	0.6	283 ^q		
+ cyclohexane	313	0	14.3	270	670	0.6	248 ^r		
+ cyclohexane	323	0	14.3	260	650	0.6	235 ^r		
p-Xylene									
+ cyclohexane	303	0	16.6	(325)	810	0.7	326 ^s		
+ cyclohexane	313	0	16.6	310	780	0.7	288 ^t		
+ cyclohexane	323	0	16.6	290	750	0.7	248 ^u		
Di-n-propyl ether									
+ n-octane	363	0	(-0)	0	-10	-0.1	-0 ^v		
+ n-heptane	343	0	5	(70)	190	0.5	68 ^w		
+ n-heptane	298	0	5	85	230	0.4	302 ^x		
Dichloro methane									
+ n-hexane	298	0.024	15	450	(1320)	0.9	1319 ^y	0.724 ^y	
+ n-heptane	298	0.05	16	420	(1395)	1.2	1395 ^y	0.782 ^y	
Chloroform									
+ n-hexane	298	0	5	320	(750)	0.3	756 ^z	0.335 ^z	
+ n-heptane	298	-0	4.5	300	(800)	0.6	797 ^z	0.501 ^z	
+ carbon tetrachloride ($\eta_{ij} = 1$)	298	0	6	(110)	300	0.3	107 ^z	230 ^{aa}	0.17 ^z
Carbon tetrachloride									
+ cyclopentane	298	0	1	(30)	50	-0.04	34 ^{ac}	77 ^{ac}	-0.035 ^{ac}
+ cyclohexane	298							80 ^{ad}	
+ cyclohexane	298	0	3	(70)	170	0.15	70 ^{ae}	148 ^{ad}	0.165 ^{ae}
+ cyclohexane	298	0						166 ^{ad}	
+ n-hexane	298	0	0	160	290	-0.2	149 ^k	316 ^f	0.044 ^f
+ n-hexane	300							297 ^g	
+ n-heptane	298	-0	0	160	350	0.1	134 ^{ah}	339 ^f	0.213 ^f
Ethyl bromide									
+ n-heptane	303	0	11	(240)	860	1.1	244 ^{ai}		
Carbon disulfide									
+ cyclohexane	293	0.01	0	170	430	0.1	-240 ^{aj}		
+ 2-methylbutane	290	0.01	0	590	1060	-0.8	-460 ^{ak}		

Diethylamine	278	0	13.8	(250)	650	0.7	251 ^{al}	740 ^{ak}	
+ n-pentane	308	0	15.4	(250)	750	1.3	248 ^{am}		
+ n-heptane	298	0	15.4	240	780	1.3	742 ^{am}		
+ n-heptane	318	0	15.4	230	720	1.4	671 ^{am}		
+ n-heptane	328	0	15.4	220	690	1.5	205 ^{am}		
Trimethylamine									
+ n-hexane	293	0	5	67	180	0.3	61 ^{an}		
+ n-hexane	283	0	5	(70)	200	0.3	71 ^{an}	(370) ^{an}	
+ n-hexane	273	0	5	76	210	0.3	82 ^{an}		
+ n-hexane	263	0	5	81	230	0.3	95 ^{an}		
+ n-hexane	243	0	5	93	260	0.3	103 ^{an}	(250) ^{an}	
+ n-hexane	223	0	5	110	290	0.3	119 ^{an}		
Triethylamine									
+ n-heptane	333	0	1	(15)	40	0.1	16 ^{ao}		
+ n-heptane	353	0	1	13	40	0.1	13 ^{ao}		
+ n-heptane	293	0	1	19	50	0.1	67 ^{ao}		
+ n-heptane	396	0	1	18	50	0.1	84 ^{ao}	0.11 ^{ao}	
+ n-heptane	318	0	1	16	50	0.1	95 ^{ao}		

^aE. W. Funk and J. M. Prausnitz, *Ind. Eng. Chem.*, **62**, 8 (1970).

^bV. Mathot and A. Demeyer, *J. Chem. Phys.*, **21**, 182 (1953).

^cP. C. Li, B. C. Y. Lu, and E. C. Chen, *J. Chem. Eng. Data*, **18**, 305 (1973).

^dG. Scatchard, S. E. Wood, and J. M. Mochel, *J. Phys. Chem.*, **43**, 119 (1939).

^eR. M. Noordzij, *Helv. Chim. Acta*, **39**, 637 (1956).

^fM. B. Ewing, K. N. Marsh, R. H. Stokes, and C. W. Tuxford, *J. Chem. Thermodyn.*, **2**, 751 (1970).

^gS. E. Wood and A. E. Austin, *J. Amer. Chem. Soc.*, **67**, 480 (1945); R. J. Powell and F. L. Swinton, *J. Chem. Eng. Data*, **13**, 260 (1968).

^hR. H. Stokes, B. J. Lovien, and K. N. Marsh, *J. Chem. Thermodyn.*, **2**, 43 (1970).

TABLE III: Excess Functions of the Binary Systems with Parameters $\eta_{ij} = \eta_{ji} = \eta_{ij} = 0$, $\Delta_{ij} > 0$, $\eta_{ij} > 0$, and $\nu_{ij} > 0$

System	T	Δ_{ij}/k	Calculated values					Observed values		
			η_{ij}/k	ν_{ij}	ν^E	H^E	ν^E	G^E	H^E	ν^E
Acetone										
+ carbon disulfide ($T^C = 265$)	308	0	134	98.5	(1350)	(1460)	2.1	1050 ^a	1460 ^b	1.06 ^b
+ methylcyclohexane ($T^C = 278$)	318	0.01	143	98.5	(1120)	2480	3.2	1118 ^c		
+ n-hexane ($T^C = 264$)	318	0.01	131	98.5	(1340)	2550	2.2	1040 ^d		
+ 2,2,4-trimethylpentane ($T^C = 251$)	308	0.048	117	98.5	(954)	2390	2.0	954 ^e		
1,4-Dioxane										
+ cyclohexane ($T^C = 265$)	298	0	110	93	(1280)	(1610)	0.8	1090 ^f	1600 ^g	0.95E ^h
+ cyclohexane	303	0	110	93	1370	1690	0.8	1067 ^f		0.97E ^h
+ cyclohexane	313	0	110	93	1350	1850	1.0	1014 ^f		1.01E ^h
Tetrafluoroethane										
+ methane ($T^C = 94.5$)	107	0	26.5	19 ⁱ	(340)	650	0.6	340 ^j		0.88 ^k
+ methane	98	0	29.0	19 ⁱ	(430)	570	0.6	435 ^m		
Perfluoropropane										
+ propane ($T^C = 196.2$)	213.6	0	83	52	(850)	(1410)	3.9	854 ⁿ	1410 ⁿ	
+ ethane ($T^C = 165.5$)	188.3	0	80	52	(690)	1200	2.7	690 ⁿ		
Perfluoro-n-butane										
+ n-butane ($T^C = 232.2$)	245	0	86	48	(1010)	(1740)	5.4	1020 ^o	1740 ^o	
Perfluoro-n-pentane										
+ n-pentane ($T^C = 265.5$)	285	0	127	75	(1180)	(2010)	8.3	1180 ^o	2010 ^o	
Perfluoro-n-hexane										
+ n-hexane ($T^C = 295.85$)	308	0	143	81	(1320)	(2160)	10.6	1320 ^o	2160 ^o	4.84 ^q
Perfluoro-n-heptane										
+ n-heptane ($T^C = 323.2$)	323	0	148	89 ^j	(1310)	1650	11.0	1310 ^o		5.7 ^r
Perfluoromethylcyclohexane										
+ cyclohexane ($T^C = 315$)	338	0	122	75 ^j	(1350)	2450	9.3	1347 ^s	2007 ^t	5.48 ^u
+ methylcyclohexane ($T^C = 320$)	338	0	125	75 ^j	(1380)	2310	9.0	1385 ^v	2800 ^v	4.96 ^v
Perfluorobenzene										
+ cyclohexane ($T^C = 225$)	313	0	79.8	67	(970)	(1520)	2.8	791 ^w	1517 ^w	2.561 ^w
+ cyclohexane	298	0	79.8	67	810	1520	2.5	1576 ^x		
+ cyclohexane	333	0	79.8	67	720	1520	3.2	728 ^y	1483 ^y	
+ methylcyclohexane ($T^C = 225$)	313	0	71.5	67	660	(1270)	2.4	1275 ^z		2.214 ^z
+ methylcyclohexane	298	0	71.5	67	690	1260	2.2	1315 ^z		
+ methylcyclohexane	333	0	71.5	67	620	1280	2.8	1239 ^z		
Methylamine										
+ n-butane ($T^C = 223$)	273	0	192.5	136	(920)	(1730)	0.2	920 ^{aa}	(1730) ^{aa}	
+ n-butane	263	0	192.5	136	950	1490	-0.1	952 ^{ab}		
+ n-butane	243	0	192.5	136	960	780	-0.7	999 ^{ab}		
+ n-butane	233	0	192.5	136	950	290	-0.9	1015 ^{ab}	(1330) ^{ab}	
+ n-butane	223	0	192.5	136	900	-490	-1.2	1026 ^{ab}		
Methylamine (cont.)										
+ n-hexane ($T^C = 223$)	283	0	229	151	(930)	(1980)	1.9	934 ^{ac}	(1980) ^{ac}	
+ n-hexane	273	0	229	151	960	1830	1.4	971 ^{ac}		
+ n-hexane	263	0	229	151	990	1580	1.0	1003 ^{ac}		
+ n-hexane	253	0	229	151	1000	1230	0.5	1030 ^{ac}	(1530) ^{ac}	
+ n-hexane	223	0	229	151	940	-560	-0.7	1084 ^{ac}		
+ n-nonane ($T^C = 225$)	283	0	242	157	(940)	(2300)	2.9	940 ^{ad}	(2300) ^{ad}	
+ n-nonane	273	0	242	157	990	2190	2.3	987 ^{ad}		
+ n-nonane	263	0	242	157	1030	1960	1.8	1029 ^{ad}		
+ n-nonane	243	0	242	157	1070	1260	0.8	1099 ^{ad}	(1870) ^{ad}	
+ n-nonane	233	0	242	157	1070	750	0.3	1125 ^{ad}		
Ethylamine										
+ n-butane ($T^C = 197$)	283	0	94.4	87	(690)	(1400)	0.6	692 ^{ae}	(1400) ^{ae}	
+ n-butane	273	0	94.4	87	720	1360	0.4	715 ^{ae}		
+ n-butane	263	0	94.4	87	740	1300	0.3	737 ^{ae}		
+ n-butane	243	0	94.4	87	780	1140	0.0	772 ^{ae}		
+ n-butane	233	0	94.4	87	790	970	-0.1	790 ^{ae}	(1080) ^{ae}	
+ n-butane	223	0	94.4	87	790	690	-0.3	797 ^{ae}		
+ n-hexane ($T^C = 202$)	283	0	95	88	700	(1580)	1.9	700 ^{af}	(1580) ^{af}	
+ n-hexane	273	0	95	88	730	1560	1.6	730 ^{af}		
+ n-hexane	263	0	95	88	760	1510	1.4	753 ^{af}		
+ n-hexane	243	0	95	88	810	1360	0.9	799 ^{af}	(1230) ^{af}	
+ n-hexane	233	0	95	88	830	1140	0.7	807 ^{af}		
n-Propylamine										
+ n-hexane ($T^C = 188$)	283	0	59.2	66	(600)	(1270)	1.2	603 ^{ag}	(1270) ^{ag}	
+ n-hexane	273	0	59.2	66	620	1250	1.0	624 ^{ag}		
+ n-hexane	263	0	59.2	66	640	1230	0.9	637 ^{ag}		
+ n-hexane	253	0	59.2	66	670	1190	0.8	659 ^{ag}		
Aniline										
+ cyclohexane ($T^C = 314$)	323	0	79	68	(1400)	(2090)	-0.2	1400 ^{ah}	2090 ^{ah}	
+ cyclohexane	343	0	79	68	1350	2360	-0.3	1353 ^{ah}		
+ methylcyclohexane ($T^C = 331$)	353	0	76.5	68	(1420)	2520	-0.2	1420 ^{ah}		
+ methylcyclohexane	363	0	76.5	68	1390	2610	-0.2	1395 ^{ah}		
+ methylcyclohexane	373	0	76.5	68	1350	2680	-0.3	1360 ^{ah}		
Pyridine										
+ cyclohexane ($T^C = 215$)	298	0	39.5	50	740	(1430)	0.2	1430 ^{ai}	0.52 ^{ai}	
+ methylcyclohexane ($T^C = 218$)	298	0.002	36	50	760	(1510)	0.2	1500 ^{ai}	0.37 ^{ai}	
+ ethylcyclohexane ($T^C = 216$)	298	0.010	36.5	50	740	(1580)	0.5	1580 ^{ai}		
+ n-heptane ($T^C = 259$)	353	0.008	39.6	50	(900)	2080	-0.1	904 ^{aj}		
+ n-octane ($T^C = 253$)	353	0.022	39	50	(870)	2140	0.5	870 ^{aj}		
+ n-nonane ($T^C = 252$)	353	0.036	38.5	50	(860)	2230	1.0	858 ^{aj}		

System	T	Δ_{ij}/k	η_{ij}/k	ν_{ij}	ν^E	H^E	ν^E
Acetonitrile							
+ n-pentane ($T^C = 347$)	363	0.024	270.5	170	(1520)	(3200)	-2.0
+ n-pentane	393	0.054	270.5	170	1370	3710	-2.1
Hydrogen chloride							
+ xenon ($T^C = 155$)	195.42	-0	(36) ^{ak}	(0) ^{ak}	650	1780	0.8
+ xenon	182.26	-0	(36)	(0)	730	1870	0.7
+ xenon	159.07	-0	(36)	(0)	870	1750	0.6

^{aj}J. Zawidzki, *Z. Phys. Chem. Stoechiom. Verwandtschaftslehre*, **35**, 129 (1900).
^{ak}L.A.K. Stevely, W.J. Tupman and K.R. Hart, *Trans. Faraday Soc.*, **51**, 323 (1955).
^{al}R.V. Oye and J.M. Prausnitz, *Trans. Faraday Soc.*, **61**, 1338 (1965).
^{am}K. Schäfer and W. Rall, *Z. Elektrochem.*, **62**, 1090 (1958).
^{an}J.L. Edwards and K. Schäfer, *Z. Naturforsch.*, **19**, 136 (1964).
^{ao}J.D. Deshpande and S.L. Oswal, *J. Chem. Soc. Faraday Trans. 1*, **68**, 1059 (1972).
^{ap}A.W. Andrews and K.W. Morcom, *J. Chem. Thermodyn.*, **3**, 513, 519 (1971).
^{aq}P.R. Naidu and V.R. Krishna, *Trans. Faraday Soc.*, **64**, 1347 (1965).
^{ar}Estimated by a correlation of ν_{ij} of perfluoro-n-alkanes.
^{as}J.N. Thorp and R.L. Scott, *J. Phys. Chem.*, **60**, 670 (1956).
^{at}J.M. Croll and R.L. Scott, *J. Phys. Chem.*, **62**, 954 (1958).
^{au}M. Simon and C.M. Knobler, *J. Chem. Thermodyn.*, **3**, 657 (1971).
^{av}J.B. Gilmore, J.O. Zwicker, J. Katz, and R.L. Scott, *J. Phys. Chem.*, **71**, 3259 (1967), and the references there given.
^{aw}R.D. Dunlap, R.G. Bedford, J.C. Woodbey, and S.D. Furrow, *J. Amer. Chem. Soc.*, **81**, 2927 (1959).
^{ax}A.G. Williamson and R.L. Scott, *J. Phys. Chem.*, **65**, 275 (1961).
^{ay}R.G. Bedford and R.D. Dunlap, *J. Amer. Chem. Soc.*, **80**, 282 (1958).
^{az}R.L. Scott, *J. Phys. Chem.*, **62**, 136 (1958).
^{ba}D.E.L. Dye, J.S. Rowlinson, and R. Thacker, *Trans. Faraday Soc.*, **55**, 903 (1959).
^{bb}J. Powell and F.L. Swinton, *J. Chem. Thermodyn.*, **2**, 87 (1970).
^{bc}W.J. Gaw and F.L. Swinton, *Trans. Faraday Soc.*, **64**, 537 (1968).
^{bd}A. Andrews, K.W. Morcom, W.A. Duncan, F.L. Swinton, and J.M. Pollock, *J. Chem. Thermodyn.*, **2**, 95 (1970).
^{be}W.A. Duncan, J.P. Sheridan, and F.L. Swinton, *Trans. Faraday Soc.*, **62**, 1090 (1966).
^{bf}H. Wolff, A. Höpfner, and H. Höpfner, *Ber. Bunsenges. Phys. Chem.*, **68**, 410 (1964).
^{bg}H. Wolff and A. Höpfner, *Ber. Bunsenges. Phys. Chem.*, **66**, 149 (1962).
^{bh}S.M. Hosseini and G. Schneider, *Z. Physik. Chem. Frankfurt am Main*, **36**, 137 (1963).
^{bi}K. Sosnkowska-Kehiaian and H. Kehiaian, *Bull. Acad. Pol. Sci. Ser. Sci. Chim.*, **14**, 573 (1966).
^{bj}G. Schneider, *Z. Physik. Chem. Frankfurt am Main*, **24**, 165 (1960).
^{bk}W. Wójcicki and K.W. Sadowska, *Bull. Acad. Pol. Sci. Ser. Sci. Chim.*, **16**, 147 (1968).
^{bl}W. Wójcicki, *J. Chem. Thermodyn.*, **4**, 1 (1972).
^{bm}Z. Moczyńska, *Bull. Acad. Pol. Sci. Ser. Sci. Chim.*, **1**, 225 (1963).
^{bn}Calculated by the authors from the liquid-vapor equilibrium data at pressures of 2 to 11 bar, determined by A.C. Zawisza and S. Głowka, *Bull. Acad. Pol. Sci. Ser. Sci. Chim.*, **17**, 373 (1969).
^{bo}J.C.G. Calado, A.F. Kozdon, P.J. Morris, M. Nunez da Ponte, L.A.K. Stevely, and L.A. Woolf, "Third International Conference on Chemical Thermodynamics," Vol. II, Baden, Austria, 1973, p. 176. The results are not discussed as they were added in the proofs. The values were predicted from eq 7 ($\nu_{ij} = \nu_{ji} = 0$; $\eta_{ij}/k = 36$ K) neglecting the effects of association of HCl ($\nu_{ij} = 0$) that appear to be moderately strong.

TABLE IV: Average Values of the Coupled Parameters η_{ij} and ν_{ij}

System	η_{ij}/k	ν_{ij}	η_{ij}/k	ν_{ij}
Benzene	11	0	Perfluoromethylcyclohexane	123
Toluene	8	0	Perfluorobenzene	79.8
n-Xylene	16.8	0	Dichloromethane	15.5
m-Xylene	14.3	0	Chloroform	5
p-Xylene	16.6	0	Carbon tetrachloride	1
Dimethyl ether	25 ^a	0 ^b	Ethyl bromide	11
Di-n-propyl ether ^c	5	0	Carbon disulfide	-0
Acetone	134	98.5	Methylamine	(192.5)
1,4-Dioxane	110	93	Ethylamine	94.7
Tetrafluoroethane	27.8	19 ^d	n-Propylamine ^d	59.2
Perfluorobenzene			Diethylamine	14.5

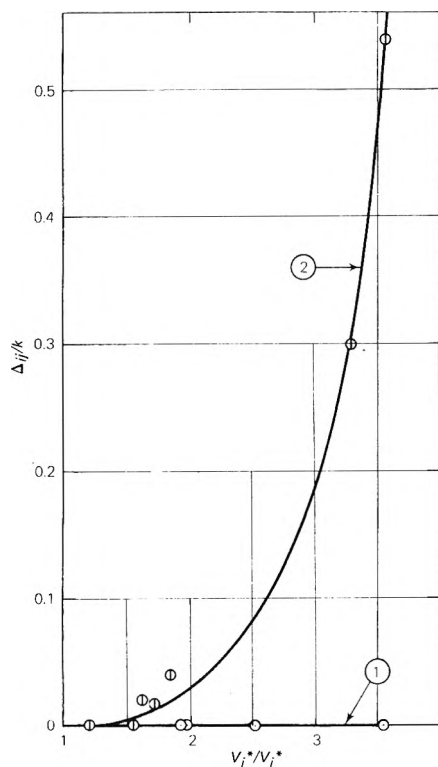


Figure 2. The parameter Δ_{ij}/k as function of V_j^*/V_i^* (where $V_i^* \geq V_j^*$). Data from Table I: line 1, two chain molecules (including CH_4 , CF_4); line 2, chain + globular or two globular molecules.

combining rule for η_{nij} of two inert components, we had to fit two parameters, n_{nij} and Δ_{ij} , to G^E and H^E or V^E data. The agreement with the observed value of V^E or H^E was always satisfactory.

Random Mixtures (Weak Specific $j + j$ Interactions). For these systems, given in Table II,¹⁴ ν_{ij} must be negligible and one parameter, η_{ij} , suffices to obtain a satisfactory agreement for the excess functions and the gas-liquid critical temperatures. The parameters $\chi_{jj}^c = \eta_{jj}/(kT_j^c)$, fitting the $T^c(\varphi)$ data, are given elsewhere.⁶ The values of V^E are less satisfactory but the errors seldom exceed 100%.

The parameters η_{jj} for a given compound, e.g., C_6H_6 , in various solvents obtained by using the simple theory of conformal mixtures are practically the same.⁶ Unfortunately, the hard-sphere equation appears to be more sensitive to the size and the shape of solvent molecules. An average value of η_{jj} , e.g., $\eta_{jj}/k = 11$ for C_6H_6 , will be suitable for estimating only the values of G^E , H^E , and $T^c(\varphi)$.

The theory of noncentral forces yields practically the same results. In this case (not shown in Table II or III)¹⁴ η_{nii} and η_{njj} were calculated from eq 7 and η_{nij} was fitted to G^E .

Nonrandom Mixtures (Moderate Specific $j + j$ Interactions). The systems exhibiting clustering, association, or both are collected in Table III.¹⁴ The value of T^{cs} used to evaluate ΔH^c and ΔG^c is given next to the name of the solvent (experimental values¹⁵ only for perfluoroalkane systems). In any case, when $T/T^{cs} \geq [B_0/(2D_0)]^2 + 1$ the corrections were neglected. The $T^c(\varphi)$ curves obtained with parameters fitting both G^E and H^E agree much better with the T^c data when Rowlinson's theory is applied (dashed curve 3 in Figure 1) as compared with that ignoring noncentral forces (curve 2). The superiority of the theory of

noncentral forces shows also in cases of large excess volumes. For the $n\text{-C}_6\text{H}_{14} + n\text{-C}_6\text{F}_{14}$ system, the observed value of $V^E/\text{cm}^3 \text{ mol}^{-1}$ is 4.84, Balescu's theory yields 10.6 (Table III), whereas the theory of noncentral forces give 5.8.

Figure 3 shows the effects of large size differences and ΔH^c on the symmetry of the excess functions. The G^E curve is well reproduced by "counting" the interactions between equivalent surfaces (surface fractions). The H^E curve appears inside the observed curve. In general, in the vicinity of T^{cs} , H^E is not only smaller than for a random mixture but the curve is flatter at the top. The term ΔH^c has the right qualitative effect on the shape of the curve, but it is not quite sufficient to give an exact agreement with the experimental results.

Among the systems for which $\nu_{ij} > 0$, given in Table III,¹⁴ aliphatic amines are particularly interesting due to their chemical nature and the availability of the outstanding data of Wolff and Höpfner. For CH_3NH_2 both G^E and H^E begin to decrease too rapidly at the lowest temperatures, whereas for $\text{C}_2\text{H}_5\text{NH}_2$, $\text{C}_3\text{H}_7\text{NH}_2$, and the other amines (R_2NH and R_3N given in Table II because $\nu_{ij} \approx 0$) the agreement is satisfactory. Thus, the behavior of CH_3NH_2 shows the limits of this treatment. We cannot expect any agreement with experimental data when the bridges (hydrogen or other) are stronger than the N...H bridge, as for example the O...H bridges in alcohols.

A Test for Ideal Associated Solutions. An ideal associated solution is formed by components whose London energies ϵ^0 and the collision diameters are equal, and thus in absence of association the mixture would be ideal. Extensive calculations of equilibrium constants were carried out for the toluene + aniline system assuming that it is an ideal associated solution¹⁶ and that toluene is an inert solvent. The results obtained in the present work allow us to estimate how much a given system deviates from this concept.

Assuming that V_i^* is the same in presence of specific interactions as it would be in their absence, we obtain from eq 2 and 3, $T_0^c = T^c[1 + (\eta/kT^c)]^{-1}$, where T_0^c is the hypothetical critical temperature due to London forces alone. For the values $\eta_{11}/k = 8$ for toluene and $\eta_{22}/k = 77.8$ for aniline (Table IV¹⁴) we get $T_{01}^c = 583.8$ ($T_1^c = 591.72$ K) and $T_{02}^c = 629$ ($T_2^c = 698.8$ K). By using these values of T_0^c and setting all the η 's and ν 's equal to zero (two inert components), we obtain at 298 K and $x = 0.5$: $G^E = 70$, $H^E = 100 \text{ J mol}^{-1}$, and $V^E = -0.1 \text{ cm}^3 \text{ mol}^{-1}$. Estimating an uncertainty of $\pm 50 \text{ J mol}^{-1}$ for G^E and $\pm 150 \text{ J mol}^{-1}$ for H^E , we confirm that the values of excess functions due to inequality of the London energies are very small and the observed large values are due to association of aniline.

Conclusions

We have established on the firm foundation made of hard spheres that, in order to evaluate a complete PVT diagram of a mixture, the calculations should be based on the theory of noncentral forces. For gases and gaseous mixtures, whose molecules are nonspherical but interact through London forces alone, a part of the ϵ 's doubtless varies with T^{-1} and so $\eta_n > 0$. Also in the liquid state, in extreme cases of large G^E and ν_{ij} , the above theory leads to better results for V^E and a better agreement with $T^c(\varphi)$ than does the theory of Balescu. However, there remains the problem of a combining rule for η_{nij} in mixtures of inert components.

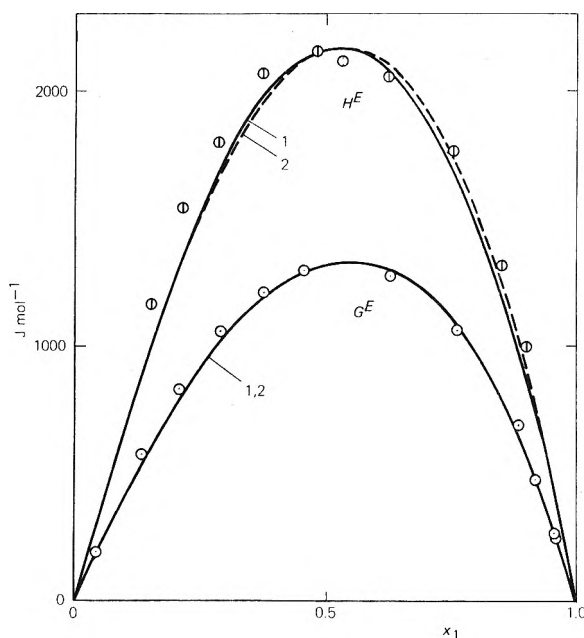


Figure 3. The excess functions of the *n*-hexane + perfluoro-*n*-hexane system at 308 K. x_1 is the mole fraction of the inert component. The experimental points were determined by Dunlap, Bedford, Woodbrey, and Furrow for G^E , and by Williamson and Scott for H^E (for references see Table III¹⁴). The curves were calculated (1) from Balescu's theory ($\eta_{ii}/k = \eta_{ij}/k = 0$, $\eta_{jj}/k = 143$, $\nu_{ij}/k = 81$), and (2) from Rowlinson's theory ($\eta_{ii}/k = 123$, $\eta_{ij}/k = 71$, $\eta_{jj}/k = 183$, $\nu_{ij}/k = 105$, where η_{ii}/k and η_{ij}/k were evaluated from eq 7). $\Delta G^E = -40$, $\Delta H^E = -640$ J mol⁻¹ at $x = 0.5$.

If we limit our aims to the correlation of liquid-vapor equilibrium diagrams, *i.e.*, G^E and H^E over a range of temperatures (where the role of V^E is negligible), the two theories leading to similar results. The theory of Balescu is more promising if our aim is the prediction of such diagrams because of the simple combining rules, eq 4 and 5. These rules and the values of η_{ij}/k and ν_{ij}/k , given in Table IV, offer an opportunity to distinguish between "physical" and "chemical" interactions in complex systems, that will be considered later in part II. For these reasons we paid in this work more attention to the theory of Balescu.

In a parallel research on the internal energies of pure liquids, we obtained additional results in favor of the theory of noncentral forces. The van der Waals parameter $a_i^c/(RT_i^c V_i^{*c})$ at the critical point evaluated from gas compressibility data was found to vary from 4.5 to 4.8 and a rounded value, 4.7, was used in the calculations of the properties of mixtures (eq 1). If critical constants, T^c , P^c , and V^c are inserted into the equation of state $PV/(RT) = \phi(\xi) - a_i/(RTV)$, where as before¹ $\xi = 0.434V_i^*/V$, one obtains a much more constant value

$$a_i^c/(RT_i^c V_i^{*c}) = 4.65 \quad (18)$$

with an average deviation ± 0.02 and a maximum deviation ± 0.04 for nine very different substances. This value, in striking agreement with that from the PVT data of gases, allows us to obtain better values of V at given T and P .

Table V¹⁴ shows the liquid molar volumes at $T/T^c = 0.6$, calculated by setting $P = 0$ and either $\eta_n/k = 0$ or $\eta_n/k =$

$0.833\omega T^c$ and compared with the observed values.⁶ By neglecting the presence of noncentral forces one obtains always too large values of V . The theory of noncentral forces predicts that the effective collision diameters will be smaller than in absence of such forces.³ We note that the liquid volumes are accordingly diminished by the presence of such forces and that the results are very satisfactory for η_n/k not exceeding about 120 K. For $C_{10}H_{22}$ and C_6F_{14} about half of η_n/k calculated from eq 7 would yield correct values of V .

On the contrary, the values of η_n/k obtained from the residual energies of liquids¹⁷ are for CF_4 and C_6F_{14} larger than η_n/k from eq 7. They imply that an additional contribution, η_s/k , mentioned in the introduction, in fact exists in fluids with specific interactions. The values of η/k obtained from U^r must be preferred because the equation of state yields satisfactory values of A^r , U^r , A^E , and H^E but is not accurate enough for predicting the much smaller quantities PV and PV^E at $P \rightarrow 0$.

In this paper, we tried to distinguish various kinds of ordering effects and to apply separate corrections for each. For many reasons they are unsatisfactory and perhaps better solutions may be found.

Acknowledgments. This investigation was supported in part by the Thermodynamics Research Center and the Texas Engineering Experimental Station of Texas A & M University.

Miniprinted Material Available. Full-sized photocopies of the miniprinted material (Tables I-V) from this paper only or microfiche (105 × 148 mm, 24× reduction, negatives) containing all of the supplementary material for the papers in this issue may be obtained from the Journals Department, American Chemical Society, 1155 16th St., N.W., Washington, D.C. 20036. Remit check or money order for \$4.00 for photocopy or \$2.00 for microfiche, referring to code number JPC-74-1961.

References and Notes

- (1) A. Kreglewski, R. C. Wilhoit, and B. J. Zwolinski, *J. Phys. Chem.*, **77**, 2212 (1973).
- (2) D. Cook and J. S. Rowlinson, *Proc. Roy. Soc., Ser. A*, **219**, 405 (1953); J. S. Rowlinson and J. R. Sutton, *ibid.*, **229**, 271 (1955).
- (3) J. S. Rowlinson, "Liquids and Liquid Mixtures," Butterworths, London, 1959.
- (4) R. Balescu, *Bull. Cl. Sci., Acad. Roy. Belg.*, **41**, 1242 (1955); see also I. Prigogine, A. Bellemans, and V. Mathot, "The Molecular Theory of Solutions," North-Holland Publishing Co., Amsterdam, 1957.
- (5) A. Kreglewski and W. B. Kay, *J. Phys. Chem.*, **73**, 3359 (1969).
- (6) A. Kreglewski, "Mixtures of Fluids," API44—TRC Publications in Science and Engineering, Thermodynamics Research Center, Texas A & M University, College Station, Tex., 1973.
- (7) B. E. F. Fender and G. C. Halsey, Jr., *J. Chem. Phys.*, **36**, 1881 (1962).
- (8) H. M. Lin and R. L. Robinson, Jr., *J. Chem. Phys.*, **54**, 52 (1971).
- (9) W. J. Gaw and R. L. Scott, *J. Chem. Thermodyn.*, **3**, 335 (1971).
- (10) M. Fixman, *Advan. Chem. Phys.*, **6**, 175 (1964).
- (11) F. Becker and M. Kiefer, "Third International Conference on Chemical Thermodynamics," Vol. II, Baden, Austria, 1973, p 131.
- (12) I. Saroiea, *J. Chem. Phys.*, **21**, 182 (1953).
- (13) R. J. Powell, F. L. Swinton, and C. L. Young, *J. Chem. Thermodyn.*, **2**, 105 (1970).
- (14) See paragraph at end of text regarding miniprinted material.
- (15) J. B. Gilmour, J. O. Zwicker, J. Katz, and R. L. Scott, *J. Phys. Chem.*, **71**, 3259 (1967).
- (16) H. Kehiaian and K. Sosnkowska-Kehiaian, *Trans. Faraday Soc.*, **62**, 838 (1966).
- (17) A. Kreglewski, *J. Phys. Chem.*, **78**, 1241 (1974).

Apparent Quadrupole Moments of Carbon Monoxide and Nitrogen and Their Librational Motion in the Liquid State

Ralph L. Amey*

Edward Davies Chemical Laboratories, University College of Wales, Aberystwyth SY23 1NE, United Kingdom (Received July 3, 1973; Revised Manuscript Received April 26, 1974)

The far-infrared absorption spectra of compressed carbon monoxide at 300 K have been measured from 10 to 100 cm^{-1} at pressures up to 102 atm ($1.03 \times 10^7 \text{ N m}^{-2}$). An apparent quadrupole moment for the compressed gas is calculated and compared with values of Q_{apparent} for pure CO and N_2 computed from published far-infrared spectra of liquid CO and liquid N_2 . It is concluded that $Q(\text{CO}) \leq Q(\text{N}_2)$, which is in disagreement with previous estimates of $Q(\text{CO})$. The molecular dynamics of liquid CO are analyzed in terms of the Larkin-modified models of Brot and Wyllie for hindered rotation. A very low barrier to molecular rotation (0.2–0.8 kJ/mol) and short dielectric relaxation (0.7–1.3 psec) and well residence times (0.7 psec) are predicted.

Introduction

A number of papers have been concerned recently with the assessment of molecular quadrupole moments of simple molecules.^{1–3} Several methods, both direct and indirect, have been used. The results in many cases have been difficult to interpret due to their large experimental uncertainty and lack of agreement with other published values. The isoelectronic character of nitrogen and carbon monoxide make them worthy of comparison. Several values of the quadrupole moments of these two molecules have been reported.¹ The values by Buckingham, *et al.*,⁴ are generally given the most serious consideration since they have been obtained by the direct method of induced birefringence.⁵ Gebbie, *et al.*,⁶ have reported the far-infrared spectrum of compressed nitrogen from which Poll⁷ calculated a quadrupole moment of 1.48×10^{-26} esu ($4.94 \times 10^{-40} \text{ C m}^2$) in good agreement with Buckingham's value of $-(1.4 \pm 0.1) \times 10^{-26}$ esu ($-4.7 \times 10^{-40} \text{ C m}^2$). The far-infrared absorption technique, though an indirect one, recently has been applied by others to both polar^{2,3} and nondipolar^{8–10} molecules with significant success.

We present here the results of far-infrared studies at room temperature on compressed carbon monoxide and the analysis of published far-infrared spectra of liquid carbon monoxide and liquid nitrogen. A maximum value for the quadrupole moment of carbon monoxide is estimated, and the molecular motions in liquid CO and liquid nitrogen are discussed in terms of the Brot–Wyllie–Larkin models of hindered rotation.

Experimental Section

The far-infrared spectra were obtained by Fourier spectroscopy¹¹ using a Grubb-Parsons NPL Michelson interferometer with a Golay detector. The range of 20–100 cm^{-1} was covered with a resolution of 4 cm^{-1} . The variable-path-length high-pressure sample cell which was used is described elsewhere.²

The gas, obtained from Matheson and Co., Ltd., was CP grade of nominal purity 99.5%. Total equivalent polar impurity concentration was less than 20 ppm. To a good first approximation, the integrated absorptions were propor-

tional to the $N\mu^2$ terms (see Results), and the presence of this level of polar impurity increased the absorption by less than 0.5% over what it would have been if no impurity had been present.

The pressure was measured on a Budenberg gauge with $\pm 1.5 \times 10^5 \text{ N m}^{-2}$ uncertainty. Gas densities were obtained from literature values.¹² All individual absorption spectra were obtained by ratioing the average of three transformed sample interferograms to the average of three transformed background interferograms. The background interferograms were obtained with the cell filled to approximately $5 \times 10^4 \text{ N m}^{-2}$ with carbon monoxide. Due to the high-pressure cell's design it was not feasible to evacuate it further without movement of the quartz windows and a resultant change in path length.

Results and Discussion

The transformed spectra are displayed in Figure 1. It is assumed that the absorption intensity arises from the pure rotational contribution of the permanent dipole and from induced dipoles resulting from the dipolar and quadrupolar fields of the CO molecule. The former effect is proportional to the number density (N) of polar molecules and the square of their dipole moment (μ^2), whereas the induced absorptions increase with N^2 .

Following the treatment of Baise² we write for the integrated intensity (I_{int})

$$\begin{aligned} I_{\text{int}} &= \int_{\text{band}} \alpha(\bar{\nu}) d\bar{\nu} = AN + A'N^2 \\ &= AN + A^\mu + A^Q \\ &= AN + (A_1 + A_2 Q^2)N^2 \\ &= 2.02 \times 10^{-20}N + (1.63 \times 10^{-44} + 2.83 \times 10^9 Q^2)N^2 \end{aligned}$$

where A^μ and A^Q are the temperature-dependent dipole- and quadrupole-induced integrated intensities respectively, $\alpha(\bar{\nu})$ is the absorption coefficient, and the molecular quadrupole moment Q is defined⁴ by $Q = \frac{1}{2} \sum_i e_i (3z_i^2 - r_i^2)$, where the notation has its usual meaning. We have

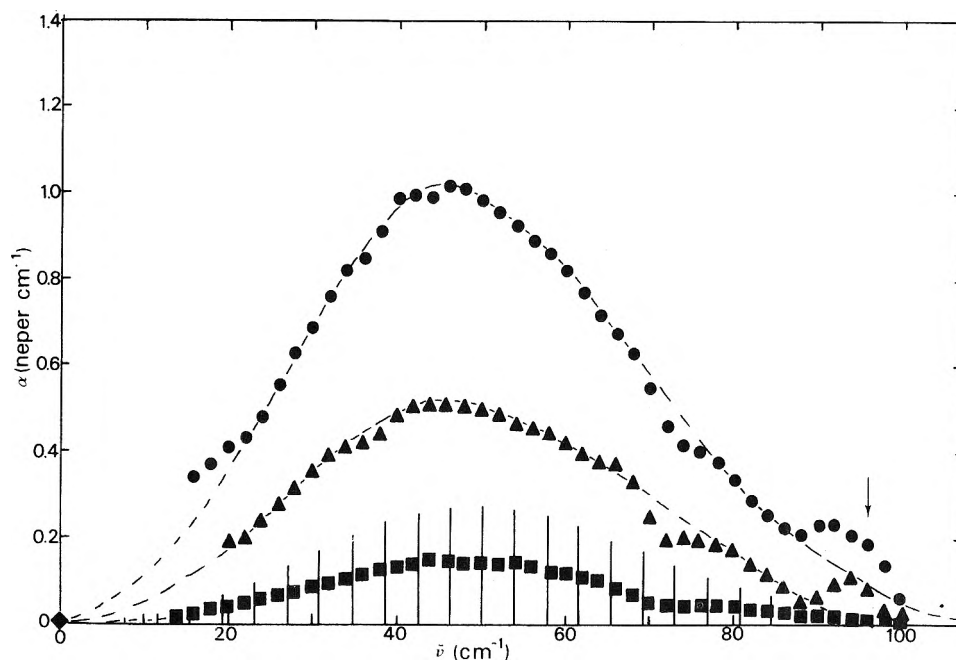


Figure 1. Far-infrared spectra of compressed gaseous carbon monoxide at 300 K: ■, 16.0 ± 0.1 atm ($10^{-20} N = 0.399 \pm 0.02$ molecule cm^{-3}); ▲, 50.0 ± 0.1 atm ($10^{-20} N = 1.24 \pm 0.02$ molecules cm^{-3}); ●, 102.0 ± 0.1 atm ($10^{-20} N = 2.47 \pm 0.02$ molecules cm^{-3}). The vertical lines give the frequencies and relative integrated intensities for some of the pure rotational ($J \rightarrow J + 1$) transitions. The dipole-induced transitions have the same frequencies and relative intensities as the pure rotational lines. The arrow indicates frequency of maximum relative integrated intensity for the quadrupole-induced ($J \rightarrow J + 2$) transitions.

evaluated A at 300 K both from Gordon's sum rules¹³ and from a summation of the individual $J \rightarrow J + 1$ transition intensities.¹⁴ These non-collision-broadened pure rotational line intensities are shown superimposed on the experimental spectra in Figure 1. Molecular parameters for CO used in these calculations were^{15,16} $\mu_{\text{gas}} = 0.112 \times 10^{-18}$ esu (0.37×10^{-30} C m) and moment of inertia 1.430×10^{-39} g cm^2 . The integrals in A^μ and A^Q were evaluated using the rotational constants¹⁶ $B = 1.9563$ cm^{-1} and $D = 6.13 \times 10^{-6}$ cm, the mean molecular polarizability¹⁷ $\alpha = 1.95 \times 10^{-24}$ cm^3 , the Lennard-Jones parameter¹⁸ $\epsilon/k = 32.8$ K (there is considerable variability in the values reported for this quantity; choice of extremum values for the calculation of Q however results in a ΔQ of only 0.1×10^{-26} esu), and the tables of Buckingham and Pople.¹⁹

A comparison of I_{int}/N and A for pressures up to 102 atm as well as an examination of Figure 1 indicates that within experimental error the absorption is due effectively to the permanent dipolar rotation spectrum and negligibly due to induced dipolar effects. The excess absorption at about 92 cm^{-1} is accepted as a foreign absorption of unknown origin (possibly water vapor) and has been neglected in establishing the CO absorption envelopes. It has been suggested that the dip at about 72 cm^{-1} may be caused by incomplete cancellation of effects produced by polyethylene in the radiation path. Hence the contours are drawn and evaluated to include a maximum absorption near 70 cm^{-1} so that Q_{app} is most likely a maximum value. The current literature values^{1,4,7} for $Q(\text{CO})$ are $Q(\text{CO})_{\text{av}} = -(2.4 \pm 0.3) \times 10^{-26}$ esu (8.0×10^{-40} C m^2). Neumann and Moskowitz recently reported²⁰ a self-consistent field MO calculation for CO which yielded a $Q_{\text{SCFMO}} = -2.1 \times 10^{-26}$ (7.0×10^{-40} C m^2). At 102 atm pressure, eq 1 indicates that a quadrupole moment of such magnitude would enhance the pure rotational spectrum by 18%, an increase which we do not observe. We estimate the uncertainty in our integrated

TABLE I: Computed Coefficients of Eq 1 for the Integrated Absorption Intensities of Carbon Monoxide and Nitrogen

	T, K	$10^{20}A, \text{cm}$	$10^{14}A_1, \text{cm}^4$	$10^{-20}A_{21}, \text{esu}^{-2}$
CO(g)	300	2.02	1.63	2.83
CO(l)	80.9	2.04	1.49	2.39
N ₂ (l)	76.4			5.34

absorption as no more than $\pm 7\%$, a value which allows an undetected value of $Q_{\text{app}} \leq 1.5 \times 10^{-26}$ esu (5.0×10^{-40} C m^2).

Since the quadrupolar contribution to the intensity increases with N^2 , we might expect an enhanced absorption in the liquid. Jones²¹ has reported the far-infrared spectra of several liquefied gases including nitrogen and carbon monoxide. We have computed the integrated absorption intensities for both liquids as well as the appropriate constants for eq 1 at the reported liquid temperatures. The computed values are listed in Table I. For nitrogen the molecular parameters used were $B = 1.961$ cm^{-1} , $D = 5.8 \times 10^{-6}$ cm, $I = 1.427 \times 10^{-39}$ g cm^2 , $\alpha_{\text{mean}} = 1.76 \times 10^{-24}$ cm^3 , $\epsilon/k = 47.6$ K. For liquid nitrogen then, the data yield an apparent quadrupole moment of $Q(\text{N}_2)_{\text{app}} = (0.8 \pm 0.1) \times 10^{-26}$ esu (2.7×10^{-40} C m^2). This value is only about half that reported from compressed gas results.⁷ Such a reduction in total absorptior from that expected on the basis of pure dipolar and binary interactions may be credited to a partial cancellation by multibody interactions in the liquid; this is due to the increased symmetry of the inducing electric fields present at high densities.²² A similar effect has been observed in nitrous oxide.²

From the spectrum of liquid CO, a similar calculation yields $Q(\text{CO})_{\text{app}} = (0.4 \pm 0.3) \times 10^{-26}$ esu (1.3×10^{-40} C m^2). This leads us to suggest that the upper limit for $Q(\text{CO})$ obtained from our compressed CO spectra may be a maxi-

TABLE II: Molecular Dipole and Apparent Quadrupole Moments of Carbon Monoxide and Nitrogen

	$10^{40}Q_{gas}, C m^2$	$10^{40}Q_{liq}, C m^2$	$10^{30}\mu, C m$
N ₂	4.9 ^a	2.7	0
CO	5.0	1.3	0.37 ^b

^a Reference 7, ^b Reference 15.

imum one. Indeed it appears that $Q(CO) \leq Q(N_2)$ and the best estimate for $Q(CO)$ may be as small as $(0.8 \pm 0.4) \times 10^{-26}$ esu $[(3 \pm 1) \times 10^{-40} C m^2]$. (See Table II.)

Although it would be anticipated that the short cylindrical CO molecule would have little hindrance on rotation in the liquid state, infrared spectra have provided some evidence of the barrier involved.²³ The small dipolar and quadrupolar fields of the molecule would imply small dispersion barriers of the order of 800 J/mol or less. Ewing has predicted²⁴ a barrier energy of approximately 500 J/mol for rotation at 80 K. We have applied the librational models of Brot and of Wyllie—as adapted by Larkin²⁵—to liquid CO. The theoretical curves have been normalized to the $\alpha(\max)$ of the experimental curve of the liquid and the results are shown in Figure 2 and Table III. Both models assume a central librating molecule with a coordination number which defines the angular aperture of the energy well containing the librator. Well definition and depth are then determined through parameters chosen to fit the observed spectrum. Ewing has suggested on the basis of infrared spectra that many of the molecules in liquid CO may experience an environment approaching that of hexagonal close packing, similar to that of the solid phase.²⁴ Neither model reproduces satisfactorily the experimental data over the entire frequency range. Adjustment of the parameters of the Wyllie model gives a somewhat improved fit with $\omega_0(\max) = 53 \times 10^{11}$ radians/sec (28 cm^{-1}), although the calculated quadrupole absorption maximum occurs at 91×10^{11} radians/sec (48 cm^{-1}). The Brot model incorporating the latter value of $\omega_0(\max)$ (which represents the librational frequency not seen as a separate center in the absorption) does not give a good fit as the Wyllie model: its half-width is too large and its high-frequency tail falls well below observations. The experimentally observed absorption maximum varies with choice of half-angular aperture (ξ) at constant V and provides a better fit at 0.75—corresponding to eight nearest neighbors—than at a coordination number of 10 ($\xi = 0.64$) found suitable for the Wyllie model.

A very low barrier to rotation is exhibited by both models: $V = 0.2$ – 0.8 kJ/mol. This can be compared with the distinctly larger barriers found for quasispherical molecules of larger electric moments ($\mu \approx 2$ D) such as 2,2-dichloropropane ($CH_3CCl_2CH_3$), 3–6 kJ/mol, and 2-chloro-2-nitropropane ($CH_3CClNO_2CH_3$) 7–8 kJ/mol, or for the slightly polar ($\mu = 0.78$ D) but distinctly anisotropic propyne ($CH_3C \equiv CH$), 5–6 kJ/mol. The lower value for liquid CO is consistent with its smaller dipole ($\mu = 0.12$ D) and its closer approximation to spherical symmetry (length/diameter = 1.3).

It is also observed that the time between weak thermal collisions (τ_i) is about the same as the duration of a jump from one well to another (τ_j) and about half the time spent while residing in a potential well (τ_r). This is consistent with relaxational mechanisms proposed by correlation function analysis of simple liquids.²⁶ Although the Debye

TABLE III: Brot and Wyllie Parameters for Liquid Carbon Monoxide at 80.9 K

Model	$V,^{b-d}$ kJ mol ⁻¹	r	$(\xi/2) -$ $kT,$				$\omega_0,$ 10^{12} radians sec ⁻¹
			10^{-12} sec	$\tau_r,$ 10^{-12} sec	$\tau_j,$ 10^{-12} sec	$\tau_i,$ 10^{-12} sec	
Brot ^a	0.81			0.7	0.3	0.5	9.1
Wyllie ^c	0.20	2.0	1.3				5.3

^a $\xi = 0.75$ radians, ^b $n_D 1.22$, calculated from the Lorentz–Lorenz equation, the mean polarizability,¹⁷ and the liquid density at 80.9 K, $\rho = 0.793$ g cm^{-3} ("Handbook of Chemistry and Physics," 49th ed, Chemical Rubber Co., Cleveland, Ohio, 1968–1969). ^c $\epsilon_{\infty} = n_D^2 = 1.480$. ^d $\epsilon_0 = 1.481$, estimated from the Clausius–Mossotti equation; $\mu = 0.112$ D, and the parameters of footnote b apply. ^e Coordination number 10.

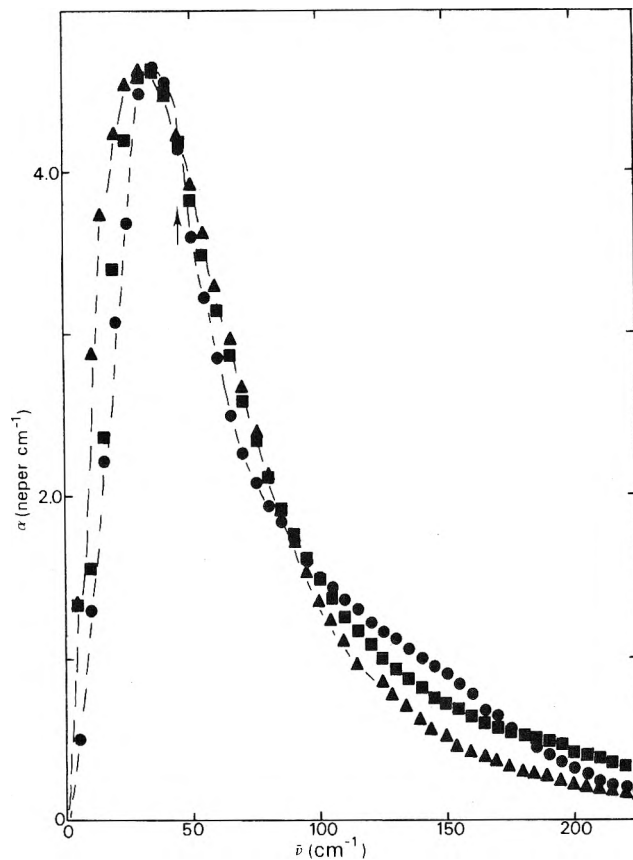


Figure 2. Far-infrared spectra of liquid carbon monoxide at 80.9 K: ●, smoothed experimental data from ref 21; ▲, data computed from Brot model; ■, data computed from Wyllie model. The arrow indicates frequency of maximum relative integrated intensity for the quadrupole-induced ($J \rightarrow J + 2$) transitions.

relaxation time (τ_D) for liquid CO has not been experimentally determined, the Brot model predicts $\tau_D \approx \tau_r \approx 0.7$ psec and the Wyllie model a value of similar magnitude: $\tau_D \approx (\xi/2)kT \approx 1.3$ psec.

We found that efforts to improve the fit of these models did not lead to significantly different computed quantities. Whether such models lead to physically correct molecular parameters is still an open question.²⁷ A further means of analyzing liquid data is in terms of the classical free rotational envelope, an expression for which has been derived recently by Brot²⁸

$$\alpha(\omega) = \frac{2\pi^2 N I \mu^2 |\omega|^3}{3(kT)^2 V} \exp\left(\frac{-I\omega^2}{2kT}\right)$$

where $\omega = 2\pi\nu c$ and I is the moment of inertia perpendicular

lar to the axis containing the dipole moment. This function has a maximum at $2\pi\nu_{\max}c = (3kT/I)^{1/2}$ which can be compared with the experimental ν_{\max} . Such a calculation for liquid CO yields $\nu_{\max}(\text{calcd}) = 26 \text{ cm}^{-1}$ and $\nu_{\max}(\text{exptl}) = 35 \text{ cm}^{-1}$ which suggests that molecules of CO in the liquid state are largely freely rotating. Thus these models are given qualitative support in that the resultant parameters are consistent with our expectations for the behavior of simple liquids: a very shallow potential well, a short dielectric relaxation time, and brief well residence times.

Acknowledgments. The author wishes to thank Professor Mansel Davies for suggesting the problem, for many helpful discussions, and for a critical reading of this manuscript. He is indebted to M. Evans for invaluable assistance with preliminary measurements and to A. Baise and I. Larkin for the use of their programs. He is also pleased to acknowledge the hospitality and assistance of the University College of Wales Chemistry Department and staff during his sabbatical stay.

References and Notes

* On sabbatical leave from Department of Chemistry, Occidental College, Los Angeles, Calif. 90041.

- (1) S. Kielich in "Dielectric and Related Molecular Processes," Vol. I, The Chemical Society, London, 1972.
- (2) (a) A. I. Baise, *J. Chem. Soc., Faraday Trans. 2*, **68**, 1904 (1972); *Chem. Phys. Lett.*, **9**, 627 (1971); (b) A. Rosenberg and I. Ozier, *ibid.*, **19**, 400 (1973).
- (3) M. Evans, *J. Chem. Soc., Faraday Trans. 2*, **69**, 763 (1973).
- (4) A. D. Buckingham, R. L. Disch, and D. A. Dunmur, *J. Amer. Chem. Soc.*, **90**, 3104 (1968).
- (5) A. D. Buckingham, *Quart. Rev., Chem. Soc.*, **23**, 183 (1959).
- (6) H. A. Gebbie, N. W. B. Stone, and D. Williams, *Mol. Phys.*, **6**, 215 (1963).
- (7) J. D. Poll, *Phys. Lett.*, **7**, 32 (1963).
- (8) D. R. Bosomworth and H. P. Gush, *Can. J. Phys.*, **43**, 751 (1965).
- (9) A. Rosenberg and G. Birnbaum, *J. Chem. Phys.*, **52**, 683 (1970).
- (10) J. E. Harries, *Proc. Phys. Soc., London (At. Mol. Phys.)*, **3**, 704 (1970).
- (11) K. D. Møller and W. G. Rothschild, "Far-Infrared Spectroscopy," Wiley-Interscience, New York, N. Y., 1971.
- (12) (a) E. P. Bartlett, H. C. Hetherington, H. M. Kvalnes, and T. H. Tremearne, *J. Amer. Chem. Soc.*, **52**, 1374 (1930); (b) *Nat. Bur. Stand. (U. S.), Circ.*, No. **564**, 219-236 (1955); "Matheson Gas Data Book," 5th ed, The Matheson Co., East Rutherford, N.J., 1971, p 105.
- (13) R. G. Gordon, *J. Chem. Phys.*, **38**, 1724 (1963).
- (14) C. H. Townes and A. L. Schawlow, "Microwave Spectroscopy," McGraw-Hill, New York, N. Y., 1955.
- (15) R. D. Nelson, D. R. Lide, and A. A. Maryott, *Nat. Stand. Ref. Data Ser., Nat. Bur. Stand.*, No. **10** (1967).
- (16) G. Herzberg, "Spectra of Diatomic Molecules" 2nd ed, Van Nostrand, New York, N. Y., 1950.
- (17) H. A. Stuart, "Molekülstruktur," Vol. 3, Springer-Verlag, West Berlin, 1967, p 35.
- (18) J. O. Hirschfelder, C. F. Curtiss, and R. B. Bird, "Molecular Theory of Gases and Liquids," Wiley, New York, N. Y., 1954.
- (19) A. D. Buckingham, J. A. Pople, *Trans. Faraday Soc.*, **51**, 1173 (1955).
- (20) D. B. Neumann and J. W. Moskowitz, *J. Chem. Phys.*, **50**, 2216 (1969).
- (21) M. C. Jones, *Nat. Bur. Stand. (U. S.), Tech. Note*, No. **390** (1970).
- (22) G. Birnbaum, W. Hó, and A. Rosenberg, *J. Chem. Phys.*, **55**, 1039 (1971).
- (23) G. E. Ewing, *Accounts Chem. Res.*, **2**, 163 (1969).
- (24) G. E. Ewing, *J. Chem. Phys.*, **37**, 2250 (1962).
- (25) R. Haffmans and I. W. Larkin, *J. Chem. Soc., Faraday Trans. 2*, **68**, 1729 (1972).
- (26) R. Gordon, *J. Chem. Phys.*, **43**, 1307 (1965).
- (27) A molecular dynamic method was used recently by J. Barojas, D. Levesque, and B. Quentrec, *Phys. Rev. A*, **7**, 1092 (1973), to simulate the behavior of liquid nitrogen. The reorientational self-correlation functions were found to predict well residence times of the same order of magnitude as those reported herein.
- (28) A. Gerschel, I. Darmon, and C. Brot, *Mol. Phys.*, **23**, 317 (1972).

Optimal Determination of Relaxation Times of Fourier Transform Nuclear Magnetic Resonance. Determination of Spin-Lattice Relaxation Times in Chemically Polarized Species¹

Kenner A. Christensen, David M. Grant,^{2*} Edward M. Schulman, and Cheves Walling*

Department of Chemistry, University of Utah, Salt Lake City, Utah 84112 (Received February 21, 1974)

Publication costs assisted by the National Institutes of Health and the National Science Foundation

The optimal conditions for determining the spin-lattice relaxation times using Fourier transform techniques are discussed and the method which has been applied to polarized species produced by chemically induced dynamic nuclear polarization (CIDNP) has been developed. A number of T_1 measurements on the polarized products of benzoyl peroxide decomposition have been made from which carbon-13 CIDNP enhancement factors are determined.

I. Introduction

In order to use chemically induced dynamic nuclear polarization as a probe to study the details of free-radical reactions, quantitative data on the enhancements of the polarized nuclei are often required. Since the observed enhancement is directly dependent on the spin-lattice relaxation time, T_1 , of the polarized nucleus,^{3,4} a reliable method of measuring T_1 values of such species in the most efficient

manner is essential to these studies. The use of Fourier transform methods provides a method for fast, accurate measurement of T_1 values of polarized nuclei in a system undergoing chemical reaction providing optimal conditions are selected for the experiment.

The T_1 value for polarized species arising from thermal decomposition may be measured by the recovery of polarization from saturation.⁵ In a photochemical reaction, T_1

values of polarized species may be obtained from the rise or decay of polarization as the light source is turned on or off.⁶ These continuous-wave methods are adequate if the polarized lines are of sufficient intensity to be observed by single scans with low radiofrequency power. This is not generally possible in studies involving polarized nuclei of low natural abundance, such as ¹³C or ¹⁵N.

The use of Fourier transform methods permits techniques with high-efficiency radiofrequency power levels and time-averaging capability. In photochemical studies where a true steady-state concentration of polarized species may be maintained, the T_1 values of the polarized species may be obtained from a progressive saturation experiment.^{7,8} Such a measurement has been made on the products of dibenzyl ketone photolysis.⁹

For thermal reactions where the rate of production of polarized species may vary at a rate similar to that of nuclear spin relaxation, it becomes especially important to collect data under time-optimized conditions. The theory for such experiments is presented, and a number of T_1 measurements have been made on both static and reacting systems.

II. Experimental Section

All experiments were performed on a Varian XL-100-15 nmr spectrometer equipped with a Varian Fourier transform pulse unit, 620f computer, Gyrocode decoupler, temperature control unit, and V-4415 probe. Carbon-13 nmr spectra were recorded at 25.2 MHz, with incoherent proton decoupling. Pulse widths were calibrated by careful determination of the 360° null as a function of the distance from the carrier frequency.

Thermal decompositions were carried out on a series of aliquots of benzoyl peroxide solutions prepared in identical 10-mm sample tubes plugged with cotton. A field-frequency lock was provided by dimethyl sulfoxide-*d*₆ in the annular region of a 12-mm tube containing the 10-mm sample tube. Tetrachloroethene solutions were maintained at 60° prior to use; cyclohexanone and hexachloroacetone solutions were maintained at 23°. A fresh 10-mm tube containing an aliquot of solution was placed in the preheated 12-mm sleeve for each measurement. Data accumulation was started 5 min after insertion into the spectrometer probe, following four preparatory pulses to ensure steady-state magnetization, and continued for 5 min. Ten to fifteen data points were taken for each T_1 determination, each with a fresh sample and at a different pulse width setting.

The thermal behavior of reacting samples in the spectrometer probe was studied by placing a glass-enclosed copper-constantan thermocouple in a reacting sample and recording the potential with a Hewlett-Packard Model 680 strip chart recorder. In the range 100–110° the reacting sample reached probe temperature within 5 min; due to the exothermic nature of the benzoyl peroxide decomposition, a maximum temperature 5° above probe temperature was reached 7 min after insertion and maintained for the duration of the experiment.

Cyclohexanone (Matheson Coleman and Bell), hexachloroacetone (Aldrich), tetrachloroethene (Matheson Coleman and Bell; ~99% by gc), and benzoyl peroxide (Lucidol Division of Wallace and Tiernan; ~98% by iodometric titration) were used as received. Cyclohexanone and hexachloroacetone solutions were 0.40 *M* in benzoyl peroxide at 25°; the tetrachloroethene solution was 0.70 *M* at 60°.

III. Theoretical Considerations

A. Dependence of Signal on Pulse Width and Pulse

Separation. If a nuclear spin system is subjected to a series of radiofrequency pulses of width θ (measured in terms of the magnetization tip angle) and with a pulse period of t the z magnetization before and after each pulse is given by M^- and M^+ , respectively. Steady state will be achieved with the pulsing radiofrequency field after four or five pulses. If t is selected to be much longer than the effective T_2^* but not necessarily long compared with the spin-lattice relaxation time, T_1 , then the following relationships between magnetizations and the parameters specifying the pulse sequence will obtain

$$M^+ = M^- \cos \theta \quad (1)$$

$$M_0 - M^- = (M_0 - M^+)e^{-t/T_1} \quad (2)$$

where M_0 is the equilibrium magnetization in the absence of the radiofrequency perturbation. The steady-state z magnetization just before the pulse is obtained by substituting (1) into (2) as in

$$M^- = M_0 \frac{e^{t/T_1} - 1}{e^{t/T_1} - \cos \theta} \quad (3)$$

Since the signal observed in the free-induction decay immediately following the pulse will be equal to $M^- \sin \theta$, then the signal intensity for N pulses is given by

$$S(\theta, r) = \frac{KN^{1/2}(\sin \theta)(e^r - 1)}{e^r - \cos \theta} \quad (4)$$

where $r = t/T_1$, N is the number of free-induction decays collected, and K is the appropriate constant of proportionality which includes the value for M_0 and the various spectrometer response coefficients. Expressions similar to (4) have been given by Waugh.¹⁰ The relative magnitude of $S(\theta, r)$ for various values of r and θ are plotted in Figure 1 assuming that the number of transients, N , is a constant in each case. It is observed that (4) maximizes for $\theta = 90^\circ$ and t very large. Actually $S(\theta, r)$ achieves 99% of its maximum value in the region of $r > 4.5$ and $\theta = 90^\circ$ as can be observed in Figure 1.

Equation 4 and, therefore, Figure 1 do not yield the true optimization of $S(\theta, r)$ per unit time spent on the experiment, however, as the points with the greatest magnitude for $S(\theta, r)$ also take the longest period of time to acquire. The relationship among N , t , and T_0 , the time over which the experiment is conducted, is given by $N = T_0/t$, and S/T_0 , the amount of usable signal gathered per unit time, now becomes

$$S'(\theta, r) = \frac{S(\theta, r)}{T_0} = \frac{K_1(\sin \theta)(e^r - 1)}{r^{1/2}(e^r - \cos \theta)} \quad (5)$$

In this expression $K_1 = K/(T_1 T_0)^{1/2}$. It is actually the maximum in $S'(\theta, r)$ and not $S(\theta, r)$ which is of the greatest importance in optimal information retrieval. The plot contained in Figure 2 illustrates the regions in which (5) has its greatest value. Contrary to the results in Figure 1 the optimal region lies at relatively small t and at angles less than 90° . One should avoid the $t \rightarrow 0$ limit as (5) contains a singularity at (0, 0) and furthermore the plot is not valid for very short t as this would invalidate the $t > T_2^*$ assumption. Figure 2 indicates that one may work in the region near $t = 0.5T_1$ and $\theta = 50\text{--}60^\circ$ and maintain high efficiency. It should be remembered that to recover the signal-to-noise ratio lost by operating at the 0.7, 0.5, or 0.3 contour

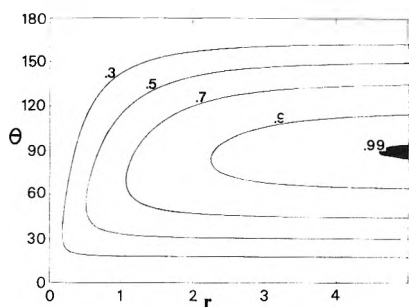


Figure 1. A contour plot of $S(\theta, r)/N$ given in eq 4. The contour lines are labeled in terms of the maximum value of $S(\theta, r)$ obtained per given number of transients, N .

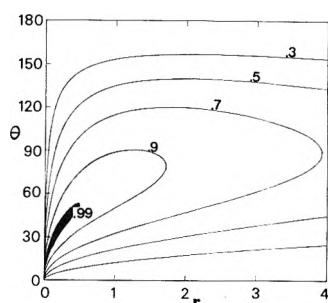


Figure 2. A contour plot of $S'(\theta, r)$ given in eq 5. The contour lines are labeled in terms of the maximum value of $S'(\theta, r)$, which measures the signal-to-noise ratio per unit time of data collection.

lines (see Figure 2) would require extended accumulation times of about $2T_0$, $4T_0$, and about $11T_0$, respectively. Thus, the importance of operating a pulse spectrometer within the shaded areas indicated in Figure 2 is apparent. One even loses almost 20% in time efficiency when working at the 0.9 signal intensity level.

B. Regions of Maximum Dependence of $S(\theta, r)$ and $S'(\theta, r)$ on T_1 . Although one should always be concerned with optimal spectrometer settings in any experiments, it becomes doubly important for measurements on samples undergoing chemical change. Short-lived intermediates must be studied under time-optimized conditions. Typical use of the progressive saturation experiment is to measure relaxation parameters under conditions specified by (4) using a given N for the various values of t . Logarithmic plots of magnetization ratios for different t values are then developed to yield the T_1 parameter. As we observed in the last section it is optimization of $S'(\theta, r)$ and not $S(\theta, r)$ which is of the greater importance in obtaining the maximum amount of information in the shortest possible time. Therefore, T_1 measurements taken in the usual manner may deviate greatly from optimal operation depending upon the individual selection of a set of t values. By differentiating $S(\theta, r)$ or $S'(\theta, r)$ with respect to $1/T_1$, functions are obtained which indicate the domain in θ and r where data should be taken which is most sensitive to the T_1 parameter. These expressions are

$$\frac{\partial S(\theta, r)}{\partial(1/T_1)} = \frac{K_2 N^{1/2} (\sin \theta)(1 - \cos \theta) r e^r}{(e^r - \cos \theta)^2} \quad (6)$$

$$\frac{\partial S'(\theta, r)}{\partial(1/T_1)} = \frac{K_3 (\sin \theta)(1 - \cos \theta) r^{1/2} e^r}{(e^r - \cos \theta)^2} \quad (7)$$

and their contour plots are given in Figures 3 and 4, respectively. $K_2 = KT_1$ and $K_3 = K(T_1/T_0)^{1/2}$. It is observed

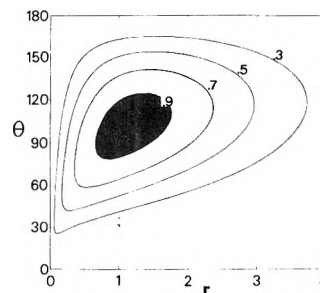


Figure 3. Contour plot of $\partial S(\theta, r)/\partial(1/T_1)$ which measures the sensitivity of $S(\theta, r)$ to the parameter $1/T_1$. The contours are related to the maximum value of the function.

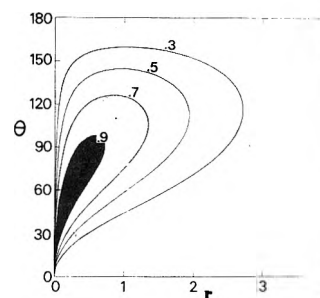


Figure 4. A contour plot of $\partial S'(\theta, r)/\partial(1/T_1)$. The function reflects the sensitivity of the time-optimized signal-to-noise ratio to the parameter $1/T_1$.

from Figure 3 that the maximum in the $\partial S(\theta, r)/\partial(1/T_1)$ plot falls in the region of $\theta = 102^\circ$ and $r = 1.15$. Normal operation at $\theta = 90^\circ$ and values of $r = 0.5$ – 2.0 of course fall in a relatively high efficient region of Figure 3, and thus the usual methods are basically satisfactory providing one is not concerned with time optimization.

Figure 4 presents a contour plot in θ and r of the regions where $S'(\theta, r)$ is most sensitive to $1/T_1$, the rate constant of spin relaxation. If one varies r while holding θ at 90° the most sensitive region is for $0.2 < r < 1.2$ (response is within the 0.7 contour line). Using standard curve-fitting techniques one can also take optimal data under constant r and variable θ . Favorable settings for this experiment are found in the region $r = 0.5$ and $50 < \theta < 120$. This approach has the convenience that a constant number of pulses is recorded for the same total time for every tip angle selected. When working on a solution undergoing chemical reaction this technique removes the time bias that otherwise exists under normal operation if different total times are selected. A multiple variable analysis of T_1 could also be used if both θ and r are allowed to vary. The function given in eq 5 must then be fit by computer to the data to yield T_1 and K_1 . While ultimately this latter approach may provide the basis for a completely automatic computer evaluation of T_1 , the single- θ -variable method is used herein because of the ease with which it may be visually portrayed. This is done of course at the expense of reducing statistical variations by increasing the degrees of freedom in going to the two-variable treatment.¹¹ Even so, the time-optimized technique is claimed to be preferable to the use of the constant transient method when time efficiency becomes a significant matter as it is in most CIDNP studies. It will also be shown that the T_1 data collected under optimum settings of r and θ as given in Figure 4 have less error in the regression fit.

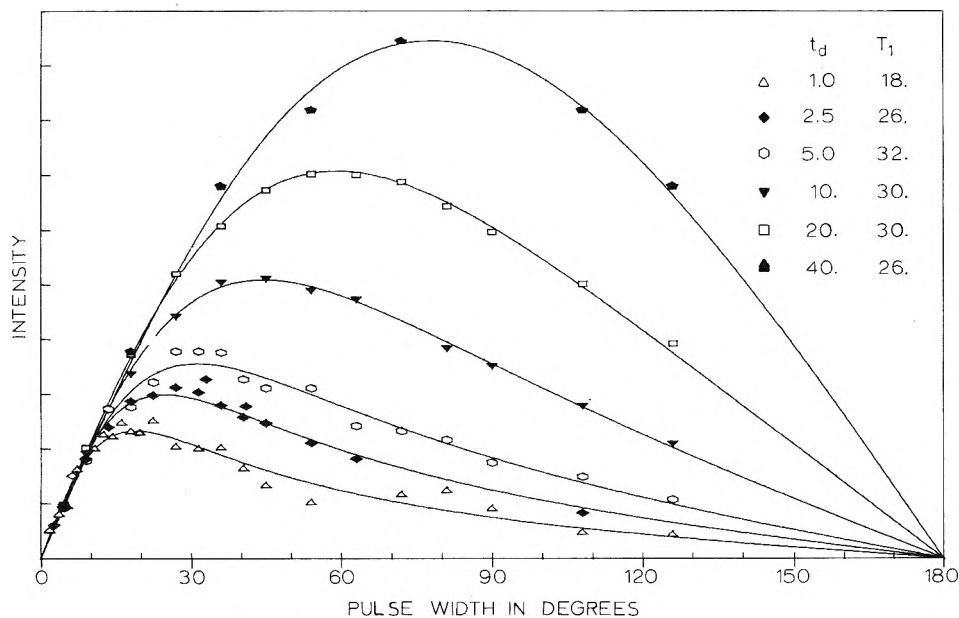


Figure 5. The effect of varying the delay time while holding the number of transients constant at 10. The data are for benzene at 40° , where a value of 29.5 sec was obtained by an inversion-recovery experiment.

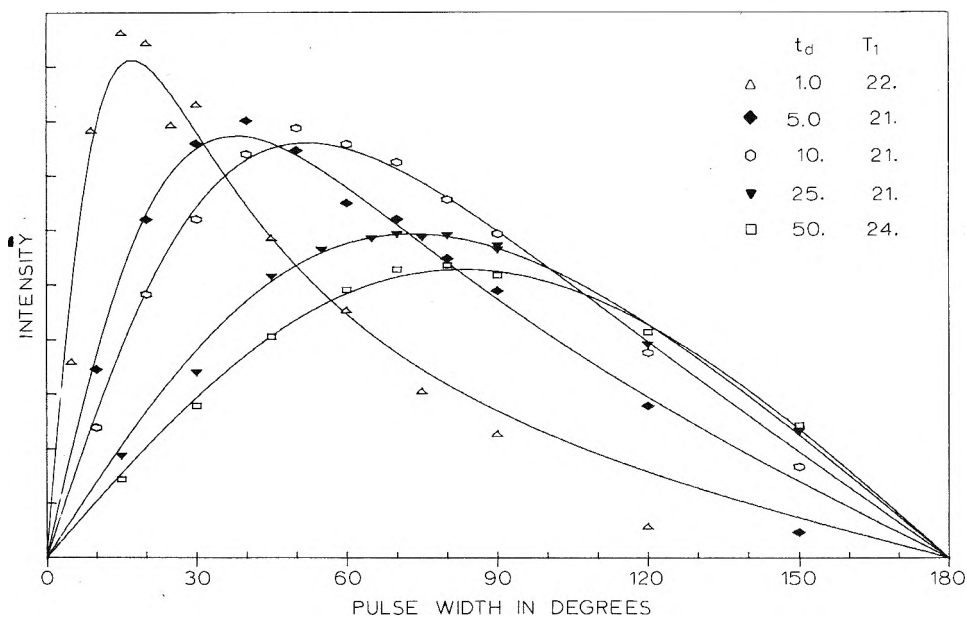


Figure 6. The effect of varying the delay time while holding the total time per data point constant (about $10T_1$ to make runs comparable to but not exactly equivalent to the best runs in Figure 5). The data are for C-3 of chlorobenzene at 40° , where a value of 21.5 sec was obtained by an inversion-recovery experiment.

IV. Results and Discussion

A. T_1 Measurements in Nonreacting Systems. The effect of varying the tip angle for different delay times on the signal-to-noise level of the observed data is shown in Figures 5 and 6 for the constant-transient and constant-time experiments, respectively.

The data illustrated in Figure 5 result from a series of measurements where the number of transients and all instrumental gain settings were held constant as the delay time and pulse angles were varied. The curves obtained illustrate the relative signal-to-noise ratio to be obtained at various settings of these two variables as a family of curves which represent vertical slices through Figure 1. The rela-

tive signal-to-noise level increases as the delay time is increased, but the total experiment time is also increased.

The best T_1 fits for various t values, as given in Figure 5, present a measure of the reliabilities of extracting T_1 from an assortment of data. The best value for T_1 obtained by a carefully executed inversion recovery experiment was 29.5 sec. It is to be observed that this value is reproduced best by the $t = 10$ and 20 sec ($r = \frac{1}{3}$ and $\frac{2}{3}$, respectively) values while for t equal to 1 sec ($r = 0.03$), 2.5 sec ($r = 0.08$), and 40 sec ($r = 1.3$) statistical deviations have greatly increased in the predicted value of T_1 from the 29.5-sec value.

The result of a series of experiments in which the spectrometer gain has been maintained constant but the number of transients has been varied to maintain a constant ac-

quisition time for each data point, neglecting the preparatory pulses, is shown in Figure 6. The signal levels have been corrected to maintain a constant noise level throughout the experiment. The plots in Figure 6 constitute vertical slices through Figure 2. The signal-to-noise ratio obtained under these conditions is greatly improved of course for shorter t values.

If the delay time chosen is much longer than T_1 , the curve obtained from a plot of intensity *vs.* pulse width lacks the accuracy in determining T_1 found for delay times which are in the range of $r = 0.25$ –1. A T_1 of 21.5 sec was obtained under carefully controlled inversion recovery conditions. If the delay time chosen is too short, errors may be introduced due to the incomplete decay of transverse magnetization between pulses (*i.e.*, $t < T_2^*$). In the compound studied here errors due to the incomplete decay of transverse magnetization began to be important when delay times fell below 5 sec. The accumulation of a large number of transients utilizing a random timing "jiggle" to prevent coherent summation of spin echoes however can decrease¹² this difficulty. Using this technique and a delay time of 1 sec indicates that reasonable results were obtained for $r \approx 0.05$ as only minor deviations from the 21.5-sec results were observed. Nonetheless it is the operation in the region of $r = 0.23$ ($t = 5$ sec) to $r = 1.15$ ($t = 25$ sec) which produces the most reliable values for T_1 . For these ranges in r , the best signal-to-noise ratio is obtained in the 30–90° region of θ as can be observed in Figure 6. These results confirm the theoretical predictions given in Figure 4.

The above considerations suggest that delay times should be chosen such that $T_1 > t > T_2^*$. For measurements on reacting systems, where the total available sampling time is limited and local short-term effects such as the periodic evolution of gas bubbles may seriously affect a few of the transients, the use of short delay times, allowing averaging of the maximum number of transients, minimizes the variation in the individual data points and permits the most accurate determination of T_1 . Thus, the experiment which forms the basis of data given in Figure 6 was selected for obtaining T_1 data on the chemically reacting species discussed in the following sections.

B. T_1 Measurements in Reacting Systems. Relaxation time measurements on the polarized products of benzoyl peroxide decomposition¹³ in various solvent systems were undertaken and the T_1 values are presented in Table I. Each data point was collected over a 5-min period during the first half-life of the reaction using delay times of 10–20 sec. The corresponding values of T_1 for unpolarized species were obtained from inversion-recovery experiments on sealed, vacuum-degassed samples to be used for comparison with the dynamically polarized species.

Two examples of the type of data obtained are given in Figures 7 and 8 for the thermal decomposition of benzoyl peroxide in cyclohexanone and hexachloroacetone, respectively. The signal-to-noise ratio is plotted *vs.* θ for $t = 10$ sec. These plots are presented to indicate the extent of scatter in the data points and to show how the position of the maximum in each plot reflects the T_1 value. It is observed that the carbons with shorter T_1 's will have their maxima in the angular plots shifted to larger tip angles. This agrees with Figure 2 where the maximum signal-to-noise ratio is found at higher θ when r is larger (*i.e.*, T_1 smaller for the same t_d). In Figure 8 the shift in the maximum of C-1 in phenyl benzoate with $T_1 = 54$ sec is sufficient that the associated line actually crosses over the C-1

TABLE I: T_1 Values (sec) of the Polarized Products of Benzoyl Peroxide Decomposition at 100°

Reaction and solvent	Carbon			
	¹³ C ₆ H ₅ - ¹³ CO ₂ C ₆ H ₅	C ₆ H ₅ CO ₂ - ¹³ C ₆ H ₅	Cl ¹³ CC ₆ H ₅	Benzene
T_1 at 100°; no reaction	76 ^a	51 ^a	111 ^b	20 ^c
0.7 M BPO in tetrachloroethene	68	50		
0.4 M BPO in cyclohexanone	72	62		32
0.4 M BPO in hexachloroacetone	87	54	88	
0.4 M BPO in 50% hexachloroacetone–50% cyclohexanone	71	64	113	24.5

^a Neat. ^b 25% in hexachloroacetone. ^c 10% in tetrachloroethene.

line in chlorobenzene with $T_1 = 88$ sec. Experimental errors in fitting these data with the T_1 parameter using regression techniques are about 10–15%.

None of these reactions showed a uniform decrease in relaxation times due to the presence of a free-radical reaction. In these experiments, the estimated radical flux is of the order of 10^{-6} M, less than the oxygen content of organic liquids in contact with the atmosphere. Such an effect would be expected under conditions of higher radical flux or for protons⁶ or fluorine nuclei where medium effects are more important than for carbon.

For species exhibiting large enhancements, the measurement of T_1 on the polarized species may prove substantially less time consuming than a conventional T_1 measurement on a neat sample of the compound providing optimal conditions are utilized to take advantage of this enhancement. In addition, the measurement is made at high dilution in the solvent of interest. If the T_1 values of the polarized species are changed by the reaction, then of course, T_1 values obtained under different conditions cannot be used for the calculation of enhancement factors. T_1 measurements must be made for these circumstances on the polarized species under reaction conditions.

C. Enhancement Factors. If the polarization is sampled as a function of time from the initiation of the reaction, the rate constant and enhancement factors may be extracted from these data by the following analysis. If we define the enhancement factor V as that where a and b are the ratios of spin-state populations for polarized and unpolarized species

$$V = a/b \quad (8)$$

then the signal at any time due to the species B will be given by

$$S = a[B^*] + b[B] \quad (9)$$

where B* denotes freshly formed product. A steady-state treatment for the first-order formation of B* from the decomposition of a peroxide P yields

$$[B^*] = k_d f [P] T_1 \quad (10)$$

where k_d is the first order rate constant for the decomposition of the peroxide P and f is the fraction of the decomposing peroxide which yields the product B. Since $S_\infty = bB_\infty$

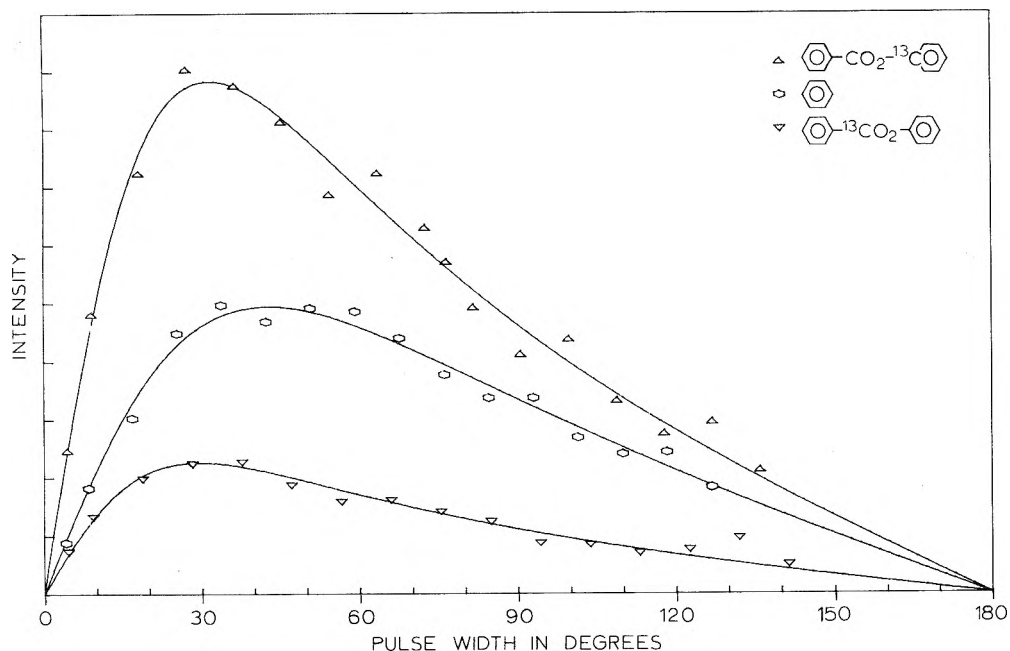


Figure 7. Pulse angle data for the major polarized products of the decomposition of 0.4 M benzoyl peroxide in cyclohexanone at 100°.

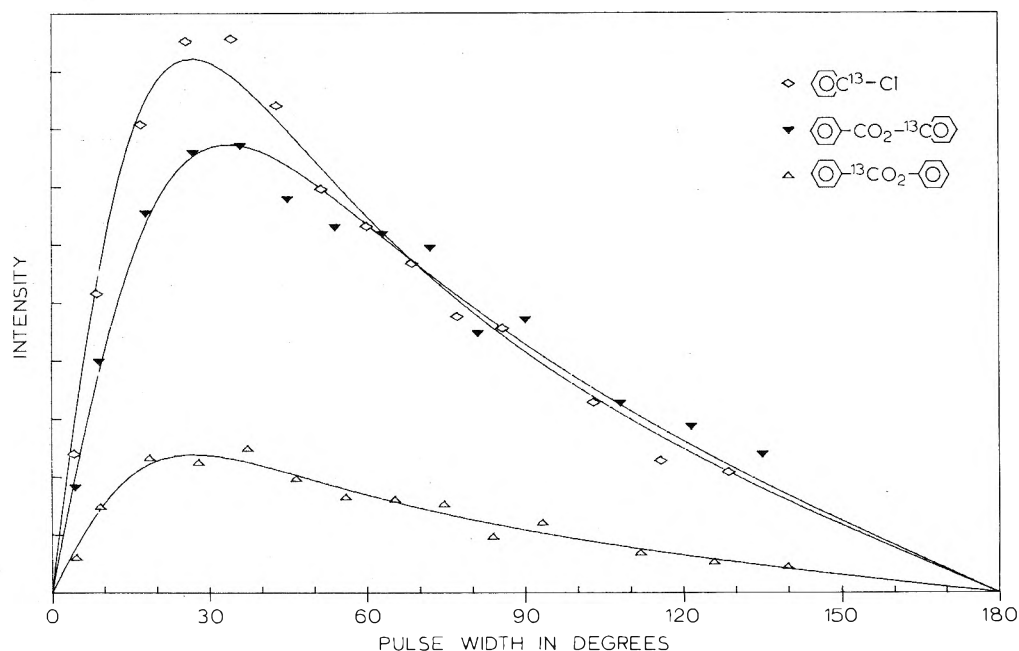


Figure 8. Pulse angle data for the major polarized products of the decomposition of 0.4 M benzoyl peroxide in hexachloroacetone at 100°.

TABLE II: Enhancement Factors at C-1' of Phenyl Benzoate Generated from the Thermal Decomposition of Benzoyl Peroxide at 100°

Solvent	$10^4 k_d, \text{min}^{-1}$	$10^{-4} V$
0.7 M in tetrachloroethene	3.1	1.5
0.4 M in cyclohexanone	4.0	1.2
0.4 M in hexachloroacetone	1.9	2.3

$$\frac{S - S_\infty}{S_\infty} = (Vk_d T_1 - 1) \exp(-k_d t) \quad (11)$$

An experimentally determined T_1 value and a set of values of S and t may be substituted into the above expression

and a regression analysis used to obtain S_∞ , V , and k_d . If V is large, i.e., S_∞ is small compared to S , then only the product VS_∞ may be accurately determined by this technique. Under these circumstances, S_∞ may be obtained from a standard sample of the reaction product if the yield of the product B is accurately known.

Table II contains rate constants and enhancement factors for C-1' of phenyl benzoate determined in the latter manner. The value of S_∞ used was calculated from the intensity of the signal observed from neat phenyl benzoate and the yield determined previously in tetrachloroethene.¹³ (Since phenyl benzoate is a cage product, the yield should be solvent independent to a first approximation, neglecting

differences in viscosity.) A notable feature of Table II is the very large values ($>10^4$) of the enhancement factors observed.

Acknowledgment. This work was supported in part by the National Institutes of Health, Grants GM-085021 and RR-0574, and by the National Science Foundation, Grant GP-36620X. Furthermore, the facilities at the California Institute of Technology were used under the sponsorship of the Sherman Fairchild Distinguished Scholars program in the final stages of this work.

References and Notes

- (1) Presented in part at the First Rocky Mountain Regional Meeting of the American Chemical Society, Fort Collins, Colo., June 30–July 1, 1972.
- (2) On leave during 1973–1974 at California Institute of Technology as a Sherman Fairchild Distinguished Scholar.
- (3) G. L. Closs and L. E. Closs, *J. Amer. Chem. Soc.*, **91**, 4549 (1969).
- (4) R. Kaptein, *J. Amer. Chem. Soc.*, **94**, 6251 (1972).
- (5) R. Kaptein, J. Brokken-Zijp, and F. J. J. deKanter, *J. Amer. Chem. Soc.*, **94**, 6280 (1972).
- (6) K. Maruyama, H. Shindo, T. Otsuki, and T. Maruyama, *Bull. Chem. Soc. Jap.*, **44**, 2756 (1971).
- (7) R. R. Ernst and W. A. Anderson, *Rev. Sci. Instrum.*, **37**, 93 (1966).
- (8) R. Freeman and H. D. W. Hill, *J. Chem. Phys.*, **54**, 3367 (1971).
- (9) R. Kaptein, R. Freeman, and H. D. W. Hill, paper presented at the 13th Experimental NMR Conference, Pacific Grove, Calif., April 30–May 4, 1972.
- (10) J. S. Waugh, *J. Mol. Spectrosc.*, **35**, 298 (1970).
- (11) Further work on this problem is being conducted in this laboratory.
- (12) R. Freeman and H. D. W. Hill, *J. Magn. Resonance*, **4**, 366 (1971).
- (13) For a discussion of the chemistry of benzoyl peroxide decomposition, see E. M. Schulman, R. D. Bertrand, D. M. Grant, A. R. Lepley, and C. Walling, *J. Amer. Chem. Soc.*, **94**, 5972 (1972), and references therein.

COMMUNICATIONS TO THE EDITOR

Direct Electron Spin Resonance Detection of Free Radicals Produced in Electron-Irradiated Liquid Alcohols¹

Publication costs assisted by Atomic Energy of Canada Limited

Sir: Although the radiation chemistry of alcohols has been extensively studied,^{2a} few reports have been published about direct observation of the free radicals formed. Pulse radiolysis studies have concentrated on the absorption spectra and reaction rates of the solvated electron.^{2,3} Simic, *et al.*,⁴ and Dainton, *et al.*,⁵ reported spectra of the radicals in pulse-irradiated alcohols but these consisted of a rising absorption edge in the ultraviolet and did not have a characteristic peak. The situation was complicated by the suggestion that both methoxy and hydroxymethyl radicals have the same absorption spectra in this region.⁶ Electron spin resonance (esr) should be able to provide a positive identification but previous esr studies have been limited to low-temperature glasses⁷ or to the products of the reactions of hydroxyl radicals.^{8,9} In this communication, we describe the first direct esr observation of the radicals formed during radiolysis of alcohols in the liquid state.

Using a method very similar to that of Fessenden,^{9,10} we have coupled an electron accelerator to an esr spectrometer. This permits the direct observation of esr spectra from the steady-state concentration of radicals formed during continuous radiolysis with a dc beam of 3-MeV electrons. The alcohols were deaerated by bubbling with argon and then flowed through the radiolysis cell. Cooling was accomplished by a coil immersed in a Dry Ice bath. For all the alcohols studied, the major radical observed during the radiolysis was derived by loss of an H atom from the carbon atom adjacent to the hydroxyl group. These will be referred

to as α radicals. In some cases the esr spectra showed the presence of secondary radicals.

The only radical observed from methanol was the hydroxymethyl, $\dot{\text{C}}\text{H}_2\text{OH}$. The coupling constants at -50° were 17.8 and 1.6 G for the α and hydroxyl protons, respectively. These values compare well with 17.4 and 1.75 G obtained by Livingston and Zeldes for $\dot{\text{C}}\text{H}_2\text{OH}$ produced by the photolysis of methanol containing 1% hydrogen peroxide at -50° .⁸ Furthermore, when the methanol was bubbled with nitrous oxide there was no change in the intensity of the CH_2OH spectrum.

The major radical observed during the radiolysis of ethanol was $\text{CH}_3\dot{\text{C}}\text{HOH}$. At room temperature, the esr couplings were $a_{\text{CH}_3\text{H}} = 22.1$ and $a_{\text{CHH}} = 15.3$ G; coupling to the hydroxyl proton was not resolved. However, at -50° , $a_{\text{OHH}} = 0.87$ G. This behavior is the same as that reported for the photochemical experiments.⁸ At -50° additional peaks were detected and were shown to be due to $\dot{\text{C}}\text{H}_2\text{OH}$. These were decreased when the alcohol was bubbled with nitrous oxide, but peaks due to $\text{CH}_3\dot{\text{C}}\text{HOH}$ were unchanged.

The spectrum observed at room temperature during radiolysis of 2-propanol was primarily due to the $(\text{CH}_3)_2\dot{\text{C}}\text{OH}$ with $a_{\text{CH}_3\text{H}} = 19.7$ and $a_{\text{OHH}} = 0.7$ G. These values are identical with those reported for the photolysis of 2-propanol containing 0.4% hydrogen peroxide.⁸ In addition to the α radical, some weaker peaks due to $\text{CH}_3\dot{\text{C}}\text{HOH}$ were observed in the esr spectrum. They decreased when the alcohol was bubbled with nitrous oxide.

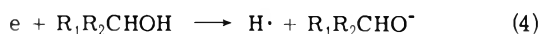
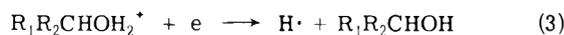
The results reported above show that the only major radicals detected by esr during the *in situ* radiolysis of alcohols were α radicals. However, previous studies by us, using a spin trapping method, have demonstrated that both α and alkoxy radicals are formed during radiolysis.¹¹ The

failure to detect alkoxy radicals, RO \cdot , in the present experiments is due to two causes. First, the lifetime of these radicals at room temperature is only 100 nsec^{5,6} and even at the lower temperatures used here, their lifetime would be short. Therefore their steady-state concentration would be very low. Second, the esr spectra of alkoxy radicals in solution would be expected to consist of one very broad, and consequently very weak, line. This is because, as for \cdot OH, these radicals have an orbitally degenerate ground state which leads, *via* spin orbit coupling, to very short spin relaxation times and hence very broad lines. This makes the detection of alkoxy radicals in solution difficult and probably impossible. The alkoxy radicals decay by H abstraction from the alcohol to produce α radicals.

The effect of saturating the alcohols with the electron scavenger, nitrous oxide, deserves further comment. The concentration of α radicals was unchanged whereas an increase was expected because of reactions 1 and 2. A possi-



ble explanation of the lack of any effect is that those electrons scavenged by nitrous oxide were already generating α radicals by the reaction series 3-5. Therefore saturation of



the alcohol with nitrous oxide merely replaces H abstraction by hydrogen atoms with H abstraction by hydroxyl radicals. The products of these reactions are expected to be the same.

The decrease in the intensity of the secondary radical peaks when nitrous oxide was used suggests that these are at least in part derived from the scavenging of electrons by the products of the radiolysis. It is well known that one of the major products is aldehyde.^{2a} This is derived from non-radical sources such as fragmentation of the primary cation

or electronically excited alcohol molecules. Aldehydes are very powerful electron scavengers. A crude calculation of the dose rate and doses in our experiment together with the known *G* values^{2a} shows that in ethanol and 2-propanol the concentration of formaldehyde and acetaldehyde respectively would be 10⁻⁴ *M*. This would be sufficient to scavenge some of the electrons to produce \cdot CH₂OH and CH₃CHOH in ethanol and 2-propanol, respectively. In the presence of nitrous oxide these reactions cannot compete with reaction 1 and therefore do not occur. Further experiments are planned to measure the dose rate in our system and to provide a better test of this interpretation.

Acknowledgment. We are indebted to R. W. Fessenden and R. H. Schuler of the Carnegie-Mellon University, E. C. Avery of the Argonne National Laboratory, and the late B. Smaller for very helpful advice in setting up the *in situ* radiolysis.

References and Notes

- (1) AECL No. 4800.
- (2) (a) G. R. Freeman in "Actions Chimiques et Biologiques des Radiations," Vol. 14, M. Haissinsky, Ed., Masson et Cie., Paris, 1970, Chapter II, p 73; (b) A. Habersbergerova, I. Janovsky, and J. Teply, *Radiat. Res. Rev.*, **1**, 109 (1968); (c) A. Habersbergerova, I. Janovsky, and P. Kourim, *ibid.*, **4**, 123 (1972).
- (3) E. Watson and S. Roy, *Nat. Stand. Ref. Data Ser., Nat. Bur. Stand.*, No. **42** (1972).
- (4) M. Simic, P. Neta, and E. Hayon, *J. Phys. Chem.*, **73**, 3794 (1969).
- (5) F. S. Dainton, G. A. Salmon, and P. Wardman, *Proc. Roy. Soc., Ser. A*, **313**, 1 (1969).
- (6) D. H. Ellison, G. A. Salmon, and F. Wilkinson, *Proc. Roy. Soc., Ser. A*, **328**, 23 (1972).
- (7) L. Kevan in "Actions Chimiques et Biologique des Radiations," Vol. 13, M. Haissinsky, Ed., Masson et Cie., Paris, 1969, p 57.
- (8) R. Livingston and H. Zeldes, *J. Chem. Phys.*, **44**, 1245 (1966).
- (9) K. Eiben and R. W. Fessenden, *J. Phys. Chem.*, **75**, 1186 (1971).
- (10) R. W. Fessenden and R. H. Schuler, *J. Chem. Phys.*, **39**, 2147 (1963).
- (11) F. P. Sargent, E. M. Gardy, and H. R. Falle, *Chem. Phys. Lett.*, **24**, 120 (1974).

Research Chemistry Branch
Atomic Energy of Canada Limited
Whiteshell Nuclear Research
Establishment
Pinawa, Manitoba, ROE 1LO, Canada

Frederick Peter Sargent*
Edward Michael Gardy

Received April 5, 1974

**New concepts
new techniques
new interpretations**

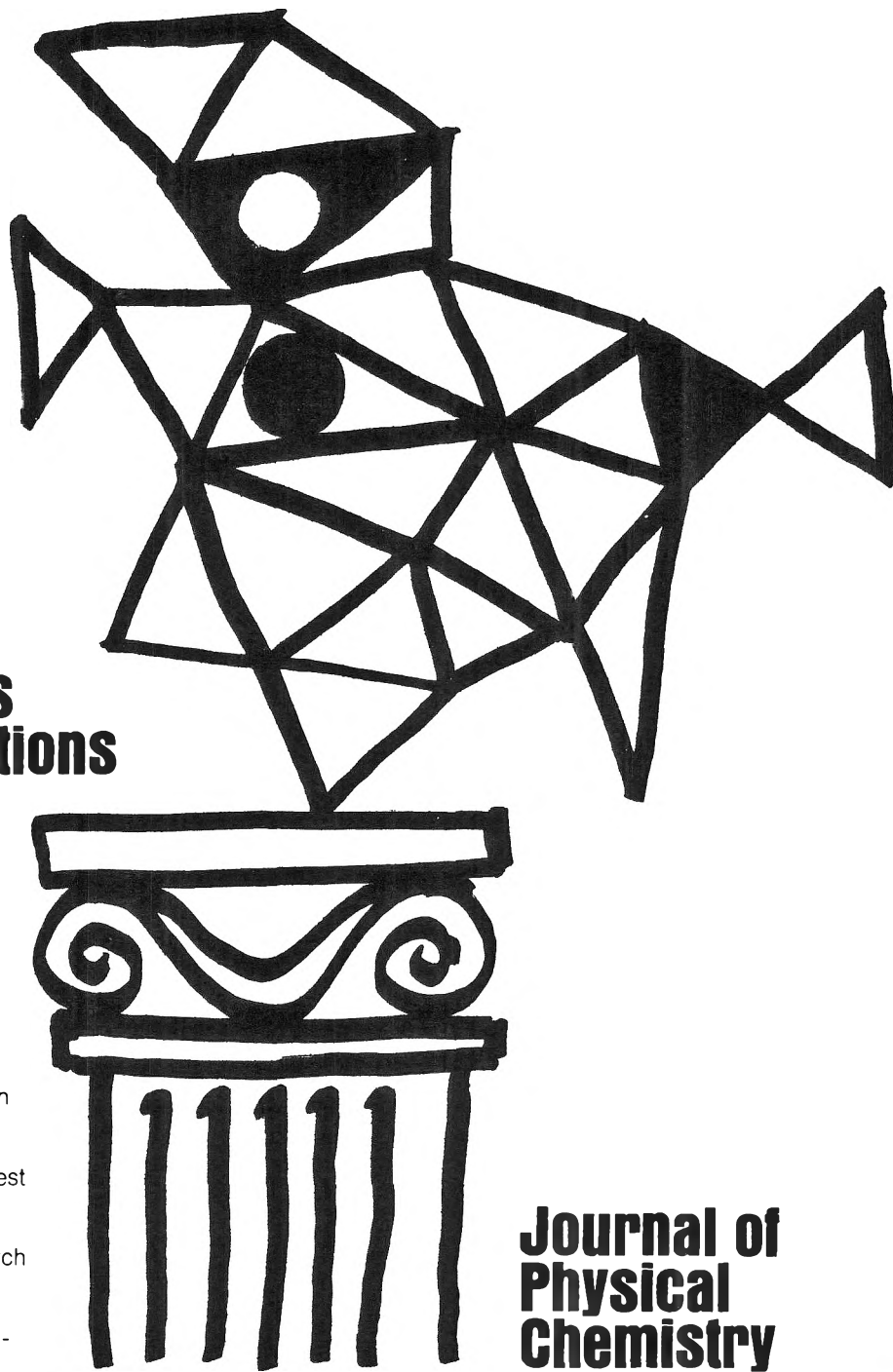
**... together
with valuable reports
on classical areas**

They are all waiting for you between the covers of our well-balanced JOURNAL OF PHYSICAL CHEMISTRY. Whatever your particular interest in physical chemistry, you'll find the JOURNAL's broad range of experimental and theoretical research reports are relevant and beneficial to your work. Each biweekly issue brings you an average of 30 authoritative, comprehensive reports on fundamental aspects of atomic and molecular phenomena, as well as timely notes, communications and reports plus the proceedings of selected symposia.

Join your fellow physical chemists who rely on JPC as an excellent biweekly source of data in both new and classical areas. Just complete and return the form to start your own subscription.



... another ACS service



**Journal of
Physical
Chemistry**

**The Journal of Physical Chemistry
American Chemical Society**

1974

1155 Sixteenth Street, N.W.
Washington, D.C. 20036

Yes, I would like to receive the JOURNAL OF PHYSICAL CHEMISTRY at the one-year rate checked below:

	<i>U.S.</i>	<i>Canada**</i>	<i>Latin America**</i>	<i>Other Nations**</i>
ACS Member One-Year Rate*	<input type="checkbox"/> \$20.00	<input type="checkbox"/> \$25.00	<input type="checkbox"/> \$25.00	<input type="checkbox"/> \$26.00
Nonmember	<input type="checkbox"/> \$60.00	<input type="checkbox"/> \$65.00	<input type="checkbox"/> \$65.00	<input type="checkbox"/> \$66.00

Bill me Bill company Payment enclosed

Air freight rates available on request.

Name _____

Street _____

Home
Business

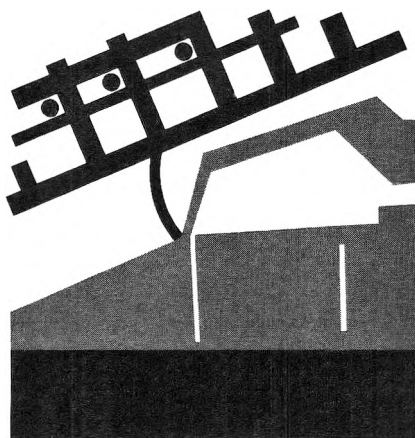
City _____

State _____

Zip _____

*NOTE: Subscriptions at ACS member rates are for personal use only. **Payment must be made in U.S. currency, by international money order, UNESCO coupons, U.S. bank draft, or order through your book dealer.

Electrodeposition of Coatings



ADVANCES IN CHEMISTRY
SERIES No. 119

A symposium sponsored by the Division of Organic Coatings and Plastics Chemistry of the American Chemical Society, with George E. F. Brewer, Chairman.

Seventeen papers report major new developments and research in the area of electrodeposition of organic coatings. This extensive collection discusses all aspects of this complex process including the advantage of better corrosion protection, lower cost, and virtual absence of pollution.

Principal topics covered:

- conversion and coatings; pretreating metals; surface changes; power supplies
- new polymers, copolymers, and pigments; preparation of resins; cathodic electrodeposition
- kinetics; dynamic simulation; throwing power
- bath maintenance; design of merchandise; influence of solvents

Each chapter offers material of permanent reference value for the industrial chemist working with automotive and appliance primers, as well as general-purpose one-coat systems.

243 pages with index Cloth (1973) \$13.45.

Postpaid in U.S. and Canada, plus 40 cents elsewhere.

Other recommended books in the ADVANCES IN CHEMISTRY SERIES include:

No. 109 Chemical Reaction Engineering

Fixed and fluid bed reactors, polymerization kinetics and reactor design, optimization of reactor performance, catalysis in gas-solid surface reactions, two-phase slurry reactors, industrial process kinetics, and transient operation.
685 pages with index Cloth (1972) \$16.50

No. 107 Industrial Color Technology

Summarizes present knowledge of colorant formulation and evaluation and its application to industrial processing. Basic colorimetry, instrumentation, color difference metrics, and color as an aspect of appearance; 32 color plates.
177 pages with index Cloth (1972) \$11.50

No. 104 Pesticides Identification at the Residue Level

Is our environment really becoming more toxic, or are pesticides falsely condemned by instruments designed as quantitative rather than qualitative tools? Eleven papers discuss philosophical aspects of ultramicroanalysis, instrumental techniques, microchemical methods, and biological assay.
182 pages with index Cloth (1971) \$8.50

No. 103 Origin and Refining of Petroleum

Twelve papers on petroleum origin, deposits, Athabasca tar sands; catalytic reforming, hydrocracking, alkylation, isomerization; ethylene, propylene, vinyl chloride in processing; homogeneous catalysis; future of oil in Canada.
230 pages with index Cloth (1971) \$10.00

No. 102 Molecular Sieve Zeolites—II

Thirty-six papers from the Second International Conference on Molecular Sieve Zeolites covering sessions on sorption and catalysis.
459 pages with index Cloth (1971) \$16.00

No. 99 Multicomponent Polymer Systems

Thirty-seven papers on systems from olefin, diene, vinyl halide, styrene, acrylic, urethane, and epoxy resins as well

as from polyamides, polyesters, polyarylenes, and others. Theory, processing, and applications are included. Nine papers on polyblends, the rest on copolymers.
598 pages with index Cloth (1971) \$16.50

No. 97 Refining Petroleum for Chemicals

Up-to-date status report on the advances made in an exciting new industry. Emphasis is on basic processing with specific discussions centering around the chemical reactions used, new developments in these reactions, products and economics, and new processing concept.
293 pages with index Cloth (1970) \$11.50

No. 96 Engineering Plastics and Their Commercial Development

A "how-to-do-it" book with discussion and case histories on developing plastics in profitable commercial products. Topics include use research, process development, and patent and legal aspects including clear warnings on contributory infringement. Engineering properties of over 50 plastic products are included.
128 pages with index Cloth (1969) \$7.50

No. 92 Epoxy Resins

Sixteen papers on formulation and performance of epoxy resins. Processes and reactions are discussed including condensation reactions, gelation, synthesis, electro-deposition, curing, and reactivity.
230 pages with index Cloth (1970) \$10.50

No. 91 Addition and Condensation Polymerization Processes

Twenty-six chapters devoted to process improvements and the polymerization kinetics of common monomers. The last 22 papers deal with new and improved polymers designed for specific uses or properties.
767 pages with index Cloth (1969) \$19.50

Order from: **Special Issues Sales**

American Chemical Society, 1155 Sixteenth St., N.W., Washington, D.C. 20036